# STUDIES ON ELECTRON SCATTERING BY MERCURY ATOMS

AND

# ELECTRON SPIN POLARIZATION DETECTOR

1977

Yasunori YAMAZAKI

Fundamental laws of Nature do not govern the world as it appears in our mental picture in any very direct way, but instead they control a substratum of which we cannot form a mental picture without introducing irrelevancies.

P.A.M. Dirac

(The Principles of Quantum Mechanics)

*Dedicated to my mother*

## Preface and Acknowledgements

Since N.F.Mott's prediction that unpolarized electrons may undergo considerable spin polarization during scattering with a heavy atom, many experimental and theoretical investigations have been performed in the area of atomic physics. Currently, experiments concerning spin polarization have attracted much attention from various fields of physics, particularly surface physics.

One of the most important considerations in spin polarization experiment is the spin polarization detector, which is markedly inefficient and structurally complex.

In the present study, a polarization detector which utilizes electron-atom scattering was systematically investigated and the optimum operation conditions has clearly been determined. For this purpose, electron-mercury scattering was studied in both an experimental and a theoretical view point. The elastic scattering cross section calculated herein has turned out to provide useful information for understanding the generation of Auger electons in solids. Furthermore, the study of the inelastic process leads to intimate insight to plasma physics.

The present paper is comprised of two sections; Part I, which includes Chapter 1-5, concerns the study of the electron-mercury scattering process. Part II, which includes Chapter 6-8, concerns the study of the electron-spin polarization detector which utilizes electron-mercury scattering.

Introducing Part I, Chapter 1 describes general concepts and the history of electron-mercury scattering.

Chapter 2 deals with the theoretical treatment of elastic scattering, based on the partial wave expansion method. The calculations of both the differential cross section and the Sherman function are also included in this chapter for incident electron energies between 300 and 2000 eV.

Chapter 3 discusses the theoretical treatment of inelastic scattering, based on distorted wave Born approximation. The calculation for both the differential cross section and the spin polarization for $6^1P$ excitation are performed for incident electron energies between 50 and 500 eV.

Chapter 4 is treating the apparatus constructed for observation of the loss-spectra of electron-mercury scattering, together with measured results of incident energies between 300 and 1000 eV and scattering angles between 50° and 110°.

Chapter 5 compares experimental (including the data in Chapter 4) and theoretical (Chapter 3) results for $6^1P$ excitation.

As an introduction to Part II, Chapter 6 generally describes the electron spin polarization detector.

Chapter 7 describes how the optimum conditions for the spin polarization detector were determined using the results of Chapters 2 and 4, and compares it to Mott detector.

Chapter 8 treats the construction of the apparatus for double scattering experiments which allows to perform experiment under the optimum conditions suggested in Chapter 7. Also described in this chapter, is the Pierce type electron gun with a single crystal $LaB_6$ cathode which was used in the experiment with considerable success and is of most practical use for high power electron beam source.

Research for the present thesis was carried out under the direction of Professor H.Hashimoto of the Department of Applied Physics, Osaka University.

The author wishes to thank Professor H.Hashimoto for the encouragement and stimulus during the course of the research. Several critical suggestions from Professors A. Mitsuishi and I. Shoji of Department of Applied Physics have been most helpful. Suggestions by Professor T.E.Everhart of Univ. of California at Berkeley provided more impetus for an investigation of Pierce type electron gun with single crystal $LaB_6$ cathode.

The author would like to express his gratitude to Professor R.Uchiyama of Faculty of Science for my initiation in the field of quantum theory of scattering.

To Associate Professor R.Shimizu, I am very thankful for critical suggestions and systematic discussion of both experiments and theory throughout the present work. The author would also like to express thanks to Dr. K. Ueda for his help with some aspects of the construction of the experimental apparatus and to Mr. Endoh for his advice on computer calculation procedures. I am thankful to my colleagues Mr.M.Shikata for his assistance in the development and successful operation of the Pierce electron gun, Messrs. S. Ichimura and T. Okutani for many stimulating discussions, Miss K.Nishiyama for her typing skill, and all other members of the Hashimoto Laboratory who supported the present work in various aspects.

I am also grateful to Mr.Y.Ogata of Central Research Lab. of Mitsubishi Electric Corp. for invaluable advice and support in manufacturing the sector-type energy analyser, Dr. S. Kawai of National Institute for Researches in Inorganic Materials for preparing $LaB_6$ single crystal and Mr. K.Goto of Nagoya Institute of Technology for his invaluable advice on detecting and counting system.

CONTENTS

# PART I ELECTRON-MERCURY SCATTERING

## CHAPTER 1 INTRODUCTION

### 1-1 General Concept of Electron-Mercury Scattering

In low and intermediate energy electron scattering by heavy atoms, electrons are strongly diffracted by an atomic potential because the electron wave length is the same order of magnitude with an atomic radius (see Appendix 1 for detailed discussion). The scattering intensity exhibits apparatent oscillatory features (diffraction pattern) as a function of both the scattering angle and incident electron energy (see Sec.2-5). From a theoretical viewpoint, this means that only a few partial waves contribute to the scattering process, as Arnot (1931) first pointed out. In contrast to atomic potential, spin-orbit interaction is usually very weak, even in electron-heavy atom scattering. However, spin-orbit interaction becomes dominant at a deep minimum of the oscillatory features, at which the effective atomic potential becomes extremely weak. Since spin-orbit interaction is non-uniform over azimuthal angles where the z-axis follows the direction of the incident electrons, it would be expected that some effects concerning electron spin polarization take place at the deep minimum of diffraction patterns.

An ensemble of electrons is referred to as polarized if the electrons are unequally populated with respect to the two spin states. The polarization $P$ of the electron ensemble is defined by $P=(N_{\uparrow}-N_{\downarrow})/(N_{\uparrow}+N_{\downarrow}) = 2\cdot\{(\frac{1}{2})\cdot N_{\uparrow}+(-\frac{1}{2})N_{\downarrow}\}/(N_{\uparrow}+N_{\downarrow})$, twice the expectation value of spin, where $N\uparrow$ and $N\downarrow$ equal the number of electrons with parallel or anti-parallel spin directions respectively in regards to a fixed direction.

### 1-2 Historical Review of Electron-Mercury Scattering

Since the historic experiment of Franck and Hertz (1914), mercury atoms were often used as a scatterer in early stages of scattering experiments because of their moderate vapour pressure and high atomic number (Z=80), which produces high scattering intensity. Quite a few experiments were performed in systems of various types (see Table 1-1). In the next decade, however, few investigations were carried out because the complicated atomic electron configuration makes theoretical application quite difficult. Success of measurement of electron spin polarization (ESP) by

electron-mercury double scattering (Deichsel 1961) revived experiments concerning electron heavy atom scattering (Kessler 1970 and 1976, and Eckstein 1970, another review papers are summarized at the top of the reference section).

It is widely known that the macroscopic magnetic field cannot orderly align the spin direction of free electrons (see Appendix 2). The detectability and producibility of polarized electrons for free states of electrons was first predicted by Mott (1929, 1932) in application of the relativistic electron theory (Dirac 1928) to double scattering, using Coulomb potential. This treatment predicted the finite ESP for high energy electrons $\gtrsim$100 keV scattered at a large angle by a gold atom. This condition corresponds to the condition that the spin-orbit interaction is larger or comparable to the electro-static potential.

In regards to the ESP experiment, since Langstroth's early experiment (1932), the first measurement using electron-gold foil double scattering was performed by Shull et al. (1943), where the measured spin polarization amounts to 12% (polarization) at an electron energy of 340 keV. This is in close agreement to Mott's theoretical prediction (10%).

Later, Bartrett and Welton (1941) and Massey and Mohr (1941) proposed that the screening effect on Coulomb potential by atomic electrons played an important role at electron impact energy of lower than 10 keV, and that a large spin polarization could be expected for gold, even at this energy region. Large polarization occurs because of diffraction effect which is referred to in Sec.1-1 and Appendix 1. Deichsel (1961) first detected spin polarization at these low impact energies for mercury double scattering at incident electron energy from 1 to 2 keV, and the maximum polarization was found to be approx. 40% for 1500 eV at a scattering angle of 90°.

Thereafter, numerous experiments were performed and theoretical calculations made for ESP with various scatterers under various scattering conditions (see Tables 1-1, 1-2 and 6-1 for detailed references). In general, close agreement has been obtained for theory and experiment, particularly in elastic scattering of electron-atom system.

Currently, ESP experiments have extended to surface physics in order to investigate the surface states of solids in detail.

On the other hand, a detailed study of the electron impact spectra for mercury has been made by Skerbele et al.(1969), and Skerbele and Lassettre (1972) for a small scattering angle at hundreds eV electron energies, in order to investigate the usefulness of Born approximation (i.e. the utility of the concept as "generalized oscillator strength").

## 1-3 Bibliographies of the Research of Electron-Mercury Scattering

The bibliographies concerning electron-mercury scattering is summarized in Table 1-1 and Table 1-2 for experiment and theory respectively. ESP experiments concerning electron-atom scattering for atoms other than mercury are also included.

As can be seen in Table 1-1, there is sufficient experimental data for elastic scattering of both the cross section and ESP at various energies and scattering angles. However, few experiments have been performed concerning inelastic scattering, particularly loss spectra at large scattering angles in an intermediate energy region. Experiments for ESP measurements of inelastically scattered electrons are equally scarce.

In regard to theoretical aspects, the case is similar. That is, for elastic scattering, many calculations on both the cross section and ESP have been made, with results comparable to experimental data. In inelastic scattering, however, only calculations for $6^1P$ and $6^3P$ excitation at low impact energies have been made.

Table 1-1. Bibliographies on experiments of electron-mercury scattering and related experiments.

| | | | | |
|---|---|---|---|---|
| Hg | | | | Franck and Hertz(1914) |
| Hg | Forward | 10-17 eV | Loss spectra retarding mesh | Davis and Goucher(1917) |
| Hg | Forward | 4.8-10.4 eV | Loss spectra, retarding mesh | Eldridge(1922) |
| Hg | Forward | threshold-40 eV | $\sigma$, inel, loss spectra | Whitney(1929) |
| Hg | Forward | 4-41 eV | $\sigma$, inel, loss spectra | Foard(1930) |
| Hg | 5-60° | | $\sigma$, el, inel. | Arnot(1930) |
| Hg | 15-125° | 8.6-800 eV | $\sigma$, el. | Arnot(1931) |
| Ar | | | | Bullard and Massey (1931) |
| | | | | Pearson and Arnquist(1931) |
| | 90° | 1,2,10 keV | P | Langstroth(1932) |
| He,Ar,Hg | 20-160° | 23-196 eV | $\sigma$, el, inel. | Mohr and Nicoll(1932) |
| Hg | 50-120° | 80-700 eV | $\sigma$, el, inel. | Tate and Palmer(1932) |
| Hg | Total | 8-200 eV | $\sigma$, el, inel. | Arnot(1935) |
| Au | 90° | 340keV | P, el. | Shull et al.(1943) |
| Au | | 194 keV | Mott Detector | Greenberg et al.(1960) |
| Hg | 60-110° | 1-2 keV | $\sigma$, P, el. | Deichsel(1961) |
| Au | 30-155° | 150-1900 eV | P, el. | Reichert(1963) |
| Hg | 30-150° | 900 eV | P, el. | Deichsel(1964) |
| Hg | 30-150° | 900-1500 eV | P, el. | Deichsel and Reichert (1965) |
| Hg | 30-150° | 300-700 eV | P, el. | Steidl et al.(1965) |
| Hg | 25-150° | 200-4000 eV | $\sigma$, el. | Kessler (1965) |
| He,Ne,Ar, Kr,Xe,Hg | Forward | 20 eV | $\sigma$, resonance scattering | Kuyatt et al.(1965) |
| Hg(solid) | 30-150° | 300 eV | $\sigma$, P, el. | Loth(1966) |

- to be continued -

| | | | | |
|---|---|---|---|---|
| Hg | 30-150° | 3.5, 7, 23, 45 eV | $\sigma$, P | Deichsel et al.(1966) |
| Hg | 30-150° | 180-1700 eV | P, el. | Jost and Kessler (1966) |
| Hg | 30-150° | 100-2000 eV | $\sigma$, P,el. | Eitel(1967) |
| He,Ne,Ar, Kr,Xe | 20-155° | 5-1000 eV | P, el. | Mehr(1967) |
| Hg | 45-135° | 46-204 keV | $\sigma$, el. | Kessler (1968) |
| He,Ne,Ar, Kr,Xe | 30-150° | 40-150 eV | P,el. | Schakert(1968) |
| Hg | | 180-900 eV | P,el. influence of plural scattering | Eitel et al.(1968) |
| Hg | Forward | 50-300 eV | $\sigma$, loss spectra | Skerbele et al.(1969) |
| Hg | 2.5, 20° | 300-500 eV | $\sigma$, el., absolute | Bromberg(1969) |
| Hg | 80-140° | 6.75 eV | P, el. | Wilmers et al.(1969) |
| Hg | 95° | 6.75 eV | P,ESP-detector | Gehenn et al.(1969) |
| Hg | 20-130° | 25,180 eV | $\sigma$, P, $6^1P$ | Eitel and Kessler(1970) |
| Hg | 20-155° | 20-300 eV | $\sigma$, el., $6^1P$ | Gronemeier(1970) |
| Hg | Forward | 300-500 eV | $6^1P$ generalized oscillator strength | Skerbele and Lassettre(1970) |
| $Sb_4$ | 20-150° | 50-1000 eV | P | Kessler et al.(1971) |
| Hg | 20-130° | 25,30,50,180 eV | P, $6^1P$ | Eitel(1971) |
| Hg | Forward | 500 eV | inel., absolute generalized oscillator strength | Skerbele and Lassettre(1972) |
| Hg | 20-150° | 30-300 eV | $\sigma$, P, $6^1P$, $6p'^3P$ | Hanne et al.(1972) |
| Hg | | 90-600 eV | $6^1P$, $6p'^3P$ generalized oscillator strength | |
| Hg | 30-150° | 4-5 eV | $\sigma$, resonance scattering | Duweke et al.(1973) |
| Hg | | | inel. | Bass (1974) |

- to be continued -

| | | | | |
|---|---|---|---|---|
| Hg | | | life time $6^3P$ | King and Adams(1974) |
| Hg | forward | 4-10 eV | exchange excitation of $6^3P$ | Hanne and Kessler(1976) |
| Hg | 30-150° | 4.4-6.1 eV | $\sigma$, P, resonance scattering | Duweke et al.(1976) |
| Hg | | | $\sigma$, electron impact excitation of $6^3P_{0,2}$ | Krause et al.(1977) |
| Xe | 20-155° | 150-1200 eV | P, el. | Kessler et al.(1977) |
| Hg | 50-110° | 300-1000 eV | $\sigma$, loss spectra | Yamazaki et al.(1977) |

Table 1-2. Bibliographies on the theory of electron-mercury scattering and the related theoretical calculations.

| | | | | |
|---|---|---|---|---|
| | | | application of Dirac theory to scattering | Darwin(1928) |
| Hg | Total | 6.7-40 eV | $\sigma$, inel | Penny(1932) |
| Au | 90° | 0.1-150 keV | P,el. screened Coulomb | Massey and Mohr(1941) |
| Hg | | 100,230 keV | $\sigma$,el. Hartree | Bartlett and Welton (1941) |
| Hg | 30-180° | 1.95-121 keV | $\sigma$, P | Mohr(1954) |
| Au | 30-150° | 150MeV | | Yennie et al.(1954) |
| Au,Cd,Hg | 15-165° | 20-650 keV | $\sigma$,P,el. Coulomb pot. | Sherman(1956) |
| Au,Al | 0-180° | 75,121 keV | $\sigma$,P,el. screened Coulomb | Sherman and Nelson(1959) |
| Hg | 0-180° | 1-2 keV | $\sigma$,P,el. rel. Hartree pot. | Bunyan(1963) |
| | | | $\sigma$,P,el. Coulomb pot. | Gluckstern and Lin(1964a) |
| | | | $\sigma$,P,el. Coulomb pot. | Gluckstern and Lin(1964b) |
| Hg,Au,Cu | 10-170° | 50-400 keV | $\sigma$,P,el. screened Coulomb | Lin(1964) |
| Au,Hg | | 0.2-290 keV | $\sigma$,P,el. | Holzwarth and Meister(1964a,b) |
| | | | quadratic correction of the potential | Bühring(1965) |
| | | | power series expansion | Bühring(1965) |
| Hg | 30-150° | 100-2000 eV | rel.Hartree $\sigma$,P,el. | Bunyan (1965) |
| Hg,Au,Bi | | 10-500 eV | $\sigma$,P,el. calculation of Hartree pot. | Schonfelder(1966) |
| | | | rel.effect | Spruch(1966) |
| | | | rel.effect | Rotenberg(1966) |
| | | | rel.effect | Browne and Bauer(1966) |
| Hg,Au,Bi | 30-150° | 10-500 eV | $\sigma$,P,el. | Schonfelder(1967) |

-to be continued-

| | | | | |
|---|---|---|---|---|
| | | | rela. effect | Dawson(1967) |
| Z=1-54 | | 10-100 keV | $\sigma$, el. | Cox(1967) |
| Hg | 0-180° | 7-180 eV | rel.effect $\sigma$,P | Meister(1968) |
| Hg | Total | 6.7-200 eV | $\sigma$,oscillator strength | McConnel and Moiseiwitsch (1968) |
| Hg | 30-150° | 20eV-150 keV | $\sigma$, rel.effect | Yates and Strand(1968) |
| Hg | 45-180° | 46-204 keV | $\sigma$, el. | Bühring(1968) |
| Hg | | 100-2000 eV | P, el.complex scattering amplitude | Bühring(1968) |
| Hg | | | tests of atomic pot. | Yates and Fink(1969) |
| Hg | | 3.5-500 eV | $\sigma$, P,el. influence of rel. and exchange | Walker(1969) |
| Hg,Ar | 0-180° | 3.5-8 eV | $\sigma$,P,el. influence of atomic polarization | Weiss(1969) |
| Hg | | | $\sigma$,el. influence of inelastic channel | Mohr(1969) |
| H,He,C,Ne, Ar,Kr,Rb, Xe,Cs,Au, Hg,Pb,Bi | | 25-800 eV | rel.Hartree-Fock-Slater | Fink and Yates(1970-a) |
| | | 100-1500 eV | | Fink and Yates(1970-b) |
| Hg | | 3.5-100 eV | $\sigma$,P,el. influence of distortion | Walker(1970) |
| Hg | 0-180° | 25-180 eV | $\sigma$,P, $6^1P$ DWB approx. | Madison and Shelton(1973) |
| Li,Na,Mg, P,K,Ca,Ga, Br,Sr,Mo, Rh,Cd,Ba, W,Os | | 25-1500 eV<br>100-1500 eV | rel. Hartree-Fock-Slater pot. | Gregory(1974)<br>(1970) |

-to be continued-

| | | | | |
|---|---|---|---|---|
| Hg | 30-150° | 300-2000 eV | $\sigma$,P.el. optimum condition of ESP detector | Yamazaki et al.(1976) |
| Hg | Forward | | $\sigma_{ex}$, P, $6^3P$ | Hanne(1976) |
| Hg | Forward | 4-12eV | $\sigma$,$6^1P$, Born-Okhur | Moiseiwitsch(1976) |
| Hg | 0-180° | 300-2000 eV | $\sigma$,P non-rel.Hartree | Yamazaki et al.(1977) |
| Hg | 0-180° | 50-500 eV | $\sigma$,P,$6^1P$ DWB | Yamazaki et al.(1977) |

# CHAPTER 2 THEORY OF ELECTRON-MERCURY ELASTIC SCATTERING ----- MODIFICATION AND EXTENTION OF CURRENT THEORY

## 2-1 Introduction

This chapter views elastic scattering theoretically employing partial wave expansion, for which detailed calculation procedures applicable to computer use have been developed by many authors (see Table 1-1). Calculation has been made for energy regions not studied previously using an accurate and fast calculation procedure developed for high speed digital computer (Yamazaki et al. 1976 and 1977). The theories are generally formulated for use in Chapter 3.

### 2-1-1 Necessity of Relativistic Treatment

In theoretical treatment of electron heavy atom scattering, particular points should be noted. First, the system should be treated relativistically even in the non-relativistic energy regions of incident electrons. This may be interpreted qualitatively as follows; The atomic potential attracts electrons and because of a high Z number, is very strong. The electrons passing through near a nucleus may be accelerated to near light velocity, which in turn necessitates relativistic correction of the electron mass as a distance function between the electron and nucleus.

Table 2-1. Comparison of phase shift calculated relativistically and non-relativistically for Hg and Ar (Meister and Weiss 1968).

| | Hg 45 eV | | | | Ar 40 eV | | | |
|---|---|---|---|---|---|---|---|---|
| | relativistic | | nonrelativistic | | relativistic | | nonrelativistic | |
| $l$ | $\delta_l$ | $\delta_{-l-1}$ | $\delta_l$ | $\delta_{-l-1}$ | $\delta_l$ | $\delta_{-l-1}$ | $\delta_l$ | $\delta_{-l-1}$ |
| 0 | −1.304 | | −0.361 | | 0.386 | | 0.402 | |
| 1 | −1.364 | −0.981 | −0.568 | −0.192 | 1.214 | 1.230 | 1.206 | 1.231 |
| 2 | −0.746 | −1.010 | −0.719 | −0.641 | 1.247 | 1.247 | 1.240 | 1.240 |
| 3 | 0.730 | −1.104 | 0.798 | 0.810 | 0.172 | 0.163 | 0.171 | 0.163 |
| 4 | 0.255 | 0.080 | 0.296 | 0.296 | 0.041 | 0.042 | 0.041 | 0.041 |

The differences between relativistic and non-relativistic treatments have been calculated for mercury by Meister and Weiss (1968). The phase shifts and ESP of these results are shown in Table 2-1 and in Fig.2-1. In Table

2-1, we see that the 0-th order relativistic phase shift differs considerably from that of the non-relativistic. This difference lessens for large $l$ because of a small mass correction. Apparent differencies of ESP are recognized in very low energies as well.

The above consideration may also lead to a theoretical explanation of the seemingly contradictory phenomena that the behaviour of apparently relativistic electron (electron energy of up to 100 keV) can be explained by Schrödinger's non-relativistic equation by modifying the electron rest mass by incident electron energy. This treatment is commonly used in high voltage electron microscopy and has explained various phenomena with considerable success(M.von Laue 1948, Fujiwara 1961 and Hashimoto et al. 1964). This is because the electron mass is not greatly affected by the atomic field in high energy regions. That is, the Hamiltonian $H_{rel}$ and $H_{non}$ for relativistic and non-relativistic cases respectively, are written

$$H_{rel} = \sqrt{1 + p^2} + V(r) \tag{2-1}$$

$$H_{non} = p^2/2 + 1 + V(r) \ , \tag{2-2}$$

where the system of units is natural unit (see Sec.2-2). From the uncertainity principle,

$$\Delta p \cdot \Delta r \sim 1 \ . \tag{2-3}$$

In simplification $V(r) = -Ze^2/r$ ,the minimum energy $H^{min}_{rel}$ and $H^{min}_{non}$ is estimated as

$$H^{min}_{rel} = \sqrt{1 - Z^2 e^4} \tag{2-4}$$

$$H^{min}_{non} = 1 - Z^2 e^4/2 \ . \tag{2-5}$$

These values amount to e.g.$H^{min}_{rel}$=2.304 keV and$H^{min}_{non}$=2.299 keV for aluminum, and$H^{min}_{rel}$=30.99 keV and$H^{min}_{non}$=30.05 keV for silver. The$H^{min}$ may be regarded as the maximum modified kinetic energy $\Delta E$ of an electron, due to the atomic field. If one takes into account that the electron microscope uses only forward scattering, i.e., uses mainly electrons scattered distant from the nucleus, it is seen that the above value for $\Delta E$ is overestimated. Thus, it may be concluded that the electron mass modified by the incident electron energy is nearly constant during scattering.

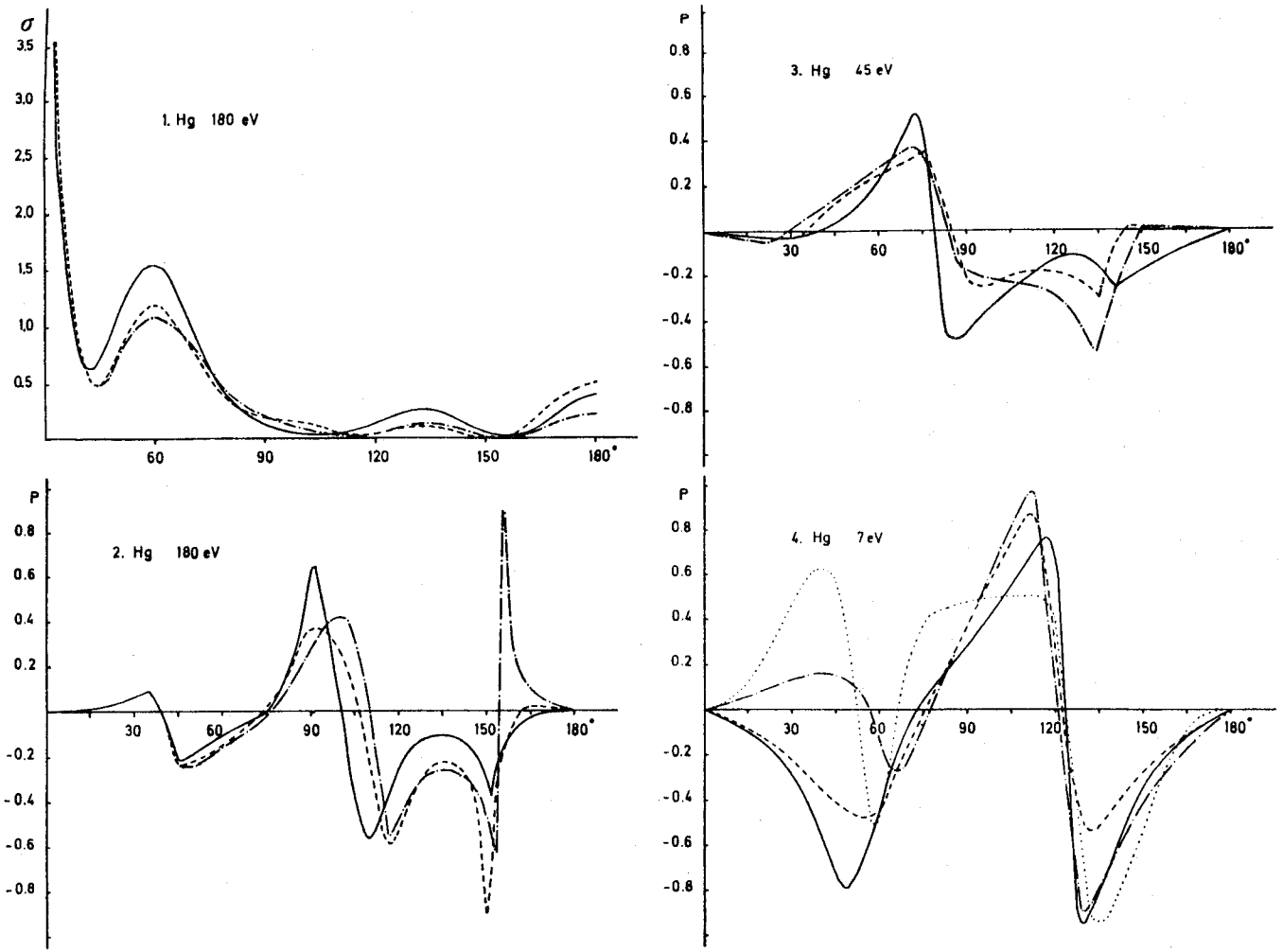


Fig. 2-1. The comparison of the relativistic and non-relativistic calculation of the differential cross section $\sigma$ and spin polarization $P$ (——relativistic and ----- non-relativistic calculation with Mayer's potential, .... relativistic and———non-relativistic calculation with Froese potential)(Meister and Weiss 1968).

It should be noted, however, that because of large mass corrections and effect of spin, large angle scattering for heavy atoms need to be treated with the proper relativistic method in even hundreds keV energy regions(e. g. for mercury $H^{min}_{rel}$=96.11 keV and $H^{min}_{non}$=87.07 keV).

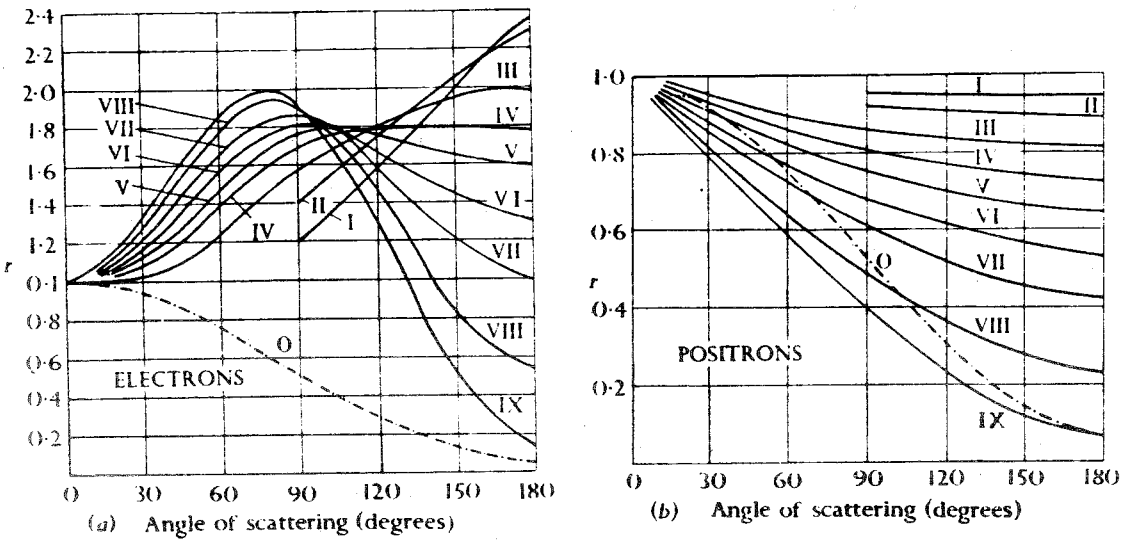


Fig. 2-2. Angular distributions (a) of electrons and (b) of positrons of various energies scattered by mercury nuclei. The scattered intensity is given as the ratio $r$ to that given by the formula

$$\frac{Z^2 e^4}{4 v^4} \cdot \frac{1}{\sin^4(\theta/2)} \cdot (1 - v^2/c^2)$$

Curves I-IX respectively correspond to particles of energies 23, 44, 74, 119, 160, 237, 340, 654, 1712 keV. Curve 0 is that given by the approximation formula (2-27) for an energy of 1712 keV (Mott and Massey 1965).

Fig. 2-2 shows the cross section for electrons and positrons normalized by the ordinary Rutherford scattering cross section. It shows that at high incident energy and large scattering angle the effect of spin becomes important (The effect of spin is discussed in Appendix 3 using Born approximation). For positron, Born-like behaviour appears clearly than for electron, this may be due to the repulsive force between the positron and nucleus (see also Appendix 1).

## 2-1-2 Origin of ESP

The occurrence of ESP(electron spin polarization) is a direct consequence of the interaction of the magnetic moment of electrons and the magnetic field induced by the atomic field. Charged particles travelling in a static-electric field "feel" the magnetic field which is written

$$\mathbf{H} = -\mathbf{v} \times \mathbf{E}, \tag{2-6}$$

where $\mathbf{v}$ the velocity of the charged particles and $\mathbf{E}$ the electric field of the atom. The interaction energy $\varepsilon$ is expressed as

$$\begin{aligned}\varepsilon &= -\mu \cdot \mathbf{H} \\ &= -e \cdot \mathbf{S} \cdot (\mathbf{v} \times \mathbf{H}) \cdot \frac{1}{er} \cdot \frac{dV}{dr} \\ &= \frac{1}{r}\frac{dV}{dr}\,\mathbf{L}\cdot\mathbf{S},\end{aligned} \tag{2-7}$$

where $\mu$ is the magnetic moment of electron, $e$ the charge of electron, $L$ the orbital angular momentum and $S$ the spin angular momentum. This term is called spin-orbit interaction which changes its sign in accordance with the direction of the spin or orbital angular momentum, causing ESP of initially unpolarized scattered electrons or initially polarized electrons to be scattered asymmetrically. On the other hand, we can obtain

$$E\psi = \left(\frac{\mathbf{p}^2}{2} + V(r) - \frac{\pi}{2}\nabla^2 V(r) + \frac{1}{2r}\frac{dV}{dr}\mathbf{L}\cdot\mathbf{S}\right)\psi \ , \tag{2-8}$$

as the non-relativistic approximation of Dirac equation(Foldy et al.1950). The 1st and 2nd terms are that of the ordinary Schrödinger Hamiltonian, and the 3rd term the so-called Darwin term, which originates from the Zitterbewegung. The 4th term is the spin-orbit term in question, which agrees with that of equation (2-7) with the exception of factor 2, which is called Thomas factor(Thomas 1927). Since the electron spin effects Hamiltonian through primarily the spin-orbit term (see equation (2-8)), the above model may provide valuable insight regarding the origin of ESP. In order for a large spin polarization to occur, the atomic potential $V(r)$ needs to be relatively small in comparison to the spin-orbit interaction. Such a condition might be to occur 1) at the minimum points of diffraction pattern of the cross section (This condition requires that incident electron energy should be low enough (e.g. lower than several keV for mercury) in order for diffraction phenomena to occur during scattering. see

Sec.1-1 and Appendix 1 , 2 at large scattering angle in order to make the factor $dV/dr$ in equation (2-8) large because impact parameter becomes small at large scattering angle and 3) for atoms of large Z-number because $1/r \cdot dV/dr$ becomes comparable to or larger than $V$ at the minimum distance between electron and nucleus (see equation (2-9)).

In these energy regions, only the partial waves of lower order contribute to scattering. Therefore, the partial wave expansion method may incur reasonable success for calculation of cross section and spin polarization.

### 2-1-3 Choice of the Atomic Potential

In theoretical treatment of electron-atom scattering, important consideration is the choice of the atomic potential. Due to the complexity of electron configuration, particularly for heavy atoms, several models based on various grades of approximation have been developed (as summarized in Table 2-2).

Table 2-2. Various calculation method of atomic potential.

| | without exchange | with exchange |
|---|---|---|
| statistical model | analytical expression of T-F (Tietz 1962, Byatt 1957) | analytical expression of T-F-D (R.A.Bonham et al.,1963)<br>Atomic energy level by T-F and T-F-D (R.Latter, 1955)<br>Consideration on exchange effect (P.A.M.Dirac 1930) |
| self-consistent model | R-H (J.L.Schonfelder 1966)<br>analytical expression of N-R-H (T.Tietz 1962, Byatt 1957)<br>R-H (S.Cohen 1960, D.F.Mayers 1960) | R-H-F-S (D.Liberman et al. 1965)<br>approximate treatment of exchange effect (V.W.Maslen 1956, J.C.Slater 1951) |

Since the schematic Hamiltonian is represented by equations (2-1) and (2-2), the distance between the (1s) atomic electrons and the nucleus is estimated as;

$$r_{rel}^{min} \sim \sqrt{1/Z^2e^4 - 1} \tag{2-9}$$

$$r_{non}^{min} \sim 1/Ze^2 \quad , \tag{2-10}$$

respectively, based on the uncertainity principle. This means that an incorporation of relativity in the calculation of atomic potentials results in greater screening and reduces both the phase shift and scattering cross section.

The ratio of the binding energy calculated relativistically to that non-relativistically is shown in Table 2-3-a (Boyd et al. 1963). The ratio for inner electrons such as (1s) or (6s) is greater than 1, which means that the attractive force becomes stronger in the relativistic case. On the other hand, the ratio for outer electrons such as (4f) and (5d) is smaller than 1, which means greater screening of the nuclear field in the relativistic case.

Table 2-3-a. Ratio of relativistic to non-relativistic eigenvalues for several electron shells. (Boyd et al. 1963)

| | 1*s* | 4*f* | 5*d* | 6*s* |
|---|---|---|---|---|
| $_{26}$Fe | 1.008 | ... | ... | ... |
| $_{74}$W | 1.09 | 0.81 | 0.84[a] | 1.16 |
| $_{78}$Pt | 1.10 | 0.86 | 0.88 | 1.27 |
| $_{80}$Hg | 1.11 | 0.87 | 0.84 | 1.20 |
| $_{92}$U | 1.15 | 0.91 | 0.95 | 1.34 |

On the other hand, the relativistic treatment of incident electrons increases the phase shift of the lower order according to a similar consideration, i.e. the attractive force in a relativistic treatment is greater than that in non-relativistic treatment.

The incorporation of exchange interaction between atomic electrons lowers the energy of the electron level, increases the screening, and reduces the phase shift (see Sec.2-3). However, the exchange interaction between incident and atomic electrons acts as an attractive force, thus increases the phase shift.

Table 2-3-b. Comparison of phase shift for mercury (Walker 1969) (H, no exchange, Hartree potential; H-F, no exchange, Hartree-Fock potential; Exchange, Hartree-Fock potential with exchange. All phases are modulo $\pi$.).

| Energy (ev) | $l$ | Spin up | | | Spin down | | |
|---|---|---|---|---|---|---|---|
| | | H | H-F | Exchange | H | H-F | Exchange |
| 3·5 | 0 | 0·86 | 0·15 | 1·35 | | | |
| | 1 | 0·30 | 0·01 | 1·00 | 0·50 | 0·12 | 1·32 |
| | 2 | 0·53 | 0·06 | 0·03 | −0·75 | 0·06 | 0·04 |
| | 3 | 0·01 | 0·00 | 0·01 | 0·01 | 0·00 | 0·01 |
| 45 | 0 | −1·09 | −1·44 | −1·01 | | | |
| | 1 | −0·58 | −0·94 | −0·48 | −0·28 | −0·65 | −0·20 |
| | 2 | −0·67 | −1·18 | −0·51 | −0·59 | −1·09 | −0·44 |
| | 3 | 0·92 | 0·51 | 1·07 | 0·93 | 0·52 | 1·07 |
| | 4 | 0·30 | 0·18 | 0·26 | 0·30 | 0·18 | 0·26 |
| | 5 | 0·12 | 0·07 | 0·09 | 0·12 | 0·07 | 0·09 |
| | 6 | 0·05 | 0·03 | 0·04 | 0·05 | 0·03 | 0·04 |
| | 7 | 0·02 | 0·01 | 0·01 | 0·02 | 0·01 | 0·01 |
| 300 | 0 | −0·24 | −0·46 | −0·26 | | | |
| | 1 | 0·60 | 0·37 | 0·58 | 0·90 | 0·67 | 0·88 |
| | 2 | 1·26 | 1·00 | 1·23 | 1·34 | 1·07 | 1·30 |
| | 3 | 1·56 | 1·23 | 1·49 | −1·56 | 1·26 | 1·51 |
| | 4 | −1·21 | −1·52 | −1·36 | −1·21 | −1·52 | −1·35 |
| | 5 | 0·99 | 0·79 | 0·84 | 1·00 | 0·79 | 0·83 |
| | 6 | 0·60 | 0·45 | 0·48 | 0·60 | 0·45 | 0·47 |
| | 7 | 0·39 | 0·28 | 0·30 | 0·39 | 0·28 | 0·29 |
| | 8 | 0·26 | 0·19 | 0·19 | 0·26 | 0·19 | 0·19 |
| | 9 | 0·18 | 0·12 | 0·12 | 0·18 | 0·12 | 0·12 |

Moreover, the electric field of the incident electron may distort the atomic potential, which in turn causes a long range attractive force for the incident electron. The calculated phase shifts for the various approximations are shown in Table 2-3-b which confirm the qualitative interpretation given above. That is, for lower order phase shifts ($l < 3$), the Hartree potential without exchange and Hartree-Fock potential with exchange comply well because of opposite effects in the two exchange interactions. For a higher order of phase shift ($l > 7$), Hartree-Fock potential without exchange and Hartree-Fock potential with exchange agree satisfactory. This occurs because the largest principal quantum number of

mercury is 6, and partial wave from $l > 6$ have little exchange interaction with atomic electrons. The difference between the Hartree potential without exchange and the Hartree-Fock potential with exchange for a higher order of partial waves is not negligible but is small and affects only at forward scattering. Therefore, the former model with relativistic treatment, despite its simplicity, is considered to give accurate results. Atomic distortion is not thought to notably affect the electron-mercury scattering at intermediate energies (Walker 1970),* thus is not considered in the present study.

Among various available expressions of atomic potentials, an analytical expression is most convenient for the present calculations. We have therefore used the non-relativistic Hartree potential, analytically expressed by Byatt(1956). The present calculation agree well with those obtained using Mayer's relativistic potential(1957, see Sec.2-4)**

---

* A recent report on $e$-Xe elastic scattering (Kessler 1970) implies that exchange scattering has relevance until 700 eV, and atomic distortion should be taken into account using the polarized orbital methods at 150 eV.

** The effects of and the relation between relativistic and non-relativistic equation, and relativistic and non-relativistic atomic potential are discussed by several authors (Spruch 1966, Rotenberg 1966, Browne 1966 and Meister and Weiss 1968). It was concluded as a vital point that one should perform relativistic and non-relativistic calculation using relativistic and non-relativistic potentials, respectively (Walker 1971). However, as is shown in Sec.2-5, the combination of relativistic treatment and non-relativistic potential gives good results in the energy region under consideration here.

## 2-2 Born Approximation

### 2-2-1 Integral Expression of Dirac Equation

The Dirac equation in common expression is written as

$$W\psi = -(\mathbf{a}\mathbf{p} + \beta + V)\psi \quad , \tag{2-11}$$

where

$$\mathbf{a} = \begin{pmatrix} 0 & \sigma \\ \sigma & 0 \end{pmatrix} \tag{2-12}$$

$$\beta = \begin{pmatrix} 1 & 0 \\ 0 & 1 \end{pmatrix} \quad , \tag{2-13}$$

$\sigma$ the Pauli matrix,* $W$ the total energy, $\mathbf{p}$ the momentum, $V$ the atomic potential energy and $\psi$ the four component spinor. The system of units is so-called natural unit, in which $c=m=\hbar=1$, where c is the light velocity, m the electron rest mass and $\hbar$ the Planck's constant devided by $2\pi$.
The unit of various quantity is tabulated in Table 2-4.

Table 2-4. Unit of various quantities in natural unit.

| | unit | value |
|---|---|---|
| energy | $mc^2$ | $8.1 \times 10^{-14}$ joul. |
| length | $\hbar/mc$ | $4.0 \times 10^{-13}$ m |
| charge | $\hbar c/m$ | $1.8 \times 10^{-18}$ coul. |
| time | $\hbar/mc^2$ | $1.2 \times 10^{-21}$ sec. |

---

* $\sigma_x = \begin{pmatrix} 0 & 1 \\ 1 & 0 \end{pmatrix}$ $\sigma_y = \begin{pmatrix} 0 & i \\ i & 0 \end{pmatrix}$ $\sigma_z = \begin{pmatrix} 1 & 0 \\ 0 & -1 \end{pmatrix}$

The formal solution of the wave equation $H\psi_j = W_j \psi_j$ is written either explicitly as

$$\psi_j^{(\pm)} = \Phi_j + \frac{1}{W_j - H \pm i\varepsilon} V\Phi_j \quad , \tag{2-14}$$

or implicitly as

$$\psi_j^{(\pm)} = \Phi_j + \frac{1}{W_j - K \pm i\varepsilon} V\psi_j^{(\pm)} \tag{2-15}$$

$$K = H - V \quad , \tag{2-16}$$

$K$ is not necessarily kinetic energy and $\Phi_j$ satisfies $K\Phi_j = W_j \Phi_j$. The sign + or - represents the asymptotic conditions which correspond to outgoing or incoming scattered states, respectively. Equation (2-15) is called the Lippmann-Schwinger equation (Lippmann and Schwinger 1950 and Gell-Mann and Goldberger 1953).

The equation (2-15) can be rewritten as follows; The operator $1/(W-K\pm i\varepsilon)$ is defined as

$$(W-K\pm i\varepsilon)\cdot 1/(W-K\pm i\varepsilon) = 1 \, , \tag{2-17-a}$$

$$1/(W-K\pm i\varepsilon)\cdot(W-K\pm i\varepsilon) = 1 \, , \tag{2-17-b}$$

and

$$W-K\pm i\varepsilon = W + (\mathbf{a}\mathbf{p}+\beta) + i\varepsilon$$

$$= \begin{pmatrix} W+1\pm i\varepsilon & \sigma\cdot\mathbf{p} \\ \sigma\cdot\mathbf{p} & W-1\pm i\varepsilon \end{pmatrix} , \tag{2-18}$$

so

$$1/(W-K\pm i\varepsilon) = 1/((W\pm i\varepsilon)^2 - \mathbf{p}^2 - 1)\begin{pmatrix} W-1\pm i\varepsilon & -\sigma\cdot\mathbf{p} \\ -\sigma\cdot\mathbf{p} & W+1\pm i\varepsilon \end{pmatrix}$$

$$= (W-\mathbf{a}\mathbf{p}-\beta)/((W\pm i\varepsilon)^2 - \mathbf{p}^2 - 1) \, , \tag{2-19}$$

which can be easily proven by direct substitution. Equation (2-15) results in

$$\psi_j^{(\pm)} = \Phi_j + \frac{W-\mathbf{a}\mathbf{p}-\beta}{(W\pm i\varepsilon)^2 - \mathbf{p}^2 - 1} V\psi_j^{(\pm)} \, . \tag{2-20}$$

Using the relation,

$$\int\int e^{-i\mathbf{k}\cdot(\mathbf{r}-\mathbf{r}')}\,d\mathbf{k}\,d\mathbf{r}' = (2\pi)^3\int\delta(\mathbf{r}-\mathbf{r}')\,d\mathbf{r}' = (2\pi)^3, \tag{2-21}$$

the second term of the right hand side of equation (2-20) can be transformed as

$$\begin{aligned}
&(W-\boldsymbol{\alpha}\mathbf{p}-\beta)/((W\pm i\varepsilon)^2-\mathbf{p}^2-1)\,V(\mathbf{r})\,\psi_j^{(\pm)}(\mathbf{r})\\
&=(W-\boldsymbol{\alpha}\mathbf{p}-\beta)/((W\pm i\varepsilon)^2-\mathbf{p}^2-1)\int\delta(\mathbf{r}-\mathbf{r}')\,d\mathbf{r}'\,V(\mathbf{r})\,\psi_j^{(\pm)}(\mathbf{r})\\
&=\frac{1}{(2\pi)^3}\iint\frac{W-\boldsymbol{\alpha}\mathbf{p}-\beta}{(W\pm i\varepsilon)^2-\mathbf{p}^2-1}\,e^{i\mathbf{k}(\mathbf{r}-\mathbf{r}')}\,V(\mathbf{r}')\,\psi_j^{(\pm)}(\mathbf{r}')\,d\mathbf{k}\,d\mathbf{r}'\\
&=\frac{1}{(2\pi)^3}\iint\frac{W-\boldsymbol{\alpha}\mathbf{p}-\beta}{(W\pm i\varepsilon)^2-K^2-1}\,e^{i\mathbf{k}(\mathbf{r}-\mathbf{r}')}\,V(\mathbf{r}')\,\psi_j^{(\pm)}(\mathbf{r}')\,d\mathbf{k}\,d\mathbf{r}',
\end{aligned} \tag{2-22}$$

where $K=|\mathbf{k}|$.

Using the residue theorem, the integrations of the variable $\mathbf{k}$ can be performed and gives

$$\frac{1}{(2\pi)^3}\int\frac{e^{i\mathbf{k}(\mathbf{r}-\mathbf{r}')}}{(W\pm i\varepsilon)^2-K^2-1}\,d\mathbf{k} = -\frac{1}{4\pi}\frac{e^{\pm i\sqrt{W^2-1}\,|\mathbf{r}-\mathbf{r}'|}}{|\mathbf{r}-\mathbf{r}'|}\,. \tag{2-23}$$

Equation (2-20) results in

$$\begin{aligned}
\psi_j^{(\pm)}(\mathbf{r}) &= \Phi_j - \frac{1}{4\pi}\int(W-\boldsymbol{\alpha}\mathbf{p}-\beta)\frac{e^{\pm iK|\mathbf{r}-\mathbf{r}'|}}{|\mathbf{r}-\mathbf{r}'|}\,V(\mathbf{r}')\,\psi_j^{(\pm)}(\mathbf{r}')\,d\mathbf{r}'\\
&\sim\Phi_j - \frac{1}{4\pi}\int(W-\boldsymbol{\alpha}\mathbf{p}-\beta)\frac{e^{\pm iK(r-(\mathbf{r}\cdot\mathbf{r}')/r)}}{r}\,V(\mathbf{r}')\,\psi_j^{(\pm)}(\mathbf{r}')\,d\mathbf{r}'\\
&=\Phi_j - \frac{1}{4\pi}\frac{e^{\pm iKr}}{r}(W-\boldsymbol{\alpha}\mathbf{k}_f-\beta)\int e^{\mp i\mathbf{k}_f\mathbf{r}'}\,V(\mathbf{r}')\,\psi_j^{(\pm)}(\mathbf{r}')\,d\mathbf{r}'
\end{aligned} \tag{2-24}$$

where $K=\sqrt{W^2-1}$, $\mathbf{k}_f=K\cdot\mathbf{r}/r$ and $r=|\mathbf{r}|$. The final expression of equation (2-24) is obtained assuming the usual scattering condition $|\mathbf{r}|\gg|\mathbf{r}'|$ (see Fig.2-3).

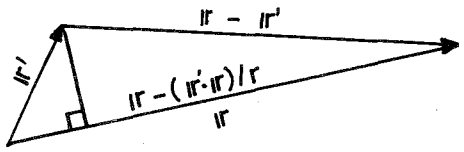


Fig. 2-3. Relation of $\mathbf{r}$ and $\mathbf{r}'$.

Equation (2-24) is the integral form of the relativistic Dirac equation (2-11). From equation (2-24), the scattering amplitude for the usual outgoing wave boundary condition is written

$$f(\theta) = -\frac{1}{4\pi}(W-\boldsymbol{\alpha}\mathbf{k}_f-\beta)\int e^{-i\mathbf{k}_f\cdot\mathbf{r}'}\,V(\mathbf{r}')\,\psi_j^{(+)}(\mathbf{r}')\,d\mathbf{r}'. \tag{2-25}$$

Note that equation (2-25) represents the exact scattering amplitude for Dirac electrons.

## 2-2-2 Born Approximation

In order to obtain an approximation of the scattering amplitude, the $\psi_j^{(+)}$ appearing in the right hand side of equation (2-25) is replaced by $\Phi_j$. This approximation is called the first Born approximation

$$f_{Born}(\theta) = -\frac{1}{4\pi}(W-\mathbf{a}\mathbf{k}_f-\beta)\int e^{-i\mathbf{k}_f\cdot\mathbf{r}'} V(\mathbf{r}')\,\Phi_j(\mathbf{r}')\,d\mathbf{r}'. \qquad (2\text{-}26)$$

For Coulomb potential $-Ze^2/r$, equation (2-26) produces the ordinary Rutherford formula with correction factors (see Appendix 3).

$$(d\sigma/d\Omega)_{Born} = \frac{Z^2e^4}{4v^4\sin^4(\theta/2)}\cdot(1-v^2\cdot\sin^2(\theta/2))\cdot(1-v^2) \qquad (2\text{-}27)$$

The first factor of equation (2-27) is that of the classical Rutherford formula, the second is that originating from the spin of electrons (see Appendix 3) and the third is the mass correction term.
It is of note that the scattering amplitude of first Born approximation gives zero spin polarization as is also shown in Appendix 3. Thus, a calculation on spin polarization of high energy electrons is often performed using second Born approximation (Walker 1971).

## 2-3. Partial Wave Expansion

For a central field of force we may separate equation (2-11) by polar coordinates. Substitution of $\psi = \begin{pmatrix} -ifX_{-\kappa\mu} \\ gX_{\kappa\mu} \end{pmatrix}$ gives (Rose 1957)

$$\left\{\begin{array}{l} -iX_{-\kappa,\mu}\left[(W-V+1)f-dg/dr-(\kappa+1)\cdot g/r\right] \\ X_{\kappa,\mu}\left[(W-V-1)g+df/dr-(\kappa-1)f/r\right] \end{array}\right\} = 0, \qquad (2\text{-}28)$$

where $f$ and $g$ are radial wave function and

$$X_{\kappa,\mu} = \sum_m C(l,\tfrac{1}{2},j;m,\mu-m)Y_{lm}\,\psi_{\frac{1}{2},\mu-m}, \qquad (2\text{-}29)$$

with

$$\mu-m = \pm\tfrac{1}{2} \qquad (2\text{-}30\text{-a})$$

$$j = |\kappa| - \tfrac{1}{2} \qquad (2\text{-}30\text{-b})$$

$$l = \begin{cases} \kappa & \kappa > 0 \quad \text{(2-30-c)} \\ -\kappa - 1 & \kappa < 0 \ , \quad \text{(2-30-d)} \end{cases}$$

$C(l, \frac{1}{2}, j; m, \mu - m)$ is the Clebsch-Gordan coefficient, the detailed form of which is shown in Table 2-5, where $Y_{lm}$ is the spherical harmonics and $\psi_{\frac{1}{2}, \mu - m}$ the spin function. As the asymptotic forms of these four components are related with one another, it suffices to treat only the lower part of equation (2-28) (Mott and Massey 1965). Hereafter this two component spinor is referred to as $\psi$ unless otherwise noted.

Table 2-5 . Clebsch-Gordan coefficients $C(j_1, 1/2, j; m-m_2, m_2)$ .

| j= | $m_2=1/2$ | $m_2=-1/2$ |
|---|---|---|
| $j_1+1/2$ | $[(j_1+m+1/2)/(2j_1+1)]^{1/2}$ | $[(j_1-m+1/2)/(2j_1+1)]^{1/2}$ |
| $j_1-1/2$ | $-[(j_1-m+1/2)/(2j_1+1)]^{1/2}$ | $[(j_1+m+1/2)/(2j_1+1)]^{1/2}$ |

Thus, the general solution of equation (2-28) in the polar coordinate system is expressed as

$$\begin{aligned} \psi &= \sum_{\kappa\mu} a_{\kappa\mu} \, g_\kappa \, X_{\kappa\mu} \\ &= \Bigg( \sum_{l=1}^{\infty} \sum_{\mu} a_{l\mu} g_l \, C(l, \tfrac{1}{2}, l-\tfrac{1}{2}; \mu-\tfrac{1}{2}, \tfrac{1}{2}) \, Y_{l, \mu-\frac{1}{2}} + \\ &\quad \sum_{l=1}^{\infty} \sum_{\mu} a_{l\mu} g_l \, C(l, \tfrac{1}{2}, l-\tfrac{1}{2}; \mu+\tfrac{1}{2}, -\tfrac{1}{2}) \, Y_{l, \mu+\frac{1}{2}} + \\ &\quad \sum_{l=0}^{\infty} \sum_{\mu} a_{-l-1, \mu} g_{-l-1} \, C(l, \tfrac{1}{2}, l+\tfrac{1}{2}; \mu-\tfrac{1}{2}, \tfrac{1}{2}) \, Y_{l, \mu-\frac{1}{2}} \\ &\quad \sum_{l=0}^{\infty} \sum_{\mu} a_{-l-1, \mu} g_{-l-1} \, C(l, \tfrac{1}{2}, l+\tfrac{1}{2}; \mu+\tfrac{1}{2}, -\tfrac{1}{2}) \, Y_{l, \mu+\frac{1}{2}} \Bigg) . \end{aligned} \quad \text{(2-31)}$$

From equation (2-28), the radial equation with respect to $g$ can be easily derived as

$$\frac{d^2 g_\kappa}{dr^2} + \left( \frac{2}{r} - \frac{a'}{a} \right) \frac{dg_\kappa}{dr} + \left\{ ab - \frac{\kappa(\kappa+1)}{r^2} + \frac{\kappa}{r} \frac{a'}{a} \right\} g_\kappa = 0 , \quad \text{(2-32)}$$

where $a = W - V + 1$ , $b = W - V - 1$ and $a' = da/dr$. For $r \to \infty$, equation (2-32) reduces to

$$\frac{d^2 g_\kappa}{dr^2} + \frac{2}{r} \frac{dg_\kappa}{dr} + \left( K^2 - \frac{l(l+1)}{r^2} \right) g_\kappa = 0 , \quad \text{(2-33)}$$

where $K^2 = W^2 - 1$. Since this differential equation is that of spherical Bessel function, the solution may be represented as follows;

$$g_\kappa \underset{r\to\infty}{\sim} j_l(Kr)\cdot\cos(\delta_\kappa) - n_l(Kr)\cdot\sin(\delta_\kappa)$$
$$\sim (Kr)^{-1}\sin(Kr - \pi/2\cdot l + \delta_\kappa), \tag{2-34}$$

where $j_l$ and $n_l$ are spherical Bessel and spherical Neumann function respectively and $\delta_\kappa$ is called the phase shift.
Corresponding to the two initial spin states with respect to z-axis, the scattering states are written

$$\psi \sim \begin{pmatrix} e^{i\mathbf{k}\cdot\mathbf{r}} + f_\uparrow(\theta',\phi')\, e^{iKr}/r \\ g_\uparrow(\theta',\phi')\, e^{iKr}/r \end{pmatrix}, \tag{2-35}$$

and

$$\psi \sim \begin{pmatrix} g_\downarrow(\theta',\phi')\, e^{iKr}/r \\ e^{i\mathbf{k}\mathbf{r}} + f_\downarrow(\theta',\phi')\, e^{iKr}/r \end{pmatrix}, \tag{2-36}$$

where $f$ and $g$ are called direct and spin-flip scattering amplitude, respectively. From the comparison between equation (2-31) and equation (2-35), $a_{\kappa,\mu}$ is fully determined as

$$a_{l,\mu} = -4\pi(l-\mu+1/2)^{1/2}(2l+1)^{-1/2} e^{i(\delta_l + \pi/2\cdot l)} Y^*_{l,\mu-1/2}(\theta,\phi) \tag{2-37-a}$$

$$a_{-l-1,\mu} = 4\pi(l+\mu+1/2)^{1/2}(2l+1)^{-1/2} e^{i(\delta_{-l-1} + \pi/2\, l)} Y^*_{l,\mu-1/2}(\theta,\phi), \tag{2-37-b}$$

for spin-up initial state, and from equations (2-31) and (2-36)

$$a_{l,\mu} = 4\pi(l+\mu+1/2)^{1/2}(2l+1)^{-1/2} e^{i(\delta_l + \pi/2\cdot l)} Y^*_{l,\mu+1/2}(\theta,\phi) \tag{2-38-a}$$

$$a_{-l-1,\mu} = 4\pi(l-\mu+1/2)^{1/2}(2l+1)^{-1/2} e^{i(\delta_{-l-1} + \pi/2\cdot l)} Y^*_{l,\mu+1/2}(\theta,\phi), \tag{2-38-b}$$

for spin-down initial state, taking into account the Rayleigh's formula,

$$e^{i\mathbf{k}\mathbf{r}} = \sum_{l=0}(2l+1)\, i^l\, j_l(Kr)\, P_l(\cos\gamma)$$
$$= 4\pi\sum_{l=0}^{\infty}\Big(\sum_m i^l\, j_l(Kr)\, Y^*_{lm}(\theta',\phi')\, Y_{lm}(\theta,\phi)\Big), \tag{2-39}$$

where $\mathbf{r}=(r,\theta',\phi')$, $K=(K,\theta,\phi)$ and $\mathbf{kr}=Kr\cos\gamma$.
Using equations (2-31) and (2-37) and setting $\theta=\phi=o$(incident along the z-axis), we can express the scattering amplitude as

$$f(\theta)=f_{\uparrow}=f_{\downarrow}=\frac{(4\pi)^{1/2}}{2iK}\sum_{l=0}^{\infty}(2l+1)^{-1/2}\{(l+1)(e^{2i\delta_{-l-1}}-1)+l(e^{2i\delta_{l}}-1)\}Y_{l0}(\theta',\phi') \tag{2-40-a}$$

$$g(\theta)=g_{\uparrow}e^{-i\phi'}=-g_{\downarrow}e^{i\phi'}=\frac{(4\pi)^{1/2}}{2iK}\sum_{l=1}^{\infty}(2l+1)^{-1/2}(l+1)^{1/2}.l^{1/2}(e^{2i\delta_{-l-1}}-e^{2i\delta_{l}})Y_{l1}(\theta',\phi'). \tag{2-40-b}$$

For further derivation let us start at the initial conditions

$$\psi=\begin{pmatrix} A\,e^{iKz} \\ B\,e^{iKz}\end{pmatrix}\quad, \tag{2-41}$$

which have the initial polarization,

$$\mathbf{P}=<\sigma>=<(A^{*}B+B^{*}A\,,\ i\,(B^{*}A-A^{*}B)\ ,\ |A|^{2}-|B|^{2})>\ , \tag{2-42}$$

under the normalization condition $|A|^{2}+|B|^{2}=1$. Here, the polarization of an electron beam is defined by statistical averaging as equation (2-42). Then, using the Sherman function $S$ defined by

$$S=i\,(fg^{*}-f^{*}g)\,/\,(|f|^{2}+|g|^{2})\ , \tag{2-43}$$

and the scattering cross-section for unpolarized electrons

$$\sigma_{0}(\theta)=|f|^{2}+|g|^{2} \tag{2-44}$$

we obtain the scattering cross section with initial polarization $\mathbf{P}$ as,

$$\begin{aligned}\sigma(\theta,\phi)&=<|Af_{\uparrow}+Bg_{\downarrow}|^{2}+|Ag_{\uparrow}+Bf_{\downarrow}|^{2}>\\&=\sigma_{0}(\theta)\quad(1+S\,\mathbf{nP})\quad,\end{aligned} \tag{2-45}$$

where

$$\mathbf{n}=(-\sin\phi,\cos\phi,0)\quad, \tag{2-46}$$

$\mathbf{n}\,S$ is a polarization vector of scattered electrons with an initially unpolarized electron beam. As the polarization $\mathbf{P}_{S}$ of scattered electrons

is derived from equation (2-42), substituting $Af_{\uparrow}+Bg_{\downarrow}$ for $A$ and $Ag_{\uparrow}+Bf_{\downarrow}$ for $B$, one obtains

$$P_S^x = \{P_z \cdot U \cdot \sin\phi - S \cdot \sin\phi + P_x - (1-T/\sigma)\cos\phi (P_x \cos\phi + P_y \sin\phi)\} / (1+S \cdot \mathbf{n} \cdot \mathbf{P}) \quad (2\text{-}47\text{-a})$$

$$P_S^y = \{P_z \cdot U \cdot \sin\phi + S \cdot \cos\phi + T \cdot P_y - (1-T/\sigma)\cos\phi \cdot (P_x \cdot \sin\phi - P_y \cdot \cos\phi)\} / (1+S \cdot \mathbf{n} \cdot \mathbf{P}) \quad (2\text{-}47\text{-b})$$

$$P_S^z = \{P_z \cdot T - U (P_x \cdot \cos\phi - P_y \sin\phi)\} / (1+S \cdot \mathbf{n} \cdot \mathbf{P}) , \quad (2\text{-}47\text{-c})$$

where $U = 2Re(fg^*)/\sigma$ and $T = (|f|^2 - |g|^2)/\sigma$. Equation (2-47) can be rewritten in simple form as,

$$\mathbf{P}_S = \frac{[\mathbf{P} \cdot \mathbf{n} + S] \cdot \mathbf{n} + T \cdot \mathbf{n} \times [\mathbf{P} \times \mathbf{n}] + U \cdot [\mathbf{n} \times \mathbf{P}]}{1 + S \cdot \mathbf{n} \cdot \mathbf{P}} . \quad (2\text{-}48)$$

From equation (2-48) we see that the polarization of incident electrons are affected as follows; the vector $S\,\mathbf{n}$ is added to the components $[\mathbf{P} \cdot \mathbf{n}] \cdot \mathbf{n}$ perpendicular to the scattering plane, i.e., perpendicular to the wave number vectors of both the incident and scattered states. The component parallel to the scattering plane is reduced by the factor $T$ ( $|T| < 1$ ). The polarization vector is rotated out of its original plane defined by $\mathbf{n}$ and $\mathbf{P}$ because of an additional component determined by $U$ (Kessler 1976). Thus this leads to the polarization of the scattered electrons for the initially unpolarized electrons as

$$\mathbf{P}_S = S\ (-\sin\phi, \cos\phi, 0) . \quad (2\text{-}49)$$

Equations (2-45) and (2-49) suggest that Sherman function $S$ has two roles, i.e. giving scattering asymmetry for initially polarized electrons and polarization of scattered electrons for initially unpolarized ones (for the qualitative explanation see Appendix 4). Equation (2-49) also shows that the direction of the ESP of the scattered electrons is perpendicular to the scattering plane.

## 2-4. Adopted Numerical Calculation Procedure

Hence the scattering amplitudes are expressed as a function of the phase shifts $\delta_l$ and $\delta_{-l-1}$ (see equation (2-40)), it is necessary to determine phase shift by clarifying the relationship with the radial wave function. Various calculation procedures have been developed for the estimation of phase shifts. Present calculation adopts one of the most advantageous procedure which were developed for accurate and fast computer calculation combining various calculation procedures (Yamazaki et al. 1976,1977). Some of them except for that shown below are summarized and compared with each other in Appendix 5.

Introducing the change of variables (Bunyan and Schonfelder, 1965),

$$F_\kappa = A_\kappa(r) \sin\phi_\kappa(r)/r \tag{2-50-a}$$

$$G_\kappa = A_\kappa(r) \cos\phi_\kappa(r)/r \tag{2-50-b}$$

we get,

$$d\phi_\kappa/dr = \kappa/r \sin 2\phi_\kappa + (W-V) - \cos 2\phi_\kappa \tag{2-51-a}$$

$$d(\ln A_\kappa)/dr = -\kappa/r \cos 2\phi_\kappa - \sin 2\phi_\kappa . \tag{2-51-b}$$

From equations (2-34) and (2-51-a) and their derivatives we obtain the expression for the phase shift

$$\tan\delta_\kappa = \frac{K \cdot j_{l+1}(Kr) - j_l(Kr)\left\{(W+1)\tan\phi_\kappa + (1+l+\kappa)/r\right\}}{Kn_{l+1}(Kr) - n_l(Kr)\left\{(W+1)\tan\phi_\kappa + (1+l+\kappa)/r\right\}} . \tag{2-52}$$

The expression on the right is evaluated at $r=a$ where $a$ satisfies $V(a) \sim 0$.

Equation (2-52) allows us to evaluate $\delta_\kappa$ using only the first order nonlinear differential equation (2-51-a), which simplifies the computer calculation procedure considerably.

As the numerical integration of differential equation (2-51-a) cannot be made from $r=0$ because of the divergence of the potential energy $V(r)$, we expand $V(r)$ and $\phi_\kappa(r)$ in a power series in order to derive initial conditions at small $r$ (Bunyan and Schonfelder 1965) as,

$$V(r) = -1/r\,(Z_0 + Z_1 r + Z_2 r^2 + Z_3 r^3) \tag{2-53}$$

$$\phi_\kappa(r) = \phi_0 + \phi_1 r + \phi_2 r^2 + \cdots \tag{2-54-a}$$

$$\ln(A_\kappa(r)) = B_0 + B_l \ln(r) + B_1 r + B_2 r^2 + \cdots \quad (2\text{-}54\text{-}b)$$

Substituting equations (2-53) and (2-54-a) into equation (2-51-a) we obtain the following equations;

$$\sin(2\phi_0) = -Z_0/\kappa \quad (2\text{-}55\text{-}a)$$

$$\phi_1 = (W + Z_1 \cos(2\phi_0))/(1 - 2\kappa\cos(2\phi_0)) \quad (2\text{-}55\text{-}b)$$

$$\phi_2 = (2\phi_1 \sin(2\phi_0)\ (1-\kappa\phi_1) + Z_2)/(2 - 2\kappa\cos(2\phi_0)) \quad (2\text{-}55\text{-}c)$$

$$\phi_3 = (2\phi_2 \sin(2\phi_0)\cdot(1-2\kappa\phi_1) + 2\phi_1^2\cos(2\phi_0)\cdot (1-2/3\,\kappa\phi_1 + Z_3))/(3 - 2\kappa\cos(2\phi_0)) \quad (2\text{-}55\text{-}d)$$

$$\phi_4 = \left[((2\phi_3 - (2\phi_1)^3/3!) - \kappa(4\phi_1\phi_3 + 2\phi_2^2 - (2\phi_1)^4/4!)) \times \sin(2\phi_0) + (1-\kappa\phi_1)4\phi_1\phi_2\cos(2\phi_0)\right]/2(2 - \kappa\cos(2\phi_0)) \quad (2\text{-}55\text{-}e)$$

$$B_l = -\kappa\cos(2\phi_0) \quad (2\text{-}56)$$

In order to keep the wave function finite at $r=0$ i.e., to maintain the positive $B_l$ in equation (2-56), we choose

$$0 \leq 2\phi_0 \leq \pi/2 \qquad \kappa < 0 \quad (2\text{-}57\text{-}a)$$

$$\pi \leq 2\phi_0 \leq 3/2 \cdot \pi \qquad \kappa \geq 0 \quad (2\text{-}57\text{-}b)$$

Integrations were carried out from $r=0.1$ by the fourth order Lunge-Kutta process which has sufficient accuracy for the present calculations. In the region $0.1 \leq r \leq 15$, to avoid the use of excessively small intervals in $r$ when performing the integration, a change of variables $r = 0.1e^t$ is introduced. The equation (2-51-a) is then rewritten as

$$d\phi_\kappa/dt = \kappa \sin(2\phi_\kappa) + 0.1e^t (W - V - \cos(2\phi_\kappa)) \quad (2\text{-}58)$$

Thereafter the ordinary equation (2-51-a) was employed for integration up

to $r=300$. We stopped the integration at $r=518$ ($=2\mathring{A}$) to reduce computing time. To make this process more appropriate, the charge distribution was reconstructed in the region $300 \leq r \leq 518$ as a quadratic form, the coefficients of which are determined so as to make the total charge equal to $Ze$, where $Z$ is the atomic number of mercury, and the charge density and its derivative continuous at $r=300$ to avoid anormalous $\delta$-function type charge distribution (Bühring 1965).

A charge reconstruction of this type may have some influence on forward scattering but may have little influence on backward scattering, since in the latter, electron is scattered by the not reconstructed potential because of small impact parameter.

According to the consideration given in Sec.2-1-3, a non-relativistic Hartree potential analytically expressed by Byatt (1957) is adopted, which is written as

$$V(r) = -Ze^2/r \cdot \sum_{i=1}^{3} a_i e^{-b_i r} , \tag{2-59}$$

where $a_i = 0.19,\ 0.56,\ 0.25$, $b_i = 9.133\times10^{-3},\ 2.768\times10^{-2},\ 1.123\times10^{-1}$, respectively. All phase shift was evaluated from $l=0$ to $|\delta_l|<10^{-5}$.

To evaluate scattering cross section and Sherman function, it may be advantageous to use the functions $E(\theta)$ and $H(\theta)$ instead of the scattering amplitudes $f(\theta)$ and $g(\theta)$ which are defined in equation (2-40) (Bühring 1968).

$$4iH(\theta) = \sum_{l=1} \left(e^{2i\delta_{l-1}} - e^{2i\delta_l}\right) L_l^- \tag{2-60-a}$$

$$4iE(\theta) = \sum_{l=1} \left(e^{2i\delta_l} + e^{2i\delta_{l-1}} - 2\right) L_l^+ , \tag{2-60-b}$$

where

$$L_n^{(\pm)}(\cos\theta) = n\left[P_n(\cos\theta) \pm P_{n-1}(\cos\theta)\right] . \tag{2-61}$$

The cross section and Sherman function are then expressed as

$$I(\theta) = K^{-2}\left(\sec^2\theta/2 \cdot |E|^2 + \operatorname{cosec}^2\theta/2 \cdot |H|^2\right) \tag{2-62}$$

$$S(\theta) = i\left(EH^* - HE^*\right) / \left(|H|^2 \cot\theta/2 + |E|^2 \tan\theta/2\right) . \tag{2-63}$$

These transformations have some advantages. At 180° the Legendre function is expressed as $P_n(-1)=(-1)^n$, thus the numerical summation of a large number of phase shifts, which is usually the case in high energy scattering, would incur error at angles near the backward scattering. However, $L_n^+$ which appears in $E(\theta)$ behaves like $\cos^2(\theta/2)$ so would be more accurate The same arguments hold for the forward scattering.

Each angular distribution of cross section and Sherman function was calculated at 1° intervals from 0° to 180° for various angular resolutions All input data such as matching radius and intervals of integrations were made sufficiently large and small, respectively, in order to make the results insensitive to those parameters.

The order of phase shifts estimated ranges from 18 to 53 for the incident energy of 300 to 2000 eV.

All the necessary additional functions such as Bessel, Neumann and Legendre functions were calculated using recurrence relations as,

$$j_{m+1}(x)=-j_{m-1}(x)+(2m+1)\ j_m(x)/x \tag{2-64-a}$$

$$n_{m+1}(x)=-n_{m-1}(x)+(2m+1)\ n_m(x)/x \tag{2-64-b}$$

with initial conditions

$$j_0(x)=\sin(x)/x\ , \qquad j_1(x)=\sin(x)/x^2-\cos(x)/x \tag{2-65-a}$$

$$n_0(x)=-\cos(x)/x\ , \qquad n_1(x)=-\cos(x)/x^2-\sin(x)/x \tag{2-65-b}$$

and

$$L^{\pm}_{n+1}(x)=\left[(2n+1)\cdot x\cdot L^{\pm}_n(x)-(n+1)\ L^{\pm}_{n-1}(x)\right.$$
$$\left.-(1\pm x)\ P_{n-1}(x)\right]/n \tag{2-66-a}$$

$$P_{n+1}(x)=\left[(2n+1)x\ P_n(x)-n\ P_{n-1}(x)\right]/(n+1) \tag{2-66-b}$$

with initial conditions,

$$L^{\pm}_0(x)=0 \qquad L^{\pm}_1(x)=x\pm 1 \tag{2-67-a}$$

$$P_0(x)=1 \qquad P_1(x)=x \tag{2-67-b}$$

respectively, throughout the present calculations.
The flow chart and the list of program for the present calculation is shown in Appendix 6.

## 2-5 Results and Discussion

In Fig.2-4, calculated results of the cross section are compared to the data of Bromberg's absolute measurements for primary energies of 300,

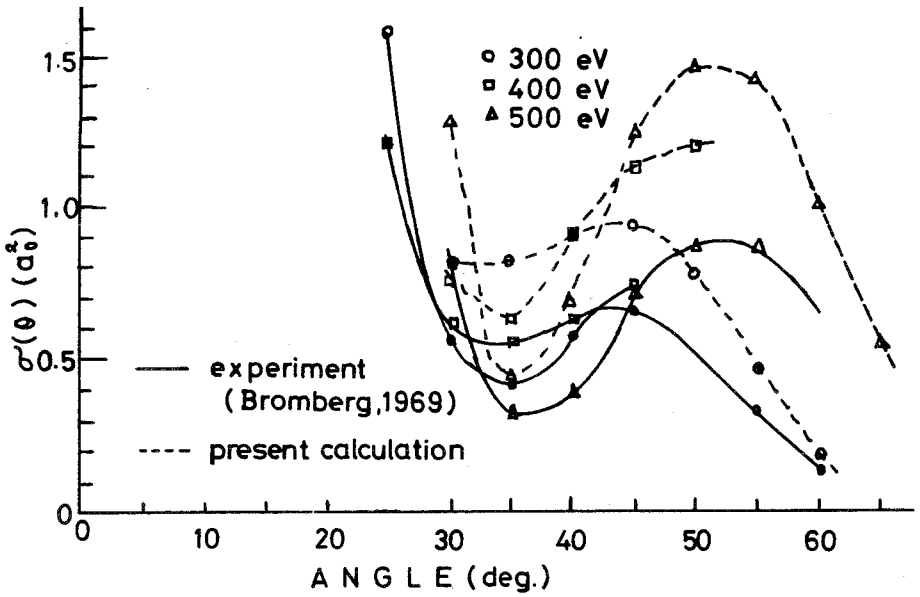


Fig. 2-4. Comparison of the cross section between the present calculation and the absolute measurements of Bromberg (1969).

400 and 500 eV(1969). Here, the theoretical calculations describe experimental curves quite well qualitatively, but in quantitative arguments the theoretical values are about 1.5 times larger for each incident electron energy. Fig.2-5 shows the calculated angular distribution of the cross section and Sherman function for various incident energies. Fig.2-5 shows comparisons to calculated results by Holzwarth and Meister (1964b), where Mayer's relativistic Hartree potential(1956) was used. Although several approximation procedures have been introduced in the present calculation, such as the scattering of relativistic electrons using a non-relativistic atomic potential, it should be noted that these calculations give satisfactory agreement with the more accurate but complicated calculation.
In Fig.2-6, results are also given as a function of incident electron energy for the purpose of convenience. Results are summarized in Fig.2-7

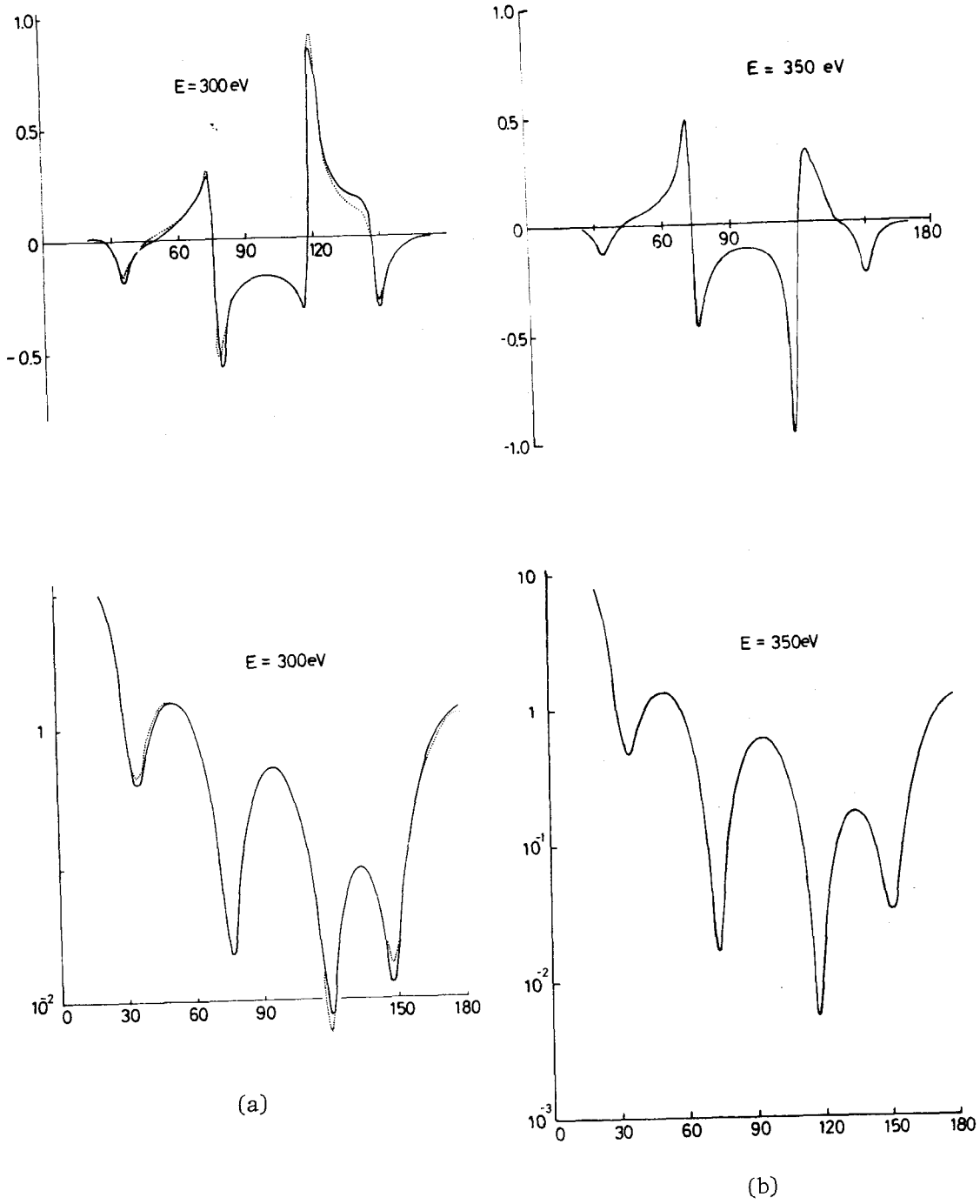


Fig. 2-5. Calculated results of spin polarization and differential cross section in unit of $a_0^2$ with respect to scattering angle. (——present calculation and --- calculated results using Mayer's relativistic Hartree potential (Holzwarth and Meister 1964b)).

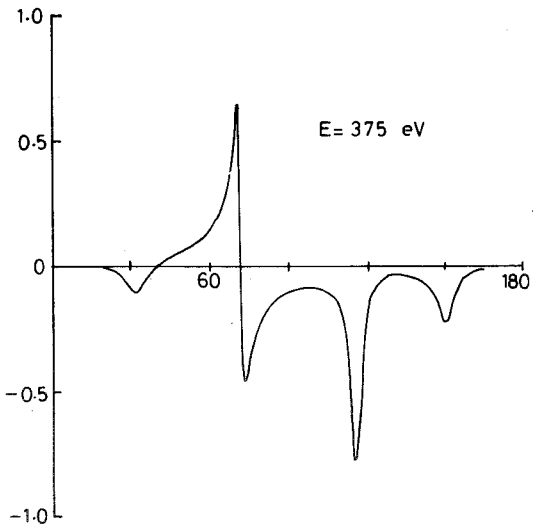
1·0
0·5
0
−0·5
−1·0
E= 375 eV
60
180

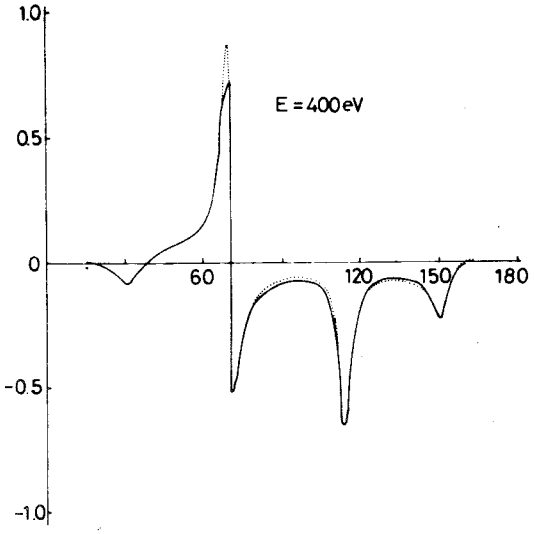
1.0
0.5
0
-0.5
-1.0
E = 400eV
60
120
150
180

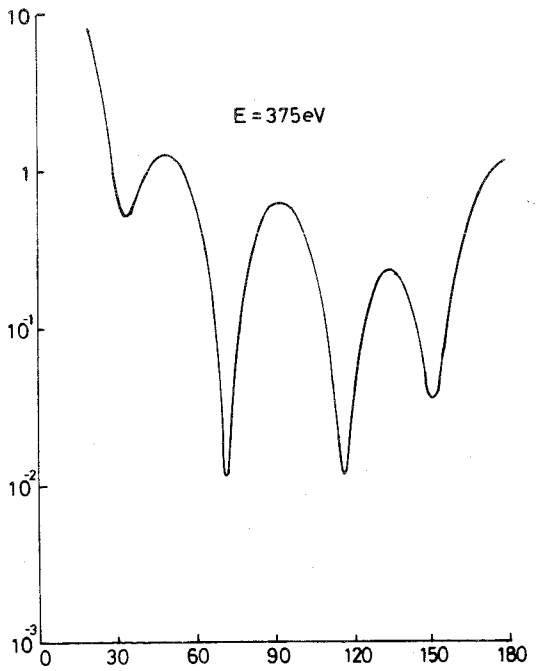
10
1
$10^{-1}$
$10^{-2}$
$10^{-3}$
E = 375eV
0
30
60
90
120
150
180

(c)

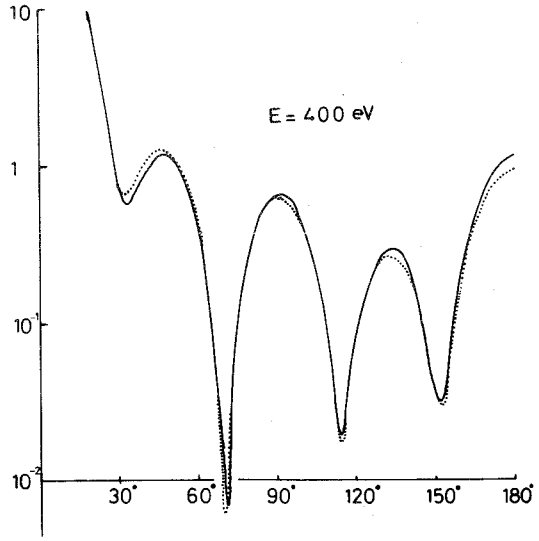
10
1
$10^{-1}$
$10^{-2}$
E = 400 eV
30°
60°
90°
120°
150°
180°

(d)

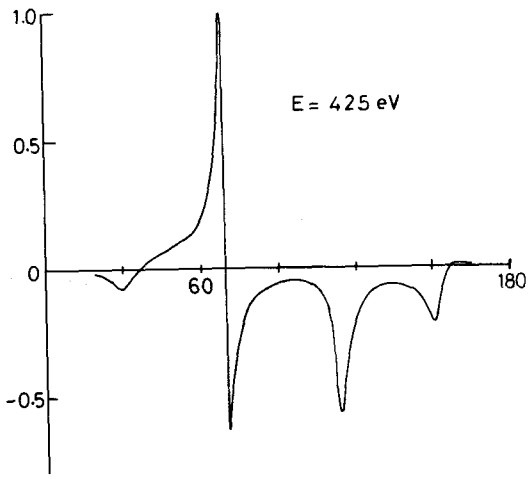
1.0
0.5
0
-0.5
E = 425 eV
60
180

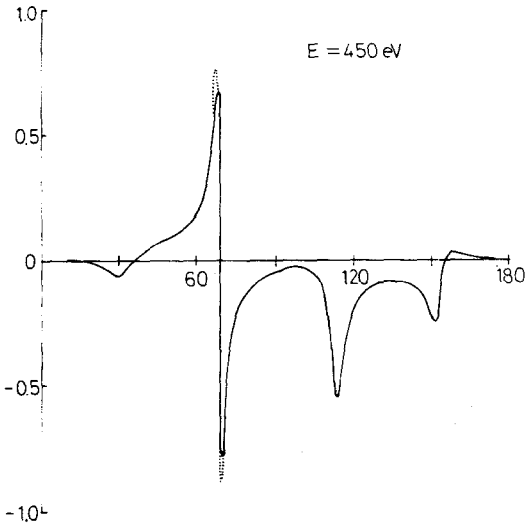
1.0
0.5
0
-0.5
-1.0
E = 450 eV
60
120
180

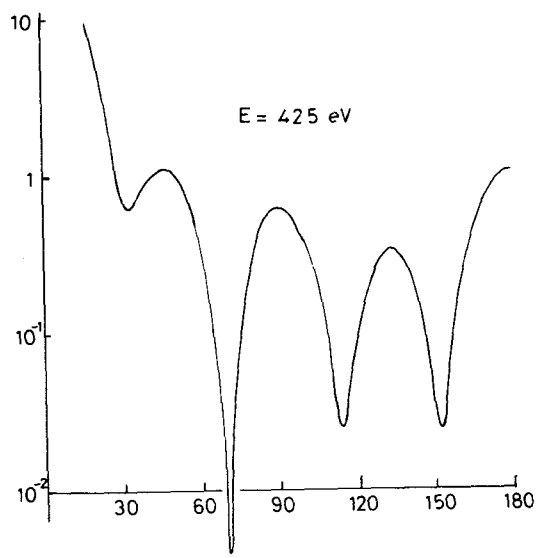
10
1
$10^{-1}$
$10^{-2}$
E = 425 eV
30
60
90
120
150
180

(e)

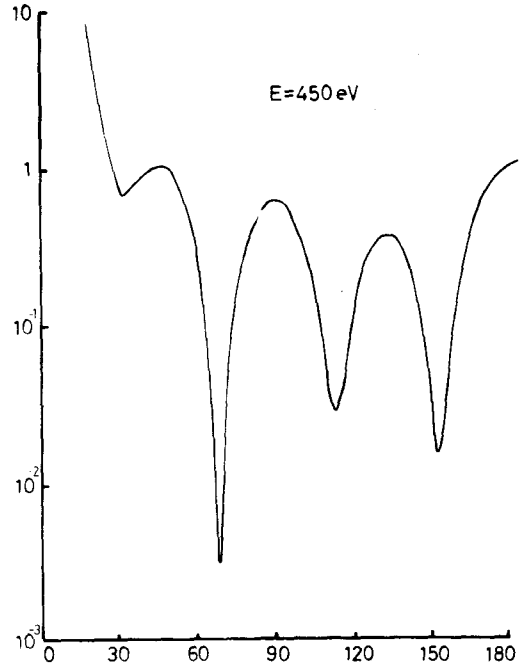
10
1
$10^{-1}$
$10^{-2}$
$10^{-3}$
E=450 eV
0
30
60
90
120
150
180

(f)

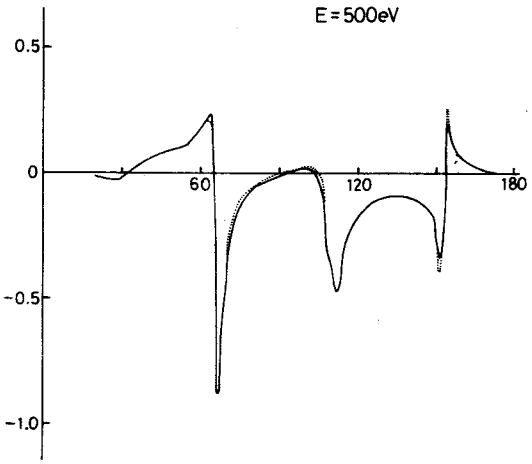
E=500eV
0.5
0
-0.5
-1.0
60
120
180

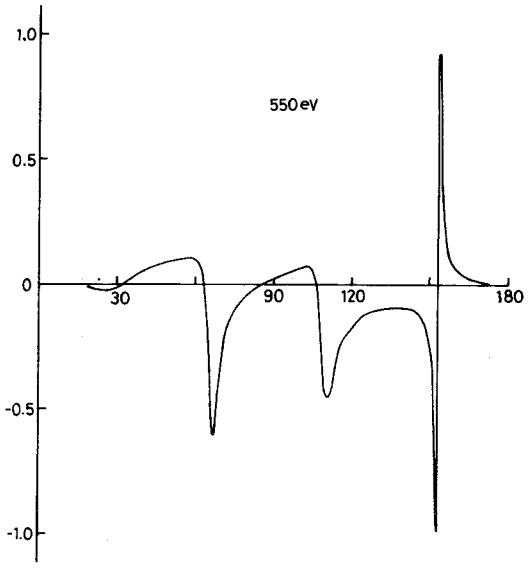
550eV
1.0
0.5
0
-0.5
-1.0
30
90
120
180

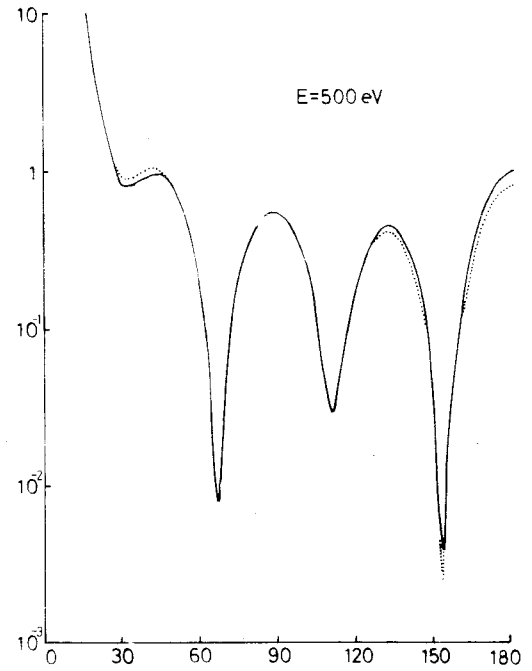
E=500 eV
10
1
$10^{-1}$
$10^{-2}$
$10^{-3}$
0
30
60
90
120
150
180

(g)

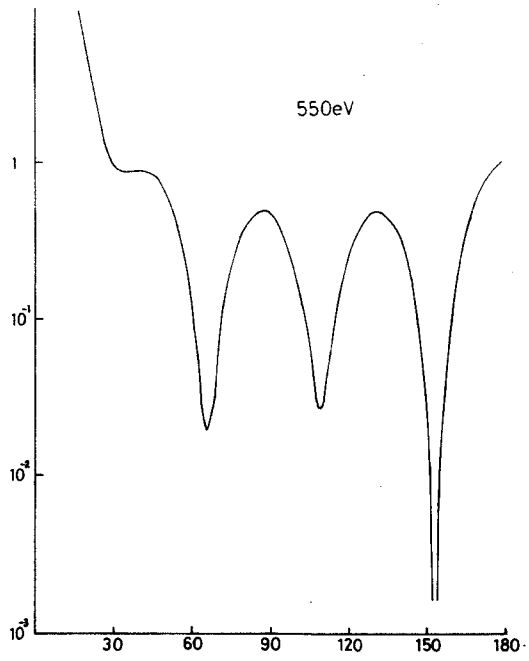
550eV
1
$10^{-1}$
$10^{-2}$
$10^{-3}$
30
60
90
120
150
180

(h)

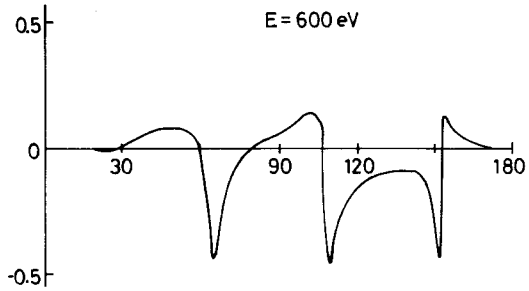
E = 600 eV
0.5
0
-0.5
30
90
120
180

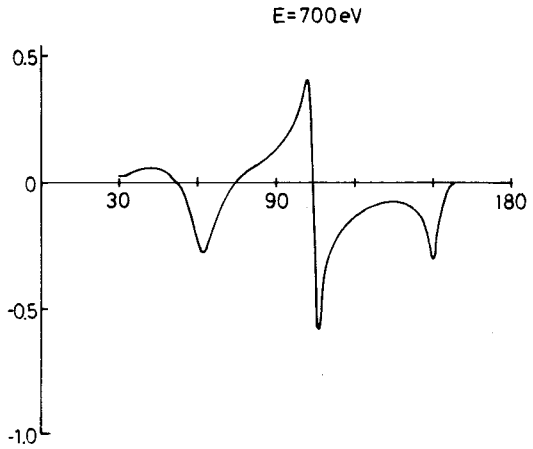
E=700eV
0.5
0
-0.5
-1.0
30
90
180

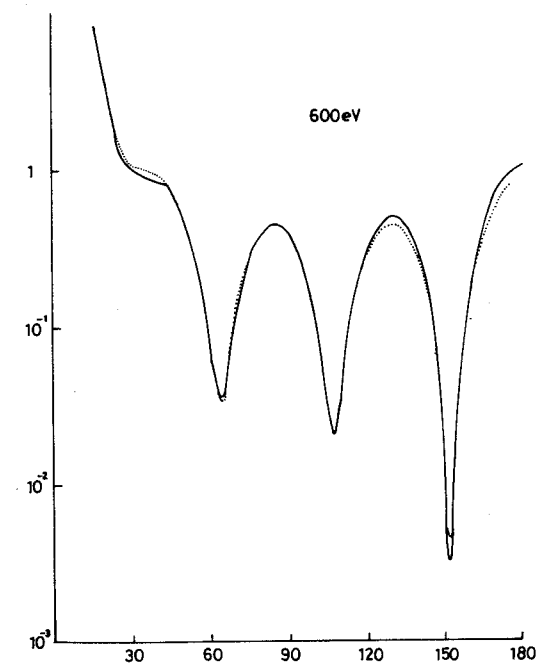
600eV
1
$10^{-1}$
$10^{-2}$
$10^{-3}$
30
60
90
120
150
180

(i)

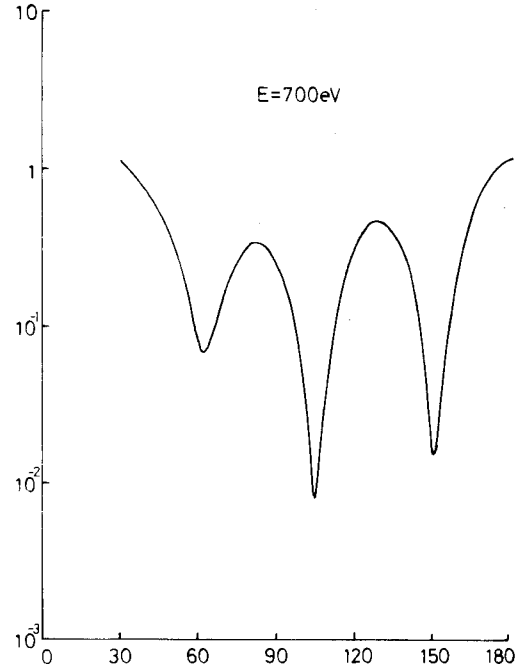
E=700eV
10
1
$10^{-1}$
$10^{-2}$
$10^{-3}$
0
30
60
90
120
150
180

(j)

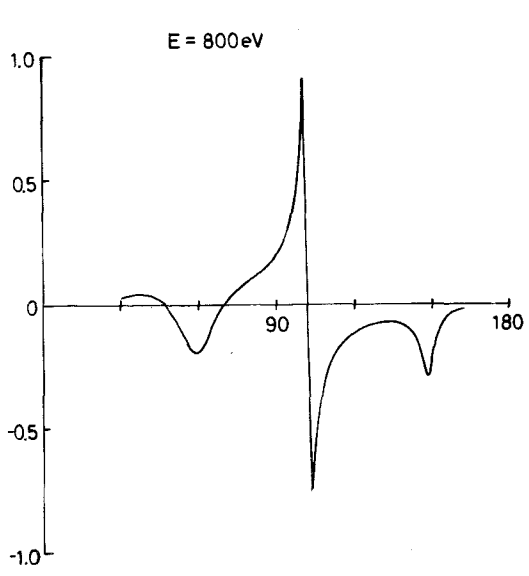
E = 800eV
1.0
0.5
0
-0.5
-1.0
90
180

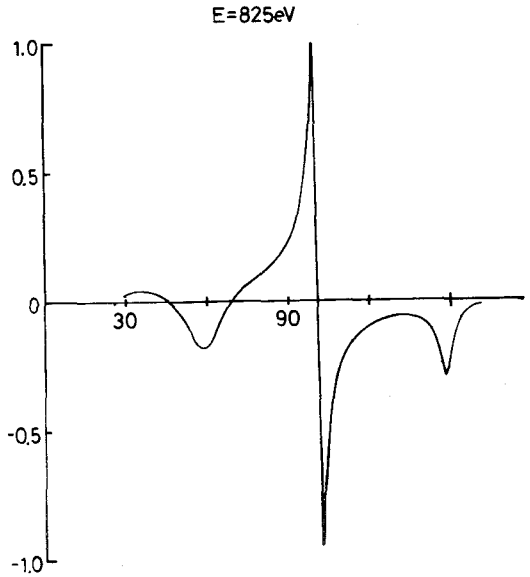
E=825eV
1.0
0.5
0
-0.5
-1.0
30
90

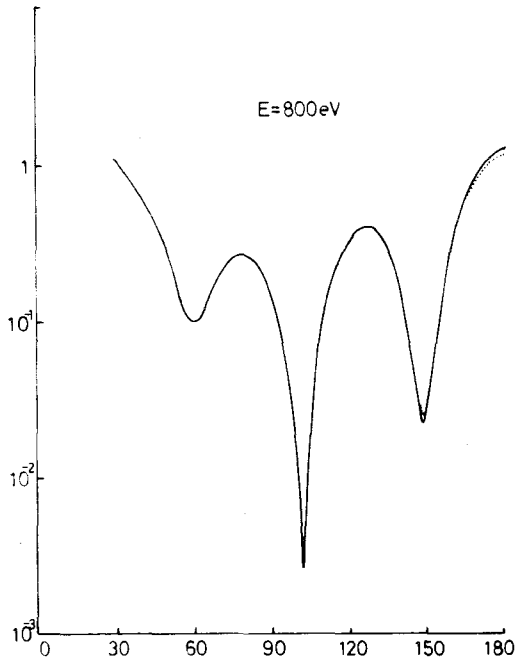
E=800eV
1
$10^{-1}$
$10^{-2}$
$10^{-3}$
0
30
60
90
120
150
180

(k)

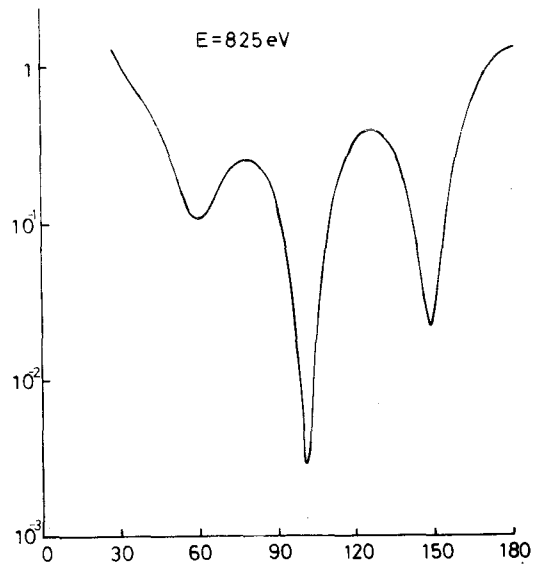
E=825eV
1
$10^{-1}$
$10^{-2}$
$10^{-3}$
0
30
60
90
120
150
180

(1)

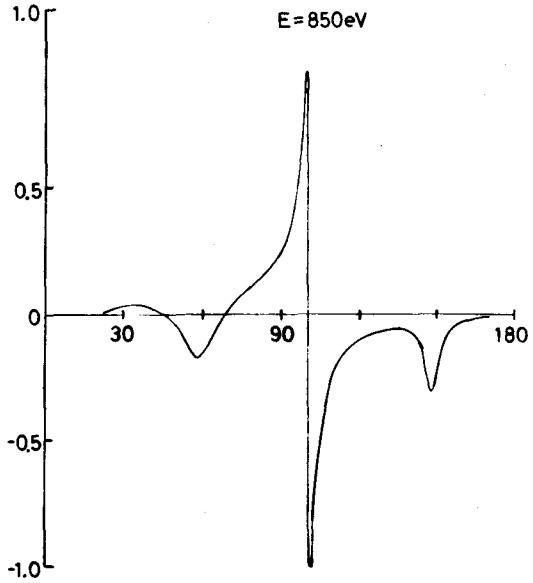
E=850eV
1.0
0.5
0
-0.5
-1.0
30
90
180

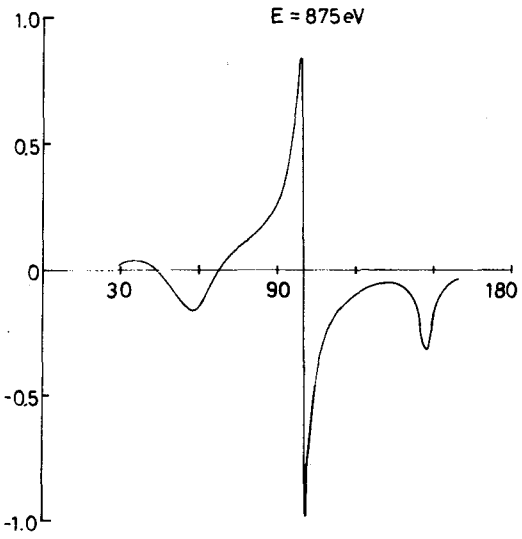
E = 875eV
1.0
0.5
0
-0.5
-1.0
30
90
180

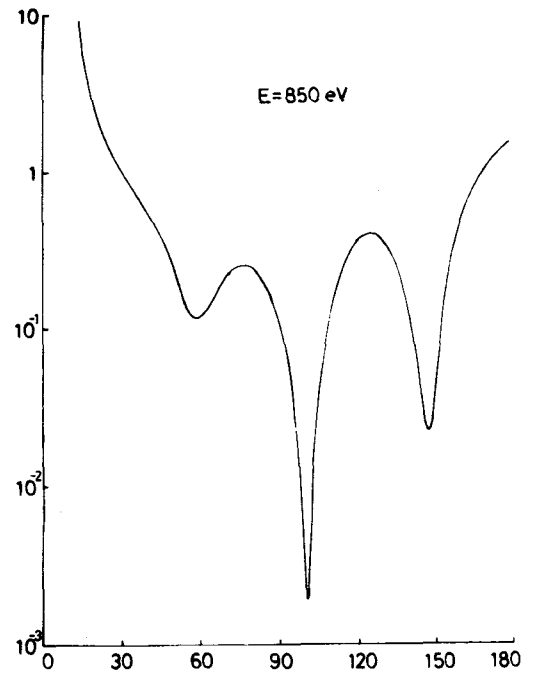
E=850 eV
10
1
$10^{-1}$
$10^{-2}$
$10^{-3}$
0
30
60
90
120
150
180

(m)

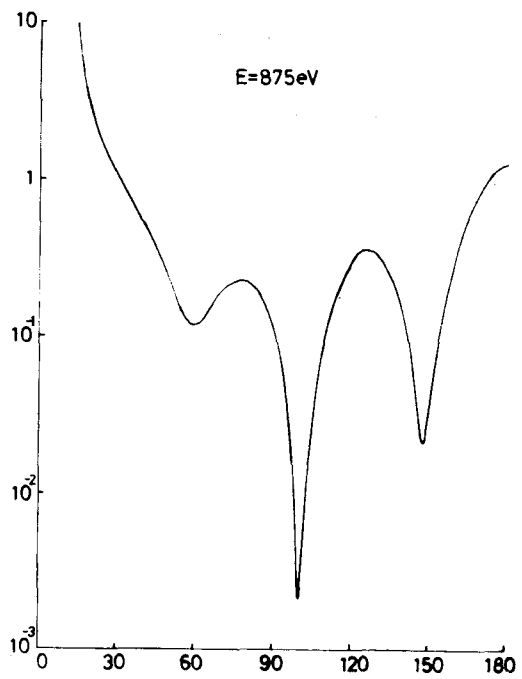
E=875eV
10
1
$10^{-1}$
$10^{-2}$
$10^{-3}$
0
30
60
90
120
150
180

(n)

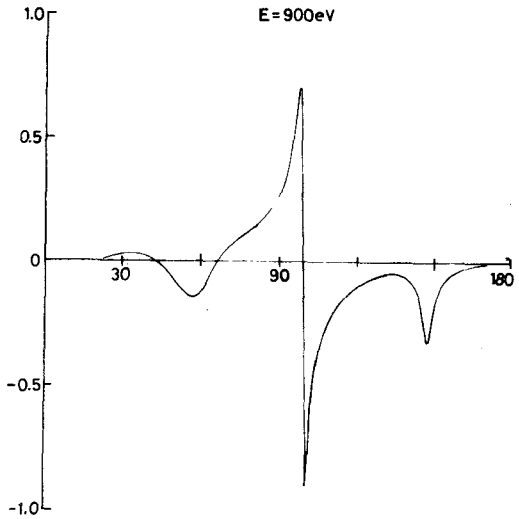
E=900eV
1.0
0.5
0
-0.5
-1.0
30
90
180

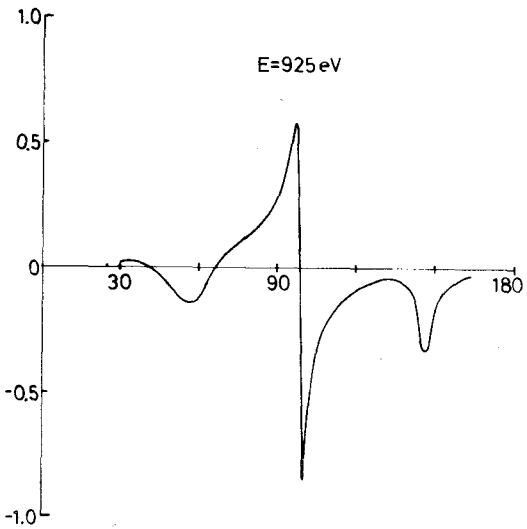
E=925eV
1.0
0.5
0
-0.5
-1.0
30
90
180

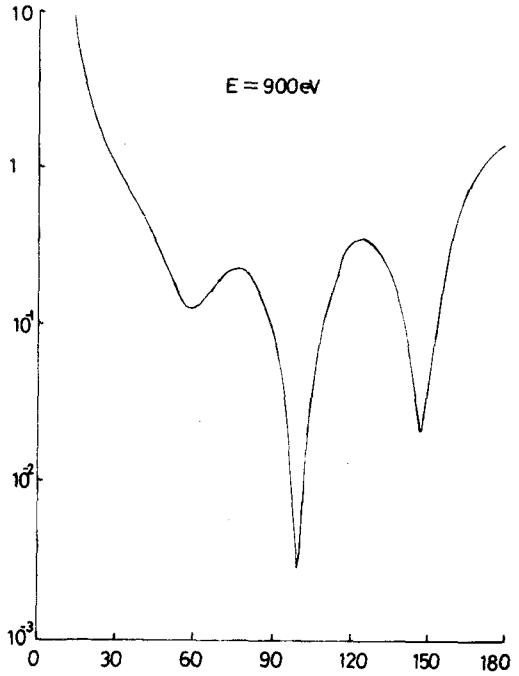
E=900eV
10
1
$10^{-1}$
$10^{-2}$
$10^{-3}$
0
30
60
90
120
150
180

(o)

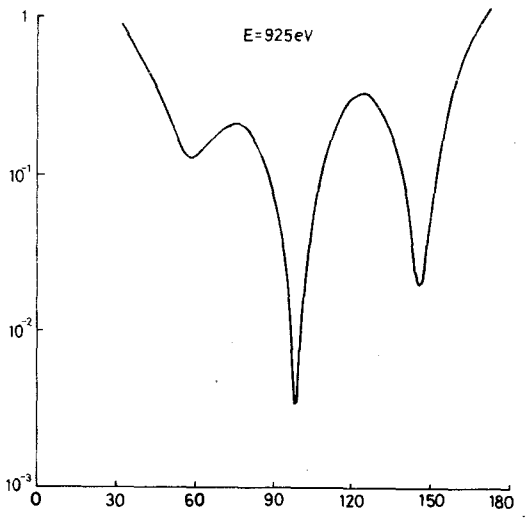
E=925eV
1
$10^{-1}$
$10^{-2}$
$10^{-3}$
0
30
60
90
120
150
180

(p)

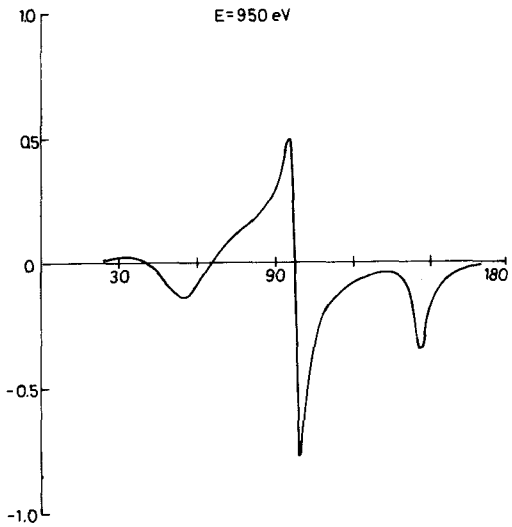
E=950 eV
1.0
0.5
0
-0.5
-1.0
30
90
180

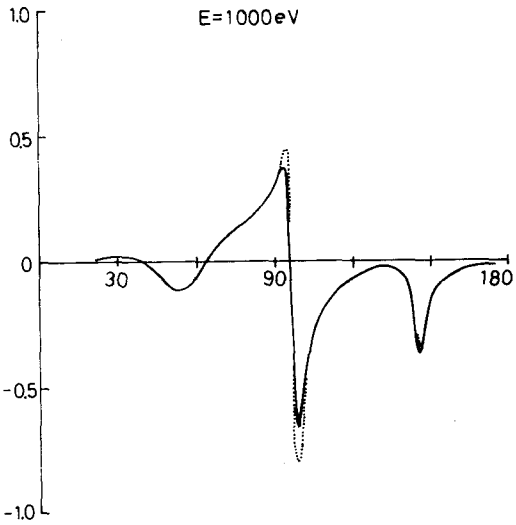
E=1000eV
1.0
0.5
0
-0.5
-1.0
30
90
180

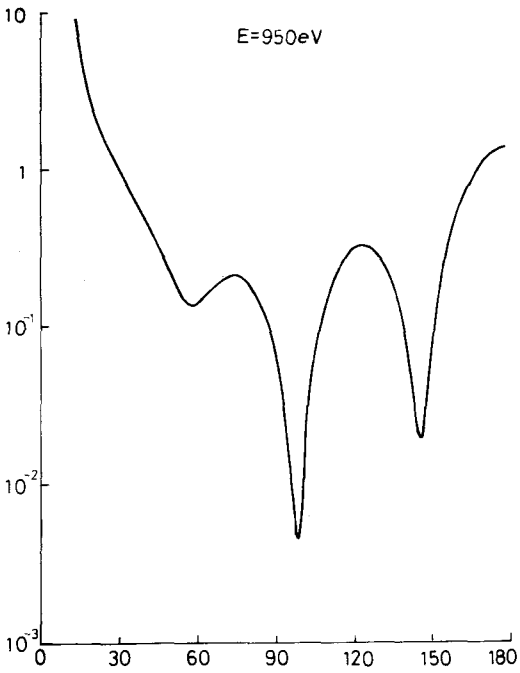
E=950eV
10
1
$10^{-1}$
$10^{-2}$
$10^{-3}$
0
30
60
90
120
150
180

(q)

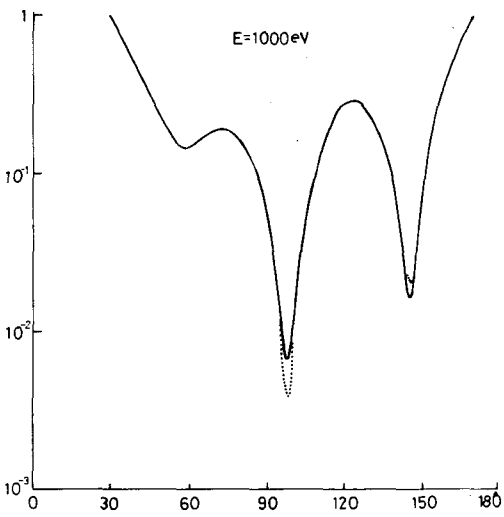
E=1000eV
1
$10^{-1}$
$10^{-2}$
$10^{-3}$
0
30
60
90
120
150
180

(r)

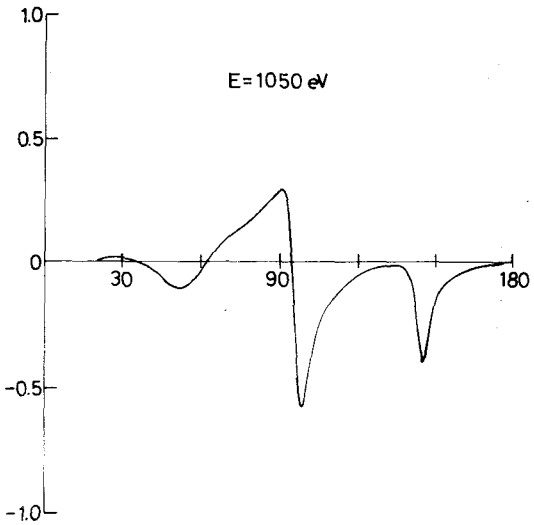
E=1050 eV
1.0
0.5
0
-0.5
-1.0
30
90
180

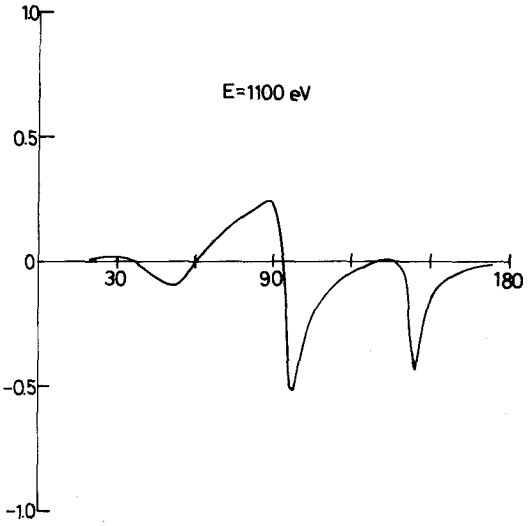
E=1100 eV
1.0
0.5
0
-0.5
-1.0
30
90
180

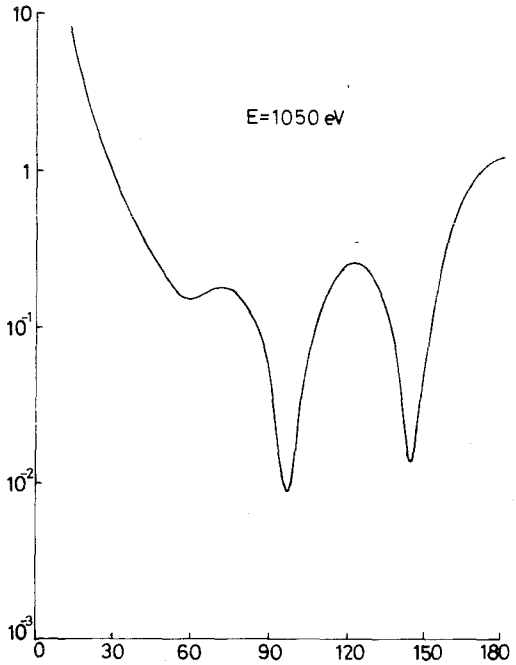
E=1050 eV
10
1
$10^{-1}$
$10^{-2}$
$10^{-3}$
0
30
60
90
120
150
180

(s)

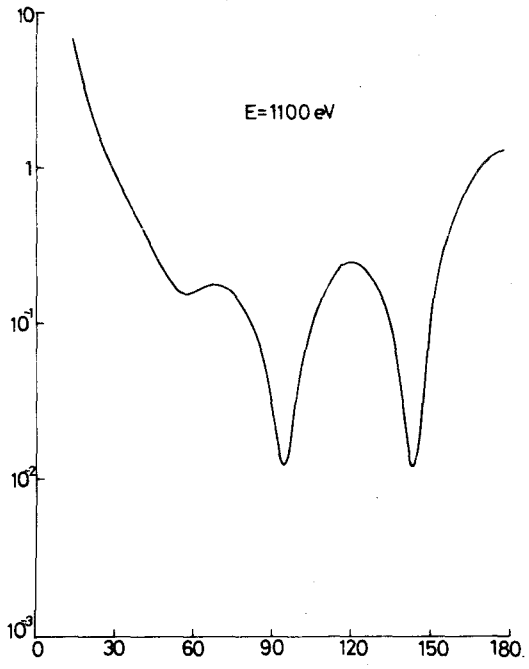
E=1100 eV
10
1
$10^{-1}$
$10^{-2}$
$10^{-3}$
0
30
60
90
120
150
180

(t)

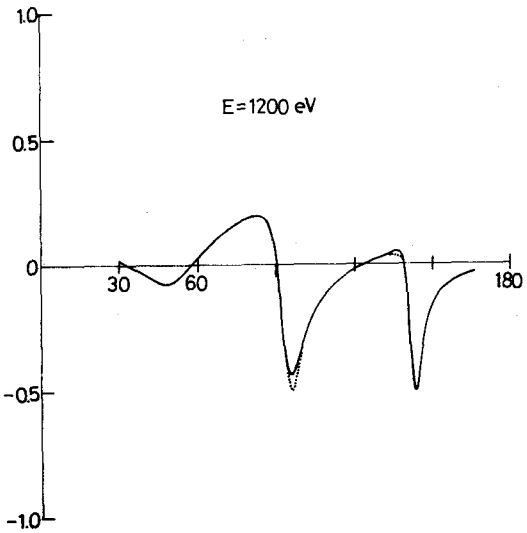
E=1200 eV
1.0
0.5
0
-0.5
-1.0
30
60
180

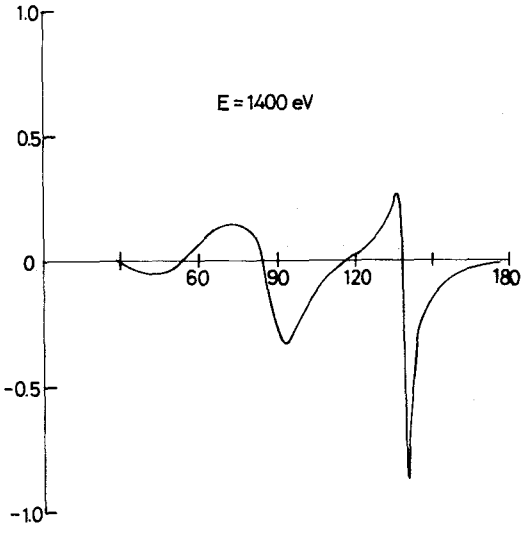
E=1400 eV
1.0
0.5
0
-0.5
-1.0
60
90
120
180

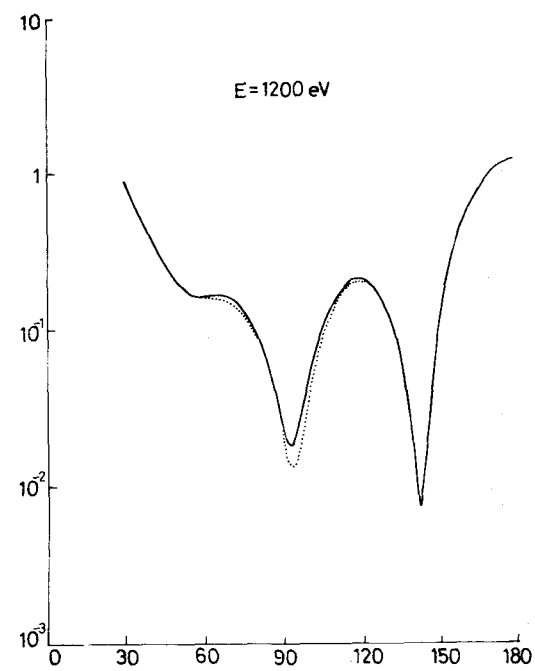
E=1200 eV
10
1
$10^{-1}$
$10^{-2}$
$10^{-3}$
0
30
60
90
120
150
180

(u)

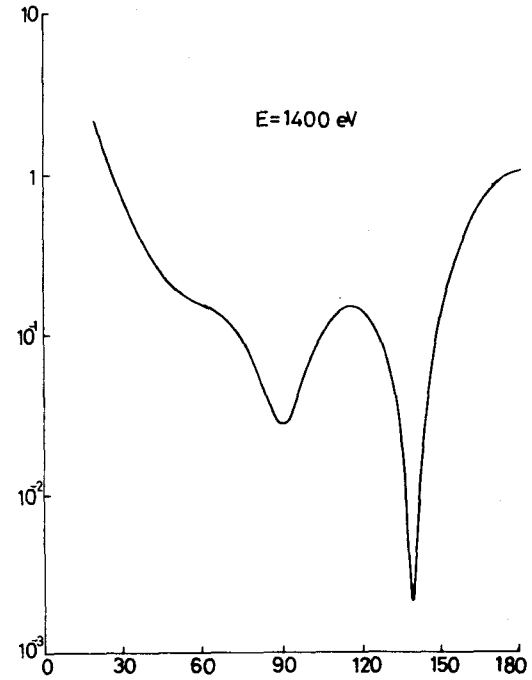
E=1400 eV
10
1
$10^{-1}$
$10^{-2}$
$10^{-3}$
0
30
60
90
120
150
180

(v)

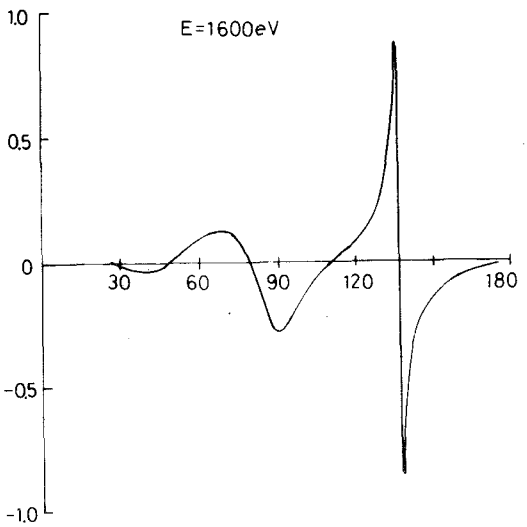
E=1600eV
1.0
0.5
0
-0.5
-1.0
30
60
90
120
180

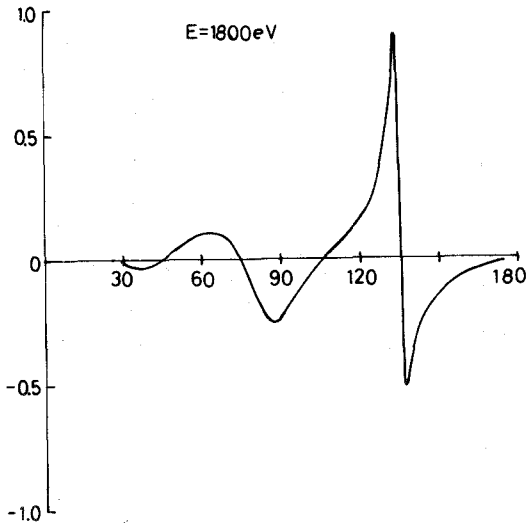
E=1800eV
1.0
0.5
0
-0.5
-1.0
30
60
90
120
180

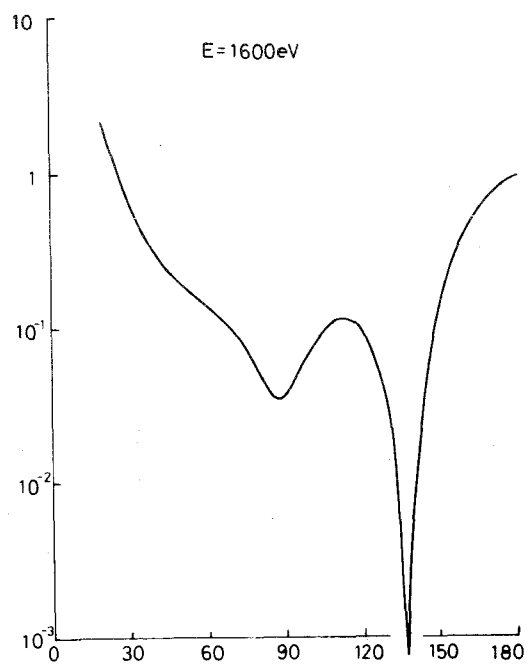
E=1600eV
10
1
$10^{-1}$
$10^{-2}$
$10^{-3}$
0
30
60
90
120
150
180

(w)

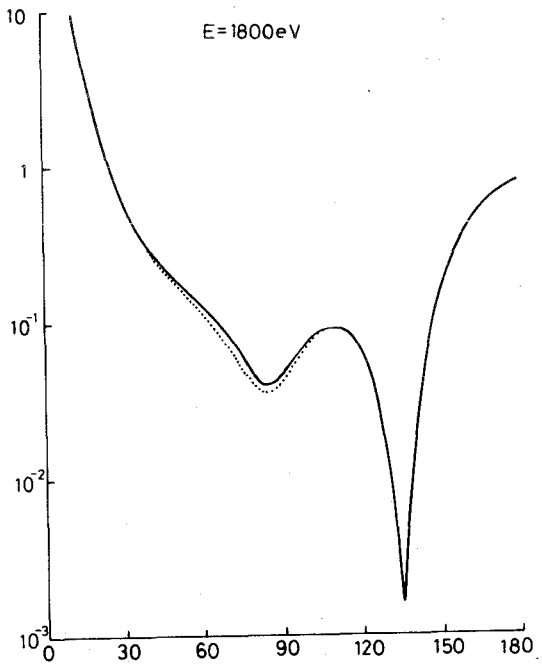
E=1800eV
10
1
$10^{-1}$
$10^{-2}$
$10^{-3}$
0
30
60
90
120
150
180

(x)

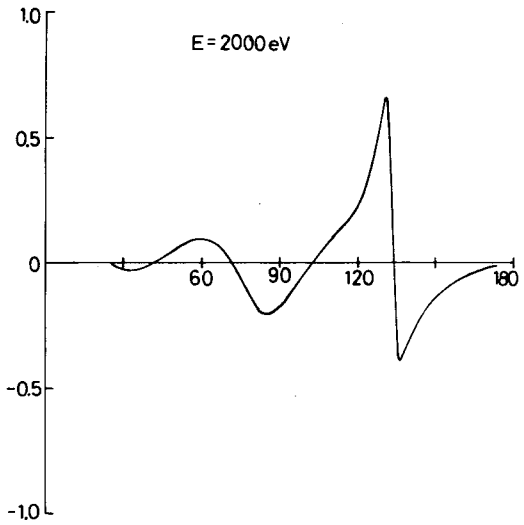
E = 2000 eV
1.0
0.5
0
-0.5
-1.0
60
90
120
180

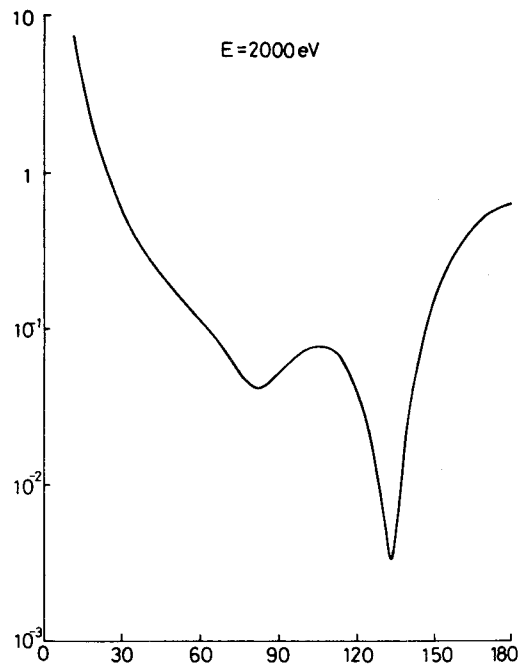
E = 2000 eV
10
1
$10^{-1}$
$10^{-2}$
$10^{-3}$
0
30
60
90
120
150
180

(y)

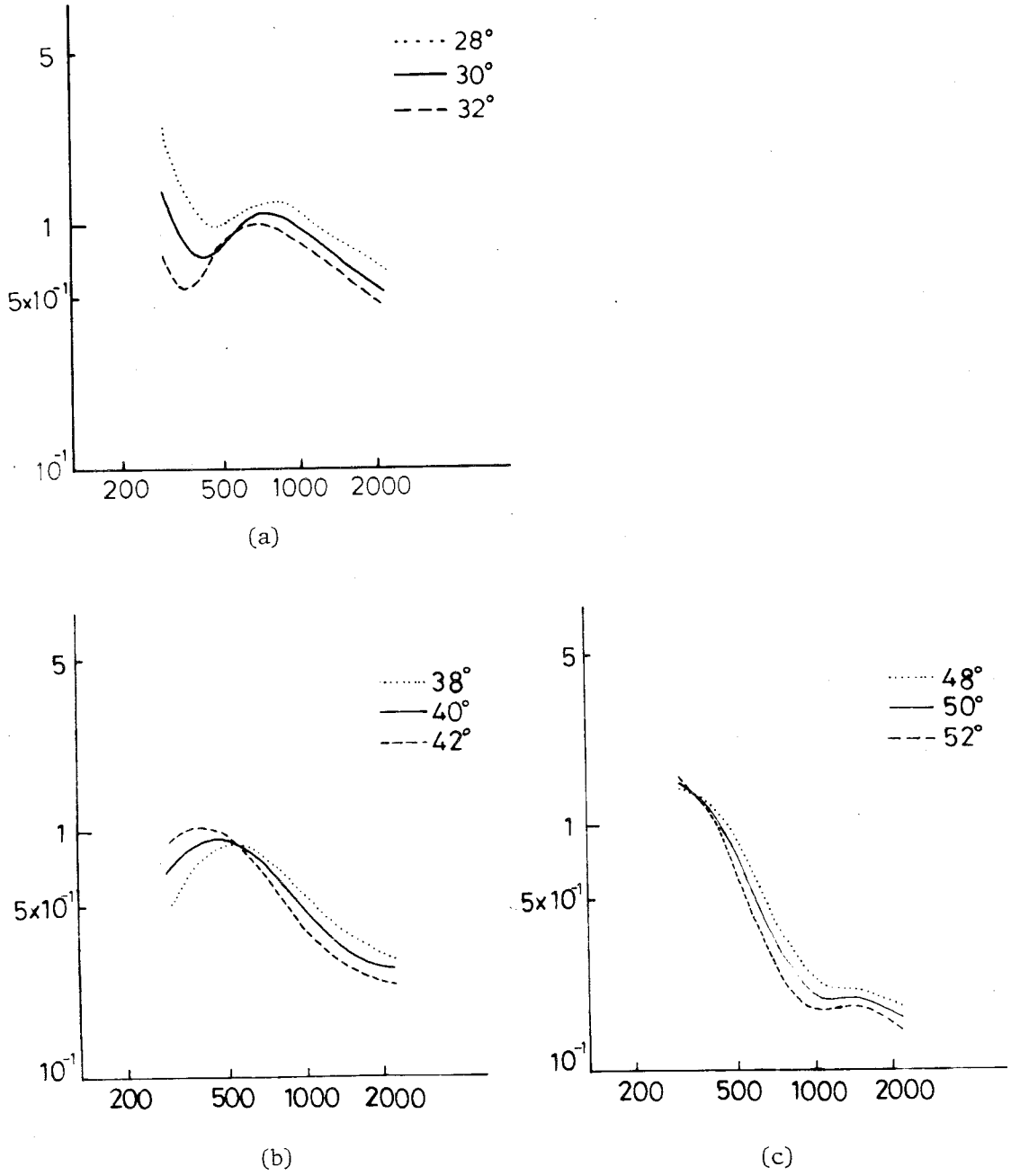


Fig. 2-6. Calculated results of differential cross section with respect to incident electron energy.

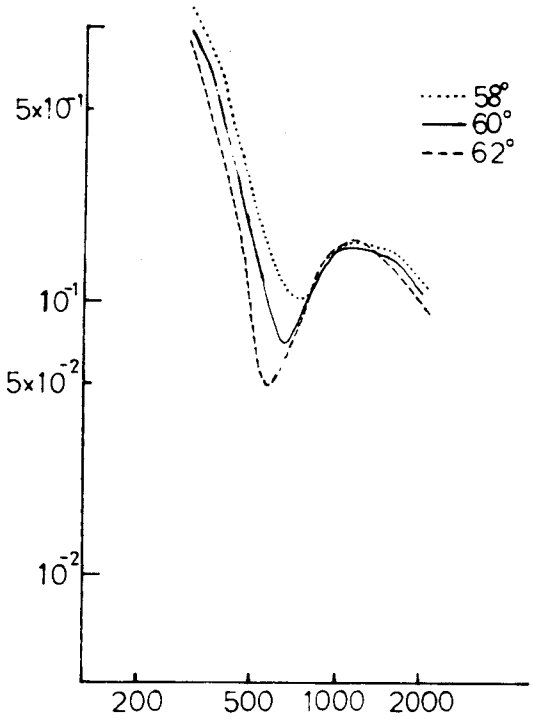
5x10⁻¹
10⁻¹
5x10⁻²
10⁻²
200
500
1000
2000
58°
60°
62°

(d)

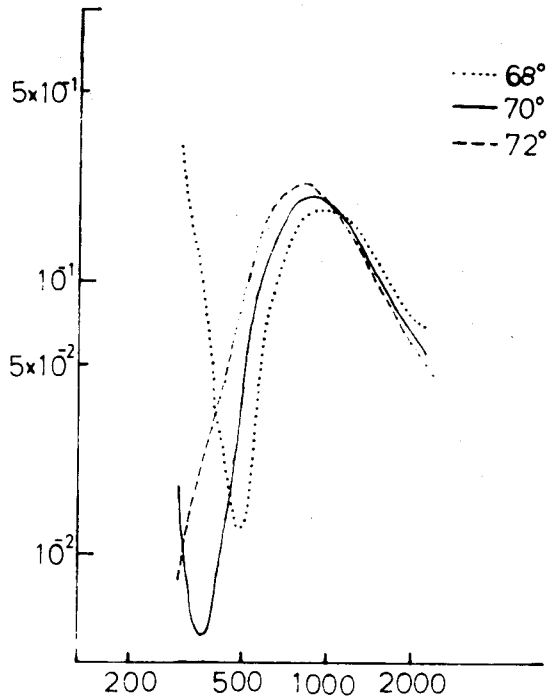
5x10⁻¹
10⁻¹
5x10⁻²
10⁻²
200
500
1000
2000
68°
70°
72°

(e)

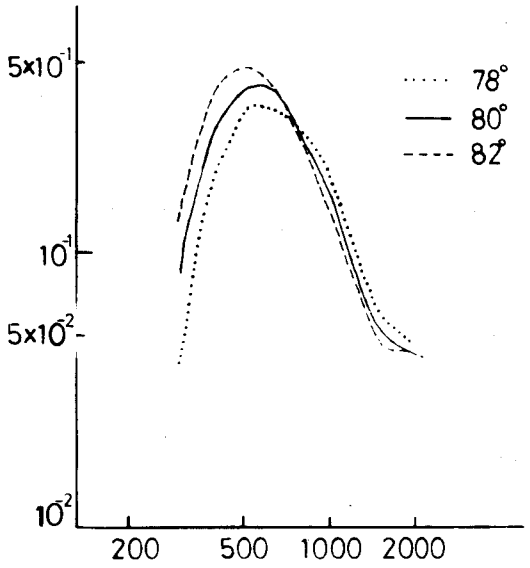
5x10⁻¹
10⁻¹
5x10⁻²
10⁻²
200
500
1000
2000
78°
80°
82°

(f)

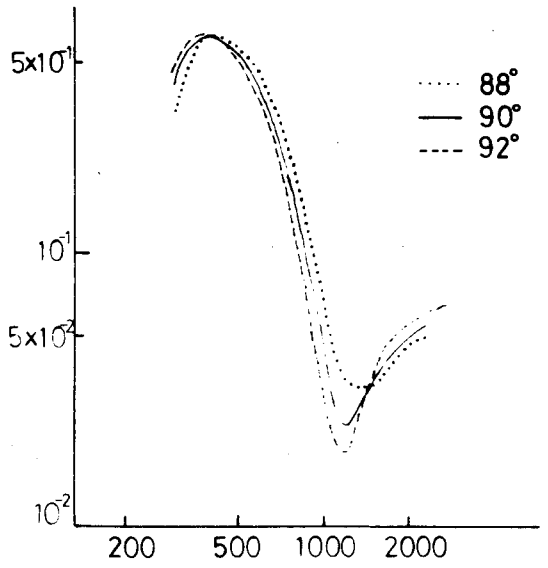
5x10⁻¹
10⁻¹
5x10⁻²
10⁻²
200
500
1000
2000
88°
90°
92°

(g)

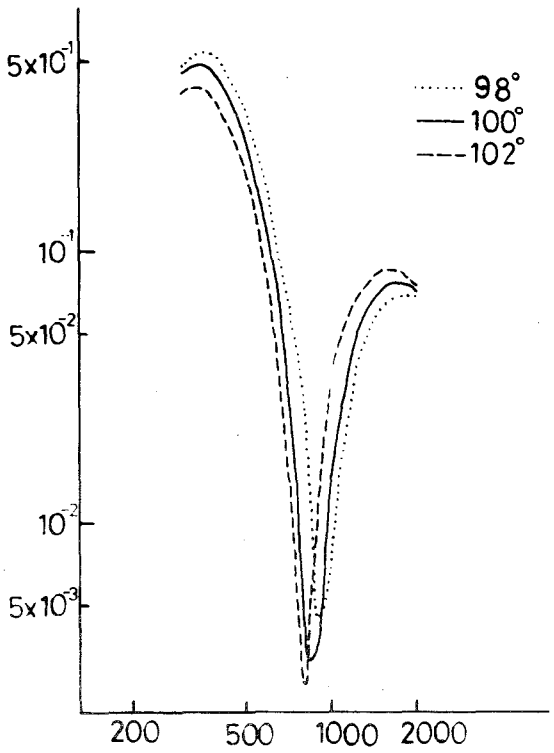
5x10⁻¹
10⁻¹
5x10⁻²
10⁻²
5x10⁻³
98°
100°
102°
200
500
1000
2000

(h)

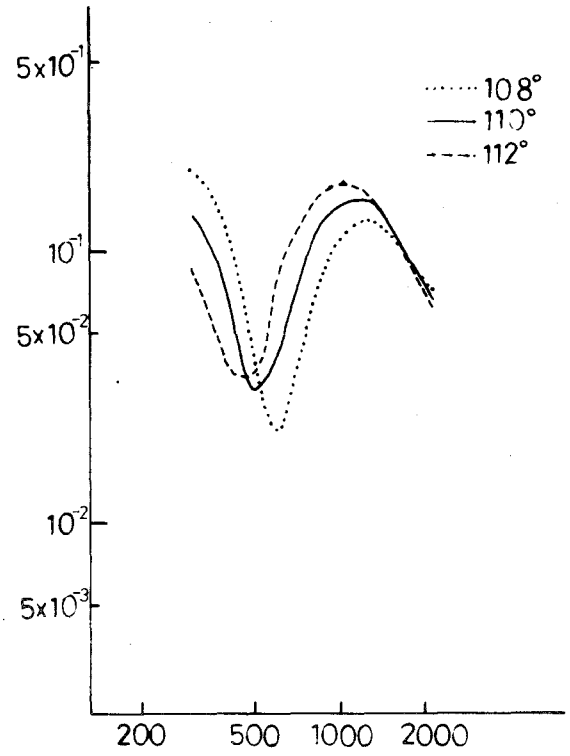
5x10⁻¹
10⁻¹
5x10⁻²
10⁻²
5x10⁻³
108°
110°
112°
200
500
1000
2000

(i)

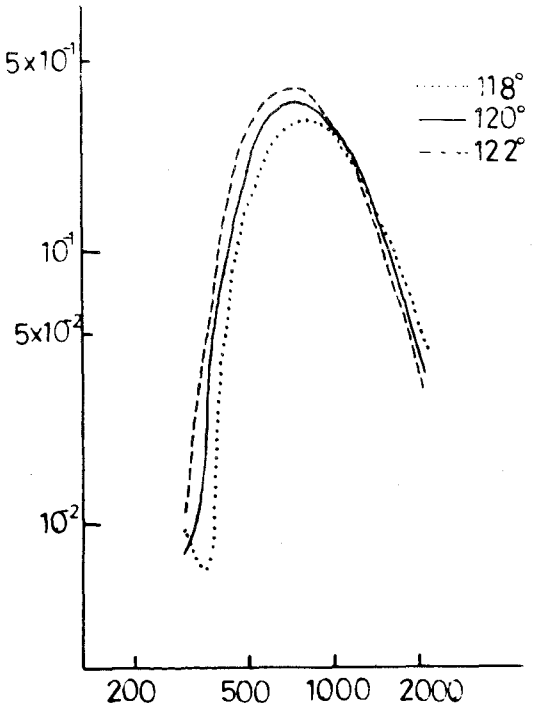
5x10⁻¹
10⁻¹
5x10⁻²
10⁻²
118°
120°
122°
200
500
1000
2000

(j)

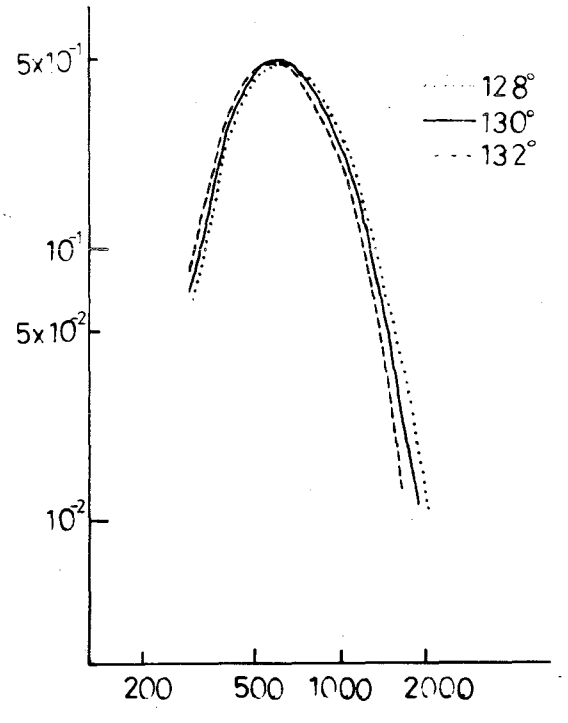
5x10⁻¹
10⁻¹
5x10⁻²
10⁻²
128°
130°
132°
200
500
1000
2000

(k)

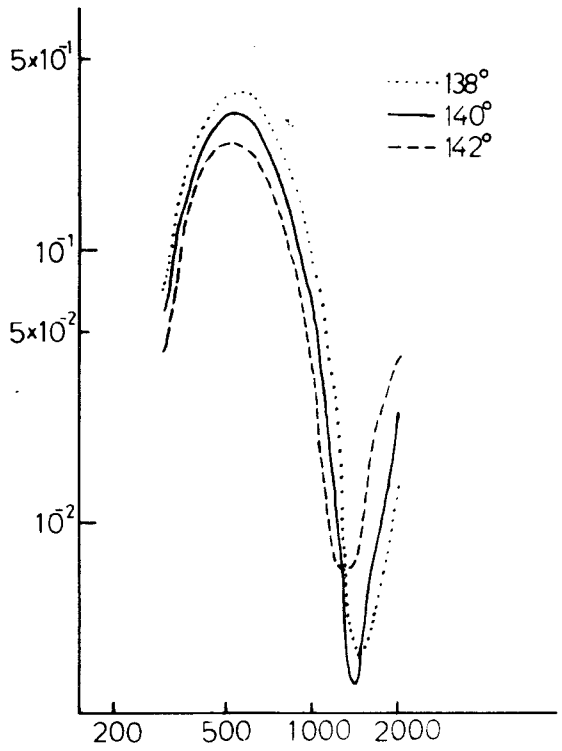
5×10⁻¹
10⁻¹
5×10⁻²
10⁻²
138°
140°
142°
200
500
1000
2000

(1)

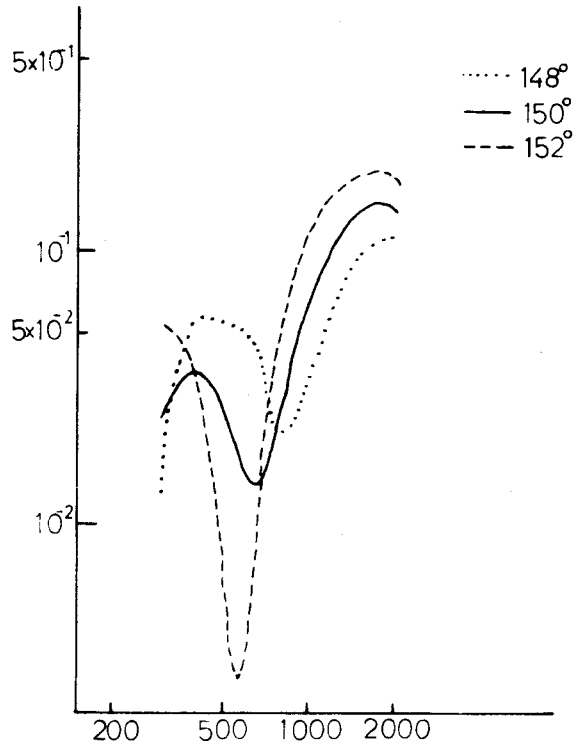
5×10⁻¹
10⁻¹
5×10⁻²
10⁻²
148°
150°
152°
200
500
1000
2000

(m)

for both cases of the angular resolution of $\Delta\theta \leqq 1$ and $\Delta\theta = 7$. This makes direct comparison with the measured spin polarization of a large acceptance angle possible(Bunyan and Schonfelder 1965). Fig.2-7 shows that the contours of constant polarization inclines to the left, i.e., the extremum points of ESP shift to lower angles as the energy increases. This corresponds to the fact that a diffraction angle becomes smaller as wave length shorter.

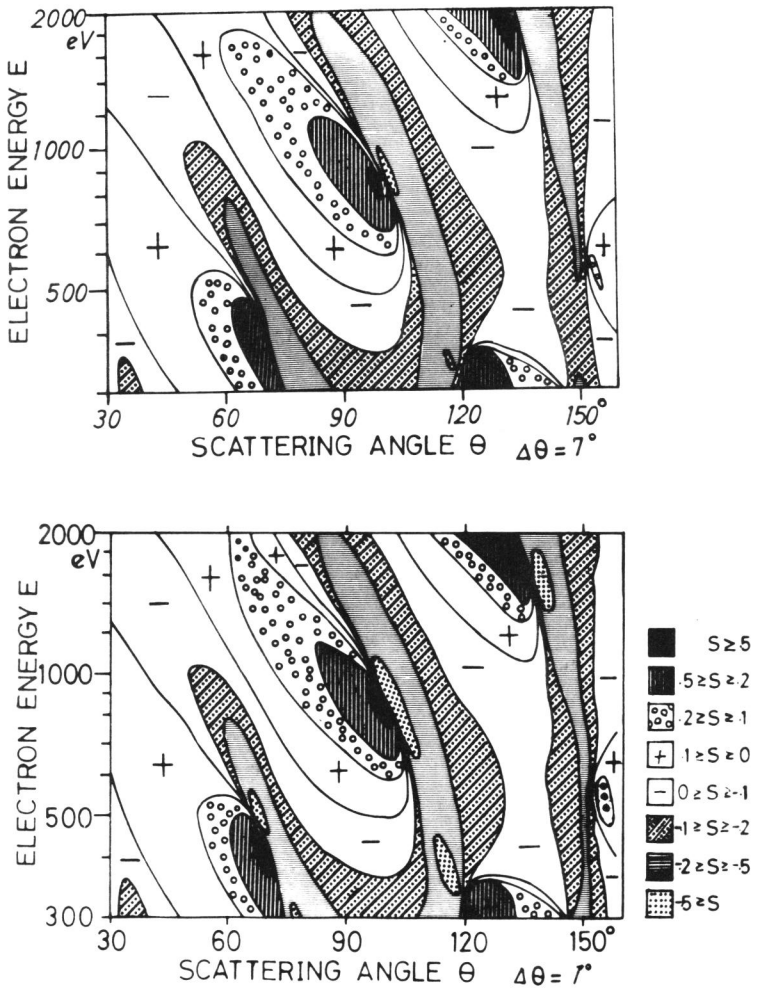


Fig. 2-7. Contours of constant polarization as function of scattering angle and electron energy with angular resolution $\Delta\theta \leqq 1°$ and $\Delta\theta = 7°$

## 2-6. Application of Partial Wave Expansion to Monte-Carlo Simulation--- Applicability of Conventional Screened Rutherford Cross Section for keV Electrons and its Failure in Low Energy Region

Krefting and Reimer (1974) have pointed out that the Rutherford cross-section (see Appendix 3) is inaccurate in describing the elastic scattering of kilovolt electrons with atoms in solids for heavy elements, and is still rather poor approximation for elements as light as aluminum. They have compared the unscreened Rutherford cross-section which diverges at a scattering angle of $\theta = 0°$, to the scattering cross-section obtained by a partial wave expansion method. However, the former method does not provide one with the total cross section, which is an important parameter in Monte-Carlo simulations. The screened Rutherford cross-section formula has been widely used in Monte-Carlo calculations (Heinrich et al. 1976), and it does provide us with the total elastic cross-section. Furthermore, Shimizu et al.(1976) have obtained close agreement between experimental and Monte-Carlo calculations based on the screened Rutherford cross-section. Hence, it is of interest to compare the partial wave expansion predictions with those obtained using screened Rutherford scattering.

From the theoretical viewpoint, although the differential cross-section for elastic scattering for electrons of energies below 1.5 keV (e.g. Fink and Yates 1970) and greater than a few tens of keV have been investigated (e.g. Sherman and Nelson 1959 and Bühring 1968b), the cross-section for intermediate energies has not yet, to our knowledge, been published. Hence it is of practical as well as theoretical use to determine the elastic scattering cross-section by partial wave expansion methods for electrons of energies between 1 and 20 keV, which are energies widely used for Monte-Carlo calculation as applied to electron microprobe and scanning electron microscopy. The differential cross-section was calculated using analytically expressed Hartree-Fock potential (T.G.Strand and Bonham 1964).

The results were compared with those published by Fink and Ingram and were found to be in satisfactory agreement with them in the region from 100 to 1500 eV.

Figures (2-8-a) and (2-8-b) show a comparison of differential cross-section for elastic scattering between the screened Rutherford and partial wave expansion calculations for aluminum at various electron energies of interest for the present study. The screening parameter $\beta_N$ adopted in the present calculation was the one derived by Nigam et al. (  Nigam et al.

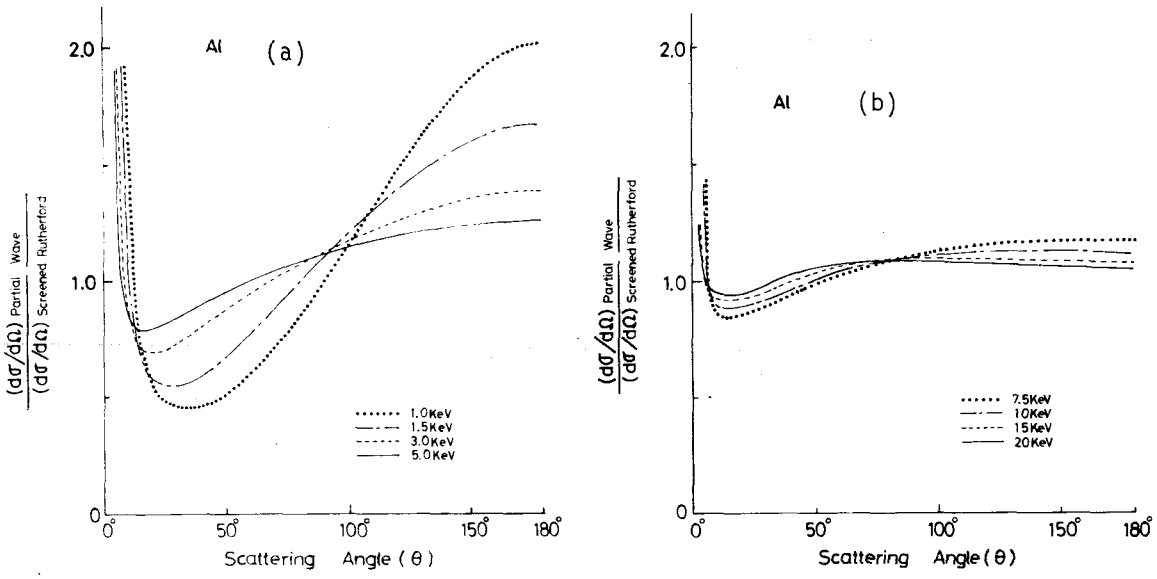


Fig. 2-8. The ratio of differential elastic scattering cross section obtained by partial wave expansion to that of screened Rutherford scattering as a function of the scattering angle $\theta$ and electron energy $E$ for aluminum.

1959) using Thomas-Fermi potential and second Born approximation. This result shows that both the differential cross-sections are in close agreement between 10 and 20 keV and that the screened Rutherford can still be extended with fairly good accuracy down to 5 keV.

Below 5 keV, however, the descrepancy between the two becomes remarkable. So far as the excitation of high energy is concerned, such as K-ionization, for which electrons with energies higher than about 3 times of K-ionization energy plays important role in practical problem (in Aluminum 3×1.5 keV=4.5 keV), these electrons of low energies below 5 keV are no more significant source of signals, i.e. K-Xrays and/or KLL Auger electrons. However, if signals of low excitation energies are treated in the argument, we have to take into account the contribution of low energy electrons.

Thus in this case it is strongly recommended to use the differential cross section obtained from partial wave expantion calculation.

Another comparison for the total cross-section is shown in Fig.2-9. The screening parameter does not cause any marked changes in the differential cross-section for scattering angles larger than several degrees in the kV region. Hence, taking an appropriate value for the screening para-

meter, i.e. 0.48 $\beta_N$ for aluminum, we can use the screened Rutherford scattering for energies ranging from 5 to 20 keV with considerable success in Monte-Carlo calculation. In Fig.2-10, total cross sections calculated by three methods are compared, i.e., partial wave expansion and first Born approximation using Hartree-Fock potential, and screened Rutherford scattering with Nigam's screening parameter $\beta_N$.

Although the partial wave expansion method is one of the most accurate theoretical approach to elastic scattering at present, it provides a differential cross-section with limited accuracy for scattering angles of less than 10 degrees because of ambiguity in the theoretical aotmic potential (Bromberg 1969). This ambiguity carries over to the total cross-section which one must use in Monte-Carlo calculation.

Thus, the present result suggests that the screened Rutherford scattering describes the elastic scattering of kV electrons with considerable accuracy for a light element such as aluminum, particularly using an appropriate value of the screened parameter, e.g., 0.48 $\beta_N$ for aluminum. Furthermore, since far better agreement between those two cross sections is theoretically expected for lighter elements, the Monte-Carlo calculation tech-

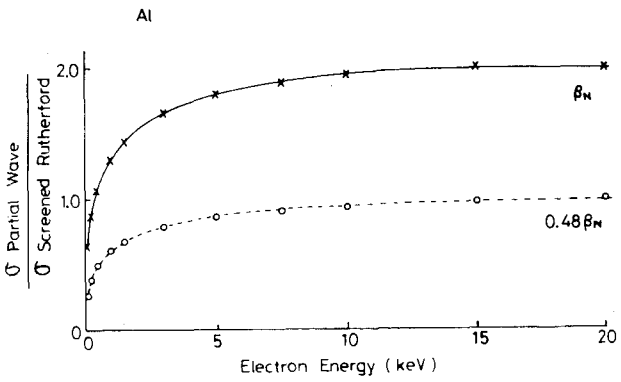


Fig.2-9. The ratio of the total cross section obtained by partial wave expansion to that of screened Rutherford scattering as a function of electron energy for different two values of the screening parameter $\beta_N$. (——after Nigam et al.(1959), ----- the best fit value.)

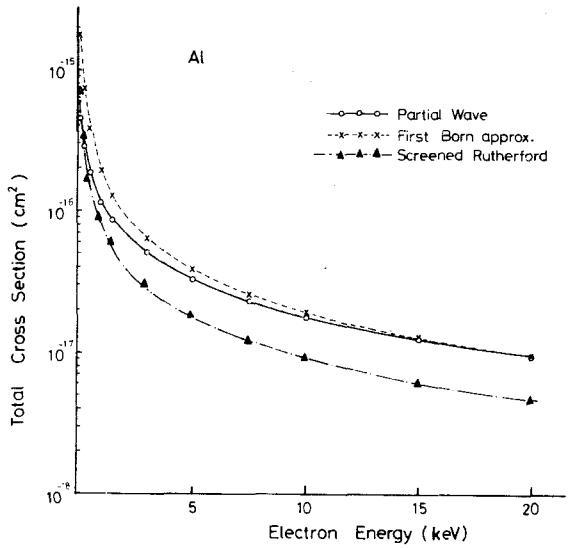


Fig. 2-10. Total cross sections obtained by partial wave expansion method, first Born approximation and screened Rutherford scattering as a function of electron energy.

nique using screened Rutherford scattering is a very useful approach for better understanding of electron penetration in organic and biological samples. However, this argument does not hold any more for such a low energy excitations as LVV Auger electron production in alminum. As a typical problem of practical importance, the application of the differential cross section obtained from partial wave expansion calculation to Monte-Carlo simulation of $Al_{LVV}$ Auger electron production will be briefly mentioned below.

Contribution of the secondary electrons to the energy distribution is seen in Fig.2-11. As is expected, the secondary electrons only contribute to the lower part of the energy distribution. The distribution

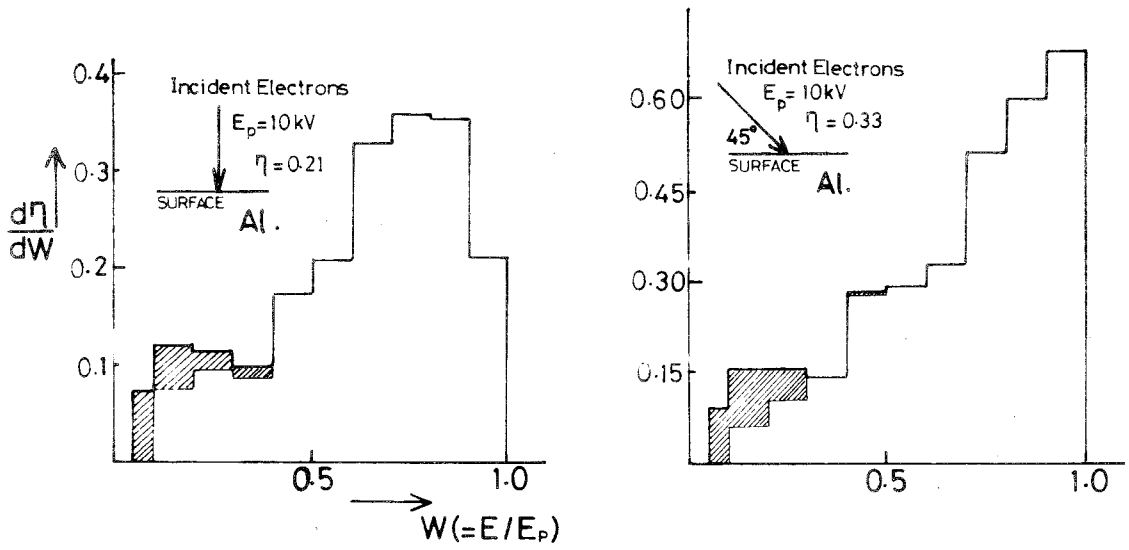


Fig. 2-11. Energy distribution of the backscattered and secondary electrons for 10-keV electrons impinging on aluminum at normal and oblique incidences. (Hatched area: signals generated by secondary electrons.)

of L-shell ionizations (corresponding to LVV- Auger electrons) produced by the secondary and backscattered electrons on the Al-specimen surface is shown in Fig.2-12 together with that of K-shell ionizations (corresponding to KLL-Auger electrons). It is worth nothing that almost half of the LVV-Auger electrons and about 30% of the KLL-Auger electrons are produced by the secondary and backscattered electrons. Another point to be noted

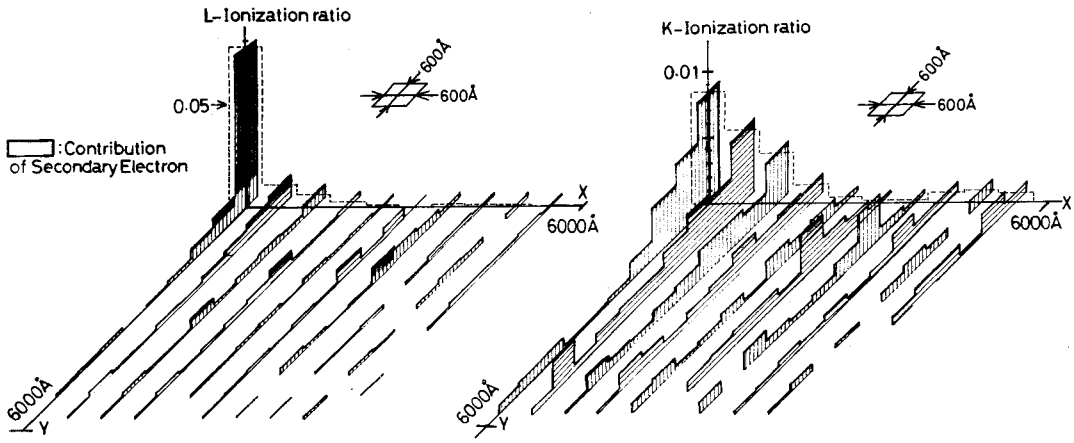


Fig. 2-12. Spatial distributions of $K$ and $L$ ionizations generated by 10 keV electrons in the surface layer of aluminum. The longitudinal axes indicate $K$- and $L$-ionization ratio of the sectional contributions per 600 Å, of backscattered and secondary electron to the contribution of an incident electron. (Solid area, signals generated by secondary electrons.)

a) $L$ ionizations in the surface layer of 1 Å by the contribution of one primary electron: $1.02\times10^{-3}$ /Å. $L$ ionizations by the total contributions of backscattered and secondary electrons: $8.9\times10^{-4}$ /Å. (b) $K$ ionizations in the surface layer of 1 Å by the contribution of one primary electron: $6.5\times10^{-6}$ /Å. $K$ ionizations by the total contributions of backscattered and secondary electrons: $2.7\times10^{-6}$/Å.

is that the contribution of secondary electrons to L ionization is remarkable at the vicinity of the incident primary beam impact as is seen in Fig.2-12-b. This is quite understandable because the secondary electrons are generated almost normal to the direction of primary electrons of high energies, and, hence, they move parallel with the surface at the vicinity of the incident point leading to a high generation rate of L ionization in the surface layer in question.

# CHAPTER 3 THEORY OF ELECTRON-MERCURY INELASTIC SCATTERING ----- APPLICATION OF DWB THEORY

## 3-1 Introduction

In electron-mercury scattering, similarities in the diffraction patterns of elastic and inelastic cases had been previously recognized by Mohr and Nicoll (1932), and Tate and Palmer (1932) for intermediate energies. Inelastic scattering experiments with an energy analyser of high energy resolution also showed a diffraction pattern similar to elastic scattering at inelastic channels of $6^1P$ excitation (Gronemeier 1970), and $6^1P$ and $6p'^3P$ excitation channels (Hanne et al. 1972, Yamazaki et al. 1977c). These are the transitions of high scattering intensities in electron-mercury loss spectra. Polarization measurements of inelastic electrons have recently been made at $6^1P$ and $6p'^3P$ excitation channels, which also resulted in patterns similar to the elastic cases (Eitel and Kessler 1970, 1971, Hanne and Kessler 1972).

Penny (1932) and Yavorskii(1947) treated the total cross sections for excitation of $6^1P$ and $6^3P$ states in mercury using Born-Oppenheimer approximation. McConnell and Moiseiwitsch (1968) refined the above treatments using Born-Ochkur approximation. In regards to oscillator strength, the above treatment gave $f(^1P_1 \rightarrow {}^1S_1)=1.17$ and $f(^3P_1 \rightarrow {}^1S_0)=0.037$ which were in close agreement to the experimental values 1.18 and 0.037 (Lulio 1965). According to development in ESP measurements of inelastic channels, theoretical calculations of differential cross section and ESP at the $6^1P$ channel would be highly expected. One theoretical calculation has been made and resulted in success in a certain aspect using distorted wave Born approximation (DWB approximation) (Madison and Shelton 1973). However, this calculation is confined to rather lower impact energies (50-180 eV) and failed to give correct cross sections.

In this chapter, the $6^1P$ excitation cross section of electron-mercury scattering is discussed. For this purpose, the DWB approximation is formulated in detail at $6^1P$ excitation for the mercury atom and calculations are made for incident electron energies of 50 to 500 eV. This may provide detailed information on the scattering process, particularly on spin polarization in unresearched areas.

The reason for adopting the DWB approximation are as follows; First, Born approximation is known to give inadequate information on the differential scattering cross section at large scattering angles and in every case

predicts zero polarization (see Sec.2-2-2), thus in spite of its simplicity and clearness, Born approximation turns out to be useless. Second, the coupling between $6^1P$ excitation and elastic channels is generally weak (the intensity ratio between $6^1P$ excitation and elastic scattering is about $10^{-2}$ in both the energy and angular regions in question). This weak coupling implies that the scattering of electrons from the inelastic channels to the elastic channel is negligible. Thus, it may not be necessary to adopt an approximation as precise as the close-coupling approximation. Third, the similarity of diffraction patterns at elastic and $6^1P$ excitation scattering suggests that the elastic scattering plays a dominant role in the $6^1P$ excitation scattering.

This leads one to expect that the present DWB approximation would provide reasonable accuracy for the interpretation of $6^1P$ excitation scattering process. Furthermore, as there exist little theoretical results using DWB approximation except for the two works for heavy atoms (Sawada et al. 1971, Madison and Shelton 1973), it is interesting to apply the relativistic DWB approximation to the calculation of cross section and spin polarization of electron-mercury scattering.

## 3-2 DWB Approximation

As is shown in Sec.2-2-1, the formal solution for the wave equation $H\psi_\alpha = W_\alpha \psi_\alpha$ is written implicitly as

$$\psi_\alpha^{(+)} = \Phi_\alpha + \frac{1}{W_\alpha - K \pm i\varepsilon} V \psi_\alpha^{(+)} \quad , \tag{3-1}$$

$$K = H - V \quad . \tag{3-2}$$

The transition rate per unit time is given by (Gell-Mann and Goldberger 1953)

$$w_{ij} = 2\pi |T_{ij}|^2 \delta(W_i - W_j) \quad , \tag{3-3}$$

where

$$T_{ij} = \langle \Phi_j | V | \psi_i^{(+)} \rangle \quad . \tag{3-4}$$

In the case of $V = V_1 + V_2$ , equation (3-4) is written

$$T_{ij}=\langle \Phi_j \mid V_1+V_2 \mid \psi_i^{(+)} \rangle \quad . \tag{3-5}$$

Introducing the eigenfunctions of $K+V_1$ as

$$X_\alpha^{(+)}=\Phi_\alpha+\frac{1}{W-K\pm i\varepsilon}\ V_1 X_\alpha^{(+)} \ , \tag{3-6}$$

we can transform the equation (3-5) as follows,

$$\begin{aligned} T_{ij} &= \langle X_j^{(-)} - \frac{1}{W-K-i\varepsilon}\ V_1 X_j^{(-)} \mid V_1+V_2 \mid \psi_i^{(+)} \rangle \\ &= \langle X_j^{(-)} \mid V_1+V_2 \mid \psi_i^{(+)} \rangle - \langle X_j^{(-)} \mid V_1 \frac{1}{W-K+i\varepsilon}\ (V_1+V_2) \mid \psi_i^{(+)} \rangle \\ &= \langle X_j^{(-)} \mid V_1+V_2 \mid \psi_i^{(+)} \rangle - \langle X_j^{(-)} \mid V_1 \mid \psi_i^{(+)} - \Phi_i \rangle \\ &= \langle X_j^{(-)} \mid V_2 \mid \psi_i^{(+)} \rangle + \langle X_j^{(-)} \mid V_1 \mid \Phi_i \rangle \ . \end{aligned} \tag{3-7}$$

The ingoing distorted waves are related to outgoing waves by time reversal, which has the form (Satschler 1964)

$$\left(X_\alpha^{(-)}(\mathbf{k},\mathbf{r})\right)_{m',m} = (-1)^{m'-m}\left(X_\alpha^{(+)}(-\mathbf{k},\mathbf{r})\right)_{-m',-m} \tag{3-8}$$

(The appearance of the ingoing wave in scattering problem is qualitatively explained by Breit and Bethe (1954), and Wu and Ohmura (1962).)
Considering the inelastic scattering of an electron-atom system, we can set $V_1$ as the atomic potential and $V_2$ as the interaction potential between the incident and atomic electrons (see Sec. 3-3). In this case, the second term of equation (3-7) vanishes because of the orthogonality of ground and excited states of atomic electrons. Then, equation (3-8) is written

$$T_{ij} = \langle X_j^{(-)} \mid V_2 \mid \psi_i^{(+)} \rangle \ . \tag{3-9}$$

Note must be made of the fact that equation (3-9) is an exact solution of the problem.

In equation (3-9), if the atomic potential $V_1$ is substantially larger than the interaction potential $V_2$, then we may substitute $X_i^{(+)}$ for $\psi_i^{(+)}$ and get

$$T_{ij}=\langle X_j^{(-)} \mid V_2 \mid X_i^{(+)} \rangle \ . \tag{3-10}$$

Equation (3-10) is called distorted wave Born (DWB) approximation, since Born approximation is obtained if $X_j^{(-)}$ and $X_i^{(+)}$ are replaced by plane waves. That is, DWB approximation introduces the effect of distortion of plane wave by the core potential on inelastic scattering.

To clarify the physical aspects of the DWB approximation, we will view scattering of electrons with hydrogen atoms non-relativistically. The wave equation for the system is written

$$\{\tfrac{1}{2}\cdot(\nabla_1^2+\nabla_2^2)+E+e^2/r_1+e^2/r_2-e^2/r_{12}\}\psi=0\ , \tag{3-11}$$

where the incident electron is distinguished by the suffix 1, the atomic electron by the suffix 2. The energy $E$ is the sum of the energy $E_0$ of the atomic electron in its ground state and of the kinetic energy of the incident electron. We may expand the function $\psi(\mathbf{r}_1, \mathbf{r}_2)$ in the form

$$\psi(\mathbf{r}_1, \mathbf{r}_2) = (\sum_n + \int)\psi_n(\mathbf{r}_2)\cdot F_n(\mathbf{r}_1) \tag{3-12}$$

where the functions $\psi_n(\mathbf{r})$ are the eigenfunction for the hydrogen atom, satisfying

$$(\tfrac{1}{2}\nabla^2 + E_n + e^2/r)\,\psi_n(r) = 0\ . \tag{3-13}$$

The integral sign denotes integration over the functions of the continuous spectrum. Substituting equation (3-12) in equation (3-11) using equation (3-13) and multiplying $\psi_n^*(\mathbf{r}_2)$ on both sides of this equation and integrating over the coordinate space of the atomic electron, we obtain

$$(\frac{\nabla_1^2}{2}+E-E_n)\,F_n(\mathbf{r}_1) = \int(e^2/r_{12}-e^2/r_1)\,\psi(\mathbf{r}_1,\mathbf{r}_2)\cdot\psi_n^*(\mathbf{r}_2)\,d\mathbf{r}_2\ . \tag{3-14}$$

Writing

$$V_{nm}(\mathbf{r}_1) = \int\psi_n^*(\mathbf{r}_2)\,e^2/r_{12}\cdot\psi_m(\mathbf{r}_2)\,d\mathbf{r}_2\ , \tag{3-15}$$

we have

$$(\nabla^2/2+E-E_n)\,F_n(\mathbf{r}) = \sum_m V_{nm}F_m(\mathbf{r})\ . \tag{3-16}$$

If $V_{nm}(n\geq 0, m\geq 1, n\neq m)$ is neglected in equation (3-16), then we obtain

$$(\nabla^2/2+E-E_0-V_{00})\,F_0 = 0 \qquad (3\text{-}17\text{-a})$$

$$(\nabla^2/2+E-E_i-V_{ii})\,F_i = V_{io}\,F_0\ . \qquad (3\text{-}17\text{-b})$$

Equation (3-17-a) is merely the ordinary equation for elastic scattering with atomic potential $V_{00}$, which can be solved by the same method developed in Sec.2-3. As $F_0$ is known, the equation (3-17-b) becomes a simple inhomogenious differential equation which can be easily solved (Mott and Massey 1965) as

$$F_i(r,\theta,\phi) \sim -\frac{1}{2\pi}\,r^{-1}\,e^{iK_i r}\int V_{io}(r',\theta',\phi')\cdot F_0(r',\theta',\phi')\,f_i(r',\pi-\Theta)\,d\mathbf{r}' \qquad (3\text{-}18)$$

where $f_i$ satisfies

$$(\nabla^2/2+E-E_i-V_{ii})\,f_i(\mathbf{r}) = 0\ , \qquad (3\text{-}19)$$

and $\cos(\Theta) = \cos\theta\cos\theta' + \sin\theta\sin\theta'\cos(\phi-\phi')$.

As equation (3-18) equals equation (3-10), the essential points concerning DWB approximation are concluded as follows:
1) neglect of the scattering from inelastic states to the elastic state and
2) neglect of the interaction between the arbitral set of inelastic states.
The "Born" of DWB stems from the approximation mentioned above.

From another view points, DWB approximation is one of the first order perturbation where $K+V$ is chosen as the unperturbed Hamiltonian. On the other hand, Born approximation is the first order perturbation theory where $K$ is chosen as the unperturbed Hamiltonian.

## 3-3. Application of DWB Approximation to Electron-Impact Excitation of $6^1P$ State of Mercury Atom

In this section, an attempt is made to rewrite the theoretical expression of DWB approximation in a more concrete form for practical use.

The electron configuration in the mercury atom is expressed as $(1s)^2(2s)^2.....(5d)^{10}(6s)^2$. In as far as the $6^1P$ excitation is concerned, the atomic electrons interacting directly with incident electrons are confined

to electrons in the 6s shell. Therefore, it is assumed that atomic electrons other than $(6s)^2$ do not interact directly with the incident electrons. Then, the total Hamiltonian $H$ is written as

$$H = H_0(\mathbf{r}) + H_1(\mathbf{r}_1, \mathbf{r}_2) + \sum_{l=1,2} \frac{e^2}{|\mathbf{r}-\mathbf{r}_l|} , \tag{3-20}$$

where $\mathbf{r}$ and $\mathbf{r}_l\,(l=1,2)$ correspond to incident and 6s electrons respectively and

$$H_0(\mathbf{r}) = K_r + V_{z-2}(\mathbf{r}) \tag{3-21}$$

$$H_1(\mathbf{r}_1, \mathbf{r}_2) = K_{r_1} + K_{r_2} + V_{z-2}(\mathbf{r}_1) + V_{z-2}(\mathbf{r}_2) + \frac{e^2}{|\mathbf{r}_1 - \mathbf{r}_2|} , \tag{3-22}$$

where $K$ is kinetic energy and $V_{z-2}$ the atomic potential energy composed of a mercury nucleus and core electrons. We will rearrange the above Hamiltonian as follows,

$$H_\alpha = K_r + V_z^\alpha(r) + H_1(\mathbf{r}_1, \mathbf{r}_2) \tag{3-23}$$

$$u_\alpha = -V_z^\alpha(r) + V_{z-2}(r) + \sum_{l=1,2} \frac{e^2}{|\mathbf{r}-\mathbf{r}_l|} , \tag{3-24}$$

where

$$V_z^\alpha(r) = V_{z-2}(r) + \langle \xi_\alpha | \sum_{l=1,2} \frac{e^2}{|\mathbf{r}-\mathbf{r}_l|} | \xi_\alpha \rangle , \tag{3-25}$$

and

$$H_1(\mathbf{r}_1, \mathbf{r}_2)\,\xi_\alpha = E_\alpha\,\xi_\alpha , \tag{3-26}$$

where $\alpha$ takes values $i$ and $j$ according to the atomic states before and after scattering, respectively. The potential $V_2$ in equation (3-10) corresponds to the $u_\alpha$ of equation (3-24). Then, the distorted wave function $X_\alpha$ is written as

$$X_\alpha(\mathbf{r}, \mathbf{r}_1, \mathbf{r}_2) = X_\alpha^0(\mathbf{r}) \cdot \xi_\alpha(\mathbf{r}_1, \mathbf{r}_2) , \tag{3-27}$$

and $X_\alpha^0$ satisfies

$$(K_r + V_z^\alpha)\, X_\alpha^0 = (W - E_\alpha)\, X_\alpha^0 . \tag{3-28}$$

The $u_i$ and $u_j$ differ outwardly from each other but have like effects on equation (3-10) because $\xi_i$ and $\xi_j$ belong to different eigenvalues of the same Hamiltonian. Namely, from equation (3-10)

$$T_{ij}=\langle X_j^{0(-)}\xi_j \mid -V_z^{\alpha}(r)+V_{z-2}(r)+\sum_{l=1,2}\frac{e^2}{\mid r-r_l\mid}\mid X_i^{0(+)}\xi_i\rangle$$

$$=\langle X_j^{0(-)}\mid\langle\xi_j\mid\sum_{l=1,2}\frac{e^2}{\mid \mathbf{r}-\mathbf{r}_l\mid}\mid\xi_i\rangle\mid X_i^{0(+)}\rangle \quad . \tag{3-29}$$

For further calculation, we take $\xi_i$ and $\xi_j$ as $(6s)^2\,{}^1S$ ground state and $(6s)(6p)\,{}^1P$ excited state respectively. We may write the wave function $\xi_i$ in the form

$$\xi_i=\phi_0(1,2)\cdot\zeta_0(1,2) \quad , \tag{3-30}$$

with

$$\phi_0(1,2)=Y_{00}(\theta_1,\phi_1)\cdot R_{00}(r_1)\cdot Y_{00}(\theta_2,\phi_2)\cdot R_{00}(r_2) \quad , \tag{3-31}$$

where $Y_{lm}(\theta,\phi)$ is a spherical harmonic, $R_{00}(r)$ the radial wave function for the 6s electrons, and $\zeta_0(1,2)$ the singlet spin function associated with spin quantum number $S=M_S=0$. Concerning $\xi_j$, we ignore spin-orbit coupling for simplicity and introduce pure Russel-Saunders P-state wave functions given by

$$\xi_j=\sum_{M_L,M_S}C(J,1,S;M_L,M_S)\cdot\phi^S_{1M_L}(1,2)\cdot\zeta_{SM_S}(1,2) \quad , \tag{3-32}$$

where the $C(J,1,S;M_L,M_S)$ are Clebsch-Gordan coefficients shown in Table 3-1,

$$\phi^S_{1M_L}(1,2)=\frac{1}{\sqrt{2}}\Big\{Y_{00}(\theta_1,\phi_1)\cdot R_{10}(r_1)\cdot Y_{1M_L}(\theta_2,\phi_2)\cdot R_{11}(r_2)$$

$$\pm Y_{00}(\theta_2,\phi_2)\cdot R_{10}(r_2)\cdot Y_{1M_L}(\theta_1\,\phi_1)\cdot R_{11}(r_1)\Big\} \tag{3-33}$$

$$(+:S=0\,,-:S=1)$$

are the spacial wave functions with radial functions $R_{10}$ and $R_{11}$ for the 6s and 6P electrons respectively and $\zeta_{SM_S}$ is the spin function for the two electrons associated with spin quantum numbers $S$ and $M_S$.

Table 3-1. Clebsch-Gordan coefficients $(J, 1, S; M-M_S, M_S)$.

| S= | $M_S=1$ | $M_S=0$ | $M_S=-1$ |
|---|---|---|---|
| J+1 | $\left[\frac{(J+M)(J+M+1)}{(2J+1)(2J+2)}\right]^{1/2}$ | $\left[\frac{(J-M+1)(J+M+1)}{(2J+1)(J+1)}\right]^{1/2}$ | $\left[\frac{(J-M)(J-M+1)}{(2J+1)(2J+2)}\right]^{1/2}$ |
| J | $-\left[\frac{(J+M)(J-M+1)}{2J(J+1)}\right]^{1/2}$ | $\frac{M}{[J(J+1)]^{1/2}}$ | $\left[\frac{(J-M)(J+M+1)}{2J(J+1)}\right]^{1/2}$ |
| J-1 | $\left[\frac{(J-M)(J-M+1)}{2J(2J+1)}\right]^{1/2}$ | $\left[\frac{(J-M)(J+M)}{J(2J+1)}\right]^{1/2}$ | $\left[\frac{(J+M+1)(J+M)}{2J(2J+1)}\right]^{1/2}$ |

The inner parenthesis of equation (3-29) can be easily calculated since the operators in equation (3-29) do not contain spin operator and the matrix elements corresponding to different spin quantum numbers vanish (This means that one of the selection rules corresponding to the conservation of multiplicity holds in DWB approximation.). It is found that

$$V^{M_L}_{1\,0}(r,\theta,\phi) \equiv <\xi_i| \sum_l \frac{e^2}{|\mathbf{r}-\mathbf{r}_l|} |\xi_j>$$

$$= \frac{(8\pi)^{1/2}}{3} e^2(\phi_{10},\phi_{00}) <\phi_{11}| F_1(r_1,r) |\phi_{00}> Y^*_{1,M_L}(\theta,\phi) \qquad (3\text{-}34)$$

$$\equiv v_{10} \cdot Y^*_{1,M_L}(\theta,\phi)$$

with

$$F_n(r_1, r) = \begin{cases} \frac{1}{r_1}\left(\frac{r}{r_1}\right)^n & r_1 > r \\ \frac{1}{r}\left(\frac{r_1}{r}\right)^n & r > r_1 \end{cases} \tag{3-35}$$

In equation (3-34) the following formulae are used

$$\frac{1}{|\mathbf{r}-\mathbf{r}_1|} = \begin{cases} \frac{1}{|\mathbf{r}_1|}\sum_{n=0}^{\infty}\left|\frac{\mathbf{r}}{\mathbf{r}_1}\right|^n P_n(\cos\gamma), & r_1 > r \\ \frac{1}{|\mathbf{r}|}\sum_{n=0}^{\infty}\left|\frac{\mathbf{r}_1}{\mathbf{r}}\right|^n P_n(\cos\gamma), & r > r_1 \end{cases} \tag{3-36}$$

where $\gamma$ is an angle formed by the two vectors $\mathbf{r}$ and $\mathbf{r}_1$,

$$P_n(\cos\gamma) = \frac{4\pi}{2n+1}\sum_m Y^*_{n,m}(\theta_1, \phi_1)\cdot Y_{n,m}(\theta_2, \phi_2) \tag{3-37}$$

and

$$\int Y^*_{n_1,m_1} Y_{1,m} Y_{n_2,m_2}\, d\Omega = \left(\frac{3}{4\pi}\right)^{1/2}\left(\frac{2n_2+1}{2n_1+1}\right)^{1/2} C(n_2, 1, n_1; m_2, m) * C(n_2, 1, n_1; 0, 0). \tag{3-38}$$

As can be seen from equations (3-34) and (3-35), the form factor $v_{01}$, the radial part of the effective potential which causes $6^1S \to 6^1P$ excitation behaves like $r^{-2}$ at large $r$, corresponding to the induction of the electric dipole moment. In general, the form factors appearing in various excitation processes behave like $r^{-n}$ in correspondence to the various multipole moment induced. This also implies that among the various transitions, those corresponding to a momentum transfer of one unit may be relatively strong since the form factor corresponding to these transitions decreases most slowly.

The wave functions $X^{(+)}$ and $X^{(-)}$ can be easily written using the equation (2-17) for the two initial spin states in Sec.2-2-1 as

$$X_i^{(-)}\uparrow = 4\pi \begin{pmatrix} \sum_{l=0}\sum_{\mu}\frac{e^{i\frac{\pi}{2}l}}{2l+1}\left\{(l+\mu+1/2)\, G_l\, e^{-i\eta_l} + (l-\mu+1/2)\, G_{-l-1} e^{-\eta_{-l-1}}\right\}\cdot \\ -\sum_{l=1}\sum_{\mu}\frac{e^{i\frac{\pi}{2}l}}{2l+1}\,(l-\mu+1/2)^{1/2}(l+\mu+1/2)^{1/2}(-G_l\, e^{-\eta_l} + G_{-l-1}\, e^{i\eta_{-l-1}})\cdot \\ Y_{l,\mu+1/2}(\theta,\phi)\cdot Y^*_{l,\mu+1/2}(\theta',\phi') \\ Y_{l,\mu+1/2}(\theta,\phi)\cdot Y^*_{l,\mu-1/2}(\theta',\phi') \end{pmatrix} \tag{3-39-a}$$

$$X_{i\downarrow}^{(-)} = 4\pi \Bigg( -\sum_{l=1}\sum_{\mu} \frac{e^{i\frac{\pi}{2}l}}{(2l+1)} (l+\mu+\tfrac{1}{2})^{\frac{1}{2}} (l-\mu+\tfrac{1}{2})^{\frac{1}{2}} (-G_l e^{-i\eta_{l+}} G_{-l-1} e^{-i\eta_{-l-1}})$$
$$\sum_{l=0}\sum_{\mu} \frac{e^{i\pi/2 \cdot l}}{(2l+1)} \{ (l-\mu+\tfrac{1}{2}) G_l e^{-i\eta_l} + (l+\mu+\tfrac{1}{2}) G_{-l-1} e^{-i\eta_{-l-1}} \}$$
$$Y_{l,\mu-\frac{1}{2}}(\theta,\phi) \cdot Y^{*}_{l,\mu+\frac{1}{2}}(\theta',\phi')$$
$$Y_{l,\mu-\frac{1}{2}}(\theta,\phi) \cdot Y^{*}_{l,\mu-\frac{1}{2}}(\theta'\ \phi') \Bigg) \qquad (3\text{-}39\text{-}b)$$

and using $Y_{l0} = \left[(2l+1)/4\pi\right]^{\frac{1}{2}}$

$$X_{j\uparrow}^{(+)} = (4\pi)^{\frac{1}{2}} \begin{pmatrix} \sum_{l=0} \dfrac{e^{i\frac{\pi}{2}l}}{(2l+1)^{\frac{1}{2}}} \{ l\, g_l\, e^{i\delta_l} + (l+1) \cdot g_{-l-1} e^{i\delta_{-l-1}} \} Y_{l,0}(\theta',\phi') \\ \sum_{l=1} \dfrac{e^{i\frac{\pi}{2}l}}{(2l+1)^{\frac{1}{2}}} \cdot (l+1)^{\frac{1}{2}} \cdot l^{\frac{1}{2}} \cdot (-g_l e^{i\delta_l} + g_{-l-1} e^{i\delta_{-l-1}}) Y_{l,1}(\theta'\ \phi') \end{pmatrix} \qquad (3\text{-}40\text{-}a)$$

$$X_{j}^{(+)} = (4\pi)^{\frac{1}{2}} \begin{pmatrix} \sum_{l=1} \dfrac{e^{i\frac{\pi}{2}l}}{(2l+1)^{\frac{1}{2}}} \cdot (l+1)^{\frac{1}{2}} \cdot l^{\frac{1}{2}} \cdot (-g_l e^{i\delta_l} + g_{-l-1} e^{i\delta_{-l-1}}) \cdot Y_{l,-1}(\theta'\ \phi') \\ \sum_{l=0} \dfrac{e^{i\frac{\pi}{2}l}}{(2l+1)^{\frac{1}{2}}} \cdot \{ l \cdot g_l \cdot e^{i\delta_l} + (l+1) \cdot g_{-l-1} \cdot e^{i\delta_{-l-1}} \} \cdot Y_{l,0}(\theta'\ \phi') \end{pmatrix} \qquad (3\text{-}40\text{-}b)$$

where the notation $G_\kappa$ and $\eta_\kappa$ are used for the state elastically scattered by the potential of the excited-state atom in the direction $\mathbf{k} = (K_f, \theta, \phi)$, $g_\kappa$ and $\delta_\kappa$ for the state elastically scattered by the potential of the ground-state atom in the direction of $\mathbf{k}' = (K_i, 0, 0)$ and the coordinates of the incident or scattered electrons are represented by $\mathbf{r}' = (r, \theta', \phi')$. The suffix 0 of $X$ is omitted for simplicity (see equation (3-29)). The sign in front of $\eta_\kappa$ changes depending upon the boundary conditions of incoming waves.

Using the $a^{i}_{l\mu}$ and $b^{i}_{l\mu}$ defined by

$$a^{1}_{l\mu} = \frac{4\pi e^{i\frac{\pi}{2}l}}{2l+1} \{ (l+\mu+\tfrac{1}{2}) \cdot G_l \cdot e^{-i\eta_l} + (l-\mu+\tfrac{1}{2}) \cdot G_{-l-1} \cdot e^{-i\eta_{-l-1}} \} \qquad (3\text{-}41\text{-}a)$$

$$b^{1}_{l\mu} = -\frac{4\pi e^{i\frac{\pi}{2}l}}{2l+1} \cdot (l-\mu+\tfrac{1}{2})^{\frac{1}{2}} \cdot (l+\mu+\tfrac{1}{2})^{\frac{1}{2}} \cdot (-G_l \cdot e^{-i\eta_l} + G_{-l-1} \cdot e^{-i\eta_{-l-1}}) \qquad (3\text{-}41\text{-}b)$$

$$a^2_l = \frac{(4\pi)^{1/2} e^{i\frac{\pi}{2}l}}{(2l+1)^{1/2}} (l \cdot g_l \cdot e^{i\delta_l} + (l+1) \cdot g_{-l-1} \cdot e^{i\delta_{-l-1}}) \qquad (3\text{-}42\text{-}a)$$

$$b^2_l = \frac{(4\pi)^{1/2} e^{i\frac{\pi}{2}l}}{(2l+1)^{1/2}} \cdot (l+1)^{1/2} \cdot l^{1/2} \cdot (-g_l \cdot e^{i\delta_l} + g_{-l-1} \cdot e^{i\delta_{-l-1}}) , \qquad (3\text{-}42\text{-}b)$$

we can rewrite equations (3-39) and (3-40) as follows;

$$X^{(-)}_{i\uparrow} = \begin{pmatrix} \sum_{l=0} \sum_{\mu} a^1_{l\mu} \cdot Y_{l,\mu+1/2}(\theta,\phi) \cdot Y^*_{l,\mu+1/2}(\theta',\phi') \\ \sum_{l=1} \sum_{\mu} b^1_{l\mu} \cdot Y_{l,\mu+1/2}(\theta,\phi) \cdot Y^*_{l,\mu-1/2}(\theta',\phi') \end{pmatrix} \qquad (3\text{-}43\text{-}a)$$

$$X^{(-)}_{i\downarrow} = \begin{pmatrix} \sum_{l=1} \sum_{\mu} b^1_{l\mu} \cdot Y_{l,\mu-1/2}(\theta,\phi) \cdot Y^*_{l,\mu+1/2}(\theta',\phi') \\ \sum_{l=0} \sum_{\mu} a^1_{l,-\mu} \cdot Y_{l,\mu-1/2}(\theta,\phi) \cdot Y_{l,\mu-1/2}(\theta',\phi') \end{pmatrix} \qquad (3\text{-}43\text{-}b)$$

$$X^{(+)}_{j} = \begin{pmatrix} \sum_{l=0} a^2_l \cdot Y_{l,0}(\theta',\phi') \\ \sum_{l=1} b^2_l \cdot Y_{l,1}(\theta',\phi') \end{pmatrix} \qquad (3\text{-}44\text{-}a)$$

$$X^{(+)}_{j} = \begin{pmatrix} \sum_{l=1} b^2_l \cdot Y_{l,-1}(\theta',\phi') \\ \sum_{l=0} a^2_l \cdot Y_{l,0}(\theta',\phi') \end{pmatrix} . \qquad (3\text{-}44\text{-}b)$$

Then T-matrix of equation (3-29) for various spin states are expressed as

$$T^m_{\uparrow\uparrow} = \langle X^{(-)}_{i\uparrow} | V^m_{01} | X^{(+)}_{j\uparrow} \rangle$$
$$= \sum_{l=0} \sum_{l'=0} \sum_{\mu} (a^{1*}_{l\mu} | v_{01} | a^2_{l'}) (Y_{l,\mu+1/2}, Y^*_{1m} \cdot Y_{l',0}) Y^*_{l,\mu+1/2}(\theta,\phi)$$
$$+ \sum_{l=1} \sum_{l'=1} \sum_{\mu} (b^{1*}_{l\mu} | v_{01} | b^2_{l'}) (Y_{l,\mu-1/2}, Y^*_{1m} \cdot Y_{l',1}) \cdot Y^*_{l,\mu+1/2}(\theta,\phi)$$

$$= \sum_{l=1} (a^{1*}_{l,-\frac{1}{2}+m} | v_{01} | a^{2}_{l-1}) \left(\frac{3}{4\pi}\right)^{\frac{1}{2}} \left(\frac{l}{2l+1}\right)^{\frac{1}{2}} C(l-1,1,l;0,m) Y^{*}_{l,m}$$

$$- \sum_{l=0} (a^{1*}_{l,-\frac{1}{2}+m} | v_{01} | a^{2}_{l+1}) \left(\frac{3}{4\pi}\right)^{\frac{1}{2}} \left(\frac{l+1}{2l+1}\right)^{\frac{1}{2}} C(l+1,1,l;0,m) Y^{*}_{l,m}$$

$$+ \sum_{l=1} (b^{1*}_{l,-\frac{1}{2}+m} | v_{01} | b^{2}_{l+1}) \left(\frac{3}{4\pi}\right)^{\frac{1}{2}} \left(\frac{l+1}{2l+1}\right)^{\frac{1}{2}} C(l+1,1,l;-1,m) Y^{*}_{l,m}$$

$$- \sum_{l=2} (b^{1*}_{l,-\frac{1}{2}+m} | v_{01} | b^{2}_{l-1}) \left(\frac{3}{4\pi}\right)^{\frac{1}{2}} \left(\frac{l}{2l+1}\right)^{\frac{1}{2}} C(l-1,1,l;-1,m) Y^{*}_{l,m}$$

(3-45-a)

$$T^{m}_{\downarrow\downarrow} = \langle X^{(-)}_{i\downarrow} | V^{m}_{01} | X^{(+)}_{j\uparrow} \rangle$$

$$= \sum_{l=1} \sum_{l'=0} \sum_{\mu} (b^{1*}_{l\mu} | v_{01} | a^{2}_{l'}) (Y_{l,\mu+\frac{1}{2}}, Y^{*}_{1m} Y_{l',0}) Y^{*}_{l,\mu-\frac{1}{2}}(\theta,\phi)$$

$$+ \sum_{l=0} \sum_{l'=1} \sum_{\mu} (a^{1*}_{l,-\mu} | v_{01} | b^{2}_{l'}) (Y_{l,\mu-\frac{1}{2}}, Y^{*}_{1m} Y_{l',1}) Y_{l,\mu-\frac{1}{2}}(\theta,\phi)$$

$$= \sum_{l=1} (b^{1*}_{l,-\frac{1}{2}+m} | v_{01} | a^{2}_{l-1}) \left(\frac{3}{4\pi}\right)^{\frac{1}{2}} \left(\frac{l}{2l+1}\right)^{\frac{1}{2}} C(l-1,1,l;0,m) Y^{*}_{l,m-1}$$

$$- \sum_{l=1} b^{1*}_{l,-\frac{1}{2}+m} | v_{01} | a^{2}_{l+1}) \left(\frac{3}{4\pi}\right)^{\frac{1}{2}} \left(\frac{l+1}{2l+1}\right)^{\frac{1}{2}} C(l+1,1\ l;0,m) Y^{*}_{l,m-1}$$

$$+ \sum_{l=0} (a^{1*}_{l,-m+\frac{1}{2}} | v_{01} | b^{2}_{l+1}) \left(\frac{3}{4\pi}\right)^{\frac{1}{2}} \left(\frac{l+1}{2l+1}\right)^{\frac{1}{2}} C(l+1,1,l;-1,m) Y^{*}_{l,-1+m}$$

$$- \sum_{l=2} (a^{1*}_{l,-m+\frac{1}{2}} | v_{01} | b^{2}_{l-1}) \left(\frac{3}{4\pi}\right)^{\frac{1}{2}} \left(\frac{l}{2l+1}\right)^{\frac{1}{2}} C(l-1,1,l;-1,m) Y^{*}_{l,-1+m}$$

(3-45-b)

$$T^{m}_{\uparrow\uparrow} = \langle X^{(-)}_{i\uparrow} | V^{m}_{01} | X^{(+)}_{j\downarrow} \rangle$$

$$= \sum_{l=0} \sum_{l'=1,\mu} (a^{1*}_{l,\mu} | v_{01} | b^{2}_{l'}) (Y_{l,\mu+\frac{1}{2}}, Y^{*}_{1m} Y^{*}_{l',-1}) Y^{*}_{l,\mu+\frac{1}{2}}(\theta,\phi)$$

$$+ \sum_{l=1} \sum_{l'=0,\mu} (b^{1*}_{l\mu} | v_{01} | a^{2}_{l'}) (Y_{l,\mu-\frac{1}{2}}, Y^{*}_{1m} Y_{l',0}) Y^{*}_{l,\mu+\frac{1}{2}}(\theta,\phi)$$

$$= \sum_{l=0} (a^{1*}_{l,m+\frac{1}{2}} | v_{01} | b^{2}_{l+1}) \left(\frac{3}{4\pi}\right)^{\frac{1}{2}} \left(\frac{l+1}{2l+1}\right)^{\frac{1}{2}} C(l+1,1,l;1,m) Y^{*}_{l,m+1}$$

$$- \sum_{l=2} (a^{1*}_{l,m+\frac{1}{2}} | v_{01} | b^{2}_{l-1}) \left(\frac{3}{4\pi}\right)^{\frac{1}{2}} \left(\frac{l}{2l+1}\right)^{\frac{1}{2}} C(l-1,1,l;1,m) Y^{*}_{l,m+1}$$

$$+\sum_{l=1}(b^{1*}_{l,m+1/2}|v_{01}|a^{2}_{l-1})(\frac{3}{4\pi})^{1/2}(\frac{l}{2l+1})^{1/2}C(l-1,1,l;0,m)Y^{*}_{l,m+1}$$

$$-\sum_{l=1}(b^{1*}_{l,m+1/2}|v_{01}|a^{2}_{l+1})(\frac{3}{4\pi})^{1/2}(\frac{l+1}{2l+1})^{1/2}C(l+1,1,l;0,m)Y^{*}_{l,m+1} \quad (3\text{-}45\text{-c})$$

$$T^{m}_{\downarrow\downarrow} = \langle X^{(-)}_{i\downarrow}|V^{m}_{01}|X^{(+)}_{j\downarrow}\rangle$$

$$= \sum_{l=1}\sum_{l'=1}\sum_{\mu}(b^{1*}_{l\mu}|v_{01}|b^{2}_{l'})(Y_{l,\mu+1/2},Y^{*}_{1m}Y_{l',-1})Y^{*}_{l,\mu-1/2}(\theta,\phi)$$

$$+\sum_{l=0}\sum_{l'=0}\sum_{\mu}(a^{1*}_{l,-\mu}|v_{01}|a^{2}_{l'})(Y_{l,\mu-1/2},Y^{*}_{1m}Y_{l',0})Y^{*}_{l,\mu-1/2}(\theta,\phi)$$

$$=\sum_{l=1}(b^{1*}_{l,m+1/2}|v_{01}|b^{2}_{l+1})(\frac{3}{4\pi})^{1/2}(\frac{l+1}{2l+1})^{1/2}C(l+1,1,l;1,m)Y^{*}_{l,m}$$

$$-\sum_{l=2}(b^{1*}_{l,m+1/2}|v_{01}|b^{2}_{l-1})(\frac{3}{4\pi})^{1/2}(\frac{l}{2l+1})^{1/2}C(l-1,1,l;1,m)Y^{*}_{l,m}$$

$$+\sum_{l=1}(a^{1*}_{l,-m-1/2}|v_{01}|a^{2}_{l-1})(\frac{3}{4\pi})^{1/2}(\frac{l}{2l+1})^{1/2}C(l-1,1,l;0,m)Y^{*}_{l,m}$$

$$-\sum_{l=0}(a^{1*}_{l,-m-1/2}|v_{01}|a^{2}_{l+1})(\frac{3}{4\pi})^{1/2}(\frac{l+1}{2l+1})^{1/2}C(l+1,1,l;0,m)Y^{*}_{l,m}\ . \quad (3\text{-}45\text{-d})$$

Here the equation (3-38) and Table 3-1 are used.

It is easily shown that

$$T^{1}_{\uparrow\uparrow}\ e^{i\phi} = -T^{-1}_{\downarrow\downarrow}e^{-i\phi} = T^{1}_{1} \quad (3\text{-}46\text{-a})$$

$$T^{0}_{\uparrow\uparrow} = -T^{0}_{\downarrow\downarrow} = T^{0}_{1} \quad (3\text{-}46\text{-b})$$

$$T^{-1}_{\uparrow\uparrow}e^{-i\phi} = -T^{1}_{\downarrow\downarrow}e^{i\phi} = T^{-1}_{1} \quad (3\text{-}46\text{-c})$$

$$T^{1}_{\downarrow\uparrow}\ e^{2i\phi} = T^{-1}_{\uparrow\downarrow}e^{-2i\phi} = T^{1}_{2} \quad (3\text{-}46\text{-d})$$

$$T^{0}_{\downarrow\uparrow}\ e^{i\phi} = -T^{0}_{\uparrow\downarrow}\ e^{-i\phi} = T^{0}_{2} \quad (3\text{-}46\text{-e})$$

$$T^{-1}_{\downarrow\uparrow} = T^{1}_{\uparrow\downarrow} = T^{-1}_{2} \quad (3\text{-}46\text{-f})$$

Comparison of the equations (3-41) and (3-42) with the equation (2-40) shows that the coefficients $a_{l\mu}^{i}$ ($b_{l\mu}^{i}$) represent the direct scattering (spin-flip) during the elastic processes occuring before and after the inelastic single process. Hence, the processes occuring during inelastic scattering are explained schematically from equation (3-45), e.g. $T_{\uparrow\downarrow(\downarrow\uparrow)}^{m}$ represents the process that initially, an incident electron undergoes a direct (spin-flip) elastic process followed by another single inelastic process and finally undergoes a spin-flip(direct) elastic process once more.

The relationship between T-matrix and scattering amplitude is given by (Schiff 1955)

$$f = -\frac{1}{2\pi} T . \tag{3-47}$$

Differential cross section and spin polarization are derived from the same procedures shown in Sec. 2-3. For the initial electron beams of $\phi_i = \binom{A}{B} e^{iKz}$ having polarization $\mathbf{p} = (p_x, p_y, p_z)$ the cross section is represented as,

$$\frac{d\sigma_{inel}}{d\Omega} = \frac{1}{4\pi^2}\frac{K_f}{K_i} < \sum_{j=1,0,-1} \left\{ |AT_{\uparrow\uparrow}^{j} + BT_{\uparrow\downarrow}^{j}|^2 + |BT_{\downarrow\downarrow}^{j} + AT_{\downarrow\uparrow}^{j}|^2 \right\} >$$

$$= \frac{1}{4\pi^2}\frac{K_f}{K_i} \sum_{j=1,0,-1} \left\{ \sum_{l=1,2} |T_l^j|^2 - 2\, Im\cdot (T_1^{j*} \cdot T_2^{j}) \cdot (-p_x \sin\phi + p_y \cos\phi) \right\} \tag{3-48}$$

where $K_i$ and $K_f$ are wave numbers of incident and scattered electrons. The comparison to equation (2-45) in Sec.2-3 shows a similar relation between the elastic and inelastic scattering cross section. Then the Sherman function $S_{inel}$ in inelastic scattering, the quantity relating to left-right asymmetry, may also be defined as

$$S_{inel} = -2 \sum_{j=-1,0,1} Im(T_1^{j*} T_2^{j}) \Big/ \sum_{l=1,2} \sum_{j=1,0,-1} |T_l^j|^2 \tag{3-49}$$

One the other hand, the ESP of inelastically scattered electrons are expressed as

$$\mathbf{P}_{inel} = \langle \sigma \rangle$$
$$= \Sigma \left( A^{*} T^{i*}_{\uparrow\uparrow} + B^{*} T^{i*}_{\downarrow\uparrow}, B^{*} T^{i*}_{\downarrow\downarrow} + A^{*} T^{i*}_{\uparrow\downarrow} \right) \sigma \begin{pmatrix} A T^{i}_{\uparrow\uparrow} + B T^{i}_{\downarrow\uparrow} \\ B T^{i}_{\downarrow\downarrow} + A T^{i}_{\uparrow\downarrow} \end{pmatrix} \quad (3\text{-}50)$$
$$= P_{inel} (-\sin\phi, \cos\phi, 0)$$

$$P_{inel} = 2 Im \left( T^{1*}_{1} T^{-1}_{2} - T^{0*}_{1} T^{0}_{2} + T^{-1*}_{1} T^{1}_{2} \right) / \sum_{l} \sum_{j} |T^{l}_{j}|^{2} , \quad (3\text{-}51)$$

where $\sigma$ denotes the Pauli matrix and < > denotes averages over all incident spin directions. The actual calculation shows that the $S_{inel}$ equals the $P_{inel}$.

As can be easily seen from equations (3-49) and (3-51), the effects of ESP becomes inexistent if all $T^{l}_{j}$ is a real or pure imaginary number i.e. the phase shifts $\eta_{\kappa}$ and $\delta_{\kappa}$ related to elastic scattering play an essential roles on the polarization effect of inelastic scattering.

## 3-4. Choice of Atomic Wave Function

The atomic potential used is the non-relativistic Hartree potential analytically expressed by Byatt (1956) (See Sec.2-2-3). The radial wave function of the ground state $(6s)^2$ and the excited state (6s)(6p) of the mercury atom used are those calculated by McConnell and Moiseiwitsch (1968) using the Coulomb approximation, since the results obtained using these wave functions were in excellent agreement with experiments as has been referred to in Sec.3-1. McConnell and Moiseiwitsch (1968) fitted these wave functions to a sum of exponentials

$$R_{00} = A_0 \exp(-a_0 r) + B_0 \exp(-b_0 r)$$
$$R_{10} = r A'_0 \exp(-a'_0 r) + B'_0 \exp(-b'_0 r)$$
$$R_{11} = r(A_1 \exp(-a_1 r) + B_1 \exp(-b_1 r)) , \quad (3\text{-}52\text{-}a)$$

with

$$A_0 = 0.907 \times 10^{-4}, a_0 = 0.612 \times 10^{-2}, B_0 = -0.425 \times 10^{-4}, b_0 = 0.144 \times 10^{-1}$$
$$A'_0 = 0.786 \times 10^{-6}, a'_0 = 0.884 \times 10^{-2}, B'_0 = -0.131 \times 10^{-3}, b'_0 = 0.196 \times 10^{-1}$$
$$A_1 = 0.103 \times 10^{-6}, a_1 = 0.410 \times 10^{-2}, B_1 = 0.303 \times 10^{-6}, b_1 = 0.164 \times 10^{-1} , \quad (3\text{-}52\text{-}b)$$

and evaluated the total $6^1P$ and $6^3P$ excitation cross section. The results calculated for these wave functions are shown in Fig.3-1, together with the

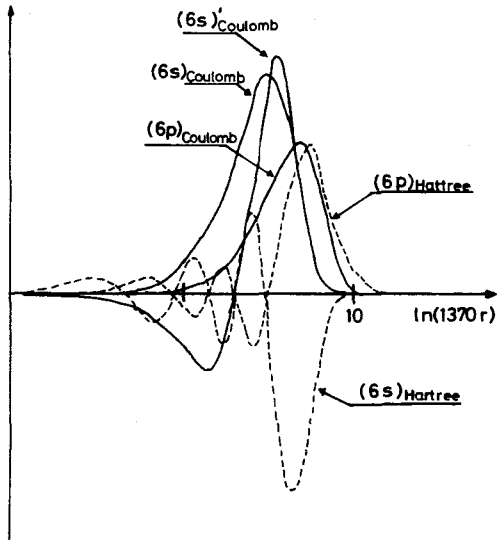


Fig.3-1. Radial wave functions for mercury, $(6s)_{Coulomb}$; Coulomb approximation for (6s) electron in $(6s)^2$ state, $(6s)'_{Coulomb}$; Coulomb approximation for (6s) electron in (6s)(6p) state, $(6p)_{Coulomb}$; Coulomb approximation for (6p) electron in (6s)(6p) state, $(6s)_{Hartree}$; Hartree approximation for (6s) electron in $(6s)^2$ and (6s)(6p) electron states and $(6p)_{Hartree}$; Hartree approximation for (6p) electron in (6s) (6p) state. (McConnell and Moiseiwitsch (1968) and Mishra (1952)).

results of self-consistent wave functions using Hartree field for the 6s orbital of the normal state $(6s)^2$ of neutral Hg (Mishra 1952). Note that the axis of abscissa is written in log-scale i.e. the departure between functions near $r \sim 0$ is emphasized too much.

It was assumed in the Coulomb approximation that the active electrons

(6s and 6p electrons in the present case) behave like the electrons moving in a Coulomb field $C/r$ having the same binding energy as the actual one, $C$ being the excess charge on the nucleus when the active electrons are removed. Although the wave functions obtained in this way are not the eigenfunctions of the Coulomb field, it is expected that they have satisfactory profiles and magnitudes except those near $r \sim 0$ (Bates and Damgaard 1949). This approximation is justified because the probability of the electrons in question, which exist in the inner part of the atom where the potential departs from $C/r$, is slight. This can be demonstrated for the oscillator strength by comparing

$$\int_0^{r_b} R_i \; R_f \; r^3 \mathrm{d}r \;, \tag{3-53-a}$$

and

$$\int_{r_b}^{\infty} R_i \; R_f \; r^3 \mathrm{d}r \;, \tag{3-53-b}$$

where $r_b$ is the boundary value of $r$ at which the atomic potential behaves like $C/r$, $R_i$ and $R_f$ initial and final radial wave functions respectively. Table 3-2 gives the relevant data for two cases of s-p transistions calculated using self-consistent wave functions (Bates and Damgaard 1949).

Table 3-2.

| System | Transition | $r_b$ (in unit of $a_0$) | $\int_0^{r_b}$ | $\int_{r_b}^{\infty}$ |
|---|---|---|---|---|
| Na I | 3s-4p | 1.5 | 0.004 | 0.386 |
| O II | 3s-3p | 2.0 | 0.05 | 4.02 |

Calculated results by McConnell and Moiseiwitsch agree well with the experiments. This confirms the usefulness of the Coulomb approximation, even though the 6s wave function used behaves like 1s or 2s electrons.
The oscillator strength for the $^1P_1 \rightarrow {}^1S_0$ transitions are given by the formulae

$$f = 2S^2\sigma^2/\lambda \;, \tag{3-54-a}$$

where

$$\sigma^2 = 1/3\left\{\int_0^\infty R_{00} R_{11} r^3 \, dr\right\}^2 \qquad (3-54-b)$$

$$S_{\cdot} = \int_0^\infty R_{00} \; R_{10} r^2 \, dr \quad , \qquad (3-54-c)$$

and $\lambda$ is the wave length of the radiation. Formula (3-54) results in the values

$$f_{coulomb} = 1.17 \qquad (3-55-a)$$

$$f_{Mishra} = 4.76 \qquad (3-55-b)$$

$$f_{Madison} = 8.8 \qquad (3-55-c)$$

corresponding to the wave functions of Coulomb approximation (McConnell and Moiseiwitsch 1965), of self-consistent approximation by Mishra(1952) and of self-consistent approximation by Madison and Shelton (1973). Madison and Shelton calculated the wave function as the eigenfunction of relativistic atomic ground-state potential. $f_{Coulomb}$ is in close agreement with the experimental value 1,18 of Lulio (1965). This implies that the Coulomb approximated wave functions can closely represent the states of the real atomic electrons, particularly their spacial distribution.

## 3-5. Adopted Numerical Calculation Procedures

The calculation procedures of $g_\kappa$ and $G_\kappa$ in equation (3-42) are like those in Sec. 2-3, but here both the phases $\phi_\kappa$ and amplitudes $A_\kappa$ will be estimated by the fourth order Lunge-Kutta process. '$B_0$', the normalization factor in equation (2-54-b) is determined by the first row of the equation (2-34).

The potential $V(r)$ is expressed using the charge distribution $\rho$ as

$$V'(r) = \frac{1}{r}\int_0^r \rho(r') \; r'^2 dr' + \int_r^\infty \rho(r') \; r' \, dr' \; . \qquad (3-56)$$

The first and second term are called inner and outer shielding, respectively (Slater 1960). From equation (3-56) and $\rho_{i(f)}(r) = e^2 | R_{i(f)} |^2$ we can construct the potential field of an excited state atom, which is necessary for evaluation of $G_\kappa$ in equation (3-39). The $V_{01}$ changes very slowly and is greater than the atomic potential $V_g$ and $V_e$ at $r \geq 340$ and $r \geq 390$ respectively. This is because $V_{01}$ behaves like $r^{-2}$ asymptotically at large $r$, as has been pointed out in Sec.3-3. As the form factor is the long range potential,

the number of partial waves necessary for the evaluation of T-matrix becomes quite large in comparison to those of elastic scattering. However, the number of partial waves distorted by the atomic potential is like those necessary in elastic scattering calculations. Contributions from the distorted partial waves are estimated as follows: 1) Equations (2-51-a) and (2-51-b) are solved numerically by the fourth order Lunge-Kutta process (see Sec.2-4), and the integrations necessary to evaluate T-matrix are performed by trapezoidal rule from $r=0.1$ to $r=r_0$ where $V(r_0)\sim 0$. 2) The phase shifts are estimated at $r=r_0$ and the T-matrix is again integrated numerically to $r=r_1$ using the first row of equation (2-34), the expression of $g_\kappa$ at large $r$ and we took $r_1=13700$ in most cases. Contributions to the T-matrix from the higher order partial waves originate from only the asymptotic region of the form factor, then analytical expression of these is possible using the formula (Watson 1966).

$$\int_0^\infty J_\mu(ax)\cdot J_\nu(bx)\cdot x^\lambda \,dx$$

$$= \frac{2^\lambda \cdot b^\nu \Gamma(\alpha)}{a^{\lambda+\mu+1}\Gamma(\nu+1)\cdot\Gamma(1-\beta)} F(\alpha,\beta,\nu+1;b^2/a^2)\ , \qquad (3-57-a)$$

where $J_\mu$ is the Bessel function of $\mu$-th order, $\mathrm{Re}(\lambda)<1$ , $\mathrm{Re}(\lambda+\mu+\nu)>-1$, $a>b>0$ , $\alpha=(\lambda+\mu+\nu+1)/2$ , $\beta=(\lambda-\mu+\nu+1)/2$ and $F(\alpha,\beta,\gamma;x)$ the hypergeometric function defined by

$$F(\alpha,\beta,\gamma;z)=\frac{\Gamma(\gamma)}{\Gamma(\alpha)\Gamma(\beta)}\sum_{n=0}^{\infty}\frac{\Gamma(\alpha+n)\Gamma(\beta+n)}{\Gamma(\gamma+n)}\frac{z^n}{n!}\ . \qquad (3-57-b)$$

Spherical harmonics are evaluated at each scattering angle using the recurrence relation as

$$Q_{l+1}^m=\left[\frac{(2l+1)(2l+3)}{(l+m+1)(l-m+1)}\right]^{1/2}\cdot z\cdot Q_l^m-\left[\frac{(2l+3)(l+m)(l-m)}{(2l-1)(l+m+1)(l-m+1)}\right]^{1/2}\cdot Q_{l-1}^m\ , \qquad (3-58)$$

where $Q_l^m(\theta)=Y_l^m(\theta,\phi)\,e^{-im\phi}$ with initial conditions

$$Q_0^0=(1/4\pi)^{1/2} \qquad (3-59-a)$$

$$Q_1^0=(3/4\pi)^{1/2}\cos\theta \qquad (3-59-b)$$

$$Q_1^{-1}=(3/8\pi)^{1/2}\sin\theta \qquad (3-59-c)$$

$$Q_2^0 = (5/4\pi)^{1/2} (3\cos^2\theta - 1)/2 \qquad (3\text{-}59\text{-d})$$

$$Q_2^{-1} = (15/8\pi)^{1/2} \sin\theta \cdot \cos\theta \qquad (3\text{-}59\text{-e})$$

$$Q_2^{-2} = (15/32\pi)^{1/2} \sin^2\theta \quad , \qquad (3\text{-}59\text{-f})$$

which are derived from

$$Q_l^m = \frac{1}{2^l\, l!} (-\sin\theta)^m (\mathrm{d}/\mathrm{d}\cos\theta)^{l+m} (\cos^2\theta - 1)^l \quad . \qquad (3\text{-}60)$$

The flow chart and the list of program for the present calculation is shown in Appendix 6.

## 3-6. Results and Discussion

The DWB calculations are performed for two form factors $F_C$ and $F_M$, where $F_C$ is obtained using the Coulomb approximated wave functions and $F_M$ is obtained from that used by Madison and Shelton (1973) with a slight modification (see Fig.3-2) which is performed to fit $F_M$ to analytical form for convenience in computer calculation. Actual calculation shows that the modification of this kind incurs little difference on calculated cross section and spin polarization. The calculated results are shown in Figs. 3-3 to 3-7 for electron impact energies between 50 and 500 eV. Each figure gives 1) a DWB calculation using $F_C$, 2) a DWB calculation using $F_M$, 3) an elastic scattering calculation of energy $E$ eV using atomic ground-state potential, 4) an elastic scattering calculation of energy $E$-6.7 eV using atomic excited-state potential and 5) experimental data when available. The experimental data are that of Hanne et al.(1972), Gronemeier (1970) and Yamazaki et al. (1977-c).

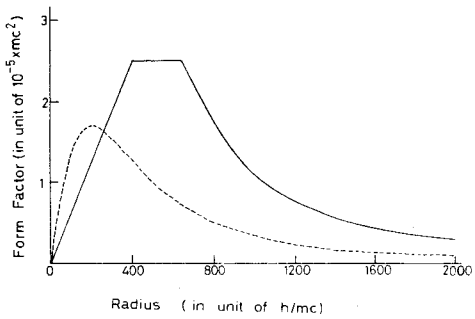


Fig.3-2. Form factor for mercury, ——; calculated using Coulomb approximated wave functions, ---- used by Madison and Shelton (1973) (calculated using Hartree wave function) with a little modification.

The elastic data of Gronemeier is normalized to the present theoretical results at $\theta$=80° ($E$=100 eV) and at $\theta$=90° ($E$=300 eV). The number of partial waves estimated numerically ranged from 15 at an incident electron energy of 50 eV, to 43 at an incident electron energy of 500 eV. The total number of partial waves ranged from 125(141) to 522(994) for $F_C$ ( $F_M$ )case in the same energy regions.

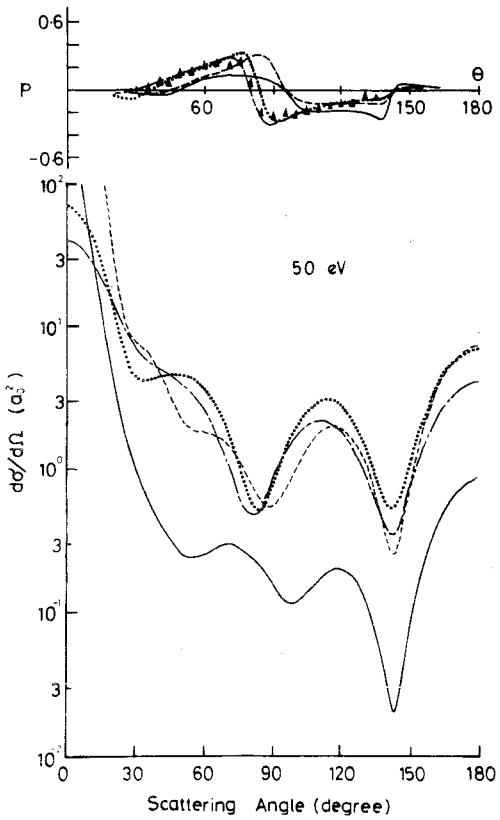


Fig.3-3. Spin polarization and differential cross section for mercury at incident electron energy of 50 eV. (——: DWB calculation for 6s6p$^1$P excitation using $F_C$, ----: DWB calculation for 6s6p$^1$P excitation using $F_M$,——————: elastic scattering by ground-state atomic potential, .....: elastic scattering by excited-state atomic potential, ▲: experimental results of spin polarization for 6$^1$P excitation (Hanne et al. 1972).

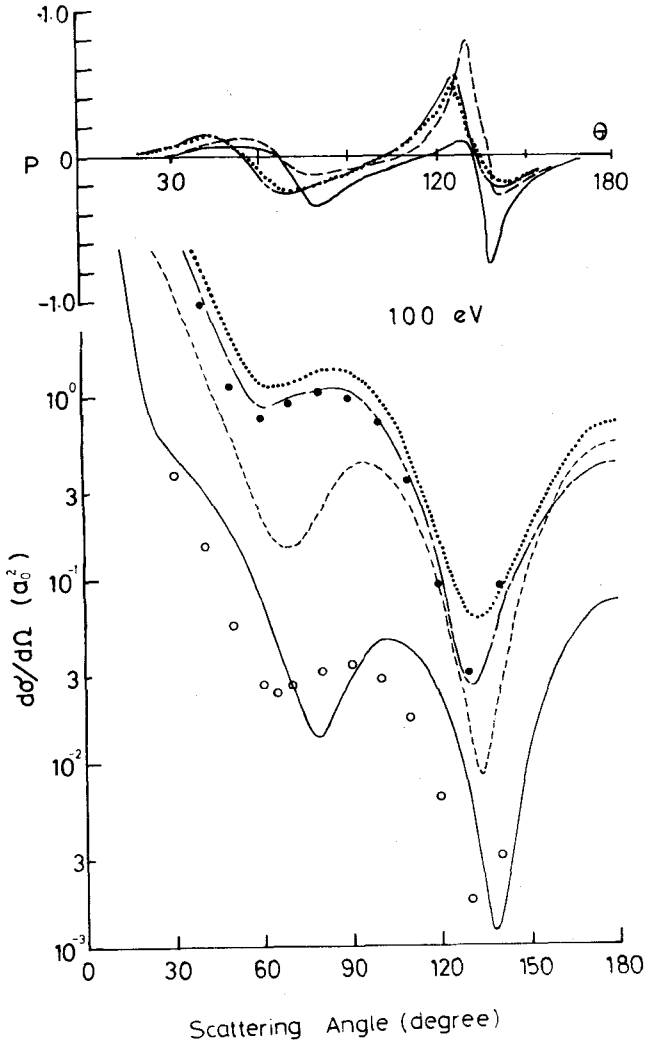


Fig.3-4. Same as Fig.3-3 except here the energy is 100 eV. (● : experimental results for the elastic scattering cross section normalized to theoretical results at $\theta$=80° and o : experimental results for the $6^1P$ excitation cross section (Gronemeier 1970)).

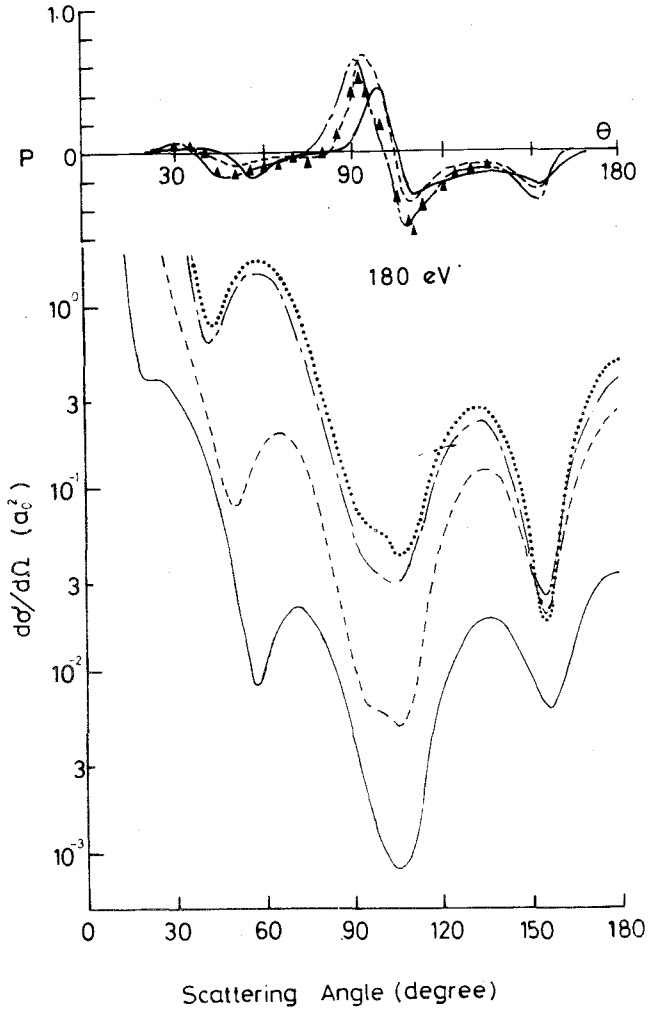


Fig.3-5. Same as Fig.3-3 except here the energy is 180 eV. The curve of spin polarization for elastic scattering by excited-state atomic potential is almost similar to that by ground-state atomic potential and is neglected for simplicity. (▲:experimental results of polarization for $6^1P$ excitation (Hanne et al. 1972))

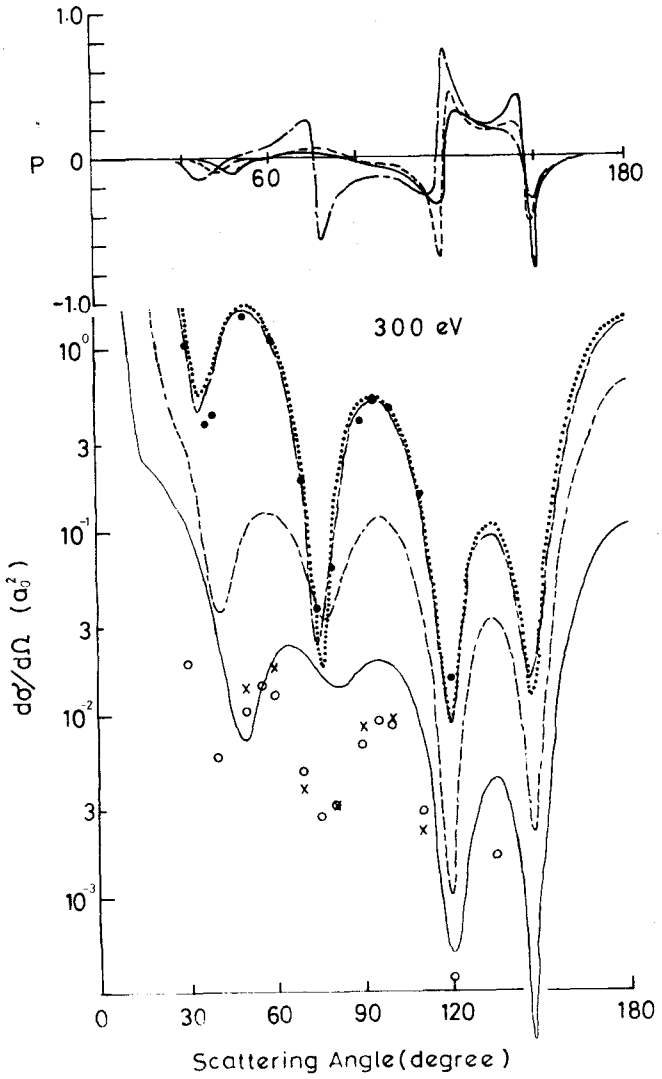


Fig.3-6. Same as Fig.3-3 except here the energy is 300 eV. ( ● : experimental results for the elastic scattering cross section normalized to theoretical results at $\theta$=90°, ○ : experimental results for the $6^1P$ excitation cross section (Gronemeier 1970) and × : experimental results for the $6^1P$ excitation cross section (Yamazaki et al. 1977c) The curve of spin polarization for elastic scattering by excited state atomic potential is neglected for simplicity.)

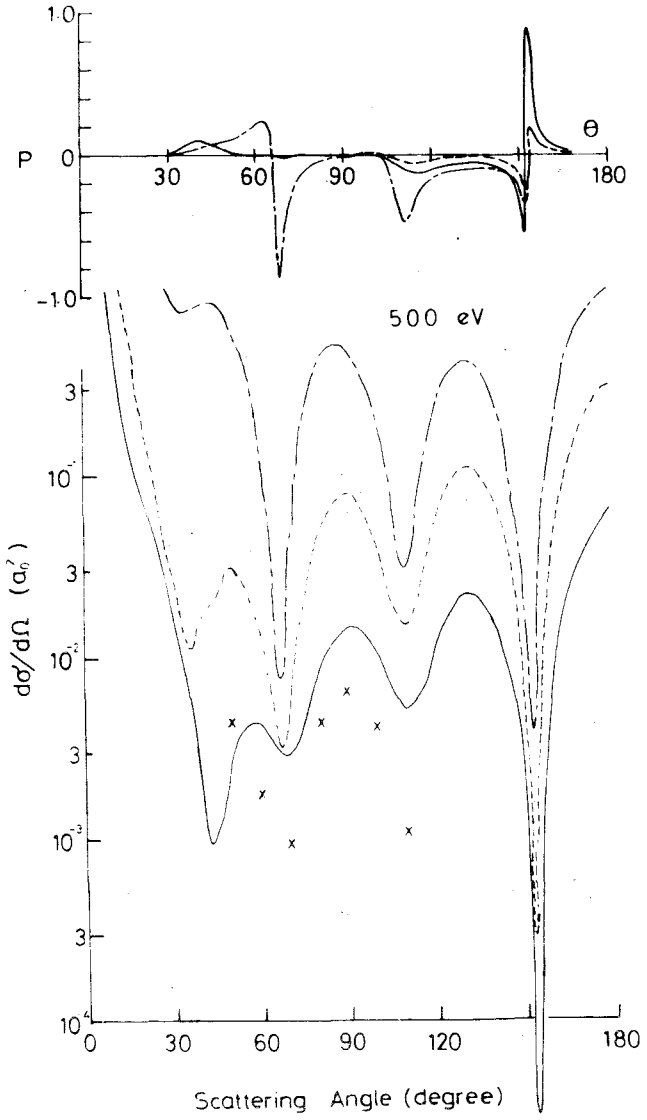


Fig.3-7. Same as Fig.3-3 except here the energy is 500 eV. (The curves of spin polarization and cross section for elastic scattering by excited-state atomic potential are neglected for simplicity).

Figures 3-3 to 3-7 show that the DWB calculation using $F_M$ gives a differential cross section several times larger than that using $F_C$ . As is seen in Fig.3-2, these differences originate from the remarkable difference between the form factors. The atomic wave functions used to calculate $F_M$ were determined by Madison and Shelton as the bound state eigenfunction of the Hartree field, in order to assure the orthogonality between the atomic and free-state wave functions, which reduces computing time drastically if exchange scattering is taken into account. The atomic wave functions obtained in this way spread over a broad radial region causing overestimations of the differential and total cross sections. On the other hand, the atomic wave functions used to calculate $F_C$ are determined as the solution of the Coulomb field, having the same binding energy as the actual one (see Sec.3-4), which provide differential and total cross sections in close agreement with experiments. The extremum points of the cross section calculated using $F_C$ shift to higher scattering angles at forward scattering in comparison to that using $F_M$ throughout the present calculations. In the case of $F_C$, the order of partial waves which contribute primarily to the T-matrix shifts lower as compared to $F_M$, which can be seen in Fig.3-2. This situation means that the "effective impact energy" in the case of $F_C$ is smaller than that in the case of $F_M$ for forward scattering where higher order partial waves play important roles, which results in shifts of the extremum points.

A comparison to experiments is discussed in Chapter 5.

In regard to the total cross section, the results obtained using $F_C$ agree well with McConnell and Moiseiwitsch, while the results using $F_M$ are about 10 times greater than those using $F_C$ (see Fig.3-8).

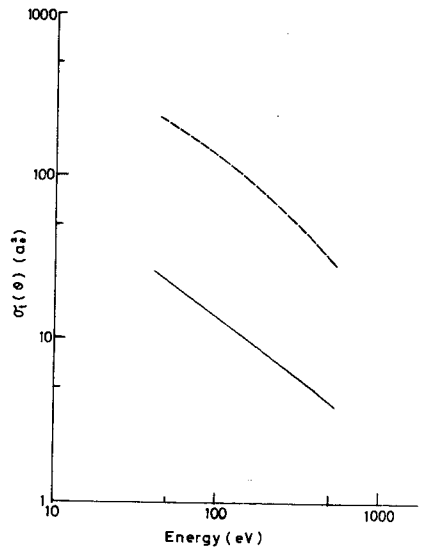


Fig. 3-8. Total cross sections for $6^1P$ excitation of mercury by electron impact calculated using DWB approximation (———; $F_C$,------; $F_M$).

# CHAPTER 4. MEASUREMENT OF LOSS SPECTRA

## 4-1 Introduction

Table 1-1 shows that a few experimental data exist concerning the loss spectra of mercury at intermediate impact energies and at large scattering angles. This situation is very surprising considering that the electron-mercury system was one of the most popular and accessible, due to its large scattering cross section and suitable vapour pressure at room temperature with little influence on the gun heater in the early stages of scattering experiments. A primary reasons for this may be deficiencies of the theoretical investigations. Theoretical treatments of inelastic scattering for heavy elements have been very difficult because of the complexities of the atomic structure and scattering process at intermediate energies. The recently developed high speed digital computer, however, makes it possible to treat accurate and complex theories, as is given in Chapter 3. Furthermore, in recent experiments on electron-mercury scattering at impact energies of several hundreds of eV at forward scattering, it was found that the relative

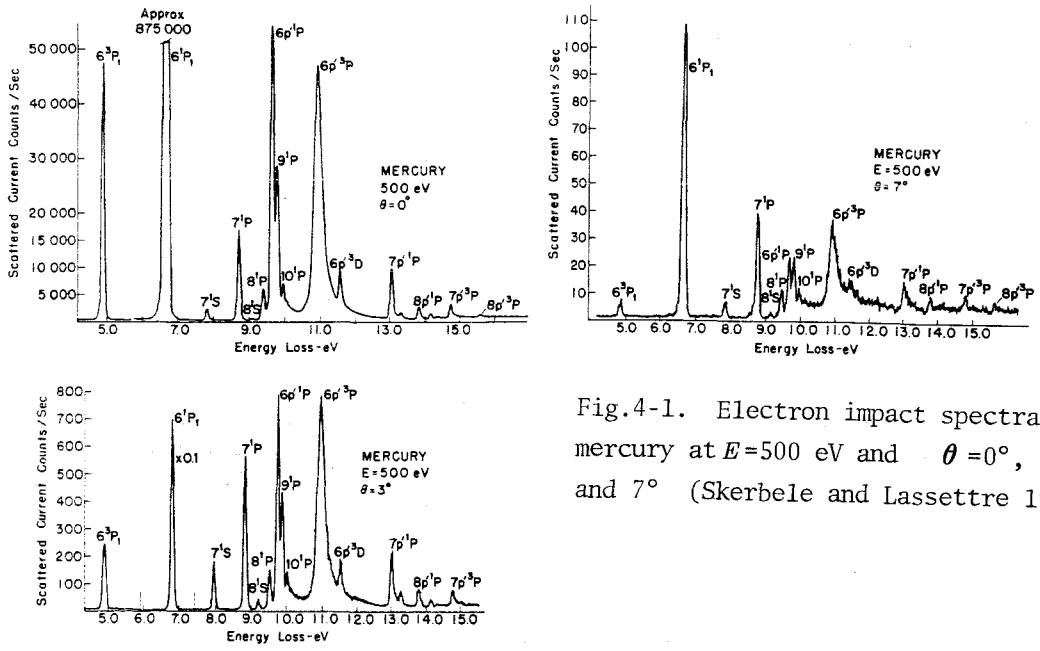


Fig.4-1. Electron impact spectra of mercury at $E$=500 eV and $\theta$=0°, 3°, and 7° (Skerbele and Lassettre 1972)

intensities between various excitation channels changed rapidly as a function of scattering angles (0° to 7°) (Skerbele and Lassettre 1972), causing interest on the behaviour of the loss spectra at large scattering angles. Fig.4-1 shows that transitions to P-state are strong in contrast to the other transitions as is surmised in Sec.3-3.

Also, from a practical viewpoint, knowledge concerning the differential cross section of inelastic scattering at large angles for mercury is of basic importance for experimental arrangement of the ESP detector using mercury vapour as a target. Optimum conditions of the ESP detector such as impact energy, scattering angle and angular resolution, can be determined by theoretical calculation of elastic differential scattering cross section and spin polarization. However, the optimum condition of energy resolution for the ESP detector can be estimated only by the cross section of inelastic scattering.

This chapter aimed at obtaining the impact spectra for mercury at intermediate energies and large scattering angles, which leads to better understanding of the optimum conditions for the ESP detector in practical use as well.

## 4-2 Apparatus — Design and Performance

### 4-2-1 Vacuum System

The apparatus used consists of a primary beam source, a gas cell as a collision chamber and 127° cylindrical type energy analyser system. The loss spectra were measured by scanning the deflecting voltage of the analyser. An outer view of the apparatus is shown in Fig.4-2 by removing the top cover of the vacuum chamber and the mercury reservoir. Fig.4-3 shows cross sectional drawings of the system. The vacuum chamber is a 20 cm high cylinder and 40 cm in diameter, evacuated by a 600 ℓ/s oil diffusion pump with

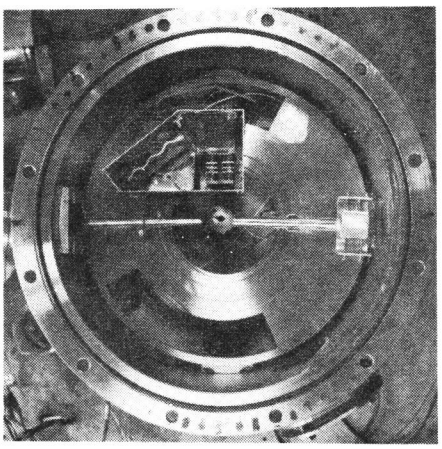

Fig.4-2. Top view of the main chamber removing the top covers of the chamber and energy analyser.

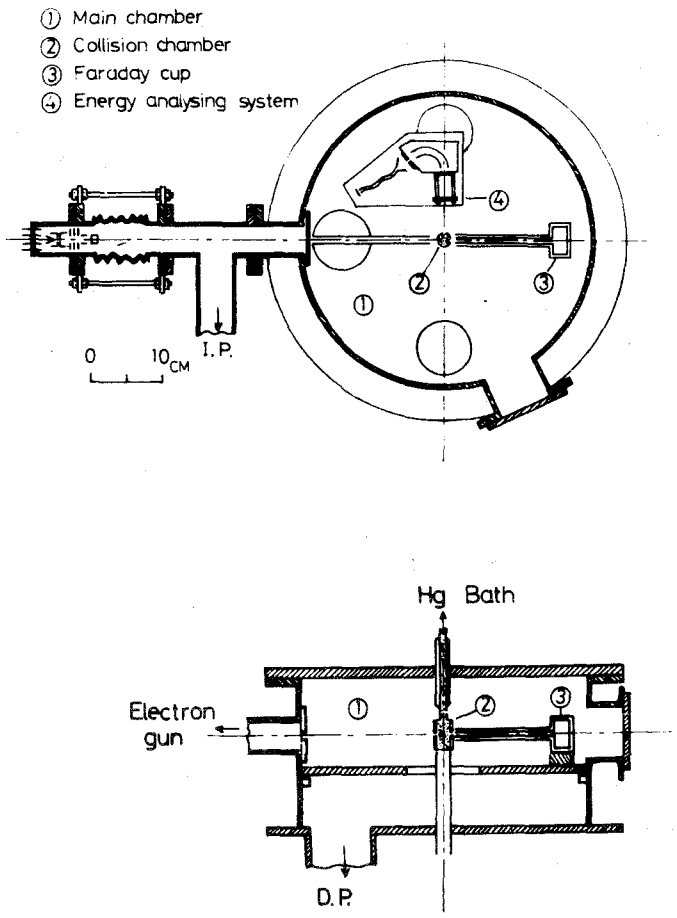


Fig.4-3. Cross section of the apparatus

a liquid nitrogen cooled baffle. The actual pumping speed is reduced to about 100 ℓ/s by the baffle and the connection tube to the chamber, which provides a residual gas pressure of $10^{-7}$ Torr. Gas pressure increases to $10^{-5}$ Torr during operation due to mercury vapour. The vacuum system is sealed with Viton O-rings.

The collision chamber at the center of the vacuum chamber, shown in Fig.4-4, consists of two tight concentric cylinders. The outer cyclinder $C_1$ is static and the inner $C_2$ rotatable. The inner cylinder is 40 mm high and 18 mm of inner diameter. The collision chamber is pumped through four apertures $A_2$, $A_3$, $A_4$ and $A'_4$ so that the incident and scattered electrons may pass. The collision chamber provides a scattering angle from 50° to

130° by utilization of the two apertures, $A_4$ and $A'_4$. The majority parts in the chamber were made of stainless steel to avoid amalgamating with mercury vapour and an excessive magnetic field. However, some parts are made of gold plated copper to avoid charging-up effects.

Tungsten ribbon (0.025 × 0.75 mm$^2$) was used as a cathode filament of the electron gun, which provides an electron beam current of 2-20 μA at the accelerating energies of 300-2000 eV with a beam diameter of less than 3 mmφ at a relative distance of 300 mm from the electron gun.

As can be seen in Fig.4-3, the gun is mechanically adjustable from outside the vacuum by means of three screws. The beam can be additionally adjusted by an electrostatic defector.

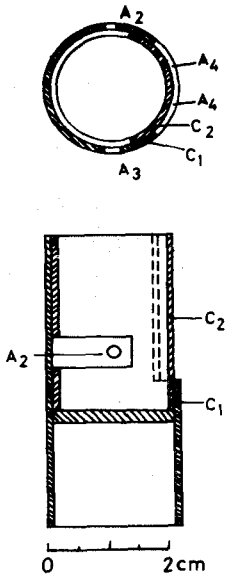


Fig.4-4. Cross section of the collision chamber.

The electron beam current is stabilized to about 0.1% for all beam current and accelerating energy ranges by controlling the filament current automatically (see Sec.4-2-5). The gun assembly is differentially pumped from the main chamber through 3 mmφ round slits by a 40 ℓ/s ion pump to approx. $5 \times 10^{-7}$ Torr to avoid instability caused by mercury vapour and to get longer life time of the filament.

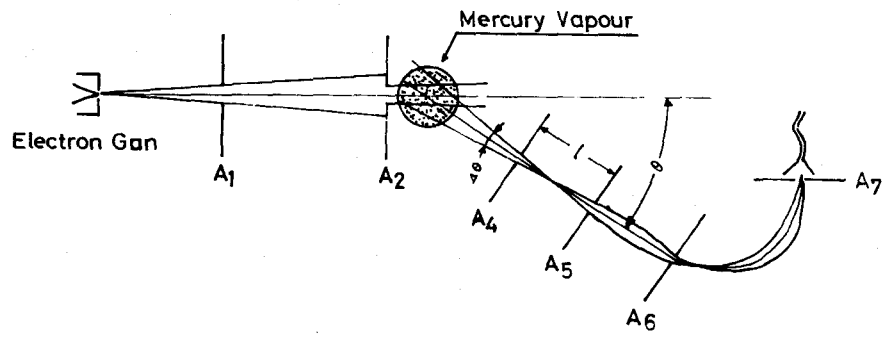


Fig.4-5. Scattering geometry ($A_1$ and $A_2$ ; round slit, $A_4$, $A_5$, $A_6$ and $A_7$; rectangular slit).

The scattering geometry is shown in Fig.4-5. Apertures $A_1$, $A_2$ and $A_3$ are round and have diameter of 3,2 and 3 mm respectively, while $A_4$, $A_5$, $A_6$ and $A_7$ are rectangular, $A_4$ is 0.7 $\times$ 5 $mm^2$ and the slit widths of $A_5$, $A_6$ and $A_7$ vary from 0.1 to 3 mm with 5 mm height and set usually at 0.1 mm. The rectangular slits were adopted to obtain a high scattering intensity even in high angular resolution experiments. The distance between $A_4$ and $A_5$ was usually set at 50 mm, so the angular resolution $\Delta\theta$ is $\simeq 1°$.

The scattering angle $\theta$ is defined as the angle formed by the line through the centers of the collimating apertures ($A_1$ and $A_2$) for the incident beam, and the line through the centers of the acceptance apertures at the collision chamber and in front of the decelerating asymmetric lens. It was estimated that the reproducibility of the scattering angle was $\pm 0.5°$ and the shift from the true scattering angle was less than $\pm 2°$, taking into account the residual magnetic field as well. The mercury vapour is produced in a mercury bath which is automatically controlled to maintain a constant temperature of about 60°C resulting in vapour pressure $\approx 10^{-2}$ Torr (see Fig.4-6), and is led to the collision chamber by a pyrex tube whose temperature is higher than the mercury bath's to prevent condensation. All the heaters used are wound so as to be inductionless.

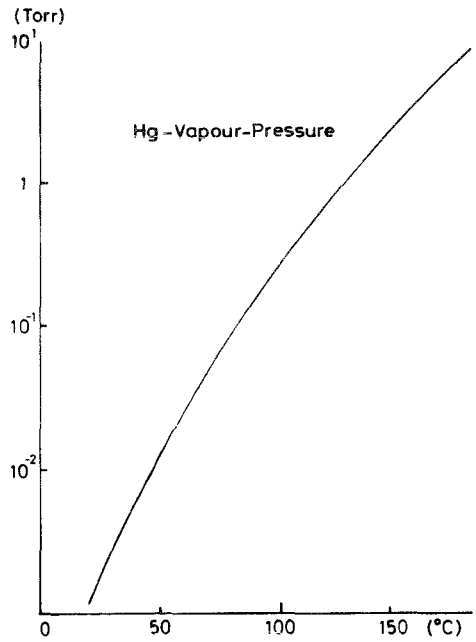


Fig.4-6. Relation of Hg vapour pressure to temperature (Weast 1972).

### 4-2-2. Magnetic Field

Charged particles in a magnetic field $B$ make a circular motion of radius $r$

$$r = \frac{\sqrt{2mE}}{qB} \quad , \qquad (4\text{-}1)$$

where $m$ is the mass of the charged particles, $E$ the kinetic energy and $q$ the charge of the particles. Then, the shift $\Delta x$ of the charged particles is expressed as

$$\Delta x = \frac{x^2}{2r} = \frac{qBx^2}{2\sqrt{2mE}} \qquad (4\text{-}2)$$

where $x$ is the path length of the electron beam (see Fig.4-7). To make the angular shift smaller than the angular resolution $\Delta\theta$, the terrestrial magnetic field $B_t$ should be reduced to

$$B_t \leqq \frac{2\sqrt{2mE}\cdot\Delta\theta}{qx} . \qquad (4\text{-}3)$$

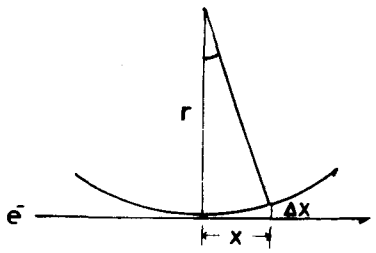


Fig.4-7. Relation between path length $x$ and shifted distance $\Delta x$ of electron in magnetic field.

Using equation (4-3), the maximum residual magnetic field allowed in the present experiments is shown in Fig.4-8 for two path lengths. The magnetic field is corrected by a Helmholz coil of 150 cm diameter and 40 cm height.

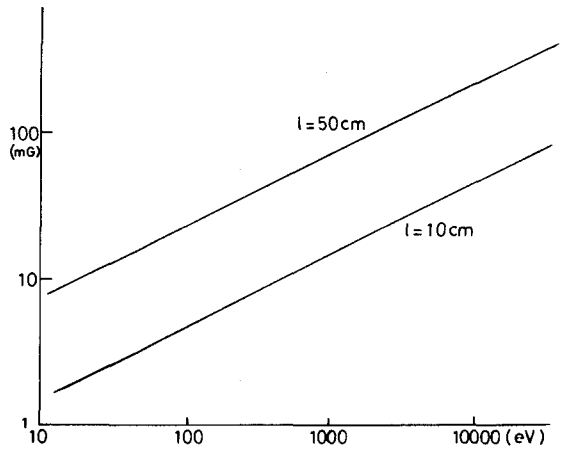


Fig.4-8. The maximum residual magnetic field allowable in the present experiments.

## 4-2-3 Energy Analyzer

The energy analyser is composed of a decelerating asymmetric three-slit lens, cylindrical 127° sector-type analyser and electron multiplier, as is shown in Figs.4-9 and 4-10. All gaps of the case of the energy analyser are sealed except for the slits, in order to prevent the secondary or backscattered electrons from straying into the electron multiplier.

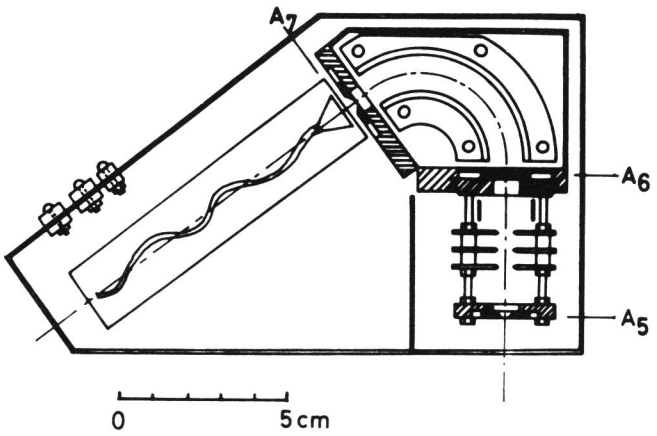


Fig.4-9. Cross section of the energy analyser composed of three-slit asymmetric lens, 127° sector type analyser and electron multiplier.

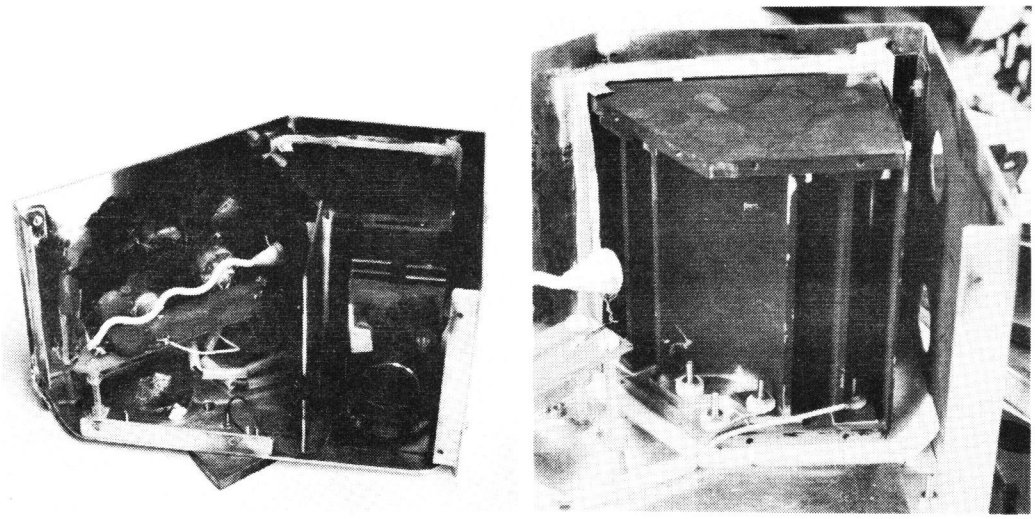

Fig.4-10. Outer view of the energy analyser removing the top and front covers (a), and sector-type 127° analyser removing the side covers (b).

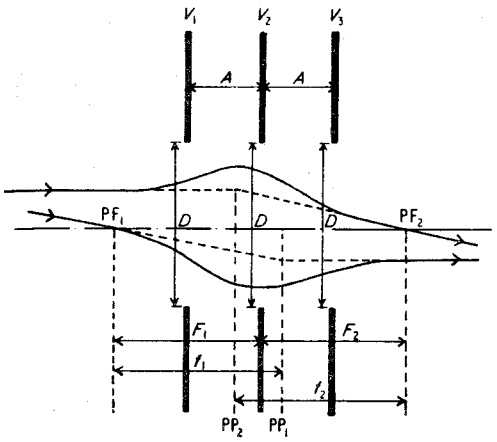


Fig.4-11. Geometry of the asymmetric three-aperture lens studied by Read (1970)

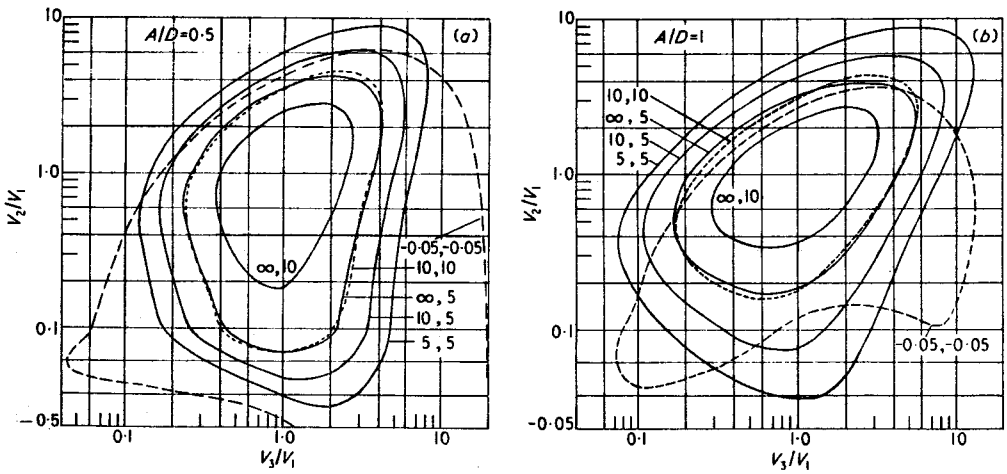


Fig.4-12. The focusing condition of the asymmetric three-aperture lens having $A/D$=0.5 and 1. The sets of numbers given in the figures show the distances between objective plane and lens, and between imaging plane and lens in unit of aperture diameter (Read, 1970).

An asymmetric three-slit lens is used to assure high energy resolution at rather high incident energies. The deflector plates are located behind this lens system for correction of the electron path.

The construction of the three-slit lens system was determined using the results calculated for the asymmetric three-aperture lens system by Read (1970,1971). The lens system studied by Read is shown in Fig.4-11, and the relationship between $V_2/V_1$ and $V_3/V_1$ is shown in Fig.4-12, where $V_1$, $V_2$ and $V_3$ are the lens potential of the entrance, mediate and exit electrodes, measured with respect to the potential at which the electrons have zero kinetic energy. It can be seen that two focusing conditions generally exist and that the ratio of acceleration (deceleration) has an upper (lower) limit corresponding to the construction of the lens system. As there are no theoretical or experimental investigations for an asymmetric three-slit lens system, the focusing conditions were examined experimentally (see Fig.4-13) . The deflecting voltage is swept sinusoidally from positive to negative values in order to sweep the image across the aperture in front of the Faraday cup (F.C.), and then the current to the

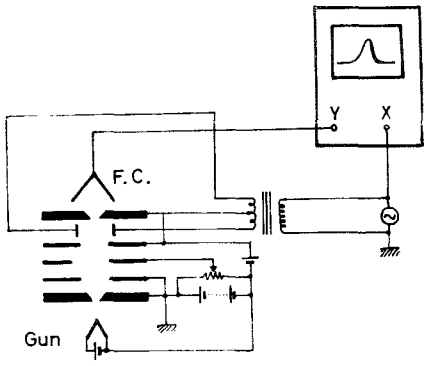


Fig.4-13. Schematic diagram of the electric circuit for the investigation of the focusing condition of the asymmetric three-slit lens.

Faraday cup goes from zero, to its maximum, and back to zero again. The shape of the curve of current measured with a Faraday cup against deflector voltage is displayed on an oscilloscope screen. The focusing condition is determined from the curve obtained in this way as conditions that provide the most high and narrow peak. The results are shown in Fig.4-14 where the dotted line shows that the theoretical results for the asymmetric three-aperture lens having a similar construction to the slit lens used in the present experiments. (Read 1970).

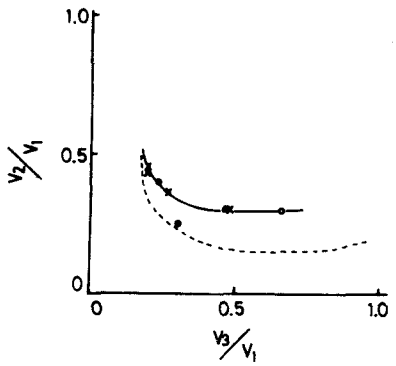


Fig.4-14. Focusing condition of the three-slit lens for V =300 eV (o) and 500 eV(×). (Dashed line shows theoretical results for an asymmetric three-aperture lens having similar construction as the three-slit lens (Read 1970).

The outer and inner radius of the sector analyser are 30 and 20 mm, respectively, and the height is 50 mm. As the width of slit $A_5$, $A_6$ and $A_7$ is set at about 0.1 mm, this analyser provides an energy resolution of $E/\Delta E \sim r/2\Delta r \sim 100$ where $E$ is electron energy entering the slit of the sector analyser, $\Delta E$ energy resolution, $r$ central radius of the slit of the analyser, and $\Delta r$ width of the slit of the analyser, and the value is confirmed experimentally by the FWHM of the elastic scattering peak (see Fig.4-22).

The sector is coated with soot produced by burning liquid benzene, to minimize the generation of secondary electrons.

### 4-2-4 Detector

The energy analysed scattered electrons are detected by a channeltron electron multiplier (Murata Co., Ceratron Type EMW-1081E, see Fig.4-10) with an acceptance cone. The multiplier pulses are inductively coupled from the analysing system at a high voltage potential into a pre-amplifier

at earth potential. The pulses the pass through a pulse height analyser and are counted by a multi-channel scaler (M.C.S.).

The pulse height distributions (P.H.D.) are shown in Fig.4-15 as a function of the multiplier voltage. The multiplier is operated at 4500 eV to

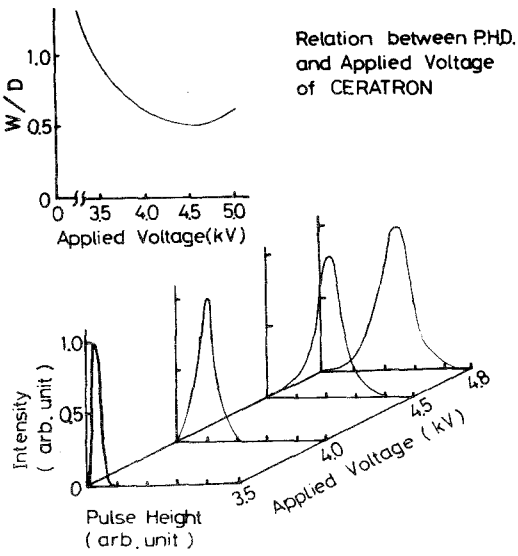


Fig.4-15. Relation between P.H.D. and applied voltage of Ceratron, and a pulse height resolution $W/D$ of Ceratron as a function of applied voltage, where $W$ is FWHM of P.H.D. and $D$ the mean value of pulse height.

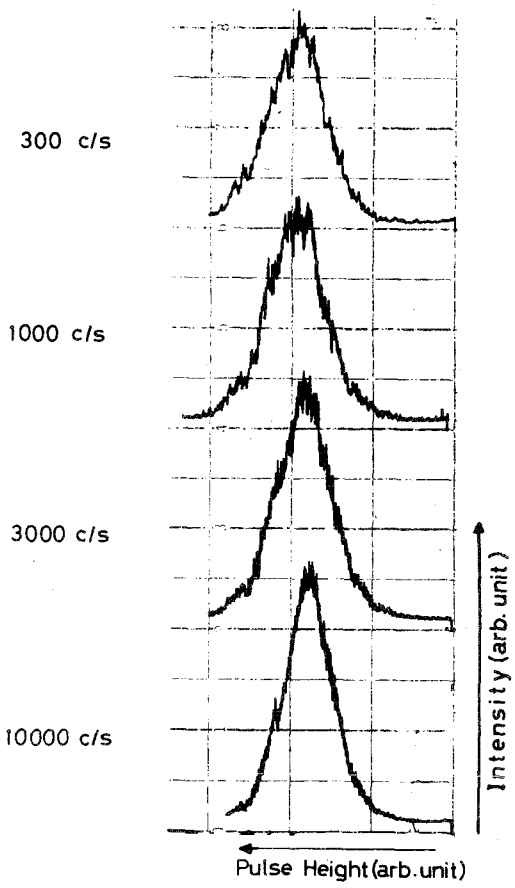


Fig.4-16. Relation between R.H.D. and count rate of Ceratron.

ensure a pulse height resolution maximum, which is defined as the ratio between the mean value of pulse height and the FWHM of P.H.D. (see Fig.4-15)

As is seen in Fig.4-16, the P.H.D. of the multiplier depends slightly on the count ratio if it is less than $10^4$ c/s. During the present experiments this condition was always satisfied.

The multiplier efficiency is not uniform over the entrance plane. For example, if an electron enters along the channel axis, it may penetrate quite a distance into the multiplier before releasing secondary electrons resulting in a lessened gain. Thus, it was always set off-axis from electron path to attain a higher pulse height. The dark current of the multiplier is less than 0.1 pulse per minute.

### 4-2-5 Measurement System

A schematic diagram of the electric circuit used in the analysing system is shown in Fig.4-17.

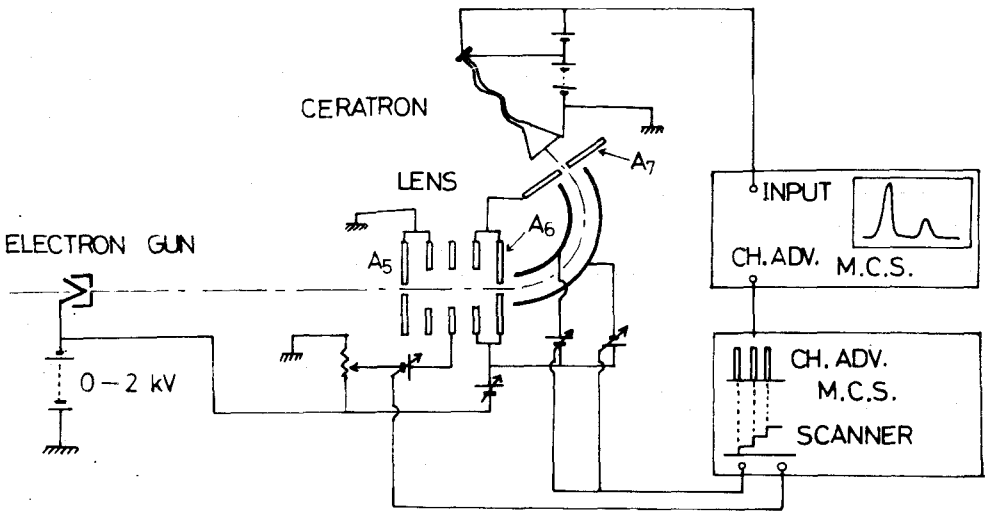


Fig.4-17. Electric circuit of the analyser system for measurements of loss spectra.

The loss spectra were obtained by scanning the potential of the sector and the lens, to obtain the best fit for the focusing condition. These potentials varied synchronously with the channel advance signal of the multi-channel-scaler (MCS) as is shown in Fig.4-17 (Ino-Tech TI-5200).

The whole electric circuit has a stability of about 0.01%. The primary electron beam current is stabilized by monitoring the current to the Faraday cup (see Fig.4-18). The monitored current using this circuit

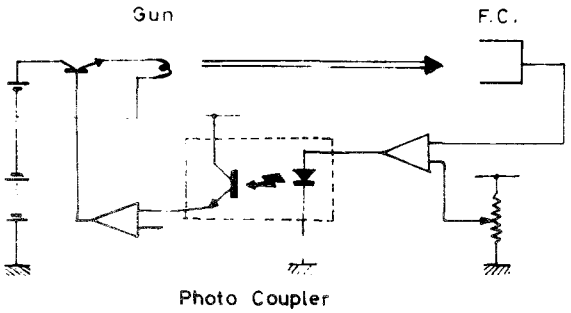


Fig.4-18 Schematic diagram of the beam current stabilized circuit.

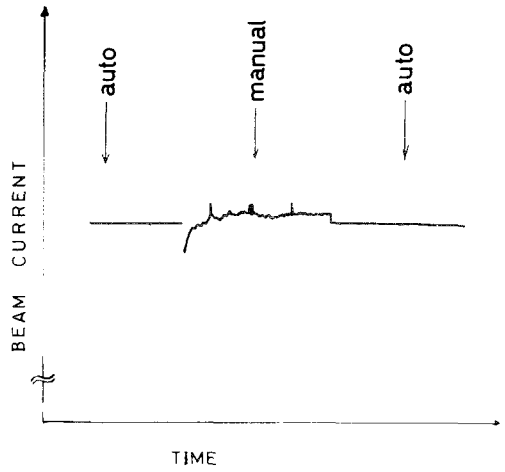


Fig.4-19 Stability of electron beam current (auto; beam-current-stabilized mode, manual; gun-heater-current stabilized mode).

is shown in Fig.4-19, together with the current obtained using a heater current stabilized circuit. As is shown in Fig.4-20, the MCS scanner is composed of a 1 MHz oscillator, counters, photo-couplers and 10-bit D-A converters (1024 steps). It serves the dwell time of $10^{-3}$ to 8 sec for each channel, and the scanning may be started or stopped at every 64 steps. The sector potential is swept linearly with regard to the MSC scanner output, however the lens potential should be swept non-linearly as can be seen in Fig.4-14. To simulate the curve, a non-linear amplifier was con-

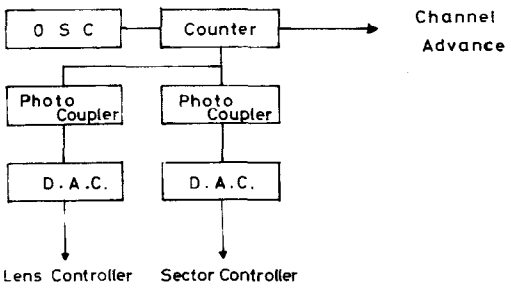


Fig.4-20. Schematic diagram of MCS scanner.

structed (see Fig.4-21). As the sweeping voltage of the sector potential is small compared to the sector potential itself, one would expect the circuit shown in Fig.4-21 to provide good results.

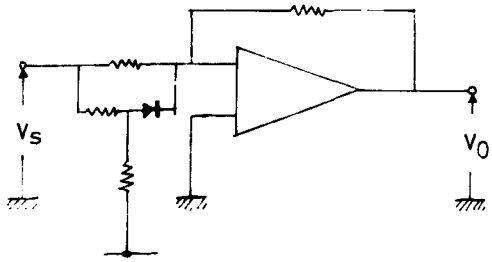


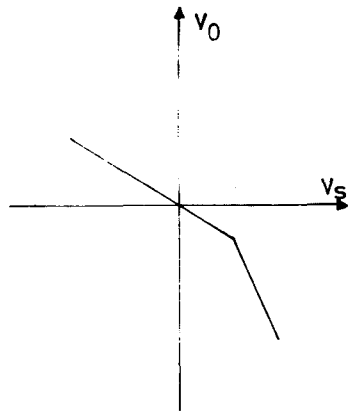


Fig.4-21. Schematic diagram of lens voltage controller.

## 4-3. Results and Discussion

### 4-3-1 Calibration

An example of the measured results of the loss spectra is shown in Fig.4-22 ($E$=300 eV, $\theta$=60°). Many peaks corresponding to various excitation processes can be observed, i.e. the excitations for $(6s)(6p)^3P$ (4.9 eV), $(6s)(6p)^1P$ (6.7 eV), $(6s)(7s)^1S$ (7.9 eV), $(5d)^9(6s)^2(6p)^1P$ (9.8 eV) and $(5d)^9(6s)^2(6p)^3P$ (11.0 eV) states.

The background is estimated as the average number of electrons counted at each channel of the M.C.S. corresponding to loss energies between 2 and 4 eV, for the lowest excited state of mercury atom exists at 4.9 eV above the ground state.

The relative transmission efficiency $\alpha$ of the analysing system was determined by measuring the scattering intensity of elastic electrons by varying the incident energies from $E$ to $E-\Delta E$. The standard transmission efficiency $\alpha_s$ was determined for each incident energy at the scattering angle where the differential cross section of an elastic scattering remains almost constant for both the variation of the incident energy and scattering angle (e.g. 300 eV 100°, 400 eV 90° etc. see Figs.2-5 to 2-7. The relative transmission efficiency $\alpha$ was measured for each incident energy

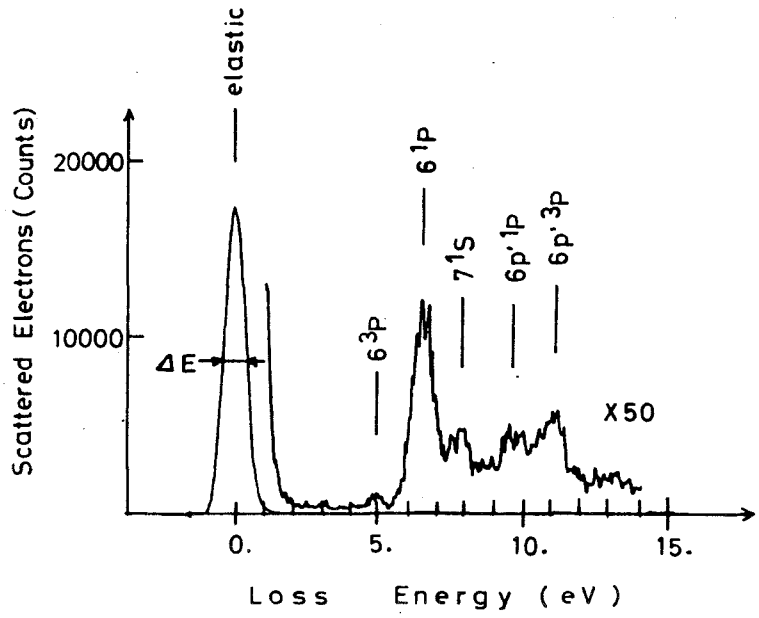


Fig.4-22. Example of the measured results of the loss spectra ($E$=300 eV and $\theta$=60°)

and scattering angle, the profiles of which were compared to $\alpha_S$ to assure a correct position for the analyser. Using the transmission efficiencies thus obtained, the ratio of the elastic and inelastic scattering cross section was determined correctly for each incident energy and scattering angle.

### 4-3-2 Loss Spectra

Fig.4-24 show the electron impact spectra for mercury corresponding to the incident electron energies from 300 eV to 1000 eV, scattering angles from 50° to 110° and loss energies from 0 eV to 15 eV. Elastic peaks are abbreviated for simplicity. Each spectrum shown in Fig.4-23 is obtained from the measured results (an example is shown in Fig.4-22) through the following procedures; 1) Transmission efficiency $\alpha$ was measured and compared with $\alpha_S$.2) The ratio between the background and the peak counts of $6^1P$ excitation was established to be less than 10 % (usually the ratio was less than 5%), otherwise the data was omitted. 3) The background was subtracted from each channel intensity and then the intensity of each channel was corrected by the transmission efficiency $\alpha$. 4) The loss spectra were normalized by the elastic scattering intensity. Finally, the data thus obtain-

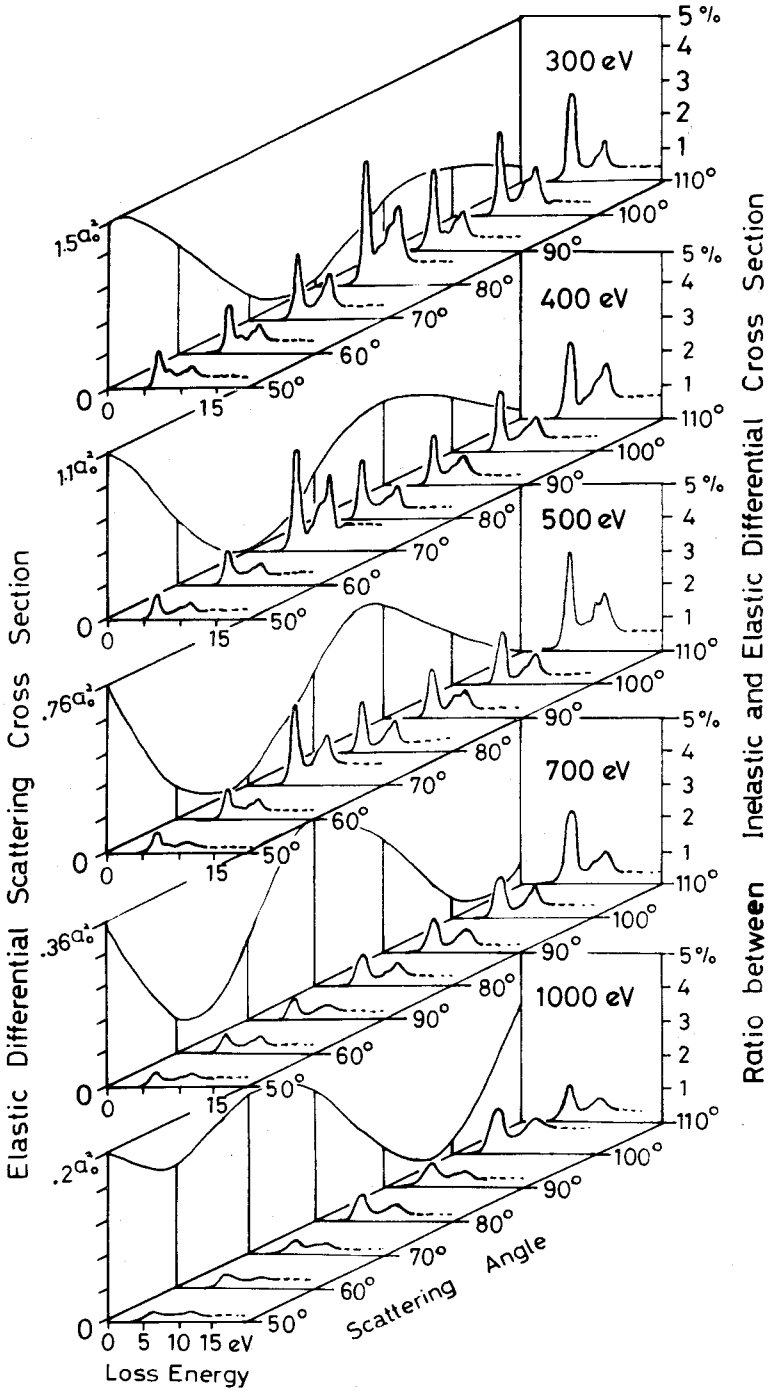


Fig.4-23. Energy loss spectra for mercury (The spectra are normalized by the elastic scattering intensity having the same impact energy and scattering angle).

ed which correspond to the same conditions as to impact energy and scattering angle were summed up and averaged to reduce the statistical deviation.

Concerning the ratio between $6^1P$ excitation and elastic scattering, it was estimated that error was less than 20 % including statistical error and the error induced by both the background and variation of transmission efficiencies. During measurement, the actual energy resolution was varied from 0.7 eV to 1.8 eV( FWHM) by controlling the electron energy entering the sector analyser in accordance with impact energy increases from 300 eV to 1000 eV. As has already been pointed out in Sec.2-4, the profiles of the theoretically calculated cross section of the elastic scattering agree well with experimental results, except that the extremum points of the calculated cross sections shift slightly to scattering angles smaller than the experimental(Walker 1969). Therefore, in Fig.4-23, the calculated results of the elastic scattering cross section, shown in Fig.2-5 are used instead of the experimental ones to avoid inaccuracies stemming from difficulties of measuring absolute transmission efficiency for various scattering angles. Concerning the absolute values of the cross section, the comparison between the experimental data and the calculated results shows that the latter is about 1.5 times larger than the former at scattering angles larger than 30° (see Sec.2-4). Thus the absolute values of the inelastic scattering cross section obtained from Fig.4-23 provides only the coarse evaluation which are probably a few times larger than the true values.

Two inelastic peaks corresponding to $6^1P((5d)^{10}(6s)(6p))$ and $6p'^3P$ $((5d)^9(6s)^2(6p))$ excitations (6.7 eV and 11.0 eV energy losses respectively), appeared clearly in every spectrum, as is shown in Fig.4-23. These were also reported in a forward scattering experiment by Skerbele and Lassettre (1972). Fig.4-23 also shows that each elastic scattering intensity varies 2 or 3 orders of magnitude as a function of scattering angle, while the ratio between inelastic and elastic intensities remains in the same order of magnitude (a few percent) for dominant inelastic scatterings. Hence these oscillatory features, which are remarkable for elastic scattering in these energy regions, also appear in each dominant inelastic scattering, although they become smoother than that for elastic scattering.

Fig.4-24 shows the ratio of intensity between $6^1P$ excitation and elastic scattering. That for 300 eV electrons agrees well with the results reported by Gronemeier (1970) (see Fig.3-6).

At other inelastic channels, in the impact energies between 300 eV

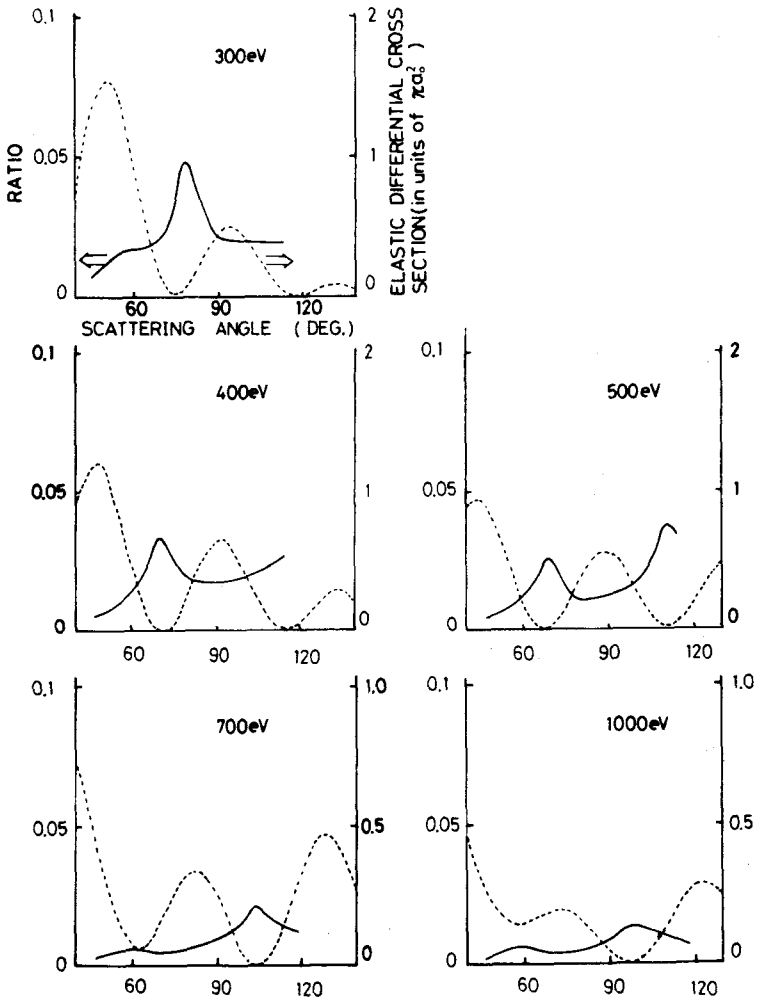


Fig.4-24. The intensity ratio of $6^1P$ excitation and elastic cross section (solid line) and differential cross section of elastic scattering (dashed line).

and 500 eV, $7^1S$(7.9 eV) and $6p'^1P$(9.8 eV) excitations were observed at shoulders of $6^1P$ and $6p'^3P$ peaks. The intensity of the strictly forbidden $7^1S$ excitation was larger than that of the $6^3P$ (4.9 eV) excitation (allowed due to spin-orbit coupling), however at forward scattering the latter was much larger than the former. The intensity ratio of $6^3P$ and $6^1P$ was equal to or less than $\sim 10^{-2}$ at the incident energy of 300 eV, and at higher impact energies $6^3P$ excitation was no longer observed because of a lower scattering intensity. The $7^1P$ excitation, the intensity of which was larger than that of $7^1S$ excitation at forward scattering, was rarely observed in the present experiment. For the ionization channels, particularly loss energy of more than about 13 eV, it seems that the variation of the intensity ratio in regard to scattering angles was not as clear as that of the excitation scattering to discrete levels.

# CHAPTER 5. $6^1P$ EXCITATION ---- COMPARISON OF THEORY AND EXPERIMENT

## 5-1 Introduction

In this chapter the theoretical and experimental results will be compared. It was found that the DWB approximation provides results in close agreement with experiments. Moreover, in regard to spin polarization, the DWB approximation predict a new phenomena at an electron impact energy greater than 300 eV.

As has already been discussed in Sec.4-3-2, the differential cross section of $6^1P$ excitation shows oscillatory features. This may be explained qualitatively by the following processes; the incident electron undergoes the inelastic process at a small angle followed by large angle elastic process, or vice versa, since the inelastic scattering cross section is very large at only forward scattering. Since this model breaks down the inelastic scattering into two elementary processes including the elastic process, the oscillatory features appearing in the inelastic scattering may be attributed to the elastic process. Futhermore, if one takes into account that the inelastics scattering at forward scattering is confined almost to optically allowed transitions, this model may also explain the dominance of the $6^1P$ excitation. Concrete theoretical treatment of this model is embodied by DWB approximation in Sec.3-2.

## 5-2 Comparison of Theory and Experiment

Figs.3-4, 3-6 and 3-7 show that the cross sections calculated using $F_C$ provide values that agree well with the experimental data for each incident energy. However, concerning the profiles, the cross sections using $F_M$ give results superior to those using $F_C$. These results suggest that the actual form factor has a profile similar to $F_M$ and a value similar to $F_C$.
This means that 1) the actual atomic field effectively acting on a 6s or 6p electron may be weak compared to the field of the Coulomb approximation, which may result in spreading of the atomic electrons over wide radial region and may originate from exchange effect and mutual shielding (see Fig.3-1), 2) the actual radial wave functions $R_{00}$ and $R_{10}$ (see equations (3-31) and (3-33)) may be much more isolated from each other than those used in $F_M$. This results in the reduction of the value of $(R_{10}, R_{00})$ appearing in the

form factor having the form (see equations (3-34) and (3-35))

$$v_{01} = \frac{(8\pi)^{1/2}}{3} (R_{10}, R_{00})(R_{11} | F_1 | R_{00}) , \qquad (5\text{-}1)$$

with

$$(R_{11} | F_1 | R_{00}) = \frac{1}{r^2}\int_0^r R_{11} R_{00} r_1^3 dr_1 + r \int_r^\infty R_{11} R_{00} dr_1 . \qquad (5\text{-}2)$$

Concerning the spin polarization, as is seen in Figs.5-1 and 5-2 the calculations using $F_M$ provide results in closer agreement to the experimen-

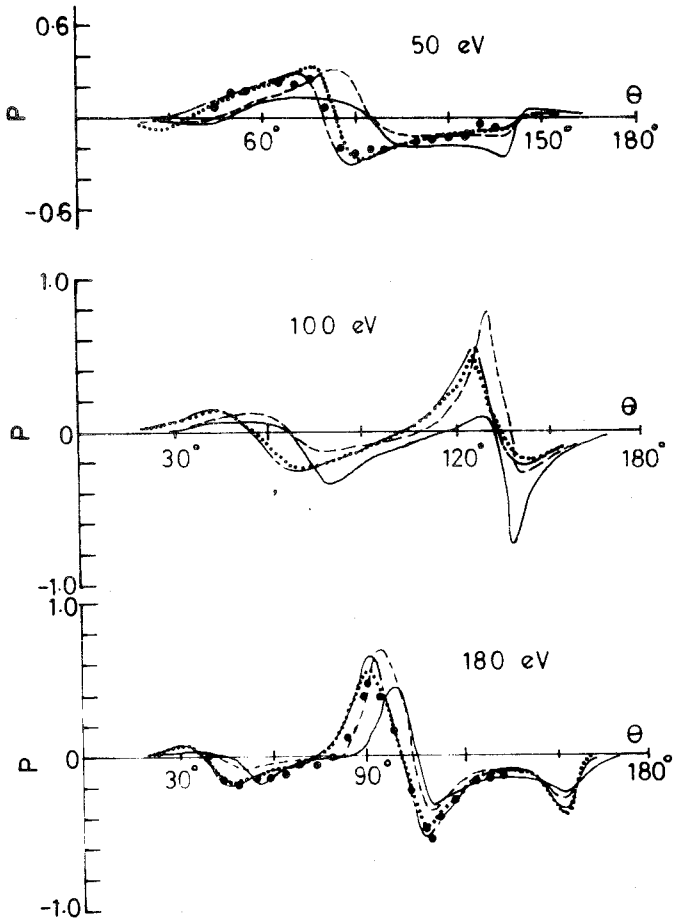


Fig.5-1. Spin polarization for mercury at incident electron energies of 50, 100 and 180 eV (——: DWB calculation for $6^1P$ excitation using $F_C$ (see Sec. 3-6), ---: DWB calculation for $6^1P$ excitation using $F_M$, ——·——: elastic scattering by ground-state atomic potential, ....: elastic scattering by excited-state atomic potential and ● : experimental results for $6^1P$ excitation (Hanne et al. 1972).

tal results than that using $F_C$ , as would be expected from the profiles of the cross section (Note that spin polarization depends not on values of cross section but on profiles of cross section. See e.g. equations (2-42),(3-51) or (7-3)). However, it should be mentioned that the experimental results of spin polarization for $6^1P$ excitation are best expressed by the calculation

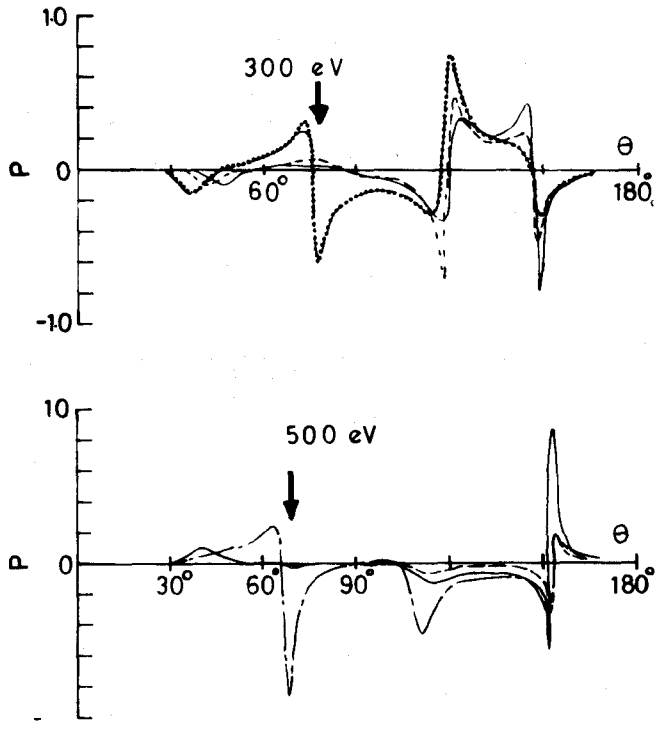


Fig.5-2. Same as Fig.5-1 except here the energies are 300 and 500 eV (Note that sharp peaks of the spin polarization appearing in the elastic scattering at the scattering angle of about 75° (300 eV) and 70° (500 eV), disappear in $6^1P$ excitation scattering.).

for elastic scattering in the present calculation. This is not the case for the calculation by Madison and Shelton (1973). They obtained results in close agreement to experimental results for incident energies between 50 and 180 eV(see Fig.5-3). It is thought that this is primarily a result of the difference in form factor used (as is seen from Fig.3-2, the profiles of $F_M$ are simplified for convenience in the present calculation).

Although the spin polarization for incident energy of 100 eV had not been measured until presently, the profiles given in Fig. 5-1 are thought to be reasonable and conceivable considering that the experimental results of

spin polarization for $6^1P$ excitation were most like that of elastic scattering. However, for incident energy of 300 eV and 500 eV, it is notable that the sharp peaks of the spin polarization appearing in the elastic cases at the scattering angle of about 75° and 70°, respectively, disappear in calculations of $6^1P$ excitations using both $F_C$ and $F_M$ (see Fig.5-2). For $6^1P$ excitation scattering and incident electron energy over 180 eV, because no experimental data on spin polarization have been reported until currently

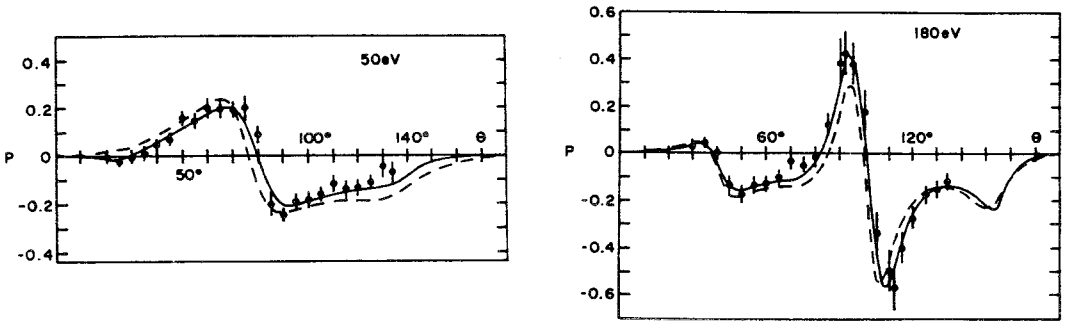


Fig. 5-3. Spin polarization for $6^1P$ excitation scattering at incident energies of 50 and 180 eV calculated by Madison and Shelton (1973) using DWB approximation for Mayer's potential (solid line, 1957), Coulthard's potential (dashed line, 1967) and experimental data by Eitel and Kessler (1970).

it is uncertain as to whether the drastic departure of spin polarization between the elastic and $6^1P$ excitation scattering means new phenomena or a breakdown of the DWB approximation. However, generally speaking, the DWB approximation provides better results at higher incident energies where a large number of partial waves contribute to forward scattering, most of which have nearly zero polarization, thus the reduction of the spin polarization is thought to be reasonable.

Further measurements of spin polarization in these energy regions would be highly desirable.

# PART II. ESP-DETECTOR USING MERCURY VAPOUR

## CHAPTER 6. INTRODUCTION

Currently, ESP experiments are being carried out by several groups in various regions of physics. These ESP experiments except for that listed in Tables 1-1 and 1-2 are summarized in Table 6-1 classifying into 5 groups, i.e. 1) the group entitled "Field Emission" treating ESP experiments or theories of field emitted electron beam usually from ferromagnetic materials, 2) the group "Photo Emission (solid)" treating those of photo electrons from ferromagnetic materials or of photo electrons from solid excited by circularly polarized light, 3) the group "LEED" treating those of diffracted electron beam in low energy electron diffraction, 4) the group "Photo Emission (vapour)" treating those of photo electrons from polarized atomic beam or photo electrons excited by circularly polarized light from unpolarized atomic beam and 5) the group "Others". In these experiments, spin polarization is usually detected using scattering of polarized electron beam with heavy atoms (Au-foil or Hg-vapour), the efficiency of which is equal to or less than $10^{-5}$ (The principle of the detector is given in Chapter 7.). It should be noted that the value is quite small compared with that of light.

A simple question arises as to whether or not a usual magnetometer can detect a direction of electron spin. Incapability of detecting electron spin with macroscopic magnetometer is qualitatively described in Appendix 2 according to Mott's consideration together with incapability of polarizing electrons with macroscopic magnetic field.

Since the first measurement of spin polarization using double scattering by gold thin film at 340 keV (Shull et al. 1943), the detection of electron spin in high energy electrons is usually performed using scattering with gold thin film, which is called Mott detector (see Fig.6-1). On the other hand, the first ESP measurement for low energy electrons was performed using

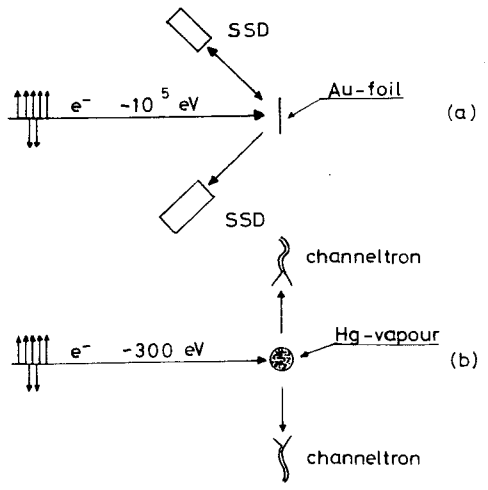


Fig.6-1. Schematic diagram of ESP detector using (a) Au-foil (Mott detector) and (b) Hg-vapour.

mercury vapour (Deichsel 1961). The ESP detector of this type is widely used for various ESP experiments such as $e^-$ -rare gas elastic scattering and $e^-$ -Ne resonance scattering. Mott detector was first used by Jost and Kessler (1965, 1966) for low energy experiments. Schematic diagrams of these two types of ESP detector are shown in Fig.6-1. Because of a high efficiency and ease of treatment in a high vacuum, the Mott detector has been widely used not only in atomic physics but also in surface physics, where ultra-high-vacuum ($10^{-10} \sim 10^{-11}$ Torr) is necessary. However, it should be noted that a Mott detector which uses high energy electrons (~100keV) is not suitable for the experiments of low and mediate energy regions in which major ESP experiments concentrate. Hence the present study attempts to develop an ESP detector suitable for low and mediate energy regions utilizing the electron-mercury scattering, which can also be used as a source of polarized electrons for e.g. surface physics study (see Sec.8-3).

Optimum conditions of ESP detector using mercury vapour are discussed and determined systematically in Chapter 7 using the results in Chapter 2, 3, 4 and 5. In Chapter 8, ESP detector and apparatus for double scattering experiments constructed according to the line shown in Chapter 7 is described. Also described in this chapter is high beam current Pierce type electron gun using single $LaB_6$ crystal as a cathode for double scattering experiments.

Another possibilities of detecting electron spin are proposed by several authors (Tolhoek 1956, Feder 1975):

1) Measurement of the spin angular momentum carried by electrons with longitudinal polarization in a mechanical way. This may be realized by measuring a torque of a suspended disk where polarized electrons are falling (A kind of Einstein-de-Haas effect).

2) Measurement of the polarization of emitted light from an atom which is excited by polarized electrons.

3) Measurement of intensity asymmetry of diffracted beams in LEED (low energy electron diffraction) experiments. The principle is like that of a Mott detector and a detector using mercury vapour as scatterer.
The methods of 2) and 3) may be more practical than that of 1).

Table 6-1

Field Emission

| | | | |
|---|---|---|---|
| Exp. | Gd (polycrystal) | Hofmann et al. | 1967 |
| Theor. | Gd | Müller et al. | 1967 |
| Exp. | Ni(single) | Gleich et al. | 1971 |
| Exp. | EuS-coated W | Müller et al. | 1972 |
| Exp. | W(single) | Regenfus and Sütsch | 1974 |
| Exp. | Ni(single) | Müller | 1975 |
| Theor. | Effect due to external field | Eckstein and Müller | 1975 |
| Exp. | Ni(single) | Eib and Alvarado | 1976 |
| Exp. | EuS coated W | Kiskev et al. | 1976 |
| Exp. | Fe,Ni,Co,rare-earth metal | Chrobok et al. | 1977 |
| Exp. | Ni(100) | Landolt and Campagna | 1977 |
| Theor. | W(001) with adatom | Feder | 1977 |

Photo Emission (Solid)

| | | | |
|---|---|---|---|
| Exp. | Ni(single,poly) | Bänninger et al. | 1970 |
| Exp. | Alkali metal | Heinzmann et al. | 1971 |
| Theor. | Ni(single) | Smith and Traum | 1971 |
| Theor. | Ni,Co | Anderson | 1971 |
| Theor. | Ni,Co | Wohlfarth | 1971 |
| Exp. | Alkali metal (circularly po.light) | Heinzmann et al. | 1972 |
| Exp. | Co | Busch et al. | 1972 |
| Theor. | Ferromagnetic metal | Murao | 1972 |
| Exp. | Ni,Co,Fe | Adler et al. | 1973a |
| Exp. | Ferro magnetic metal | Adler et al. | 1973b |
| Theor. | EuO(100) | Eastmann | 1973 |
| Summary | | Campagna et al. | 1973 |
| Theor. | Ferromagnetic metal | Murao | 1974 |
| Exp. | EuO(La doped) | Meier et al. | 1975 |
| Exp. | EuO | Sattler and Siegmann | 1975 |
| Exp. | GaAs | Pierce et al. | 1975 |
| Exp. | Ferrite ($Fe_3O_4$, $Li_{0.5}Fe_{2.5}O_4$) | Alvarado et al. | 1975b |
| Exp. | La-doped EuO | Meier et al. | 1975 |

| | | | |
|---|---|---|---|
| Theor. | Ce by circularly po. light | Koyama and Merz | 1975 |
| Theor. | Photo Emission (circularly po light) | Koyama | 1975 |
| Theor. | Ni(single) | Wohlfarth | 1975 |

L E E D

| | | | |
|---|---|---|---|
| Theor. | | Jennings | 1970 |
| Theor. | E(001) | Jennings | 1971 |
| Theor. | | Jennings | 1972 |
| Theor. | Fe(001) | Feder | 1973 |
| Theor. | W(110), W(001) | Feder | 1974 |
| Exp. | W(001) | O'Neill et al. | 1975 |
| Theor. | W(001) | Jennings | 1975 |
| Theor. | W(001) | Feder | 1976 |
| Theor. | W(001) | Feder et al. | 1976 |
| Theor. | Ni(111) | Feder | 1977 |

Photo Emission (vapour)

| | | | |
|---|---|---|---|
| Theor. | | Fano | 1969 |
| Exp. | Ce | Heinzmann et al. | 1970 |
| Exp. | Po. Alkali Atom | W. Hughes et al. | 1972 |
| Exp. | Ce Po.light | Drachenfels et al. | 1974 |
| Exp. | Th | Heinzmann et al. | 1975 |
| Exp. | Ce | Granneman et al. | 1976 |
| Theor. | | Feder | 1977 |

Others

| | | | |
|---|---|---|---|
| Theor. | exchange scattering | Byrne and Farago | 1965 |
| Theor. | Ne(resonance scattering) | Franzen and Gupta | 1965 |
| Exp. | K, exchange scattering | Farago and Siegmann | 1966 |
| Theor. | electron-magnon scattering | DeWames and Vredevoe | 1967 |
| Exp. | K, exchange scattering | Campbell et al. | 1971 |
| Theor. | excitation process of po. atom | Kleinpoppen | 1971 |

| | | | |
|---|---|---|---|
| Exp. | Ne(resonance scattering) | Heindorff et al. | 1973 |
| Theor. | Ne(resonance scattering) | Suzuki and Tanaka | 1973 |
| Theor. | excitation process of po. atom | Blum and Kleinpoppen | 1974 |
| Theor. | Ne(resonance scattering) | Suzuki et al. | 1975 |
| Theor. | surface of ferromagnetic metal | Penn | 1975 |
| | Hg(resonance scattering) | Düweke et al. | 1976 |
| Exp. | Hg(exchange scattering) | Hanne and Kessler | 1976 |
| Theor. | Hg(exchange scattering) | Hanne | 1976 |

# CHAPTER 7. OPTIMUM CONDITIONS OF THE ESP DETECTOR

## 7-1. Introduction

The ESP detector constructed by Deichsel (1961) is shown in Fig.7-1. It consists of a mercury reservoir, two sector type energy analysers and two electron multipliers. This was used to investigate the spin polarization of the electrons elastically scattered by the mercury atom. The energy resolution was set at less than 4.9 eV, the lowest excitation energy of mercury corresponding to $6^3P$ excitation. The scattering angle and angular resolution were set at 90° and 6° respectively. However, the

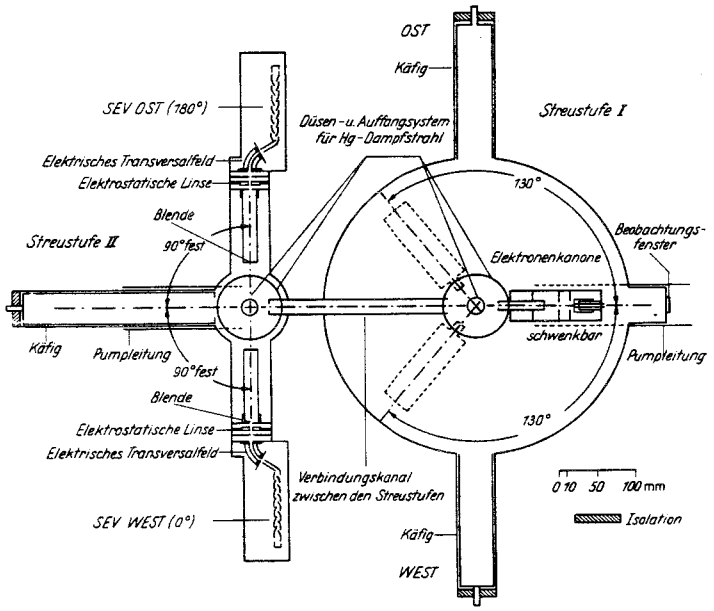


Fig.7-1. Electron spin polarization (ESP) detector (left side chamber) and polarizer (right side chamber) used by Deichsel (1961).

theoretical basis for these values was not shown with the exception of the energy resolution for the ESP detector.

Gronemeier (1970) measured the $6^1P$ excitation scattering, which is usually the most dominant inelastic process in electron-mercury scattering for electron impact energies between 20 and 300 eV and Yamazaki et al. (1977c) measured the loss spectra of mercury atom for electron impact energies between 300 and 1000 eV (see Secs. 3-6 and 4-3-2). The results

show that these inelastic electrons have little influence on the determination of the spin polarization when used in hundreds eV energy regions.

In this chapter, optimum conditions of the ESP detector using electron-mercury scattering are systematically studied and a high efficient ESP detector of simple construction is proposed.

## 7-2. Determination of $E$, $\theta$ and $\Delta\theta$

From equation (2-45), we can see that transverse spin polarization of electrons (i.e. spin polarization perpendicular to the scattering plane which is described by primary beam and direction of observation) can be analyzed by the scattering asymmetry. Substituting $\theta = 0$ and $\pi$, and $\mathbf{P} = (O, P, O)$ in equation (2-45), we obtain

$$\sigma_L = \sigma_0 (1 + S P) \tag{7-1}$$

$$\sigma_R = \sigma_0 (1 - S P) , \tag{7-2}$$

respectively (see Fig.7-2-a). Equations (7-1) and (7-2) lead to

$$N_R / N_L = (1 - PS) / (1 + PS) , \tag{7-3}$$

where $N_{R(L)} = N_{in} \cdot N_{Hg} \sigma_{R(L)} \mathrm{d}\Omega$, $N_{in}$ is the number of incident electrons per unit area, $N_{Hg}$ the number of mercury atom in collision volume, and $\mathrm{d}\Omega$ the acceptance solid angle of electron detector. Thus, we can determine the polarization of incident electrons by measuring the ratio of left-right asymmetry $N_R / N_L$.

Fig.7-2-b shows the differential cross section for a totally polarized incident electron beam of 300 eV. It seems that the grater the absolute value of the Sherman function, the greater the detectability of spin polarization becomes. However, from a practical point of view it should be noted that in these energy and angular regions, the differential cross section becomes extremely small, so the efficiency of the detector is reduced. Moreover, the Sherman function $S$ in these regions is in general rapidly varying for both the scattering angle and the impact energy (see Figs.7-3 to 7-6). This makes it difficult to estimate the Sherman function both theoretically and experimentally. The theoretical value of Sherman function differs considerably from the experimental one in these regions.

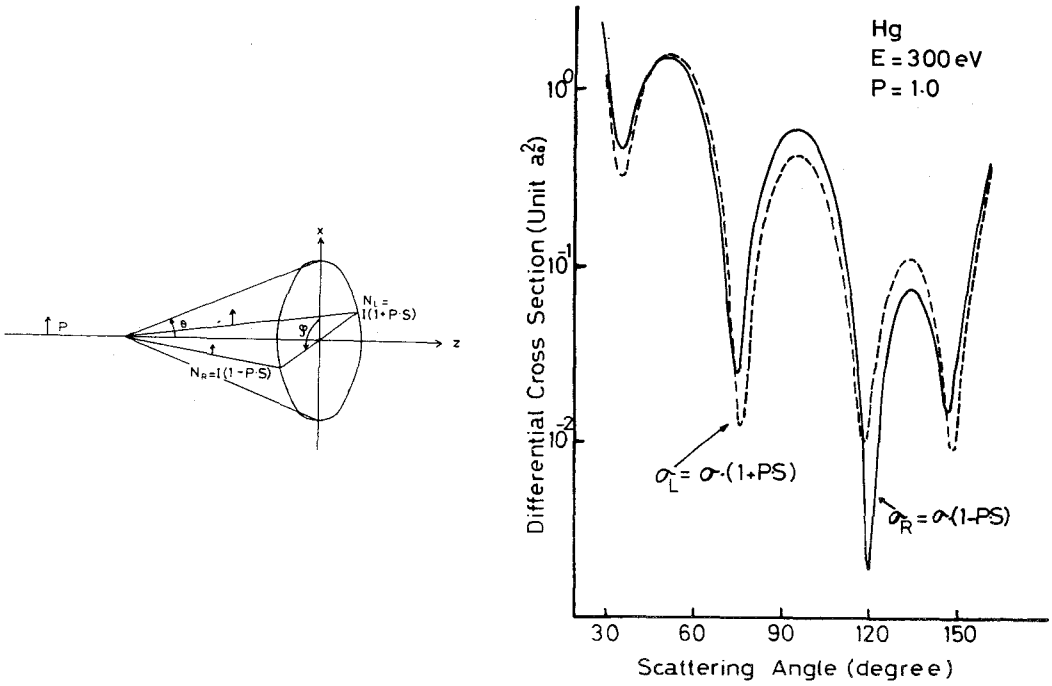


Fig.7-2. (a) Schematic diagram of left-right scattering asymmetry of a beam polarized perpendicular to scattering plane.
(b) Cross section for a totally polarized electron beam scattered by mercury atom at $E$ = 300 eV.

Furthermore, experimentally determined Sherman function in these regions depends strongly on the accuracy of the scattering angle and the angular resolution of the system.

To determine the best condition of the ESP detector systematically from these various parameters, first, the statistical error of the measured polarization is estimated from equation (7-3) as

$$\Delta P_{rel} = (2N)^{1/2} \cdot \Delta P / P \sim \left\{ (\sigma P^2 S^2)^{-1} - \sigma^{-1} \right\}^{1/2} \qquad (7\text{-}4)$$

Calculating the right hand side of equation (7-4) and taking into account both the differential cross section and ESP we can estimate the suitable regions for the energy, scattering angle and angular resolution necessary for the detector. Examples of the results are shown in Figs.7-3 to 7-6, together with the cross section and spin polarization. The results are summarized in Fig.7-7 for cases of the two different angular resolutions.

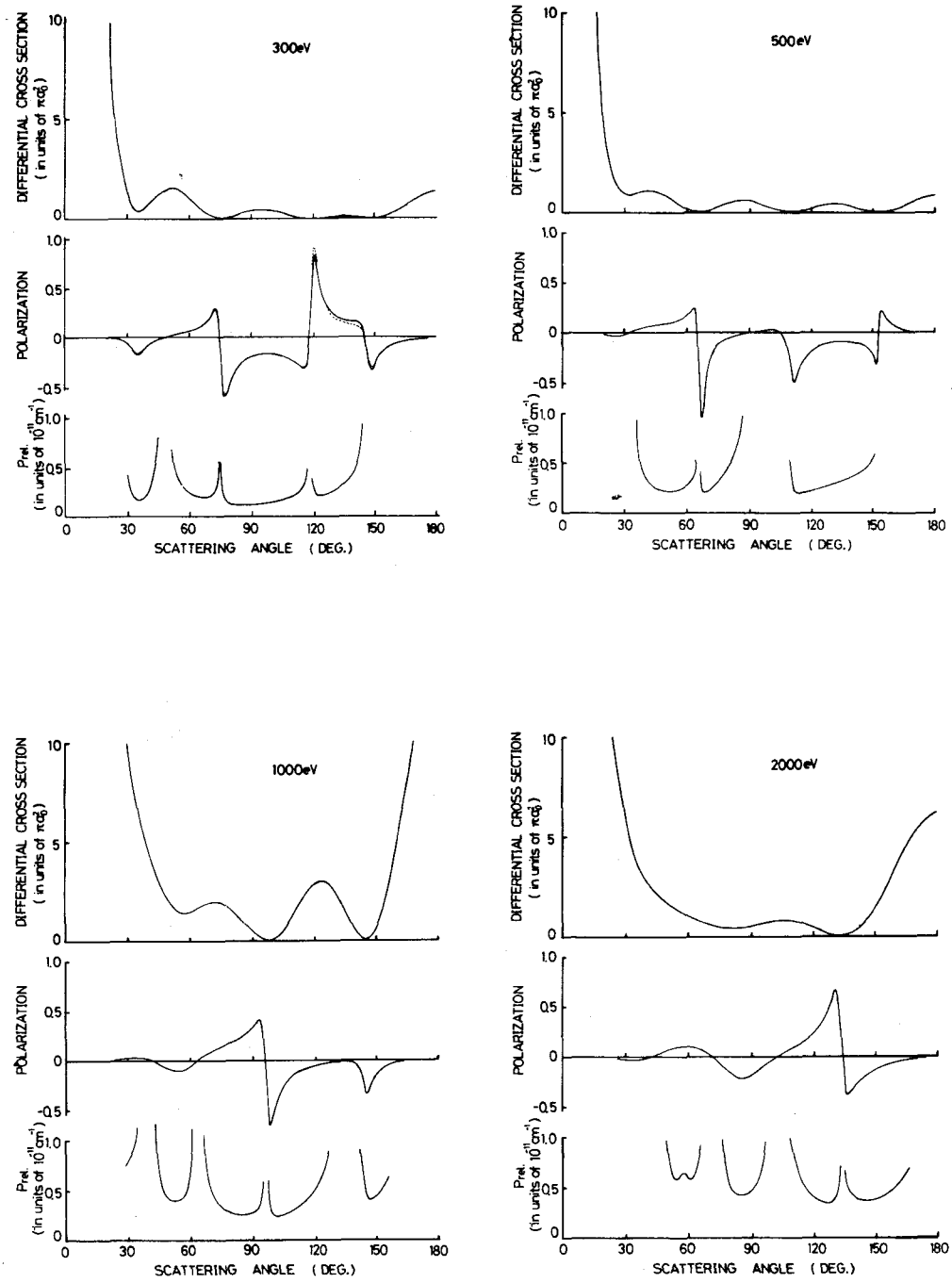


Fig.7-3 to 7-6. Relation between cross section, spin polarization and $\Delta P_{rel}$ for initial spin polarization of $P$= 0.1.

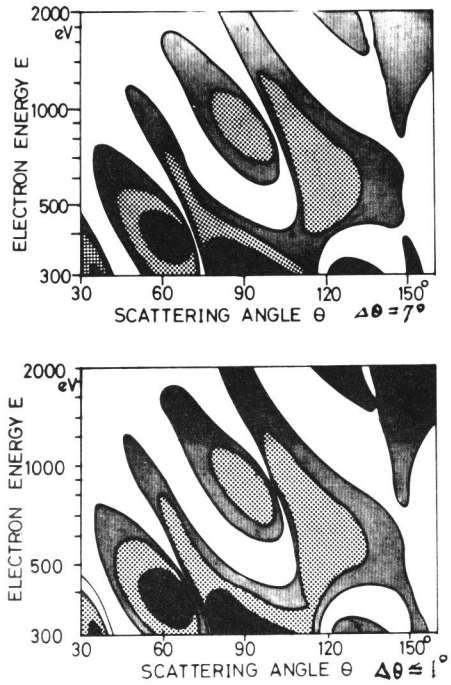


Fig.7-7. Contours of constant $\Delta P_{rel}$ for initial polarization of $P$ = 0.1 as function of scattering angle and electron energy for angular resolution of $\Delta\theta \leqq 1°$ and $\Delta\theta$ = 7°.

These results show that the optimum conditions do not concentrate around extremum points of Sherman function, but exist around 1) 300 eV, 90°, 2) 400 eV, 70°, 3) 600 eV, 120° and 4) 1000 eV, 90°. In these energy and angular regions, particularly at 300 eV, both the cross section and Sherman function are slowly changing functions with respect to scattering angle, so it is concluded that high angular resolution and high accuracy of angular setting are not necessary for the ESP detector to achieve high ESP resolution.

Other important points are 1) the Sherman function necessary for determination of polarization has nearly the same value for several theoretical calculations and experiments in these energy and angular regions, so the accurate Sherman function can be easily obtained both theoretically and experimentally, 2) S/N ratio may increase because of high scattering intensity.

It was concluded that an electron energy of 300 eV and a scattering angle of about 95° is the best condition for the optimum operation of the ESP detector in the hundreds eV energy regions.

As can be seen in equation (7-3), the left-right asymmetry remains constant over the region of scattering angle where Sherman function $S$ remains constant. From equation (7-3), for the angular resolution of $\Delta\theta$, the

observed spin polarization $P_{obs}$ is expressed as

$$P_{obs}/P = 1 + \frac{(\Delta\theta)^2}{24}\left(\frac{S''}{S} + \frac{2\sigma' S'}{\sigma S}\right) \qquad (7\text{-}5)$$

where $S' = \partial S/\partial\theta$ , $\sigma' = \partial\sigma/\partial\theta$ and $S'' = \partial^2 S/\partial\theta^2$

From equation (7-5), the error caused by the variation of the Sherman function in the angular range of 90° to 105° for incident energy of 300 eV is estimated to be less than about 1%.

The number of doubly scattered electrons $N_2$ may be roughly estimated as

$$N_2(\alpha) = N_{in} N_{Hg}^2 \int \sigma(\theta)\, \sigma(\alpha-\theta)\, d\theta \qquad (7\text{-}6)$$

where $\alpha$ and $\theta$ are the final and intermediate scattering angle respectively. Equation (7-6) shows that ratio of double scattering to single scattering is proportional to mercury vapour density, so in general sufficiently low density of mercury vapour is required for precise measurement of spin polarization (W. Eitel et al. 1968). Fig.7-8 shows $\sigma(\theta)\,\sigma(\alpha-\theta)$ as a function of $\theta$ for $\alpha$ = 95° and 75°. It shows that for $\alpha$ = 95°, the probability of the double scattering is dominant only near $\theta \sim 0°$ or 95°. A polarization **P** of incident electron is transformed to $\mathbf{P}_s$ after scattering according to the equation (2-48). Equation (2-48) shows that at forward scattering, initial polarization **p** is conserved during scattering, because $S \sim U \sim 0$ and $T \sim 1$ at forward scattering as is seen from Figs.7-9 and 2-9.

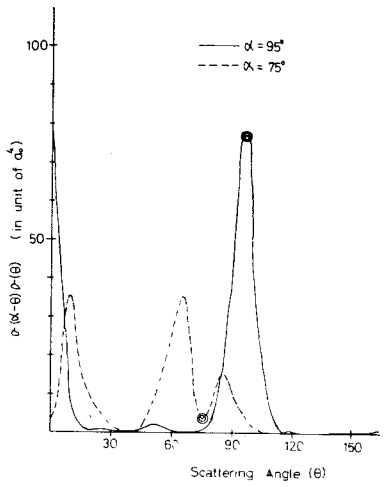


Fig.7-8. Contribution of doubly scattered electrons for incident electron energy of $E$ = 300 eV and final scattering angle of $\alpha$ = 95° ( solid line ) and $\alpha$ = 75° (dashed line) as a function of scattering angle of first scattering.

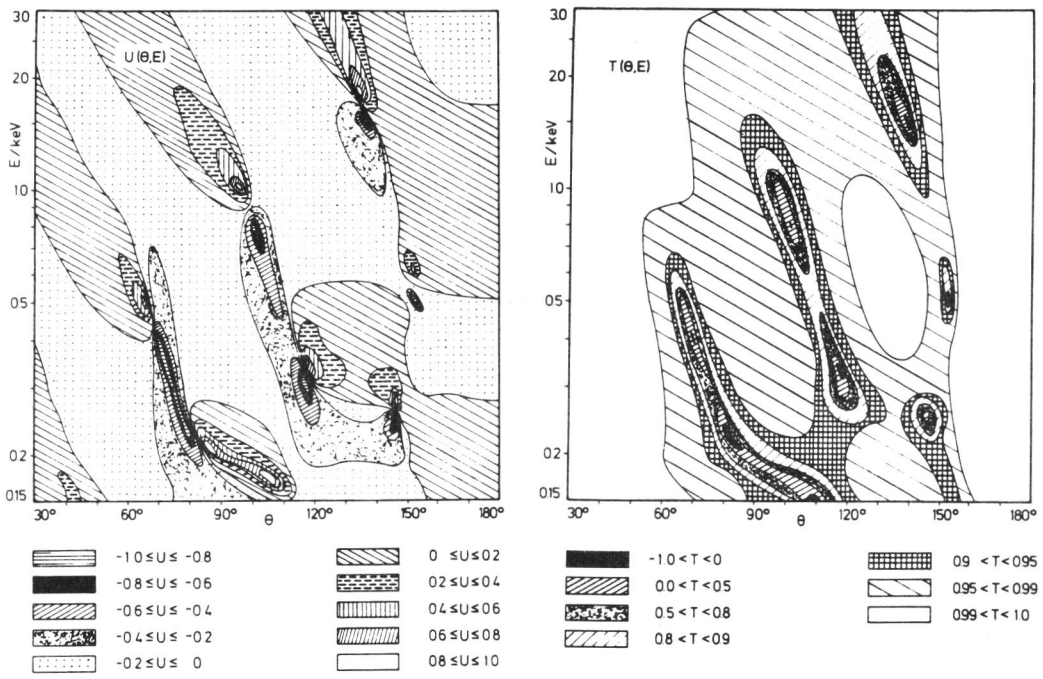


Fig.7-9. Contours of constant $U$ (a) and $T$ (b) for mercury as function of scattering angle and electron energy. $U$ describes the rotation of the polarization out of its initial plane. $T$ describes the reduction of the polarization component due to scattering (Kessler 1976).

(Note that $S^2+U^2+T^2 = 1$). This affects little on the determination of spin polarization. It is not the case at $\alpha$ =75° where an effective Sherman function originating from double scattering is modified by the Sherman function at $\theta$ =65° and 85°. It is concluded that the region of large cross section is desirable to make the affect of double scattering relatively less.

## 7-3. Determination of $\Delta E$

In this section, the energy resolution necessary for an ESP detector is investigated. From equation (7-3), the observed spin polarization $P_{obs}$ is expressed as

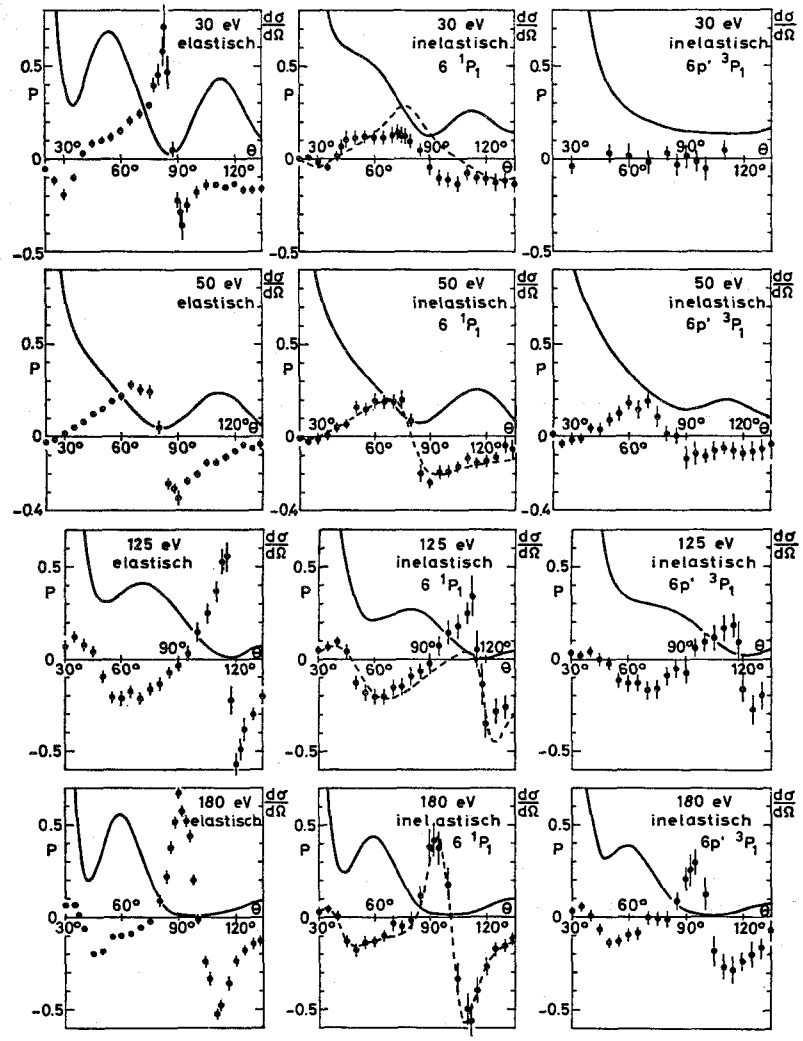


Fig.7-10. Experimental results of cross section and spin polarization for $6^1P$ and $6p'^3P$ excitation scattering.

$$P_{obs}\cdot S = (N_R - N_L + n_R - n_L) \,/\, (N+n)$$
$$= P\cdot S\cdot\left\{1 - S_{inel}/S)\, n/N\right\}\ , \qquad (7\text{-}7)$$

where $n_{R\ (L)}$ is the number of inelastically scattered electrons to the right (left) side, $S_{inel}$ the Sherman function of inelastically scattered electrons

$$N = N_R + N_L \qquad (7\text{-}8\text{-a})$$
$$n = n_R + n_L \qquad (7\text{-}8\text{-b})$$

From equation (7-7), if $P_{inel}=0$, i.e. inelastically scattered electrons are not polarized, the error induced by these electrons is estimated to be $n/N$, the ratio of inelastic electrons to elastic ones.

As was experimentally investigated in Chapter 4, the ratio $n/N$ for a hundreds eV electron remains within a few percent (see Fig.4-24). It increases when elastic cross section decrease. This implies that the error induced by inelastic electrons can be reduced if we adopt a condition where the elastic cross section is large.

Moreover, as was experimentally investigated by Hanne et al. (1972), inelastically scattered electrons corresponding to $6\,^1P$ and $6p'\,^3P$ excitations are polarized to some extent and show the similar profiles of spin polarization to elastically scattered electrons (see Fig.7-10). These facts suggest that the error originating from inelastic scattering can be less than $n/N$ (see equation 7-7).

It is concluded that the energy resolution of $\sim$ 13 eV (6.7 eV $\times$ 2) or more may not cause significant error (less than 2% see Fig.4-24) in the ESP detector, particularly at region near the maximum points of cross section.

## 7-4. Conclusion

The optimum condition proposed in this chapter is of practical importance for reducing unnecessary labor in both the construction of the ESP detector and precise measurement of spin polarization. From the discussions developed in Secs. 7-2 and 7-3, it is concluded that

$$
\begin{aligned}
E &\sim 300 \quad eV \\
\Delta E &\sim 13 \quad eV \\
\theta &\sim 95^\circ \\
\Delta\theta &\sim 15^\circ
\end{aligned}
\tag{7-9}
$$

may give the best condition for the ESP detector. Advantages of the condition are summarized as follows;

1) In this region , the Sherman function can be determined accurately.

2) The high accuracy of angular setting is not necessary, which results in simple construction of the ESP detector.

3) A large acceptance angle is allowable which results in high efficiency of the ESP detector.

4) The scattering cross section is large which results in better S/N ratio.

5) The ratio of inelastic to elastic scattering cross section is small which results in high efficiency and simple construction of the ESP detector.

6) The affect of multiple scattering is small which allows high density mercury vapour so results in high efficiency of the ESP detector.

For this condition and the mercury density of $10^{15}/cm^3$ (corresponding to the vapour pressure of $\sim 3 \times 10^{-2}$ Torr), the efficiency $\alpha_{eff}$ of the ESP analyser amount to approx. $10^{-6}$ where

$$
\alpha_{eff} = S_{eff}^2 \cdot I/I_0 \quad , \tag{7-10}
$$

$S_{eff}$ is an effective Sherman function and $I/I_0$ the intensity ratio of scattered to incident electrons. Equation (7-10) is derived from equation (7-4) taking into account the usual experimental condition of $S \cdot P \ll 1$.

A common Mott detector provides an efficiency of approx. $10^{-5}$ (see e.g. Kessler 1976) which is about one order larger than the value now obtained. However, the ESP detector using mercury has various advantages, primarily 1) electrons need not be accerelated to energies as high as 100 keV, which results in simple construction and easy operation of ESP detector, 2) this detector can also be used as a polarized electron source (see Chapter 8).

# CHAPTER 8. DOUBLE SCATTERING EXPERIMENT

## 8-1 Introduction

The optimum conditions of the ESP detector have been systematically determined in Chapter 7. In this chapter, the apparatus for double scattering experiments will be described (see Fig.8-1).

The first and second scattering is for production and detection of polarization, respectively. The arrangement of the ESP detector, the second scattering, is determined according to the line shown in Chapter 7. As a standard polarized electron beam source, electron-mercury elastic scattering is used, because the spin polarization in the electron mercury elastic scattering has been investigated in detail by several authors (see Tables 1-1 and 1-2). Since the intensity of an electron beam after double scattering is extremely weak, a Pierce-type electron gun of high intensity was constructed using a single crystal $LaB_6$ cathode.

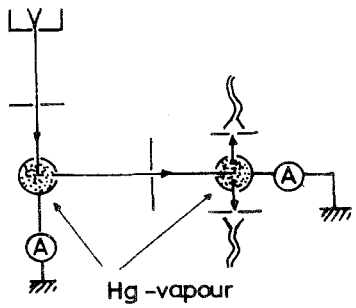


Fig.8-1. Schematic diagram of the double scattering experiment for mercury vapour.

## 8-2. Apparatus -- Design and Performance

### 8-2-1. Construction

The apparatus consists of an electron beam source, a first vacuum chamber as an electron spin polarizer and a second vacuum chamber as an ESP detector. An outer view of the apparatus shown in Fig.8-2 removing the top cover of the vacuum chamber. Fig. 8-3 shows cross sectional drawings of the system. The scattering angle at the first chamber is set at ~100° where highly polarized electrons are provided at E ~ 850 eV (see Fig.2-5). Fig.8-4 shows the block diagram of the vacuum system.

The first vacuum chamber is a 20 cm high cylinder of 12.4 cm inner diameter pumped by a 120 ℓ/s oil diffusion pump evacuating the system to residual gas pressure of $10^{-5}$ Torr, but the pressure increases to $5 \times 10^{-5}$ Torr during operation due to mercury vapour. The gun part is differential-

ly pumped by a 600 ℓ/s oil diffusion pump which provides a residual gas pressure of $\sim 5 \times 10^{-6}$ Torr. In the center of the second chamber, a collision chamber is set which is also used as the mercury reservoir and the Faraday cup from monitoring the primary electron beam current. The density of the mercury vapour is controlled by the inductionless heater wound around the

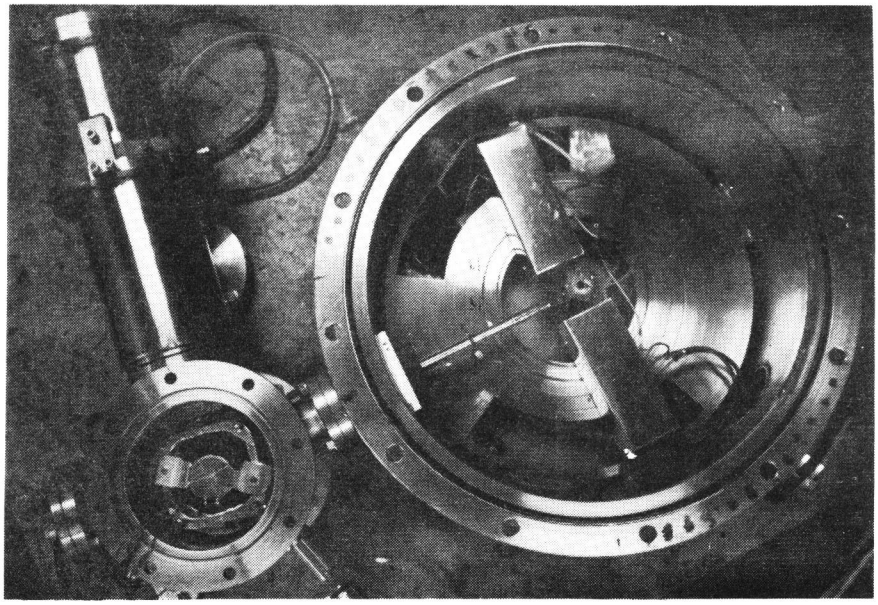

Fig.8-2. Top view of the apparatus for the double scattering removing the top cover of both 1st and 2nd chambers.

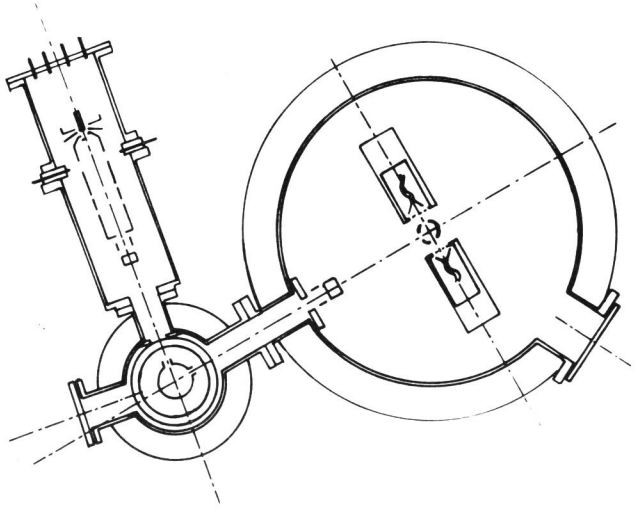

Fig.8-3. Schematic diagram of the apparatus constructed for the double scattering.

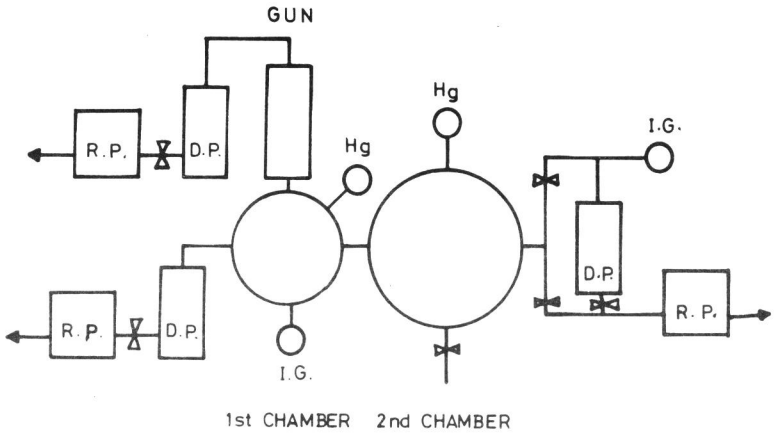


Fig.8-4. Schematic diagram of the vacuum system.

collision chamber which is pumped through two apertures (inner diameter of 4mm) which allow the incident and scattered electrons to pass.

The construction of the second chamber is like that used in Chapter 4 except the energy analyser and the collision chamber which is also used as a Faraday cup. Two energy analysers are set in the left and right sides of the collision chamber (in the scattering plane) at symmetric position with respect to incident beam axis at a scattering angle of approx.95°.

The cross sectional drawings of the energy analyser are shown in Fig. 8-5. The energy analysis is performed by a twofold retarding mesh (gold plated tungsten of 100 mesh) instead of a sector type analyser, the construction of which is confirmed by the investigation in Chapter 7. (It was shown that even energy resolution of approx.13 eV was still practically feasible). The outer view of the analyser is shown in Fig.8-6.

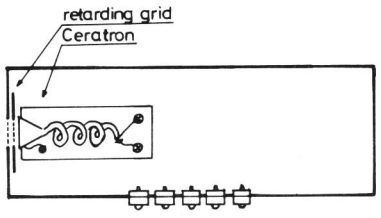


Fig.8-5. Schematic diagram of the energy analyser to the ESP detector.

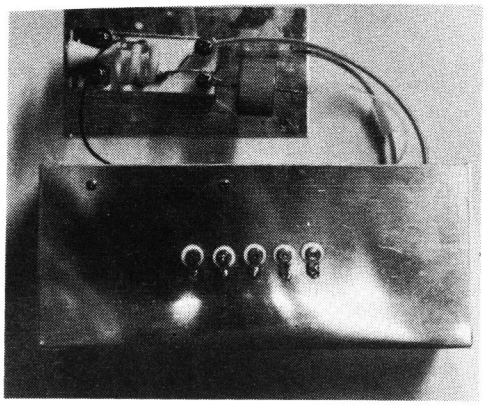

Fig.8-6. View of the electron multiplier and the case of energy analyser.

The electron multiplier used is a kind of channeltron (Murata Co., Ceratron Type EMS-6081B) with an acceptance cone and a holding stage.

### 8-2-2. Pierce-Type Electron Gun Using $LaB_6$ Single Crystal as a Cathode

As the intensity of an electron beam after double scattering is extremely weak, an electron gun of high beam intensity is necessary for double scattering experiment. For this purpose, a Pierce-Type electron gun of high beam intensity was constructed (Pierce 1954). The Pierce-Type electron gun is designed for use in space-charge limited regions and provides a parallel electron beam. The main part of this gun consists of a cathode with flat

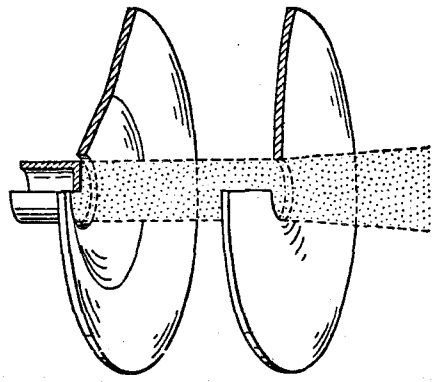

Fig.8-7. Schematic diagram of cathode and anode electrodes of Pierce type electron gun (Pierce 1954).

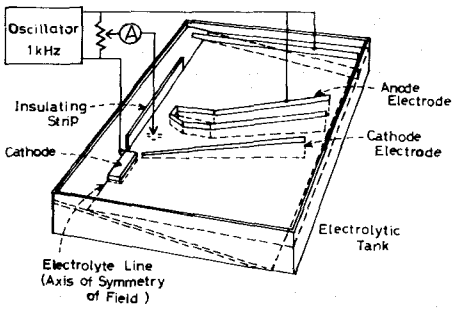


Fig.8-8. Schematic diagram of the electrolytic tank.

surface, a cathode electrode and an anode electrode as is schematically shown in Fig.8-7. The actual shapes of these electrode are determined using an electolytic tank (see Fig.8-8). It was concluded that the shape of the cathode electrode should have the same shape as the usual Pierce gun with an angle of 67.5° between the electrode and the beam axis.

The cathode are heated by electron-bombardment. To prevent the bombarding electrons from straying into the electron beam from the cathode, a shielding electrode is set between the cathode electrode and the heater for electron bombardment. Parts of both the cathode and shielding electrodes near the cathode consist of Ta to obtain stable performance during operation at high temperatures. Fig.8-9 is a cross sectional drawing of the Pierce

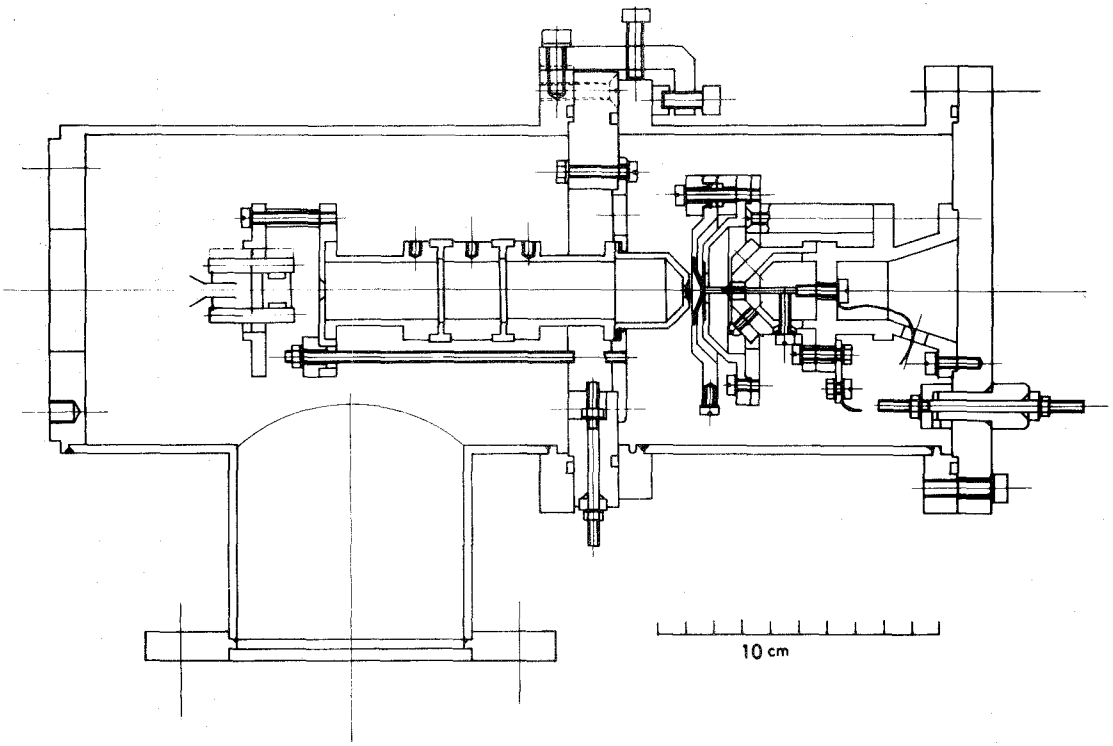


Fig.8-9. Cross section of the Pierce-type electron gun with einzel lens and deflector, and its vacuum chamber.

gun constructed. An asymmetric three cylindrical lens with deflector is set in front of the anode electrode.

$LaB_6$ single crystal is used as a cathode because of its high emission current and stable performance over a long period of time (long service life) which originates from the low values of both the work function and the vapour pressure (J.M. Lafferty 1951). Moreover, the $LaB_6$ single crystal has flat surface plane of stochiometric uniformity (T. Tanaka et al. 1975) which enables one to obtain a beam of higher current intensity with good parallelism and spatial uniformity.

The cathode consists of a $LaB_6$ single crystal rod with a diameter of 2mm and length of 7mm held in a Ta cylinder. The Ta cylinder is connected to a 2mm diameter W-rod with three spot welded Ta wires in order to limit power consumption. Furthermore, this prevents the gun assembly from deteriorating the vacuum by heating the area surrounding the cathode. The distance between the anode and the cathode was 5.5 mm and the perveance was $2.42 \times 10^{-7}$ $A/V^{3/2}$. Two Ta ribbons ($0.025 \times 0.75$ mm) were held around the $LaB_6$ cathode. The two Ta ribbons had heating currents of opposite direction in order to reduce the current-induced magnetic field around the emitter.

Fig.8-10 is an outer view of the cathode and bombarding system with both the cathode and the shielding electrode removed.

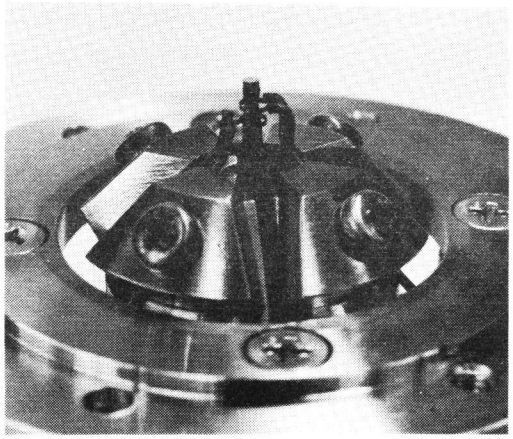

Fig.8-10. View of the single crystal $LaB_6$ cathode and its holding system removing anode, cathode and shielding electrodes.

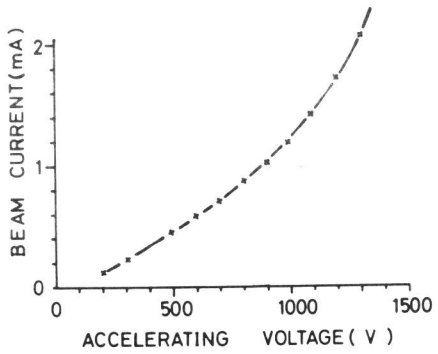


Fig.8-11. Relationship between beam current and accelerating voltage (×: beam current).

To evaluate the performance, $LaB_6$ was heated up to ~1600°C with accelerating voltage range of 200-1300 eV. With these operating conditions, the gun was being operated in the space charge limited region, with approx. 12W of power consumed. During operation, evaporated $LaB_6$ is continually deposited on the Ta-ribbons which reduces the work function of the ribbons, which in turn reduces the heating power to approx. 6 W. The beam diameter was observed with a fluorescent screen situated 10 cm along the beam path from the anode. The spot size of the beam was found to be 3-4 mm in diameter for the above accelerating voltages. The beam current was measured by a Faraday cup having an inner diameter of 4 mm at a vacuum pressure of $3 \times 10^{-6}$ Torr. Fig. 8-11 shows the relationship between the beam current and the accelerating voltage. The rapid variation of the beam current in current stability measurements was rarely observed and the beam current drift was less than 0.1 %. As in seen in Fig.8-11 the actual perveance was found to be $3.8 \times 10^{-8}$ $A/V^{3/2}$.

## 8-2-3. System of Measurement

A schematic diagram of the electric circuit used for the double scattering experiment is seen in Fig.8-12. The memory section of M.C.A. was devided into two parts to treat the signals of the two origins. A pulse is at first amplified and then arrives at A.D.C. input in the M.C.A. through the mixer. At the same time, the memory region is selected based

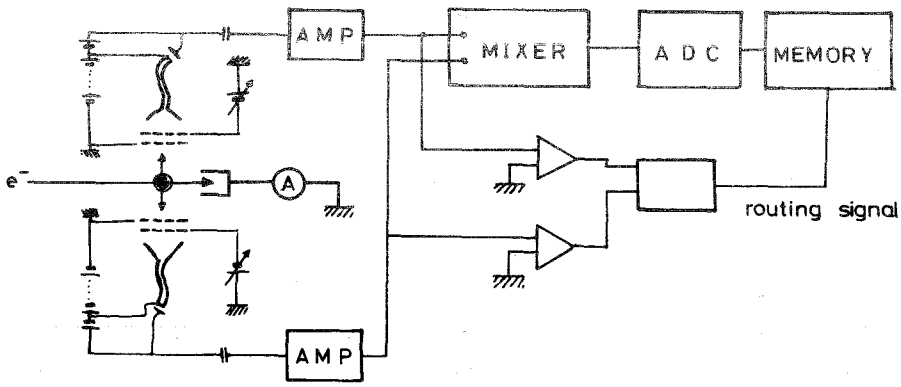


Fig.8-12. Schematic diagram of the electric circuit for double scattering experiment

on which multipliers the pulse originates. This is a successful method when counting ratio of both the multipliers are low because switching time or dead time of M.C.A. has little effect on measurements. Moreover, we can correct the external and internal background by direct observation of P.H.D.

The system used was Ortec "Spectroscopy Amplifier 472A (×2), Ortec "Dual Sum and Invert Amplifier, 433A", and Ino-Tech IT-5200 Multi-Channel-Analyser.

## 8-3. Proposal for an Application of Electron-Mercury Scattering to a Polarized Beam Source

As is shown in Sec.2-3 and Appendix 3, polarizing and analysing powers are expressed by the same function $S$ (Sherman function) in the case of elastic scattering. In a certain type of scattering experiment, an intensity measurement using an initially polarized electron beam is superior to a polarization measurement using initially unpolarized electron beam.* This is precisely the case in studies of surface physics, where primary electron beam should be sufficiently weak so as not to damage a sample surface.

Kessler (1976) summarized various polarized sources and estimated its beam qualities, which is shown in Table 8-1. '$P^2 I$', appearing at the top of the 5th column in Table 8-1, may serve as a kind of parameter for an estimation of beam quality (see Sec.7-4, where the similar quantity $\alpha_{eff}$ is used for the estimation of efficiency of the ESP detector.). The 6-th column Beam quality $q$ is determined by

$$q = \frac{P^2 I}{r_0^2 \alpha_0^2 E_0} \quad , \tag{8-1}$$

---

* Recently, an experiment of similar conception is reported to be in progress (Unertl et al. 1977) where photo electrons from GaAs surface are used as a polarized electron source for LEED study.

where $r_0$ is the radius of a beam-cross-section minimum, $\alpha_0$ the corresponding semi-aperture of the beam and $E_0$ the energy of electrons leaving the source. We can see that $q$ takes into account the polarization, intensity and collimation of the beam. From Table 8-1, the beam source using "scatter-

| Method | $P$ | $I$ | | $P^2I$ (Ampere) | Beam quality $q$ Eq. (7.19) |
|---|---|---|---|---|---|
| | | d.c. (Ampere) | pulsed($\approx 1\mu s$) (el./pulse) | | |
| Scattering from unpolarized targets | 0.2 | $3.5 \cdot 10^{-8}$ | | $10^{-9}$ | Medium |
| Exchange scattering from polarized atoms | 0.5<br>0.2 | | $10^4$<br>$10^7$ | $2 \cdot 10^{-14}$<br>$7 \cdot 10^{-12}$ | Low to medium |
| Photoionization of polarized atoms | 0.76 | | $8 \cdot 10^8$ | $10^{-8}$ | Medium |
| Fano effect | 0.65<br>0.9 | $1.5 \cdot 10^{-9}$ | $3 \cdot 10^9$ | $6 \cdot 10^{-10}$<br>$2 \cdot 10^{-11}$ | Medium |
| Collisional ionization in optically pumped He discharge | 0.3 | $5 \cdot 10^{-7}$ | | $5 \cdot 10^{-8}$ | Medium to high |
| Field emission from ferromagnets | 0.89 | $10^{-6}$ | | $8 \cdot 10^{-7}$ | High |

Table 8-1. Comparison of various sources of polarized electrons (Kessler 1976).

ing from unpolarized targets" is ranked "medium". Thus, the ESP detector using mercury vapour may work well as a polarized beam source, if an electron gun is mounted together with the electron multiplier.

It is worth noting that this system provides precise information on the scattering process by comparing the polarizing and analysing power, i.e., these two values are not equal to each other e.g. in exchange scattering as is shown in Appendix 4.

## SUMMARY

The present work consists of two parts, Part I which consists of Chapter 1-5 and Part II , Chapter 6-8. The main subject of Part I is "Electron-Mercury Scattering" and that of Part II , "ESP detector using Mercury Vapour". The results obtained in the present study are summarized chapter by chapter as follows.

### Part I Electron-Mercury Scattering

Chapter 1; Introduction

1) The characteristics of electron-heavy atom scattering are briefly described.
2) A historical view of electron-mercury scattering is given together with bibliographies. It becomes apparent that the studies have been strongly biased toward elastic scattering for both experimental and theoretical studies.

Chapter 2; Theory of Electron-Mercury Elastic Scattering --- Modification and Extention of Current Theory

1) Particular attention needed for the theoretical treatment of electron-heavy atom scattering is described.
2) $e^-$-Hg elastic scattering is treated relativistically using a non-relativistic Hartree potential. The scattering amplitude is written down for an arbitral incident direction of electron beam.
3) The efficient and accurate computer program is developed for electron-atom elastic scattering. Theoretical calculation is made for both the differential cross section and spin polarization of the incident electron energy between 300 and 2000 eV. In these energy regions, the calculated results agree well with both experimental results and other theoretical results calculated by more accurate but complex theories, which include exchange effect between incident and atomic electrons, and distortion of atom by electric field of incident electrons.
4) The cross section calculated in this way provides important information concerning study on the behaviour of Auger electrons in solids using Monte-Carlo calculation. Because the screened Rutherford scattering formula which is usually used in the Monte-Carlo calculation breaks down for low energy electron scattering.

Chapter 3; Theory of Electron-Mercury Inelastic Scattering
--- Application of DWB Theory

1) DWB approximation is applied to electron-impact excitation of $6^1P$ state of mercury.
2) The computer program is developed for electron-atom inelastic scattering using the DWB approximation. The DWB calculation is performed for atomic wave functions constructed using Coulomb approximation and Hartree approximation in the incident electron energy of 50 to 500 eV.
3) It is shown that at an impact energy greater than 300 eV, the spin polarization of inelastic electrons differs considerably from that of elastic electrons at scattering angles less than 90° for both the atomic wave functions.

Chapter 4; Measurement of Loss Spectra

1) Construction of an apparatus for the measurement of loss spectra is described.
2) The loss spectra of electron-mercury scattering are obtained in the energy region between 300 and 1000 eV at a scattering angle of 50 to 110°.
3) Allowed transitions such as $6^1P$ and $6p'^3P$ excitation are dominant in these energies and scattering angles, and show similar diffraction pattern to elastic scattering. However, the transition rate to $7^1S$ state (strictly forbidden transition) is higher than that to $6^3P$ state, and $6^3P$ state is higher than that to $7^1P$ state (allowed transition).

Chapter 5; $6^1P$ Excitation --- Comparison of Theory and Experiment

1) The results in Chapters 3 and 4 are compared.
2) The DWB calculation using Coulomb approximated atomic wave function provides values of cross section in close agreement with experiment, however, the DWB approximation using Hartree atomic wave function provides profiles of angular dependence of cross section and spin polarization in close agreement with experiment.
3) From this result, it is conjectured that the actual 6s and 6p wave functions of mercury may have similar profiles to that of Hartree wave functions. However, (6s) wave function for $(6s)^2$ state and that for (6s)(6P) state may be much more isolated from each other in the actual case than in Hartree case.

## Part II. ESP-Detector Using Mercury Vapour

### Chapter 6; Introduction

1) Studies on ESP experiments and ESP detectors used for these experiments are briefly reviewed.

### Chapter 7; Optimum Conditions of the ESP Detector.

1) Optimum conditions of ESP detector are systematically investigated utilizing the results in Chapters 2,3 and 4.
2) The conclusions obtained are $E$=300 eV, $\theta$=95°, $\Delta E \approx$13 eV and $\Delta\theta \approx$10°.
3) The spin-polarization detector using mercury is compared to the conventional Mott detector to draw out the conclusion that the former type is more appropriate for wider application.

### Chapter 8; Double Scattering Experiment

1) An apparatus for double scattering experiments is described, using the conclusion derived in Chapter 7.
2) The Pierce-type electron gun using $LaB_6$ single crystal cathode is designed and constructed for double scattering experiment.
3) It is proposed that an ESP detector of this type may be also used as a polarized electron source which provides a powerful method particularly in the region of surface physics.

## APPENDIX 1. QUALITATIVE EXPLANATION OF THE DIFFRACTION EFFECT IN e-ATOM SCATTERING

One of the most important reason for the occurrence of the diffraction effect is that a wave length of low and intermediate energy electrons is comparable to the radius of an atom as has already been mentioned in Sec.1-1. Although the atomic radius of various elements is comparable with each other, the diffraction effect becomes clear and complex for heavier elements. Furthermore, the maximum impact energy for the diffraction effect to occur shifts to higher energies for heavier elements. For example they are 6 eV for H and 15 eV for He (Mott and Massey 1965), however, higher than 10 keV for Hg. The following consideration provides a qualitative explanation for these phenomena. The diffraction pattern appears if only several partial waves with considerable values of phase shifts contribute to scattering. For this, atomic potential should be narrow and deep enough, and attractive. This is because for attractive case, atomic potential can pull in considerable cycles of wave if the deepness of the potential is sufficient, which results in large phase shift. This is not the case for narrow and repulsive potential because the cycles that can be swept out of the potential region are very small, which results in small phase shift. If the potential is long range, a number of partial waves contribute to scattering, so diffraction phenomena can not be observed for both attractive and repulsive potentials.

The radial wave equation is written as

$$\frac{d^2L}{dr^2}+\frac{2}{r}\frac{dL}{dr}+\left(K^2-U(r)-\frac{l(l+1)}{r^2}\right)L=0\ , \qquad \text{(A-1-1)}$$

for non-relativistic case (cf. equation 2-32). It is seen that an effective potential consists of an attractive atomic potential and repulsive centrifugal potential. Putting $U(r)=-2\frac{Ze^2}{r}\exp(-r/a_0)$ for simplicity, we obtain condition for atomic number,

$$Z>l\ (l+1)\ /a_0\cdot e^2\sim l\ (l+1)\ , \qquad \text{(A1-2)}$$

which is the condition that the atomic potential dominates the centrifugal potential in a certain radial regions. In equation (A1-2), the screening parameter $a_0$ is assumed to be the order of Bohr radius. It is seen from equation (A1-2) that the number of partial waves which undergo an atomic potential dominantly becomes larger as the $Z$-number increases. This means

that the diffraction pattern becomes complex for heavier element. Furthermore, a main part of an $l$-th partial wave exists around the principal region of the effective potential if

$$Ka_0 < 1 \ , \tag{A1-3}$$

where $K$ is a wave number of incident electron. From equation (A1-2) and (A1-3), the maximum impact energy where the diffraction effect occures clearly is estimated as i.e. 13 eV for H and 1000 eV for Hg. Large discrepancy for mercury will be reduced if the depth of the atomic potential is taken into consideration.

## APPENDIX 2. INCAPABILITY OF POLARIZING AND ANALYZING ELECTRON SPIN BY MACROSCOPIC METHOD

Let us consider at first producing polarized electrons by macroscopic field (a kind of Stern-Gerlach experiment).

Suppose that a beam of electrons travels along the z-axis with velocity $v_z$ in an unhomogeneous magnetic field **H**. It is assumed that $H_z$ is everywhere zero, and that in the xz-plane $H_y$ is also zero i.e. an actual shape of magnet has a same cross section with respect to xy-plane along z-axis and is symmetric with respect to xz-plane (see Fig.A-1). The force on the electron tending to split the beam is

$$e \frac{\partial H_x}{\partial x} \ . \tag{A2-1}$$

On the other hand, because of the finite breadth of the electron beam, electrons travelling at a distance $\Delta y$ from the xz-plane will be subject to a force

$$e v_z H_y \ , \tag{A2-2}$$

in the x-direction. Considering that

$$\mathbf{div}\,(\mathbf{H}) = 0 \ , \tag{A2-3}$$

equation (A2-2) can be rewritten as

$$e\, v_z\, \partial H_x / \partial x \cdot \Delta y \quad . \tag{A2-4}$$

This force causes a spreading of the beam, so should be smaller than (A2-1), i.e.,

$$e\, v_z\, \partial H_x / \partial x \cdot \Delta y \; < e\, \partial H_x / \partial x \, . \tag{A2-5}$$

However, the uncertainity principle states, that

$$\Delta v_y \cdot \Delta y \sim 1 \quad . \tag{A2-6}$$

Inequality (A2-5) therefore leads to the inequality

$$\Delta v_y \; > v_z \quad . \tag{A2-7}$$

That is to say, the slit must be so narrow (of the order of the de Broglie wave length) that we have not got a beam at all, but a cylindrical wave emerging from it (Mott 1929).

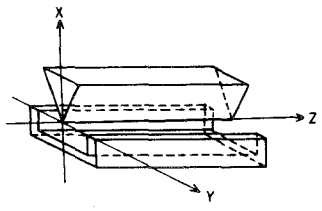


Fig. A-1. Schematic diagram of the magnet.

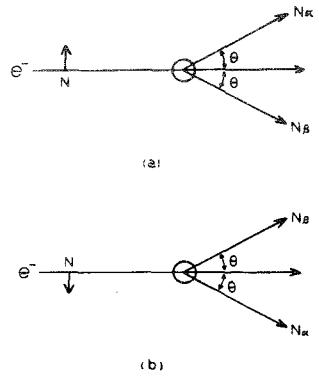


Fig. A-2. Scattering asymmetry for totally polarized incident electron beam.

The situation is similar for detecting electron spin. Suppose the electron was at distance $R$ from the magnetometer, then the order of magnitude of the magnetic field due to the spin is

$$e/R^3 \quad . \tag{A2-8}$$

There may be a magnetic field due to the motion of the electron, the order of which is

$$e\,v/R^2 \quad , \tag{A2-9}$$

where $v$ is the velocity of the electron. From the uncertainity principle

$$\Delta R \;\; \Delta v \sim 1 \quad , \tag{A2-10}$$

where $\Delta R$ and $\Delta v$ are the uncertainities in our knowledge of $R$ and $v$. Now in order that equation (A2-8), the effect of the spin, shall be observable, it must be greater than the uncertainity in equation (A2-9). That is to say,

$$e/R^3 > e\,\Delta v/R^2 \quad . \tag{A2-11}$$

Hence from equation (A2-10)

$$\Delta R > R \quad . \tag{A2-12}$$

Measurement will therefore be impossible (Mott 1929).

## APPENDIX 3. RELATIVISTIC RUTHERFORD SCATTERING FORMULA

For Coulomb potential $-Ze^2/r$, the integral in equation (2-26) can be performed and results in

$$\begin{aligned} f_{Born} &= Ze^2 \left\{ H(\mathbf{k}_f) + W \right\} / (\mathbf{k}_i - \mathbf{k}_f)^2 \cdot u(\mathbf{k}_i) \\ &= Ze^2/(4\mathbf{k}^2 \cdot \sin^2\theta/2) \left\{ H(\mathbf{k}_f) + W \right\} u(\mathbf{k}_i) \quad , \end{aligned} \tag{A3-1}$$

where $\phi_j(r') = e^{i\mathbf{k}_i \mathbf{r}} u(\mathbf{k}_i)$ and $W + H(\mathbf{k}_f) = W - \boldsymbol{\alpha}\mathbf{k}_f - \beta$. The operator $W + H(\mathbf{k}_f)$ gives 0 when operated to negative energy states and gives finite value when operated to positive energy states, which assures the final states being in positive energy states. Thus

$$d\sigma/d\Omega = |f_{Born}|^2 = \left\{ Ze^2/(4K^2 \cdot \sin^2\theta/2) \right\}^2 2W\, u(\mathbf{k}_i)^{+} \left\{ H(\mathbf{k}_f) + W \right\} u(\mathbf{k}_i) \quad . \tag{A3-2}$$

The linearly independent solution of free states can be written as

$$u_1(\mathbf{k}_i)=\sqrt{(W+1)/2W}\begin{Bmatrix}1\\0\\K_{iz}/(W+1)\\(K_{ix}+iK_{iy})/(W+1)\end{Bmatrix}, \tag{A3-3}$$

and

$$u_2(\mathbf{k}_i)=\sqrt{(W+1)/2W}\begin{Bmatrix}0\\1\\(K_{ix}-iK_{iy})/(W+1)\\-K_{iz}/(W+1)\end{Bmatrix}, \tag{A3-4}$$

which is proved by direct substitution. For the state expressed by equation (A3-3), equation (A3-2) gives

$$\begin{aligned}d\sigma/d\Omega &= \frac{Z^2e^4}{4K^4\sin^4\theta/2}\cdot\frac{1}{2}\left\{(W^2+1)+(\mathbf{k}_i,\mathbf{k}_f)\right\}\\ &= \frac{Z^2e^4}{4K^4\sin^4\theta/2}(W^2-K^2\cdot\sin^2\theta/2)\\ &= \frac{Z^2e^4}{4v^4\sin^4\theta/2}(1-v^2\cdot\sin^2\theta/2)(1-v^2),\end{aligned} \tag{A3-5}$$

where $v=K/W$ Equation (A3-5) is just equal to equation (2-27). The calculation for the state expressed by equation (A3-4) also results in the same equation as (A3-5), this means that Sherman function always equals to zero in Born approximation. So for the analysis of phenomena concerning spin polarization, the Born approximation is an ineffective approximation.

To investigate the origin of the second factor of equation (A3-5), we shall treat a spin 0 particle by Klein-Gordon equation, i.e.

$$\left\{(W-V)^2-(\mathbf{p}^2+1)\right\}\psi=0\ . \tag{A3-6}$$

A similar procedure adopted in Sec.2-2-1 gives the integral equation of (A3-6) as follows; The Lippmann-Schwinger equation of (A3-6) is written as

$$\psi=\Phi+\frac{1}{W^2-\mathbf{p}^2-1+i\varepsilon}(2WV-V^2)\psi\ . \tag{A3-7}$$

Using equation (2-21),

$$\psi = \Phi - \frac{1}{4\pi}\frac{e^{iKr}}{r}\int e^{-i\mathbf{k}_f\mathbf{r}'}\,(2WV(\mathbf{r}') - V(\mathbf{r}')^2)\,\psi(\mathbf{r}')\,d\mathbf{r}', \qquad \text{(A3-8)}$$

the notation used here is same as that used in Sec.2-2-1.

Introducing first Born approximation, i.e. $\psi \to \Phi$, $2WV + V^2 \to 2WV$ equation (A3-8) results in

$$\psi = \Phi - \frac{e^{iKr}}{r} \cdot Ze^2 2W/(\mathbf{k}_i - \mathbf{k}_f)^2 \quad . \qquad \text{(A3-9)}$$

Thus

$$f_{KG} = -Ze^2 W/(2K^2 \cdot \sin^2\theta/2) \quad , \qquad \text{(A3-10)}$$

and

$$\left(\frac{d\sigma}{d\Omega}\right)_{KG} = \frac{Z^2 e^4}{4K^4 \sin^4(\theta/2)}\,W^2 = \frac{Z^2 e^4}{4v^4 \sin^4(\theta/2)}(1-v^2) \quad . \qquad \text{(A3-11)}$$

The comparison with equation (A3-5) or (2-27) shows that the factor $(1 - v^2 \cdot \sin^2\theta/2)$ is dropped out in the case of spin 0 Klein-Gordon particle. It may be concluded that this factor reflects the effect of electron spin (Nishijima, 1973).

## APPENDIX 4. QUALITATIVE EXPLANATIONS OF THE TWO ROLES OF SHERMAN FUNCTION

Let scattering efficiencies be $\alpha$ and $\beta$ for spin-up electrons scattered to left and right side respectively, then $\alpha$ and $\beta$ are also the scattering efficiencies for spin-down electrons scattered to right and left side respectively (see Fig.A-2). Then for an initially unpolarized electron beam, the spin polarization $P_L$ after scattering to left side may be expressed as

$$P_L = \frac{N\alpha - N\beta}{N\alpha + N\beta} = \frac{\alpha - \beta}{\alpha + \beta} \quad . \qquad \text{(A4-1)}$$

On the other hand, the left-right asymmetry for a totally polarized incident electron beam (spin-up state) may be expressed as

$$N_R / N_L = \beta / \alpha = (1 - P_L) / (1 + P_L) \ . \tag{A4-2}$$

From equation (3-7), it is seen that $P_L$ plays also a role of Sherman function.

On the other hand, for example in the case of exchange scattering, $P$ and $S$ are not equal to each other. Putting direct and exchange scattering amplitude as $f(\theta)$ and $g(\theta)$, we have the cross section for an unpolarized electrons scattered by totally polarized atoms as follows (Kessler 1976);

| Process | | Cross Section | |
|---|---|---|---|
| $e_\downarrow + A_\uparrow$ | $e_\downarrow + A_\uparrow$ | $\lvert f(\theta)\rvert^2$ | |
| $e_\downarrow + A_\uparrow$ | $e_\uparrow + A_\downarrow$ | $\lvert g(\theta)\rvert^2$ | (A4-3) |
| $e_\uparrow + A_\uparrow$ | $e_\uparrow + A_\uparrow$ | $\lvert f(\theta) - g(\theta)\rvert^2$ | |

and

| | | | |
|---|---|---|---|
| $e_\uparrow + A_\downarrow$ | $e_\uparrow + A_\downarrow$ | $\lvert f(\theta)\rvert^2$ | |
| $e_\uparrow + A_\downarrow$ | $e_\downarrow + A_\uparrow$ | $\lvert g(\theta)\rvert^2$ | (A4-4) |
| $e_\downarrow + A_\downarrow$ | $e_\downarrow + A_\downarrow$ | $\lvert f(\theta) - g(\theta)\rvert^2$ | |

for spin-up and spin-down atomic state respectively. Then the spin polarization $P$ of initially unpolarized electrons scattered by totally polarized spin-up atoms is expressed as

$$P = \frac{\lvert f(\theta) - g(\theta)\rvert^2 + \lvert g(\theta)\rvert^2 - \lvert f(\theta)\rvert^2}{\lvert f(\theta) - g(\theta)\rvert^2 + \lvert f(\theta)\rvert^2 + \lvert g(\theta)\rvert^2} \ . \tag{A4-5}$$

On the other hand, the scattering intensity of totally polarized spin-up and spin-down electrons scattered by totally polarized spin up atoms are $\lvert f(\theta) - g(\theta)\rvert^2$ and $\lvert f(\theta)\rvert^2 + \lvert g(\theta)\rvert^2$, respectively. So the value corresponding to the value $P$ in equation (A3-5) may be expressed as

$$S = \frac{\lvert f(\theta) - g(\theta)\rvert^2 - \lvert f(\theta)\rvert^2 - \lvert g(\theta)\rvert^2}{\lvert f(\theta) - g(\theta)\rvert^2 + \lvert f(\theta)\rvert^2 + \lvert g(\theta)\rvert^2} \ . \tag{A4-6}$$

It is worth noting that this is not a left-right asymmetry but a "spin-up-down" asymmetry (Kessler, 1976).

## APPENDIX 5. VARIOUS CALCULATION PROCEDURES FOR THE ESTIMATION OF PHASE SHIFT

1) A direct integration of equation (2-28) by Runge-Kutta process was performed by Bunyan (1962). This method was usually used in the calculation of atomic wave function. (e.g. Mayer 1957)

2) Putting $g_K = a^{1/2} G_K / r$ and substituting in equation (2-32) one gets

$$d^2 G_l / dr^2 + \left[ K^2 - l\ (l+1) / r^2 - U_l(r) \right] G_l = 0 , \qquad \text{(A5-1)}$$

where $-U_l = 2WV + V^2 + \frac{(l+1)}{r}\frac{a'}{a} - \frac{3}{4}\frac{a'^2}{a^2} + \frac{1}{2}\frac{a''}{a}$ .

Equation (A5-1) shows that the difference from the non-relativistic equation is only the potential that should be adopted. This method is quite suitable if there has already existed a computer program for non-relativistic equation (Madison and Shelton 1973) or if one wants to compare the results between relativistic and non-relativistic calculations. (Meister and Weiss 1968).

3) Another method is the power expansion method developed by Bühring (1965). He divided the radial region into three and put

$$V^I(r) = \sum_{m=-1}^{\infty} v_m^I r^m \qquad \text{(A5-2-a)}$$

$$V^M(r) = \sum_{n}^{\infty} \sum_{N} v_m^M(y)\ (r-y)^m \qquad \text{(A5-2-b)}$$

$$V^E(r) = v_{-1}^E r^{-1} , \qquad \text{(A5-2-c)}$$

and

$$\left.\begin{matrix} f^I(r) \\ g^I(r) \end{matrix}\right\} = \alpha r^{-1+s} \left\{ \begin{matrix} \sum_{n=0} a_n^I r^n \\ \sum_{n=0} b_n^I r^n \end{matrix} \right. \qquad \text{(A5-3-a)}$$

$$\left.\begin{matrix} f^M(r) \\ g^M(r) \end{matrix}\right\} = r^{-1} \left\{ \begin{matrix} \sum_{n=0} a_n^M (r-y)^n \\ \sum_{n=0} b_n^M (r-y)^n \end{matrix} \right. \qquad \text{(A5-3-b)}$$

$$\left.\begin{matrix} f^E(r) \\ g^E(r) \end{matrix}\right\} \sim C e^{tr} r^s \left\{ \begin{matrix} \sum_{n=0} a_n r^{-n} \\ \sum_{n=0} b_n r^{-n} \end{matrix} \right. , \qquad \text{(A5-3-c)}$$

corresponding to the three regions. Substituting in equation (2-28), one obtains series of coefficients. This method provides one a method to escape from truncation errors.

4) Fourth method is the one developed by Lin et al. (1963) and used by Bunyan and Schonfelder (1965), and in the present calculation (see Sec. 2-4). As is shown, equation (2-51), is a non-linear equation, so it is very difficult to treat it in an analytical manner. However, this method separates the wave function into two parts i.e. amplitude and phase parts, in order to obtain a slowly changing variables. Furthermore, these equations are first order differential equations and for the evaluation of phase shift, it suffices to treat only the former. (see equation (2-51-a)).

It is expected that the fourth method provides a sufficient accuracy and simple calculation procedures for the calculation using high speed digital computer.

APPENDIX 6. COMPUTER PROGRAM LIST

a) Elastic scattering case

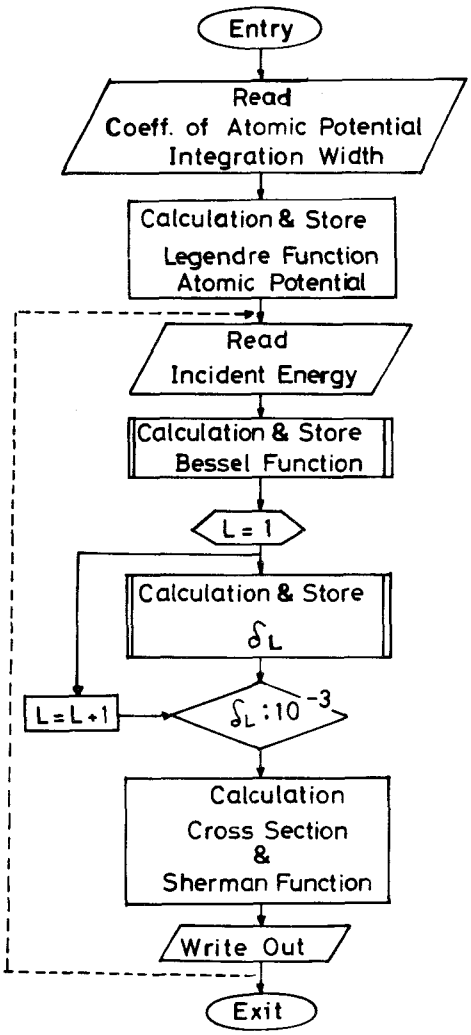

```
      C       ASYMMETRY OF ELECTRON SCATTERING FROM MERCURY
      DIMENSION FLI(10,300),FLJ(10,300),P(9),TANDL(300,2),S(3),SWIG(3)
      COMMON/DRC/ZZ(10000),RR(10000),ZZZ(15000),NN,H1,H2,H3,ERADI,NNN,NN
     1NN
      COMMON /BES/FJ(300),FNEU(300),RK,KR
      READ(5,100)PA1,PA2,PA3,PB1,PB2,PB3,RADIUS,H
  100 FORMAT(6F8.4,F10.4,F8.4)
      WRITE(6,100)PA1,PA2,PA3,PB1,PB2,PB3,RADIUS,H
      DO 1100 N=1,300
      TANDL(N,1)=0.0
      TANDL(N,2)=0.0
      FJ(N)=0.0
      FNEU(N)=0.0
 1100 CONTINUE
      DO 10 NX=1,10
      NX1=50+10*NX
      FNX=NX1
      FNX=FNX*0.01745329252
      X=COS(FNX)
      P0=1.0
      P1=X
      FL10=0.0
      FL20=0.0
      FL11=X+1.0
      FL21=X-1.0
      FLI(NX,1)=FL10
      FLI(NX,2)=FL11
      FLJ(NX,1)=FL20
      FLJ(NX,2)=FL21
      DO 10 NY=3,300
      FNY=NY
      FLI(NX,NY)=((2.0*FNY-3.0)*X*FL11-(FNY-1.0)*FL10-(1.0+X)*P0)/(FNY-2
     1.0)
      FLJ(NX,NY)=((2.0*FNY-3.0)*X*FL21-(FNY-1.0)*FL20-(1.0-X)*P0)/(FNY-2
     1.0)
      P2=((2.0*FNY-3.0)*X*P1-(FNY-2.0)*P0)/(FNY-1.0)
      FL10=FL11
      FL11=FLI(NX,NY)
      FL20=FL21
      FL21=FLJ(NX,NY)
      P0=P1
      P1=P2
   10 CONTINUE
      DO 20 NY=3,10
      NY1=NY-1
      FNY=NY1
      FNY2=FNY*2.
      DO 30 NX=1,7
      NX1=NX
      P(NX)=(FLI(NX1,NY)+FLJ(NX1,NY))/FNY2
   30 CONTINUE
      WRITE(6,200)NY1,(P(NX),NX=1,7)
  200 FORMAT(1H0,I2,7E15.7)
   20 CONTINUE
C  IZYO DE LEGENDRE NO KEISAN OWARI%%%%%
C
C
C
      PB1=PB1*3.553022E-2
      PB2=PB2*3.553022E-2
      PB3=PB3*3.553022E-2
      PA1=PA1*.58377491
      PA2=PA2*.58377491
      PA3=PA3*.58377491
      Z0=PA1+PA2+PA3
      Z1=PA1*PB1+PA2*PB2+PA3*PB3
      Z2=PA1*PB1*PB1+PA2*PB2*PB2+PA3*PB3*PB3
      Z3=PA1*PB1**3.0+PA2*PB2**3.0+PA3*PB3**3.0
      Z1=-Z1
      Z2=Z2*0.5
      Z3=-Z3/6.
      RADIUS=RADIUS/10.0**8.0
      RADIUS=RADIUS/3.8145E-11
      RAD=.1
      RAD1=5.
      RADIU=200.
      ERADI=RAD*EXP(RADI)
      FFN=RADI/H*2.*ERADI+.1
      NN=INT(FFN)
      NN=NN/2*2+1
      H1=RAD1/FLOAT(NN-1)
      DO 40 N=1,NN
      FF=FLOAT(N-1)*H1
      RR(N)=RAD*EXP(FF)
      ZZ(N)=PA1*EXP(-PB1*RR(N))+PA2*EXP(-PB2*RR(N))+PA3*EXP(-PB3*RR(N))
   40 CONTINUE
      H1=2.*H1
      NN1=NN+1
      DO 41 N=NN1,10000
      RR(N)=.0
      ZZ(N)=.0
   41 CONTINUE
      FFNN=(RADIU-ERADI)/H*2.+1
      NNN=INT(FFNN)
      NNN=NNN/2*2+1
      H2=(RADIU-ERADI)/FLOAT(NNN-1)
      H=H2*2.
      DO 42 N=1,NNN
      FF=FLOAT(N-1)*H2+ERADI
      ZZZ(N)=PA1*EXP(-PB1*FF)+PA2*EXP(-PB2*FF)+PA3*EXP(-PB3*FF)
   42 CONTINUE
      NNN1=NNN+1
      DO 43 N=NNN1,15000
      ZZZ(N)=.0
   43 CONTINUE
      FFNNN=(RADIUS-RADIU)/H/2.+1
      NNNN=INT(FFNNN)
      H3=(RADIUS-RADIU)/FLOAT(NNNN-1)
      WRITE(6,9400)H,H1,H2,H3,NN,NNN,NNNN
 9400 FORMAT(//1H0,4E15.7,3I15)
      WRITE(6,9450)(RR(N),N=1,1201,200)
      WRITE(6,9450)(ZZ(N),N=1,1201,200)
      WRITE(6,9450)(ZZZ(N),N=1,1201,200)
 9450 FORMAT(7E15.6)
      RADIU1=PB1*RADIU
      RADIU2=PB2*RADIU
      RADIU3=PB3*RADIU
      D0=PA1*EXP(-RADIU1)+PA2*EXP(-RADIU2)+PA3*EXP(-RADIU3)
      D1=PA1*PB1*EXP(-RADIU1)+PA2*PB2*EXP(-RADIU2)+PA3*PB3*EXP(-RADIU3)
      RADIUU=RADIUS-RADIU
      D1=RADIUU*D1
      D2=PA1*PB1*PB1*EXP(-RADIU1)+PA2*PB2*PB2*EXP(-RADIU2)+PA3*PB3*PB3*E
     1XP(-RADIU3)
      D2=RADIUU*RADIUU*D2
      SGM=D2*.5-D1*3.+D0*8.
      FMUU=-D2+D1*5.-D0*8.
      FMUU=-FMUU
      FNUU=D2*.5-D1*2.+D0*3.
      WRITE(6,9500)RADIU,RADIUS,SGM,FMUU,FNUU
 9500 FORMAT(/7H RADIU=,E10.3,8H RADIUS=,E10.3,5H SGM=,E10.3,6H FMUU=,E1
     10.3,6H FNUU=,E10.3)
      READ(5,9000)NEN
 9000 FORMAT(I10)
      NENN=1
 9200 READ(5,9100)NENERG
 9100 FORMAT(I10)
      WRITE(6,900) NENERG
  900 FORMAT(///1H0,18H ********* ENERGY=,I10,19H EV DESU **********)
      ENERGY=FLOAT(NENERG)/511000.0+1.0
      FK=ENERGY*ENERGY-1.0
      FK=FK**0.5
      RK=RADIUS*FK
      CALL BESSEL
      WRITE(6,300) KR
  300 FORMAT(1H0,30H KEISANSARETA BESSEL NO JISU =,I4,5H DESU)
      WRITE(6,350)RK
  350 FORMAT(1H0,16H HASU = RADIUS =,E15.7,5H DESU)
      WRITE(6,360)(FJ(N),N=1,7)
  360 FORMAT(////1H0,7E15.6)

      WRITE(6,370)(FNEU(N),N=1,7)
  370 FORMAT(1H0,7E15.6///)
      L=0
```

```
      19 K=L-1
      17 FL=L
         FKK=K
         PHAIOS=Z0/FKK
         PHAIOC=(1.0-PHAIOS*PHAIOS)**0.5
         IF(K)1,2,3
       1 GO TO 1050
       2 WRITE(6,400)
     400 FORMAT(1H0,10H OKASHIIYO)
         GO TO 9999
       3 PHAIOC=-PHAIOC
    1050 PHAI1=(ENERGY+Z1-PHAIOC)/(1.0-2.0*FKK*PHAIOC)
         PHAI2I=2.0*(PHAI1+PHAIOS*(1.0-FKK*PHAI1)*Z2
         PHAI2=2.0*(1.0-FKK*PHAIOC)
         PHAI2=PHAI2I/PHAI2
         PHAI31=2.0*PHAI2*PHAIOS*(1.0-2.0*FKK*PHAI1)*Z3
         PHAI32=2.0*PHAI1*PHAI1*PHAIOC*(1.0-2.0*FKK*PHAI1/3.0)
         PHAI3=3.0-2.0*FKK*PHAIOC
         PHAI3=(PHAI31+PHAI32)/PHAI3
         PHAIO=ARSIN(PHAIO5)
         IF(PHAIO)5,*,4
       5 PHAIO=3.141592654-PHAIO
       4 PHAI=PHAIO-.5*RAD*(PHAI1+RAD*(PHAI2+RAD*PHAI3))
         CALL DIRAC(PHAI,FKK,L,ENERGY,PA1,PA2,PA3,PB1,PB2,PB3,RADIUS,PHAIL,
        1H,SGM,FNUU,FNUU,RADI,RADIU,RADIUU)
         TANPHL=TAN(PHAIL)
         TANDL1=(ENERGY+1.0)*TANPHL+(1.0+FL*FKK)/RADIUS
         L1=L+1
         L2=L+2
         TANDLU=FK*FJ(L2)-FJ(L1)*TANDL1
         TANDLL=FK*FNEU(L2)-FNEU(L1)*TANDL1
         IF(K)9,11,12
       9 TANDL(L1,1)=TANDLU/TANDLL
         WRITE(6,1052)L,K,PHAI,PHAIL,TANDL(L1,1)
    1051 FORMAT(1H ,3H L=,I5,3X,3H K=,I5,3X,6H PHAI=,E15.6,10X,7H PHAIL=,E1
        15.6,10X,7H TANDL=,E15.6)
    1052 FORMAT(1H0,3H L=,I5,3X,3H K=,I5,3X,6H PHAI=,E15.6,10X,7H PHAIL=,E1
        15.6,10X,7H TANDL=,E15.6)
         IF(L)13,14,15
      13 WRITE(6,600)
     600 FORMAT(1H0,16H OKASHIIYO PART2)
         GO TO 9999
      14 TANDL(L1,2)=0.0
         L=L+1
         GO TO 19
      15 K=L

      11 WRITE(6,500)
     500 FORMAT(1H0,16H OKASHIIYO PART3)
         GO TO 9999
      12 TANDL(L1,2)=TANDLU/TANDLL
         WRITE(6,1051)L,K,PHAI,PHAIL,TANDL(L1,2)
         DEL1=ATAN(TANDL(L1+1))
         DEL2=ATAN(TANDL(L1+2))
         DEL1=ABS(DEL1)
         DEL2=ABS(DEL2)
         IF(DEL1-GT-0.001)GO TO 16
         IF(DEL2-GT-0.001)GO TO 1A
         GO TO 1B
      16 L=L+1
         IF(L-GT-300)GO TO 18
         GO TO 19
      18 CONTINUE
         WRITE(6,750)L
     750 FORMAT(1H0,10X,26H KEISANSARETA PHASE SHIFT=,I4,5H DESU)
         WRITE(6,720)
     720 FORMAT(/91H ***********************************************************
        1**********************************)
         WRITE(6,700)
     700  FORMAT(3H  *,3X,6H THETA,6X,10H CROSS SEC,6X,10H NORM  C S,6X,10H
        1 SHER  FUN,10X,2H F,7X,10H MOD  ASYM,3H  *)
         DO 70 N=1,3
         S(N)=0.0
         SHIG(N)=0.0
      70 CONTINUE
         L=L+1
         WRITE(7,701)((TANDL(N,I),I=1,2),N=1,L)
     701 FORMAT(4E16.8)
         N=1
         DO 50 NX=1,10
         NX1=50+10*NX
         FNX1=NX1
         FNX=FNX1/2.0
         FNX=FNX+1.7453292E-2
         FNX1=FNX1+1.7453292E-2
         ER=0.0
         EI=0.0
         HR=0.0
         HI=0.0
         DO 60 M1=1,L1
         M2=M1+1
         A1=TANDL(M1,1)*TANDL(M1,1)+1.0
         A2=TANDL(M2,2)*TANDL(M2,2)+1.0
         HR1=(TANDL(M1,1)/A1-TANDL(M2,2)/A2)*FLJ(NX,M2)
         HI1=(1.0/A1-1.0/A2)*FLJ(NX,M2)
         ER1=(TANDL(M1,1)/A1+TANDL(M2,2)/A2)*FLI(NX,M2)
         EI1=(2.0-1.0/A1-1.0/A2)*FLI(NX,M2)

         ER=ER+ER1
         EI=EI+EI1
         HR=HR+HR1
         HI=HI+HI1
      60 CONTINUE
         ER=ER*0.5
         EI=EI*0.5
         HR=HR*0.5
         HI=-HI*0.5
         EE=ER*ER+EI*EI
         HH=HR*HR+HI*HI
         SHIGM1=EE/COS(FNX)/COS(FNX)+HH/SIN(FNX)/SIN(FNX)
         SHIGM2=EE+HH-(EE-HH)*COS(FNX1)
         SHIGMA=SHIGM1/FK/FK
         SHIGMA=SHIGMA*1.49107E-21
         SHINOR=SHIGMA/2.80008E-17
         SHERM=2.0*SIN(FNX1)*(ER*HI-EI*HR)/SHIGM2
         F=TAN(FNX)*EE+HH/TAN(FNX)
         F1=(ER*HR+EI*HI)*4.0/TAN(FNX1)
         F=(F+F1)/SHIGM1
         N=MOD(N,3)+1
         SHIG(N)=SHIGMA
         S(N)=SHERM
         ASYMOD=S(1)*SHIG(1)+S(2)*SHIG(2)+S(3)*SHIG(3)
         ASY=SHIG(1)+SHIG(2)+SHIG(3)
         ASYMOD=ASYMOD/ASY
         WRITE(6,800) NX1,SHIGMA,SHINOR,SHERM,F,ASYMOD
     800 FORMAT(1H ,2H *,I11,5E15.5,2H *)
         WRITE(6,810)
     810 FORMAT(1H ,2H *,86X,2H *)
      50 CONTINUE
         WRITE(6,720)
         WRITE(6,950)
     950 FORMAT(1H0,40H TADASHI MOD ASYMM IGYO SHITA C YOMUKOTO)
         WRITE(6,960)ER,EI,HR,HI
     960 FORMAT(1H0,4E15.5////)
         NENN=NENN+1
         IF(NENN-GT-NEN)GO TO 9999
         GO TO 9200
    9999 CONTINUE
         STOP
         END
```

```
0001        SUBROUTINE DIRAC(PHAI,FKK,L,ENERGY,PA1,PA2,PA3,PB1,PB2,PB3,RADIUS,
           1PHAIL,H,SGM,FMUU,FNUU,RAD1,RADIU,RADIUU)
0002        COMMON/DRC/ZZ(10000),RR(10000),ZZZ(15000),NN,H1,H2,H3,ERAD1,NNN,NN
           1NN
0003        Y1=2.*PHAI
0004        NN1=NN-2
0005        DO 3100 N=1,NN1,2
0006        N1=N+1
0007        N2=N+2
0008        RK1=FKK*SIN(Y1)+ZZ(N)+RR(N)*(ENERGY-COS(Y1))
0009        RK1=H1*RK1
0010        RK2=FKK*SIN(Y1+RK1)+ZZ(N1)+RR(N1)*(ENERGY-COS(Y1+RK1))
0011        RK2=H1*RK2
0012        RK3=FKK*SIN(Y1+RK2)+ZZ(N1)+RR(N1)*(ENERGY-COS(Y1+RK2))
0013        RK3=H1*RK3
0014        RK4=FKK*SIN(Y1+2.*RK3)+ZZ(N2)*RR(N2)*(ENERGY-COS(Y1+2.*RK3))
0015        RK4=H1*RK4
0016        Y1=Y1+(RK1+2.*(RK2+RK3)+RK4)/3.
0017  3100  CONTINUE
0018        NNN1=NNN-2
0019        R1=ERAD1
0020        R2=R1+H2
0021        R3=R2+H2
0022        DO 3200 N=1,NNN1,2
0023        N1=N+1
0024        N2=N+2
0025        RK1=(FKK*SIN(Y1)+ZZZ(N))/R1+ENERGY-COS(Y1)
0026        RK1=H*RK1
0027        RK2=(FKK*SIN(Y1+RK1)+ZZZ(N1))/R2+ENERGY-COS(Y1+RK1)
0028        RK2=H*RK2
0029        RK3=(FKK*SIN(Y1+RK2)+ZZZ(N1))/R2+ENERGY-COS(Y1+RK2)
0030        RK3=H*RK3
0031        RK4=(FKK*SIN(Y1+2.*RK3)+ZZZ(N2))/R3+ENERGY-COS(Y1+2.*RK3)
0032        RK4=H*RK4
0033        Y1=Y1+(RK1+2.*(RK2+RK3)+RK4)/3.
0034        R1=R1+H
0035        R2=R2+H
0036        R3=R3+H
0037  3200  CONTINUE
0038        NNNN1=NNNN-1
0039        R2=R1+H3*.5
0040        R3=R1+H3
0041        DO 3300 N=1,NNNN1
0042        RRA1=R1-RADIUS
0043        RRA2=R2-RADIUS
0044        RRA3=R3-RADIUS
0045        RRA1=RRA1/RADIUU
0046        RRA2=RRA2/RADIUU
0047        RRA3=RRA3/RADIUU

0048        Z1=RRA1*(SGM+RRA1*(FMUU+RRA1*FNUU))
0049        Z2=RRA2*(SGM+RRA2*(FMUU+RRA2*FNUU))
0050        Z3=RRA3*(SGM+RRA3*(FMUU+RRA3*FNUU))
0051        RK1=(FKK*SIN(Y1)+Z1)/R1+ENERGY-COS(Y1)
0052        RK1=H3*RK1
0053        RK2=(FKK*SIN(Y1+RK1)+Z2)/R2+ENERGY-COS(Y1+RK1)
0054        RK2=H3*RK2
0055        RK3=(FKK*SIN(Y1+RK2)+Z2)/R2+ENERGY-COS(Y1+RK2)
0056        RK3=H3*RK3
0057        RK4=(FKK*SIN(Y1+2.*RK3)+Z3)/R3+ENERGY-COS(Y1+2.*RK3)
0058        RK4=H3*RK4
0059        Y1=Y1+(RK1+2.*(RK2+RK3)+RK4)/3.
0060        R1=R3
0061        R2=R2+H3
0062        R3=R3+H3
0063  3300  CONTINUE
0064        PHAIL=Y1/2.
0065        RETURN
0066        END
```

```
0001        SUBROUTINE BESSEL
0002        COMMON/BES/FJ(300),FNEU(300),RK,KR
0003        FJ0=SIN(RK)/RK
0004        FJ1=(SIN(RK)/RK-COS(RK))/RK
0005        FNEU0=-COS(RK)/RK
0006        FNEU1=-(COS(RK)/RK+SIN(RK))/RK
0007        FJ(1)=FJ0
0008        FJ(2)=FJ1
0009        FNEU(1)=FNEU0
0010        FNEU(2)=FNEU1
0011        KR=INT(RK)+50
0012        KR=MIND(KR,300)
0013        KR2=KR-1
0014        DO 2100 KR1=3,KR2
0015        FKR1=KR1
0016        FJ(KR1)=-FJ0+(2.0*FKR1-3.0)*FJ1/RK
0017        FNEU(KR1)=-FNEU0+(2.0*FKR1-3.0)*FNEU1/RK
0018        FJ0=FJ1
0019        FJ1=FJ(KR1)
0020        FNEU0=FNEU1
0021        FNEU1=FNEU(KR1)
0022  2100  CONTINUE
0023        DO 2200 KR1=KR,300
0024        FJ(KR1)=0.0
0025        FNEU(KR1)=0.0
0026  2200  CONTINUE
0027        RETURN
0028        END
```

b) Inelastic scattering case

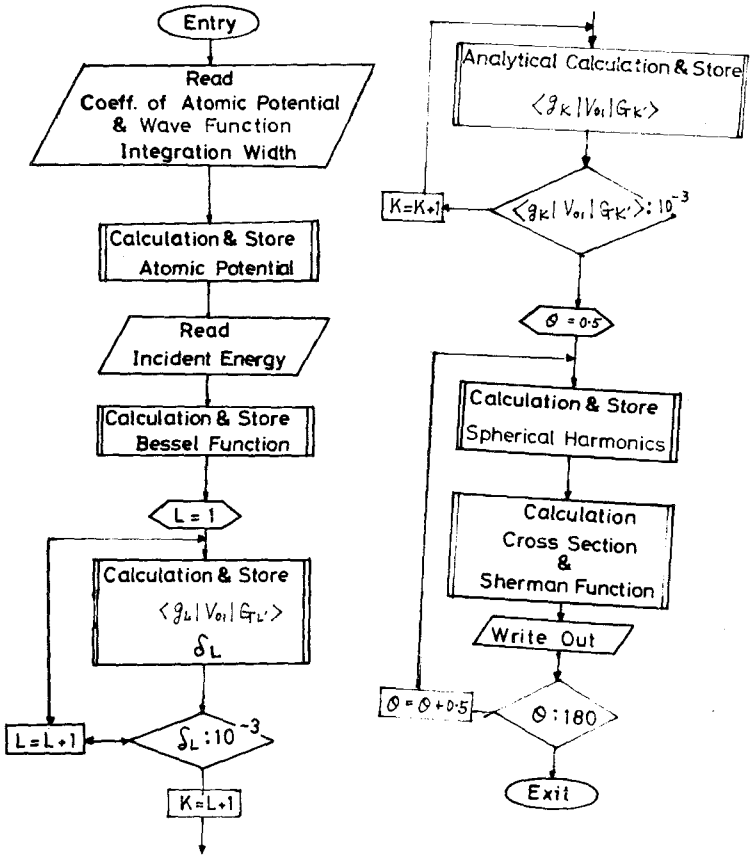

```
      INELASTIC SCATTERING CROSS SECTION FOR MERCURY
00001       DIMENSION GRAPH (121)
00002       DIMENSION      ABTAN (2,2)
00003       DIMENSION FUNC(2,2,2)
00004       COMMON/SCDL/SINDL(300,2,2),COSDL(300,2,2),SCSQ(300,2,2)
00005       COMMON/RRADAL/RADIUS(6),RADIAL(10000)
00006       COMMON/FKF/FK(2)
00007       COMMON/HHABA/HABA(4)
00008       COMMON/KKAISU/KAISU(4)
00009       COMMON/WAVPOT/POTE(2,3),WAVEFU(3,2,2)
00010       COMMON/VVPOT/VPOT(10000,2),VPOTEI(10000)
00011       COMMON/AASSLG/ASSLEG(2000,3)
00012       COMMON/BES/FJ(300,2),FNEU(300,2),RK(2),KR(2)
00013       COMMON/ZZB/ZBE(4,2)
00014       COMMON/PPHAI/PHAI(2,4,2),AMPL(2,4,2)
00015       COMMON/PPHAIO/PHAIO(2,2),AMPO(2,2)
00016       COMMON/MATRIX/FMATRX(2000,2,2,2)
00017       COMMON/L1L/L(2,2)/ENERG/ENERGY(2)
00018       COMMON/PPHAI1/AMP1(2,2,10000)
00019       COMMON/TANDEL/TANDL(300,2,2)
00020       COMMON/AAAAMP/AAMP(2000,2,3,2),BBMP(300,2,3,2),ABMP(300,2,3,2)
           1,BAMP(300,2,3,2)
00021       COMMON/SIG/SIGMA(4),SHERM(4,2)
00022       COMMON/FFSC/FSC(2,3,2)
00023       DIMENSION HI(360)
00024       DIMENSION SIGMAA(360,6)
00025       DIMENSION SHERMM(360,4)
00026       DIMENSION FRE(2),FIM(2),GRE(2),GIM(2)
C     ABTAN(I,J)   I,L OR -L-1,, J,ELASTIC OR INELASTIC
C     WAVEFU  (I,J,K) I,STATE,,J,ATAMA OR KATA NOKEISU
C     VPOT(I,J)  J,ELASTIC OR INELASTIC
C     RK=RADIUS*(WAVE NUMBER),KR=PHYSE NUMBER
C     VOTENTIAL NO TENKAIKEISU
C     PHAI(I,J,K) I,L OR -L-1,,J,KEISU,,K,,ELASTIC OR INELASTIC
C     FMATRX(I,J,K,M)  I,L,,J,L OR -L-1 OF ELASTIC,,K,PLUS OR MINUS SIGNS OF
C     INELASTIC,,M,  ABSOLUTE MAGNITUDE OF L OF INELASTIC
C     PHAI1(I,J,K),AMP1(I,J,K)  KIOKU SARETA INELATIC NO WAVE FUNCTION  1,
C    -1,,J,NWE OR OLD ONE
C     TANDLD(I,J,K)  JAL OR -L-1,,K,ELASTIC OR INELASTIC
C     AAMP(I,J,K,L)  J,(L,L+1)  OR (L,L-1) ,,K MAGNETIC UUANTUM NUMBER,,L,R
C     MAGINARY PART
C
C
00027       NPN=2000
00028       NPP=300
00029       NSEK=10000
00030       READ(5,100)RADIUS
00031   100 FORMAT(6F10.2)
00032       READ(5,200)HABA(2)
00033   200 FORMAT(F10.5)
00034       READ(5,300)((POTE(I,J),I=1,2),J=1,3)
00035   300 FORMAT(3E15,5)
00036       READ(5,400)(((WAVEFU(I,J,K),J=1,2),K=1,2),I=1,3)
00037   400 FORMAT(4E15.5)
00038       READ(5,701)IP,DEL
00039   701 FORMAT(I10,E10.1)
00040       READ(5,500)NEN
00041   500 FORMAT(I10)
00042       WRITE(6,102)
00043   102 FORMAT(/////////38H **** YOMIKOMI DATA NOHAJIMARI *****)
00044       WRITE(6,702)IP,DEL
00045   702 FORMAT(1HO,13H PHASE LIMIT=,I10,19H PHASE SHIFT LIMIT=,E10.1)
00046       WRITE (6,101)RADIUS
00047   101 FORMAT(1HO,8H RADIUS =,6F10.2)
00048       WRITE(6,201)HABA (2)
00049   201 FORMAT(1H,17H SEKIBUN HABA(2)=,F10.5)
00050       WRITE(6,301)
00051   301 FORMAT(1HO,33H YOMIKIMARETA POTENTIAL NO KEISU=)
00052       WRITE(6,300)POTE
00053       WRITE(6,401)
00054   401 FORMAT(1HO,36H YOMIKOKARETA 6S 6P NO WAVE FUNCTION)
00055       WRITE(6,400)WAVEFU
00056       CALL POTENT(NSEK)
00057       WRITE(6,610)((VPOT(I,J),I=100,NSEK,2000),J=1,2)
00058       WRITE(6,610)(VPOTEI(I),I=100,NSEK,1000)
00059   610 FORMAT(1H ,10X,10E10.3)
00060       CALL DIRAC1
00061       WRITE(6,650)
00062   650 FORMAT(////27H POTENTIAL*R=Z(R) NO TENKAI)
00063       WRITE(6,700)((ZBE(I,J),I=1,4),J=1,2)
00064   700 FORMAT(4E15.5)
00065       DO 600 I=1,NEN
00066          READ(5,5100)ENERG
00067  5100 FORMAT(F10.3)
00068       DO 50 M=1,2
00069       DO 50 J=1,2
00070       DO 50 K=1,NSEK
00071       AMP1(M,J,K)=0.
00072    50 CONTINUE
00073       DO 61 J=1,2
00074       DO 61 K=1,4
00075       DO 61 M=1,2
00076       AMPL(J,K,M)=0.
00077       PHAI(J,K,M)=0.
00078    61 CONTINUE
00079       DO 60 M=1,3
00080       DO 60 J=1,NPN
00081       ASSLEG(J,M)=0.
00082    60 CONTINUE
00083       DO 810 JJ=1,2
00084       DO 810 J=1,2
00085       AMPO(J,JJ)=0.
00086   810 CONTINUE
00087       FFF=0.
00088       ENERGY(1)=ENERG
00089       ENERGY(2)=ENERG-6.703
00090       WRITE(6,800)ENERG
00091   800 FORMAT(1H1,/////////20X,21H ***** NYUSHA ENERGY=,F10.1,6H *****)
00092       DO 5150 J=1,NPP
00093       DO 5150 JJ=1,2
00094       DO 5150  JJJ=1,2
00095       TANDL(J,JJ,JJJ)=0.
00096       SINDL(J,JJ,JJJ)=0.
00097       COSDL(J,JJ,JJJ)=1.
00098       SCSQ(J,JJ,JJJ)=1.
00099  5150 CONTINUE
00100       DO 5200 J=1,2
00101       ENERGY(J)=ENERGY(J)/511008.+1.
00102       FK(J)=(ENERGY(J)*ENERGY(J)-1.)**.5
00103       RK(J)=FK(J)*RADIUS(5)
00104  5200 CONTINUE
00105       CALL BESSEL(NPP)
00106       WRITE(6,900)RK
00107   900 FORMAT(///13H HASU*RADIUS=,2E15.5)
00108   950 FORMAT(30H KEISANSARETA  BESSEL NO JISUU,2I15)
00109       WRITE(6,950)KR
00110       WRITE(6,1000)((FJ(II,JJ),II=1,5),JJ=1,2)
00111       WRITE(6,1000)((FNEU(II,JJ),II=1,5),JJ=1,2)
00112  1000 FORMAT(/5E15.5)
00113       DO 5250 LL=1,NPN
00114       DO 5250 M=1,2
00115       DO 5250 J=1,2
00116       DO 5250 K=1,2
00117       FMATRX(LL,M,J,K)=0.
00118  5250 CONTINUE
00119       READ(5,703)KLUNG,KTAE,KANKAK
00120   703 FORMAT(3I1)
00121       IF(KLUNG.EQ.1)GO TO 704
00122       LL=-1
00123  5300 CONTINUE
00124       CALL DIRAC2(LL,FFF)
00125       WRITE(6,1200)LL,L
00126       WRITE(6,1210)
00127       WRITE(6,6300)
00128  6300 FORMAT(22X,2H 0,13X,2H 1,11X,2H 2,11x,2H 3,19X,2H 0,11X.2H 1,11X,2
           1H 2,11X,2H 3)
00129  1210 FORMAT(//16X,9(2H *),7X,2H L,7X,9(2H *),9X,9(2H *),5X,5H -L-1,4X,
           19(2H *))
00130       DO 1150 II=1,2
00131       IF(II.EQ.2)GO TO 6000
00132       WRITE(6,1100)((PHAI(JJ,KK,II),KK=1,4),JJ=1,2)
00133  6100 CONTINUE
00134       WRITE(6,1160)((AMPL(JJ,KK,II),KK=1,4),JJ=1,2)
00135       GO TO 6200
00136  6000 CONTINUE
00137       WRITE(6,1110)((PHAI(JJ,KK,II),KK=1,4),JJ=1,2)
00138       GO TO 6100
00139  6200 CONTINUE
00140  1150 CONTINUE
00141  1100 FORMAT(1HO,15H ELASTIC  PHAI=,4E13.4,8X,4E13.4)
00142  1110 FORMAT(1H ,15HINELASTIC PHAI=,4E13.4,8X,4E13.4)
```

```
00143     1160 FORMAT(10X,6H AMPL=,4E13.4,8X,4E13.4)
00144          WRITE(6,8000)
00145     8000   FORMAT(///5X,2X,9(2H *),4X,6H PHAIO,5X,10(2H *),10X,11(2H *),4X,
                15H AMPO,5X,12(2H *))
00146          WRITE(6,8100)
00147     8100 FORMAT(14X,8H ELASTIC,20X,10H INELASTIC,30X,8H ELASTIC,20X,10H INE
               1LASTIC)
00148          WRITE(6,8200)
00149     8200 FORMAT(2(8X,2H L,12X,5H -L-1,3X),10X,2(8X,2H L,12X,5H -L-1,3X))
00150          ARITE(6,8300)
00151     8300 FORMAT(5H R=,1)
00152          WRITE(6,1220)((PHAIO(K,J),K=1,2),J=1,2),((AMPO(K,J),K=1,2),J=1,2)
00153     1220   FORMAT(4E15.5,10X,4E15.5)
00154     1200 FORMAT(1H1,/////15(2H__),5X,4H LL=I10,20X,416,5X,15(2H__))
00155          CALL LUNGE(LL,NPN,NSEK)
00156          LL2=LL+2
00157          LL1=LL+1
00158          JJJ=1
00159          KKK=1
00160          IF(LL)5450,5320,5310
00161     5450 CONTINUE
00162          JJJ=2
00163          KKK=2
00164          GO TO 5310
00165     5320 CONTINUE
00166          JJJ=2
00167          J=1
00168          K=2
00169          TANU=FK(J)*FJ(LL2,J)-FJ(LL1,J)*((ENERGY(J)+1.)*TAN(PHAIO(K,J))+
               1(1.+FLOAT(L(1,J)+L(K,J)))/RADIUS(5))
00170          TANL=FK(J)*FNEU(LL2,J)-FNEU(LL1,J)*((ENERGY(J)+1.)*TAN(PHAIO(K,J))
               1+(1.+FLOAT(L(1,J)+L(K,J)))/RADIUS(5))
00171          TANDL(LL1,K,J)=TANU/TANL
00172          SINDL(LL1,K,J)=TANU*EXP(AMPO(K,J))*COS(PHAIO(K,J))/RADIUS(5)
00173          SINDL(LL  ,K,J)=SINDL(LL1,K,J)/(FJ(LL2,J)*FNEU(LL1,J)-FJ(LL1,J)
               1*FNEU(LL2,J))/FK(J)
00174          COSDL(LL1,K,J)=TANL*EXP(AMPO(K,J))*COS(PHAIO(K,J))/RADIUS(5)
00175          COSDL(LL1,K,J)=COSDL(LL1,K,J)/(FJ(LL2,J)*FNEU(LL1,J)-FJ(LL1,J)
               1*FNEU(LL2,J))/FK(J)
00176            SINDL(LL1,K,J)=-SINDL(LL1,K,J)
00177          COSDL(LL1,K,J)=-COSDL(LL1,K,J)
00178          SCSQ(LL1,K,J)=(SINDL(LL1,K,J)**2 +COSDL(LL1,K,J)**2 )**.5
00179          IF(SCSQ(LL1,K,J).EQ..0)SCSQ(LL1,K,J)=1.
00180          COSDL(LL1,K,J)=COSDL(LL1,K,J)/SCSQ(LL1,K,J)
00181          SINDL(LL1,K,J)=SINDL(LL1,K,J)/ SCSQ(LL1,K,J)
00182          GO TO 5310
00183     5310 CONTINUE
00184          DO 5500 J=JJJ,2
00185          IF(J.EQ.2)GO TO 5410
00186          GO TO 5420
00187     5410 CONTINUE
00188          LL1=LL2
00189          LL2=LL2+1
00190     5420 CONTINUE
00191          DO 5400 K=KKK,2
00192          TANU=FK(J)*FJ(LL2,J)-FJ(LL1,J)*((ENERGY(J)+1.)*TAN(PHAIO(K,J))+
               1(1.+FLOAT(L(1,J)+L(K,J)))/RADIUS(5))
00193          TANL=FK(J)*FNEU(LL2,J)-FNEU(LL1,J)*((ENERGY(J)+1.)*TAN(PHAIO(K,J))
               1+(1.+FLOAT(L(1,J)+L(K,J)))/RADIUS(5))
00194          TANDL(LL1,K,J)=TANU/TANL
00195          SINDL(LL1,K,J)=TANU*EXP(AMPO(K,J))*COS(PHAIO(K,J))/RADIUS(5)
00196          SINDL(LL1,K,J)=SINDL(LL1,K,J)/(FJ(LL2,J)*FNEU(LL1,J)-FJ(LL1,J)
               1*FNEU(LL2,J))/FK(J)
00197          COSDL(LL1,K,J)=TANL*EXP(AMPO(K,J))*COS(PHAIO(K,J))/RADIUS(5)
00198          COSDL(LL1,K,J)=COSDL(LL1,K,J)/(FJ(LL2,J)*FNEU(LL1,J)-FJ(LL1,J)
               1*FNEU(LL2,J))/FK(J)
00199            SINDL(LL1,K,J)=-SINDL(LL1,K,J)
00200          COSDL(LL1,K,J)=-COSDL(LL1,K,J)
00201          SCSQ(LL1,K,J)=(SINDL(LL1,K,J)**2 +COSDL(LL1,K,J)**2 )**.5
00202          IF(SCSQ(LL1,K,J).EQ..0)SCSQ(LL1,K,J)=1.
00203          SINDL(LL1,K,J)=SINDL(LL1,K,J)/ SCSQ(LL1,K,J)
00204          COSDL(LL1,K,J)=COSDL(LL1,K,J)/ SCSQ(LL1,K,J)
00205     5400 CONTINUE
00206     5500 CONTINUE
00207          DO 5600 J=1,2
00208          LL1=LL+1
00209          LL2=LL+2
00210          IF(J.EQ.2)GO TO 5610
00211          GO TO 5620
00212     5610 CONTINUE
00213          LL1=LL2
00214          LL2=LL2+1
00215     5620 CONTINUE
00216          DO 5600 K=1,2
00217          ABTAN(K,J)=ABS(TANDL(LL1,K,J))
00218     5600 CONTINUE
00219          AMTAN=1.
00220          IF(LL.LT.0)GO TO 7002
00221          AMTAN=AMAX1(ABTAN(1,1),ABTAN(1,2),ABTAN(2,1),ABTAN(2,2))
00222          WRITE(6,5376)
00223          WRITE(6,5375)
00224     5376 FORMAT(1H0)
00225     5375 FORMAT(15X,8H (L,L+1),6X,11H (-L-1,L+1),4X,9H (L,-L-2),4X,12H (-L-
               11,-L-2), 9X,8H (L,L-1),5X,11H (-L-1,L-1),7X,7H (L,-L),8X,10H (-L-1
               2,-L))
00226          WRITE(6,5370)(((FMATRX(LL+1,K,M,N),K=1,2),M=1,2),N=1,2)
00227     5370 FORMAT(1H ,8H FMATRX=,4E15.5,5X,4E15.5)
00228          LL11=LL+1
00229          LL22=LL+2
00230          WRITE(6,5381)(SINDL(LL11,K,1),K=1,2),(SINDL(LL22,K,2),K=1,2)
00231          WRITE(6,5382)(COSDL(LL11,K,1),K=1,2),(COSDL(LL22,K,2),K=1,2)
00232          WRITE(6,5380)(TANSL(LL11,K,1),K=1,2),(TANDL(LL22,K,2),K=1,2)
00233          WRITE(6,5386)( SCSQ(LL11,K,1),K=1,2),( SCSQ(LL22,K,2),K=1,2)
00234     5380 FORMAT(1HO,8H TANDL= ,10H (ELASTIC),2E15.5,12H (INELASTIC),2E15.5)
00235     5381 FORMAT(1HO,8H SINDL= ,10H (ELASTIC),2E15.5,12H (INELASTIC),2E15.5)
00236     5382 FPRMAT(1HO,8H COSDL= ,10H (ELASTIC),2E15.5,12H (INELASTIC),2E15.5)
00237     5386 FORMAT(1HO,8H  SCSQ= ,10H (ELASTIC),2E15.5,12H (INELASTIC),2E15.5)
00238          GO TO 7003
00239     7002 CONTINUE
00240          WRITE(6,7004)(SINDL(LL+2,K,2),K=1,2)
00241          WRITE(6,7005)(COSDL(LL+2,K,2),K=1,2)
00242          WRITE(6,7006)(TANDL(LL+2,K,2),K=1,2)
00243          WRITE(6,7007)( SCSQ(LL+2,K,2),K=1,2)
00244     7004 FORMAT(1HO,8H SINDL= ,12H (INELASTIC),2E15.5)
00245     7005 FORMAT(1HO,8H COSDL= ,12H (INELASTIC),2E15.5)
00246     7006 FORMAT(1HO,8H TANDL= ,12H (INELASTIC),2E15.5)
00247     7007 FORMAT(1HO,8H  SCSQ= ,12H (INELASTIC),2E15.5)
00248     7003 CONTINUE
00249          IF(LL.LT.0)GO TO 7001
00250          LL11=LL+1
00251          DO 5383 J=1,2
00252          IF(J.EQ.2)LL11=LL+2
00253          DO 5383 K=1,2
00254          FUNC(K,J,1)=EXP(AMPO(K,J))*COS(PHAIO(K,J))/RADIUS(5)/SCSQ(LL11,K,J
               1)
00255          FUNC(K,J,2)=FJ(LL11,J)*COSDL(LL11,K,J)-FNEU(LL11,J)*SINDL(LL11,K,
               1J)
00256     5383 CONTINUE
00257          WRITE(6,5385)
00258     5385 FORMAT(1HO,32H WAVE FUNCTION NO TSUNAGARI GUAI)
00259          WRITE(6,5384)(((FUNC(K,J,JJJ),JJJ=1,2),K=1,2),J=1,2)
00260     5384 FORMAT(//8E15.5)
00261     7001 CONTINUE
00262          IF(LL.GE.IP)GO TO 7000
00263          LL=LL+1
00264          IF(AMTAN.GE.DEL )GO TO 5300
00265          GO TO 7100
00266     7000 CONTINUE
00267          LL=LL+1
00268          WRITE(6,7200)
00269     7200 FORMAT(/////35H ***** CAUTION ***** PHAISE IS OVER)
00270     7100 CONTINUE
00271          WRITE(6,7300)
00272     7300 FORMAT(25(2H *),19H PHAISE SHIFT OWARI,25(2H *))
00273          DO 5000 J=1,LL
00274          NN=2
00275          IF(J.EQ.1)NN=1
00276          DO 5000 N=1,NN
00277          JI=J+1
00278          IF(N.EQ.1)JI=J-1
00279          DO 5000 M=1,2
00280          DO 5000 K=1,2
00281          FMATRX(J,K,M,N)=FMATRX(J,K,M,N)/SCSQ(J,K,1)/ SCSQ(JI,M,2)
00282     5000 CONTINUE
00283          WRITE(6,5371)RADIUS(5)
00284     5371 FORMAT(1H1,///10X,3H R=,F10.1,10X,25H DE NORMALIZE SARETA ATAI)
00285          WRITE(6,5375)
00286          WRITE(6,5373)
00287          WRITE(6,5372)(J,(((FMATRX(J,K,M,N),K=1,2),M=1,2),N=1,2),J=1,LL)
00288     5373 FORMAT(1H ,8H FMATRX=)
00289     5372 FORMAT(1H ,I8,4E15.5,5X,4E15.5)
00290          IF(KATE.EQ.1)GO TO 707
00291          KK=11
```

```
00292          CALL TAE(LL,NPN,NPP)
00293          GO TO 707
00294      704 CONTINUE
00295          READ(5,705)LL,LK
00296      705 FORMAT(2110)
00297          READ(5,5360)((((FMATRX(J,K,M,N),K=1,2),M=1,2)N=1,2),J=1,LK)
00298          READ(5,5360)((FMATRX(J,1,1,N),N=1,2),J=LK+1,LL)
00299          READ(5,5360)(((TANDL(J,K,M),K=1,2),M=1,2),J=1,LK)
00300          READ(5,5360)(((COSDL(J,K,M),K=1,2),M=1,2),J=1,LK)
00301          READ(5,5360)(((SINDL(J,K,M),K=1,2),M=1,2),J=1,LK)
00302          DO 708 J=LK+1,LL
00303          DO 708 K=1,2
00304          DO 707 M=1,2
00305          DO 708 N=1,2
00306          FMATRX(J,K,M,N)=FMATRX(J,1,1N)
00307      708 CONTINUE
00308          FMATRX(LK+1,1,1,2)=-FMATRX(LK+1,1,1,2)
00309          FMATRX(LK+1,2,1,2)=-FMATRX(LK+1,2,1,2)
00310          FMATRX(LK+2,1,1,2)=-FMATRX(LK+2,1,1,2)
00311          FMATRX(LL+2,2,1,2)=-FMATRX(LK+2,2,1,2)
00312          GO TO 706
00313      707 CONTINUE
00314          I111=1
00315          I222=0
00316          WRITE(7,5362)ENERG
00317      5362 FORMAT(F10.1)
00318          WRITE(7,5363)I111,I222
00319      5363 FORMAT(2I1)
00320          WRITE(7,5361)LL,LK
00321      5361 FORMAT(2I10)
00322          WRITE(7,5360)((((FMATRX(J,K,M,N),K=1,2),M=1,2),N=1,2),J=1,LK)
00323          WRITE(7,5360)(((FMATRX(J,K,M,N),N=1,2),J=LK+1,LL)
00324          WRITE(7,5360)(((TANDL(J,K,M),K=1,2),M=1,2),J=1,LK)
00325          WRITE(7,5360)(((COSDL(J,K,M),K=1,2),M=1,2),J=1,LK)
00326          WRITE(7,5360)(((SINDL(J,K,M),K=1,2),M=1,2),J=1,LK)
00327      706 CONTINUE
00328          WRITE(6,5371)RADIUS(6)
00329          WRITE(6,5375)
00330          WRITE(6,5372)((((FMATRX(J,K,M,N),K=1,2),M=1,2),N=1,2),J=1,LK)
00331          WRITE(6,5374)((, (FMATRX(J,1,1N),N=1,2)J=LK+1,LL)
00332      5374 FORMAT(1H ,3(I4,2E15.5,6X))
00333          WRITE(6,5364)
00334      5364 FORMAT(7H TANDL=)
00335          WRITE(6,5365)(J,((TANDL(J,K,M),K=1,2),M=1,2),J=1,LK+2)
00336          WRITE(6,5366)
00337          WRITE(6,5365)(J,((COSDL(J,K,M),K=1,2),M=1,2),J=1,LK+2)
00338          WRITE(6,5367)
00339          WRITE(6,5365)(J,((SINDL(J,K,M),K=1,2),M=1,2),J=1,LK+2)
00340      5366 FORMAT(7H COSDL=)
00341      5367 FORMAT(7H SINDL=)
00342      5365 FORMAT(2(15,4E15.5))
00343      5360 FORMAT(4E15.9)
00344          CALL NAD(LL,LK,NPN,NPP)
00345          WRITE(6,8900)
00346      8900 FORMAT(1H1)
00347          DO 9200 K=KANKAK,360,KANKAK
00348          AK=FLOAT(K)*.5
00349          CALL SPHERI(K,LL,NPN)
00350          CALL RET(LL,LK,NPN,NPP)
00351          DO 9201 J=1,4
00352          SIGMAA(K,J)=SIGMA(J)
00353      9201 CONTINUE
00354          SHERMM(K,1)=SHERM(4,2)
00355          SHERMM(K,4)=SHERM(4,1)
00356          FRE(1)=.0
00357          FRE(2)=.0
00358          FIM(1)=.0
00359          FIM(2)=.0
00360          GRE(1)=.0
00361          GRE(2)=.0
00362          GIM(1)=0.
00363          GIM(2)=.0
00364          DO 4100 JJ=1,2
00365          DO 4000 J=1,LK
00366          AL=FLOAT(J -1)
00367          FRE(JJ)=FRE(JJ)+(2.*AL+1.)**(-.5)*2.*(AL*SINDL(J,1,JJ)*COSDL(J,1,J
               1J)+(AL+1.)*SINDL(J,2,JJ)*COSDL(J,2,JJ))*ASSLEG(J,1)
00368          FIM(JJ)=FIM(JJ)+(2.*AL+1.)**(-.5)*2.*(AL*SINDL(J,1,JJ)**2
               1+(AL+1.)*SINDL(J,2,JJ)**2)**ASSLEG(J,1)
00369          GRE(JJ)=GRE(JJ)+2.*((AL+1.)*AL/(2.*AL+1.))**.5*(SINDL(J,1,JJ)*COSD
               1L(J,1,JJ)-SINDL(J,2,JJ)*COSDL(J,2,JJ)*ASSLEG(J,2)
00370          GIM(JJ)=GIM(JJ)+2.*((AL+1.)*AL/(2.*AL+1.))**.5*(SINDL(J,1,JJ)**2-S
               1INDL(J,2,JJ)**2)*ASSLEG(J,2)
00371      4000 CONTINUE
00372          SIGMAA(K,JJ+4)=FRE(JJ)**2+FIM(JJ)**2+GRE(JJ)**2+GIM(JJ)**2
00373          SHERMM(K,JJ+1)=2.*(FRE(JJ)*GIM(JJ)-FIM(JJ)*GRE(JJ))/SIGMAA(K,JJ+4)
00374          SIGMAA(K,JJ+4)=SIGMAA(K,JJ+4)*3.14159265/FK(JJ)**2
00375          SIGMAA(K,JJ+4)=SIGMAA(K,JJ+4)*5.3249E-05
00376      4100 CONTINUE
00377           WRITE(6,9000)AK,(((FSC(II,JJ,KK),II=1,2),KK=1,2),JJ=1,3)
00378      9100 FORMAT(1H ,F10.1,3(2E10.2,2X,2E10.2))
00379      9200 CONTINUE
00380          WRITE(6,4450)
00381      4450 FORMAT(1H1)
00382          WRITE(6,4400)
00383      4400 FORMAT(2X,5H KAKU,3X,18(2H *),6H SIGMA,17(2H *),5X,8(2H *),7H SHER
               1MA,7(2H *))
00384          A1A=8.7266463E-03*FLOAT(KANKAK)
00385          SIGT01=0.
00386          SIGT02=0.
00387          SIGT03=0.
00388          SIGT04=0.
00389          DO 4300 K=KANKAK,360,KANKAK
00390          AK=FLOAT(K)*.5
00391          AK1=AK*1.745329252E-02
00392          AK1=SIN(AK1)
00393          KIK=MOD(K,10)
00394          IF(KIK.EQ.1)GO TO 4401
00395          GO TO 4402
00396      4401 CONTINUE
00397          WRITE(6,4403)
00398      4403 FORMAT(1HO,5(2H -))
00399      4402 CONTINUE
00400          WRITE(6,4200)AK,(SIGMAA(K,J),J=1,4),(SHERMM(K,J),J=1,4)
00401      4200 FORMAT(F6.1,6E12.4,5X,4E12.4)
00402          SIGT01=SIGT01+SIGMAA(K,1)*AK1
00403          SIGT02=SIGT02+SIGMAA(K,2)*AK1
00404          SIGT03=SIGT03+SIGMAA(K,3)*AK1
00405      4300 CONTINUE
00406          SIGT01=SIGT01*A1A*6.283185307
00407          SIGT02=SIGT02*A1A*6.283185307
00408          SIGT03=SIGT03*A1A*6.283185307
00409          SIGT04=SIGT01+SIGT02+SIGT03
00410      4404 FORMAT(1HO,20H TOTAL CROSS SECTION,4E20.3)
00411          WRITE(6,4404)SIGT01,SIGT02,SIGT03,SIGT04
00412          DATA BLANK,SIG,HI1,KYO,ZERO/1H ,1H,.1H*.1HO,1HI/
00413          WRITE(6,4450)
00414          DO 4410 K=10,180,2
00415          K1=2*K
00416          SIG1=SIGMAA(K1,5)/(SIGMAA(360,5)*20.
00417          NSIG1=INT(SIG1)
00418          IF(NSIG1.GT.120)NSIG1=120
00419          HI2=SIGMAA(K1,4)/SIGMAA(360,4)*20.
00420          NHI2=INT(SHERMM(K1,4)*25.+101.)
00421          NHI1=INT(HI2)
00422          IF(NHI1.GT.120)NHI1=120
00423          NSHE1=INT(SHERMM(K1,2)*25.+101.)
00424          NSHE1=INT(SHERMM(K1,2)*25.+101.)
00425          DO 4411 J=1,121
00426          GRAPH(J)=BLANK
00427      4411 CONTINUE
00428          GRAPH(1)=ZERO
00429          GRAPH(81)=KYO
00430          GRAPH(101)=ZERO
00431          WRITE(6,4412)K,GRAPH,K
00432          GRAPH(NSIG1)=SIG
00433          GRAPH(NHI1)=HI1
00434          GRAPH(NHI2)=KYO
00435          WRITE(6,4413)GRAPH
00436          GRAPH(NSHE1)=SIG
00437          GRAPH(NSHE2)=HI1
00438          WRITE(6,4413)GRAPH
00439      4413 FORMAT(1H+,6X,121A1)
00440      4412 FORMAT(1H ,I4,2X,121A1,I4)
00441      4410 CONTINUE
00442       600 CONTINUE
00443          STOP
00444          END
```

```
00445         SUBROUTINE SPHERI(K,LL,NPN)
00446         COMMON/AASSLG/ASSLEG(2000,3)
00447         DIMENSION F(3,2)
00448         FK=FLOAT(K)*.01745329252*.5
00449         CFK=COS(FK)
00450         SFK=SIN(FK)
00451         ASSLEG(1,1)  =0.2820947918
00452         ASSLEG(2,1)  =0.4886025119*CFK
00453         ASSLEG(2,2)  =0.3454941495*SFK
00454         ASSLEG(3,1)  =0.3153915653*(3.*CFK*CFK-1.)
00455         F(1,1)=ASSLEG(3,1)
00456         ASSLEG(3,2)  =0.772548404*SFK*CFK
00457         F(2,1)=ASSLEG(3,2)
00458         ASSLEG(3,3)  =0.386274202*SFK*SFK
00459         F(3,1)=ASSLEG(3,3)
00460         ASSLEG(4,1)  =0.3731763326*CFK*(5.*CFK*CFK-3.)
00461         F(1,2)=ASSLEG(4,1)
00462         ASSLEG(4,2)  =.3231801841*SFK*(5.*CFK*CFK-1.)
00463         F(2,2)=ASSLEG(4,2)
00464         ASSLEG(4,3)  =1.021985476*CFK*SFK*SFK
00465         F(3,2)=ASSLEG(4,3)
00466         DO 200 I=5,LL+2
00467         FI=FLOAT(I)-2.
00468         DO 300 J=1,3
00469         FJ=-(FLOAT(J)-1.)
00470         ASSLEG(I,J)  =((2.*FI+1.)*(2.*FI+3.)/(FI+FJ+1.)/(FI-FJ+1.))**.5*CF
            1K*F(J,2)-((2.*FI+3.)*(FI+FJ)*(FI-FJ)/(2.*FI-1.)/(FI+FJ+1.)/(FI-FJ+
            2I.))**0.5*F(J,1)
00471       300 CONTINUE
00472         DO 200 J=1,3
00473         F(J,1)=F(J,2)
00474         F(J,2)=ASSLEG(I,J)
00475       200 CONTINUE
00476         RETURN
00477         END
```

```
00478         SUBROUTINE POTENT(NSEK)
00479         COMMON/WAVPOT/POTE(2,3),WAVEFU(3,2,2)
00480         COMMON/RRADAL/RADIUS(6),RADIAL(10000)/HHABA/HABA(4)
00481         COMMON/KKAISU/KAISU(4)
00482         COMMON/ VVPOT/VPOT(10000,2),VPOTEI(10000)
00483         HABA(1)=HABA(2)/RADIUS(2)
00484         KAISU(1)=INT(ALOG(10.*RADIUS(2))/HABA(1))
00485         HABA(1)=ALOG(10.*RADIUS(2))/FLOAT(KAISU(1))
00486         KAISU(2)=INT((RADIUS(3)-RADIUS(2))/HABA(2))
00487         HABA(2)=(RADIUS(3)-RADIUS(2))/FLOAT(KAISU(2))
00488         HABA(3)=2.*HABA(2)
00489         KAISU(3)=INT(RADIUS(4)-RADIUS(3))/HABA(3))
00490         HABA(3)=(RADIUS(4)-RADIUS(3))/FLOAT(KAISU(3))
00491         HABA(4)=2.5*HABA(3)
00492         KAISU(4)=INT((RADIUS(5)-RADIUS(4))/HABA(4))
00493         HABA(4)=(RADIUS(5)-RADIUS(4))/FLOAT(KAISU(4))
00494         DO 100 I=1,KAISU(1)
00495         RADIAL(I)=0.1*EXP(HABA(1)*FLOAT(I))
00496       100 CONTINUE
00497         J=1+KAISU(1)
00498         JJ=KAISU(1)+KAISU(2)
00499         DO 200 K=2,4
00500         DO 300 I=J,JJ
00501         RADIAL(I)=RADIUS(K)+HABA(K)*FLOAT(I-J+1)
00502       300 CONTINUE
00503         J=JJ+1
00504         KK=K+1
00505         IF(KK.GE.5)GO TO 210
00506         JJ=JJ+KAISU(KK)
00507       200 CONTINUE
00508       210 CONTINUE
00509         JJ=JJ+1
00510         IF(JJ.GE.NSEK)GO TO 2000
00511         GO TO 2100
00512      2000 CONTINUE
00513         WRITE(6,2300)
00514         WRITE(6,2200)
00515         WRITE(6,2300)
00516      2200 FORMAT(29H SEKIBUN KAISU DIMENSION OVER)
00517      2300 FORMAT(1H ,50(2H**))
00518      2100 CONTINUE
```

```
00519         DO 400 I=JJ,NSEK
00520         RADIAL(I)=RADIUS(5)+HABA(4)*FLOAT(I-JJ)
00521       400 CONTINUE
            C     RADIAL NO KETSAN OWARI     GOKUROSAN
00522         JJ=JJ-1
00523         WRITE(6,1000)HABA
00524      1000 FORMAT(1HO,14H SEKIBUN HABA=,4E15.5)
00525         WRITE(6,1100)KAISU
00526      1100 FORMAT(1H ,15H SEKIBUN KAISU=,4I15)
00527         WRITE(6,1200)(RADIAL(I),I=100,NSEK,1000)
00528      1200 FORMAT(1HO,3H R=,7X,12E10.2)
00529         DO 500 NN=1,NSEK
00530         R=RADIAL(NN)
00531         VPOT(NN,1)=0.
00532         VPOT(NN,2)=0.
00533         VPOTEI(NN)=0.
00534         DO 600 I=1,3
00535         VPOT(NN,1)=VPOT(NN,1)-POTE(1,I)*EXP(-POTE(2,I)*R)
00536       600 CONTINUE
00537         VPOT(NN,1)=VPOT(NN,1)/R
00538         DO 700 I=1,2
00539         DO 700 J=1,2
00540         A1=WAVEFU(1,1,I)*WAVEFU(1,1,J)
00541         A2=WAVEFU(1,2,I)*WAVEFU(1,2,J)
00542         VPOT(NN,2)=VPOT(NN,2)+A1/A2/A2*(2./A2/R*(1.-EXP(-A2*R))-EXP(-A2*R)
            1)
00543       700 CONTINUE
00544         VPOT(NN,2)=2.*VPOT(NN,2)
            C     IZYO KITEIZYOTAI KARANO POTENTIAL
00545         A1=WAVEFU(2,1,1)**2
00546         A2=WAVEFU(2,2,1)*2.
00547         VPOT(NN,2)=VPOT(NN,2)-A1/A2/A2*(24./A2**3.*(1.-EXP(-A2*R))/R-EXP(-
            1A2*R)*(18./A2/A2+6./A2*R+R*R))
00548         DO 800 I=1,2
00549         DO 800 J=1,2
00550         A1=WAVEFU(3,1,I)*WAVEFU(3,1,J)
00551         A2=WAVEFU(3,2,I)*WAVEFU(3,2,J)
00552         VPOT(NN,2)=VPOT(NN,2)-A1/A2/A2*(24./A2**3.*(1.-EXP(-A2*R))/R-EXP(-
            1A2*R)*(18./A2/A2+6./A2*R+R*R))
00553       800 CONTINUE

00554         A1=WAVEFU(2,1,1)*WAVEFU(2,1,2)
00555         A2=WAVEFU(2,2,1)*WAVEFU(2,2,2)
00556         VPOT(NN,2)=VPOT(NN,2)-2.*A1/A2/A2*(6./A2/A2*(1.-EXP(-A2*R))/R-EXP(
            1-A2*R)*(4./A2+R))
00557         A1=WAVEFU(2,1,2)*WAVEFU(2,1,2)
00558         A2=WAVEFU(2,2,2)*2
00559         VPOT(NN,2)=VPOT(NN,2)-A1/A2/A2*(2./A2*(1.-EXP(-A2*R))/R-EXP(-A2*R)
            1)
00560         VPOT(NN,2)=VPOT(NN,1)-VPOT(NN,2)
            C     POT OF INELA     OWARI       MATAMATA GOKUROSAN
00561         DO 900 I=1,2
00562         DO 900 J=1,2
00563         A1=WAVEFU(1,1,I)*WAVEFU(3,1,J)
00564         A2=WAVEFU(1,2,I)*WAVEFU(3,2,J)
00565         VPOTEI(NN)=VPOTEI(NN)+3.*A1/A2/A2*(8./A2**3.*(1.-EXP(-A2*R))/R/R-(
            18./A2/A2/R+4./A2  +R)*EXP(-A2*R))
00566       900 CONTINUE
00567         VPOTEI(NN)=VPOTEI(NN)*1.5437488
00568       500 CONTINUE
00569         WRITE(6,5000)((I,RADIAL(I),VPOTEI(I)),I=1,NSEK,10)
00570      5000 FORMAT(4(I7,2E13.4))
00571         RETURN
00572         END
```

```
00573         SUBROUTINE BESSEL(NPP)
00574         COMMON/BES/FJ(300,2),FNEU(300,2),RK(2),KR(2)
00575         DO 100 J=1,2
00576         R=RK(J)
00577         FJO=SIN(R)/R
00578         FJ1=(SIN(R)/(R)-COS(R))/R
00579         FNEUO=-COS(R)/R
00580         FNEU1=-(COS(R)/R+SIN(R))/R
00581         FJ(1,J)=FJO
00582         FJ(2,J)=FJ1
00583         FNEU(1,J)=FNEUO
00584         FNEU(2,J)=FNEU1
```

```
      KR(J)=INT(R)+50
      KR(J)=MINO(KR(J),NPP)
      KR2=KR(J)-1
      DO 200 KR1=3,KR2
      FKR1=KR1
      FJ(KR1,J)=-FJO+(2.*FKR1-3.)*FJ1/R
      FNEU(KR1,J)=-FNEU0+(2.*FKR1-3.)*FNEU1/R
      FJO=FJ1
      FJ1=FJ(KR1,J)
      FNEU0=FNEU1
      FNEU1=FNEU(KR1,J)
  200 CONTINUE
      DO 300 KR1=KR(J),NPP
      FJ(KR1,J)=1.
      FNEU(KR1,J)=1.
  300 CONTINUE
  100 CONTINUE
      RETURN
      END
```

```
      SUBROUTINE BESEL1(LL,I,NPP)
      COMMON/BES/FJ(300,2),FNEU(300,2),RK(2),KR(2)
      DO 100 J=1,2
      R=RK(J)
      FJO=SIN(R)/R
      FJ1=(SIN(R)/(R)-COS(R))/R
      FNEU0=-COS(R)/R
      FNEU1=-(COS(R)/R+SIN(R))/R
      FJ(1,J)=FJO
      FJ(2,J)=FJ1
      FNEU(1,J)=FNEU0
      FNEU(2,J)=FNEU1
      KR(J)=LL+3
      KR(J)=MINO(KR(J),NPP)
      KR2=KR(J)-1
      DO 200 KR1=3,KR2
      FKR1=KR1
      FJ(KR1,J)=-FJO+(2.*FKR1-3.)*FJ1/R
      FNEU(KR1,J)=-FNEU0+(2.*FKR1-3.)*FNEU1/R
      FJO=FJ1
      FJ1=FJ(KR1,J)
      FNEU0=FNEU1
      FNEU1=FNEU(KR1,J)
  200 CONTINUE
      IF(   I.GE.3)GO TO 150
      DO 300 KR1=KR(J),NPP
      FNEU(KR1,J)=0.
      FJ(KR1,J)=0.
  300 CONTINUE
  150 CONTINUE
  100 CONTINUE
      RETURN
      END
```

```
      SUBROUTINE DIRAC1
      COMMON/WAVPOT/POTE(2,3),WAVEFU(3,2,2)
      COMMON/ZZB/ZBE(4,2)
      DO 100 I=1,4
      DO 100 J=1,2
      ZBE(I,J)=0.
  100 CONTINUE
      DO 200 I=1,3
      DO 200 J=1,2
      ZBE(1,J)=ZBE(1,J)+POTE(1,I)
      ZBE(2,J)=ZBE(2,J)-POTE(1,I)*POTE(2,I)
      ZBE(3,J)=ZBE(3,J)+POTE(1,I)*POTE(2,I)*POTE(2,I)/2.
      ZBE(4,J)=ZBE(4,J)-POTE(1,I)*POTE(2,I)**3./6.
  200 CONTINUE
      ZBE(2,2)=3./8.*WAVEFU(2,1,1)*WAVEFU(2,1,1)*WAVEFU(2,2,1)**(-4.)+4.
     1*WAVEFU(2,1,1)*WAVEFU(2,1,2)*(WAVEFU(2,2,1)+WAVEFU(2,2,2))**(-3.)+
     2.25*WAVEFU(2,1,2)*WAVEFU(2,1,2)*WAVEFU(2,2,2)**(-2.)+ZBE(2,2)
      ZBE(4,2)=ZBE(4,2)-WAVEFU(2,1,2)*WAVEFU(2,1,2)/6.
      DO 300 I=1,2
      DO 300 J=1,2
      ZBE(2,2)=ZBE(2,2)+6.*WAVEFU(3,1,I)*WAVEFU(3,1,J)*(WAVEFU(3,2,1)+WA
     1VEFU(3,2,J))**(-4.)-2.*WAVEFU(1,1,I)*WAVEFU(1,1,J)*(WAVEFU(1,2,1)+
     2WAVEFU(1,2,J))**(-2.)
      ZBE(4,2)=ZBE(4,2)+WAVEFU(1,1,I)*WAVEFU(1,1,J)/3.
  300 CONTINUE
      RETURN
      END
```

```
      SUBROUTINE DIRAC2(LL,FFF)
      COMMON/PPHAI/PHAI(2,4,2),AMPL(2,4,2)
      COMMON/ZZB/ZBE(4,2)
      COMMON/PPHAIO/PHAIO(2,2),AMPO(2,2)
      COMMON/LIL/L(2,2)/EENERG/ENERGY(2)
      COMMON/HHABA/HABA(4)
      L(1,1)=LL
      L(1,2)=LL+1
      L(2,1)=-LL-1
      L(2,2)=-LL-2
      IF(LL) 100,150,200
  100 L(1,2)=1
      L(2,1)=1
      GO TO 200
  150 L(1,1)=+1
      GO TO 200
  200 CONTINUE
      DO 300 I=1,2
      DO 400 J=1,2
      PHAI(I,1,J)=-ZBE(1,J)/FLOAT(L(I,J))
  400 CONTINUE
      DO 300 J=1,2
      PHAI(I,1,J)=ARSIN(PHAI(I,1,J))
      IF(PHAI(I,1,J)) 501,502,502
  501 PHAI(I,1,J)=3.141592654-PHAI(I,1,J)
  502 CONTINUE
      PH1=PHAI(I,1,J)
      FLL=FLOAT(L(I,J))
      PHAI(I,2,J)=(ENERGY(J)+ZBE(2,J)-COS(PH1))/(1.-2.*FLL*COS(PH1))
      PHAI(I,3,J)=2.*PHAI(I,2,J)*SIN(PH1)*(1.-FLL*PHAI(I,2,J))+ZBE(3,J)
      PHAI(I,3,J)=PHAI(I,3,J)/2./(1.-FLL*COS(PH1))
      PHAI(I,4,J)=2.*PHAI(I,3,J)*SIN(PH1)*(1.-2.*FLL*PHAI(I,2,J))+2.*PHA
     1I(I,2,J)*PHAI(I,2,J)*COS(PH1)*(1.-2./3.*FLL*PHAI(I,2,J))+ZBE(4,J)
      PHAI(I,4,J)=PHAI(I,4,J)/(3.-2.*FLL*COS(PH1))
      AMPL(I,1,J)=AMPL(I,1,J)- AMPO(I,J)
      AMPL(I,2,J)=(FLL*FLL-ZBE(1,J)*ZBE(1,J))**0.5
      ANPL(I,3,J)=SIN(PH1)*(2.*FLL*PHAI(1,2,J)-1.)
      AMPL(I,4,J)=PHAI(I,2,J)*COS(PH1)*(FLL*PHAI(I,2,J)-1.)+FLL*PHAI(I,3
     1,J)*SIN(PH1)
  300 CONTINUE
      DO 500 I=1,2
      DO 500 J=1,2
      PHAI(I,1,J)=PHAI(I,1,J)/2.
      PHAIO(I,J)=0.
  500 CONTINUE
      DO 600 I=1,2
      DO 600 J=1,2
      DO 650 K=1,4
      FK=FLOAT(K)
      PHAIO(I,J)=PHAIO(I,J)+(.1*EXP(HABA(1)))**(FK-1.)*PHAI(I,K,J)
  650 CONTINUE
      AMPO(I,J)=AMPL(I,1,J)+AMPL(I,2,J)*ALOG(.1*EXP(HABA(1)))+AMPL(I,3,J
     1)*1.*EXP(HABA(1))+AMPL(I,4,J)*.01*EXP(2.*HABA(1))
  600 CONTINUE
      RETURN
      END
```

```
      SUBROUTINE LUNGE(LL,NPN,NSEK)
      DIMENSION DELTA(4),DELAMP(4)
      COMMON/HHABA/HANA(4)/KKAISU/KAISU(4)
      COMMON/BRADAL/RADIUS(6),RADIAL(10000)/EENERG/ENERGY(2)
```

```
      COMMON/MATRIX/FMATRX(2000,2,2,2)/VVPOT/VPOT(10000,2),VPOTEI(10000)
      COMMON/PPHAI1/AMP1(2,2,10000)
      COMMON/L1L/ L(2,2)/PPHAIO/PHAIO(2,2),AMPO(2,2)
      LL1=LL+1
      KKK=1
      KAI=1
      KAIS=KAISU(1)
      HAB=HABA(1)
  100 CONTINUE
      DO 200 I=KAI,KAIS
      DO 300 J=1,2
      DO 300 K=1,2
      FL=FLOAT(L(K,J))
      PHA=PHAIO(K,J)
      DELTA(1)=FL*SIN(2.*PHA)+RADIAL(I)*(-VPOT(I,J)+ENERGY(J)-COS(2.*PHA
     1))
      DELTA(1)=HAB*DELTA(1)
      DELTA(2)=FL*SIN(2.*PHA+DELTA(1))+(RADIAL(I)+RADIAL(I+1))/2.*((-VPO
     1T(I,J)-VPOT(I+1,J))/2.+ENERGY(J)-COS(2.*PHA+DELTA(1)))
      DELTA(2)=HAB*DELTA(2)
      DELTA(3)=FL*SIN(2.*PHA+DELTA(2))+(RADIAL(I)+RADIAL(I+1))/2.*((-VPO
     1T(I,J)-VPOT(I+1,J))/2.+ENERGY(J)-COS(2.*PHA+DELTA(2)))
      DELTA(3)=HAB*DELTA(3)
      DELTA(4)=FL*SIN(2.*(PHA+DELTA(3)))+RADIAL(I+1)*(-VPOT(I+1,J)+ENERG
     1Y(J)-COS(2.*(PHA+DELTA(3))))
      DELTA(4)=HAB*DELTA(4)
      PHAIO(K,J)=PHAIO(K,J)+(DELTA(1)+2.*(DELTA(2)+DELTA(3))+DELTA(4))/6
     1.
      DELAMP(1)=-FL*COS(2.*PHA)-RADIAL(I)*SIN(2.*PHA)
      DELAMP(2)=-FL*COS(2.*PHA+DELTA(1))-(RADIAL(I)+RADIAL(I+1))/2.-SIN(
     1 2.*PHA+DELTA(1))
      DELAMP(3)=-FL*COS(2.*PHA+DELTA(2))-(RADIAL(I)+RADIAL(I+1))/2.*SIN(
     1(2.*PHA+DELTA(2)))
      DELAMP(4)=-FL*COS(2.*(PHA+DELTA(3)))-RADIAL(I+1)*SIN(2.*(PHA+DELTA
     1 3)))
      AMPO(K,J)=AMPO(K,J)+HAB*(DELAMP(1)+2.*(DELAMP(2)+DELAMP(3))+DELAMP
     1(4))/6.
  300 CONTINUE
      IF(LL.LT.0)GO TO 270
      DO 250 J=1,2
      DO 250 K=1,2
      IF(AMPO(K,1).LE.-170.)GO TO 251

      FMATRX(LL1,K,J,2)=FMATRX(LL1,K,J,2)+EXP(AMPO(K,1))*COS(PHAIO(K,
     11))*VPOTEI(I)*AMP1(J,2,I)*HAB*RADIAL(I)**2
      IF(AMPO(J,2).LE.-170.)GO TO 251
      FMATRX(LL1,K,J,1)=FMATRX(LL1,K,J,1)+EXP(AMPO(K,1))*COS(PHAIO(K,1))
     1* VPOTEI(I)*EXP(AMPO(J,2)*COS(PHAIO(J,2))*HAB*RADIAL(I)
  251 CONTINUE
  250 CONTINUE
  270 CONTINUE
      AMP1(1,2,I)=AMP1(1,1,I)
      AMP1(2,2,I)=AMP1(2,1,I)
      AMP1(1,1,I)=EXP(AMPO(1,2))*COS(     PHAIO(1,2))/RADIAL(I)
      AMP1(2,1,I)=EXP(AMPO(2,2))*COS(     PHAIO(2,2))/RADIAL(I)
  200 CONTINUE
      WRITE(6,1100)
 1100    FORMAT(5H R=15)
      WRITE(6,1000)((PHAIO(I,J),I=1,2),J=1,2),((AMPO(I,J),I=1,2),J=1,2)
 1000     FORMAT(4E15.5,10X,4E15.5)
  210 CONTINUE
      KKK2=KKK
      KKK=KKK+1
      KAI=KAI+KAISU(KKK2)
      KAIS=KAIS +KAISU(KKK)
      HAB=HABA(KKK)
      DO 500 I=KAI,KAIS
      DO 400 J=1,2
      DO 400 K=1,2
      FL=FLOAT(L(K,J))
      PHA=PHAIO(K,J)
      DELTA(1)=FL*SIN(2.*PHA)/RADIAL(I)+ENERGY(J)-VPOT(I,J)-COS(2.*PHA)
      DELTA(1)=HAB*DELTA(1)
      DELTA(2)=FL*SIN(2.*PHA+DELTA(1))/(RADIAL(I)+RADIAL(I+1))*2.+ENERGY
     1(J)-(VPOT(I,J)+VPOT(I+1,J))/2.-COS(2.*PHA+DELTA(1))
      DELTA(2)=DELTA(2)*HAB
      DELTA(3)=FL*SIN(2.*PHA+DELTA(2))/(RADIAL(I)+RADIAL(I+1))*2.+ENERGY
     1(J)-(VPOT(I,J)+VPOT(I+1,J))/2.-COS(2.*PHA+DELTA(2))
      DELTA(3)=HAB*DELTA(3)
      DELTA(4)=FL*SIN(2.*(PHA+DELTA(3)))/RADIAL(I+1)+ENERGY(J)-VPOT(I+1,
     1J)-COS(2.*(PHA+DELTA(3)))
      DELTA(4)=DELTA(4)*HAB
      PHAIO(K,J)=PHAIO(K,J)+(DELTA(1)+2.*(DELTA(2)+DELTA(3))+DELTA(4))/
     16.
      DELAMP(1)=-FL*COS(2.*PHA)/RADIAL(I)-SIN(2.*PHA)
      DELAMP(2)=-FL*COS(2.*PHA+DELTA(1))/(RADIAL(I)+RADIAL(I+1))*2.-SIN(
     12.*PHA+DELTA(1))
      DELAMP(3)=-FL*COS(2.*PHA+DELTA(2)/(RADIAL(I)+RADIAL(I+1))*2.-SIN(
     12.*PHA+DELTA(2))
      DELAMP(4)=-FL*COS(2.*(PHA+DELTA(3)))/RADIAL(I+1)-SIN(2.*(PHA+DELTA
     1(3)))
      AMPO(K,J)=AMPO(K,J)+HAB*(DELAMP(1)+2.*(DELAMP(2)+DELAMP(3))+DELAMP
     1(4))/6.
  400 CONTINUE
      IF(LL.LT.0)GO TO 370
      DO 350 J=1,2
      DO 350 K=1,2
      FMATRX(LL1,K,J,2)=FMATRX(LL1,K,J,2)+EXP(AMPO(K,1))*COS(PHAIO(K,
     11))*VPOTEI(I)*AMP1(J,2,I)*HAB*RADIAL(I)
      FMATRX(LL1,K,J,1)=FMATRX(LL1,K,J,1)+EXP(AMPO(K,1))*COS(PHAIO(K,1))
     1*VPOTEI(I)*EXP(AMPO(J,2))*COS(PHAIO(J,2))*HAB
  350 CONTINUE
  370 CONTINUE
      AMP1(1,2,I)=AMP1(1,1,I)
      AMP1(2,2,I)=AMP1(2,1,I)
      AMP1(1,1,I)=EXP(AMPO(1,2))*COS(     PHAIO(1,2))/RADIAL(I)
      AMP1(2,1,I)=EXP(AMPO(2,2))*COS(     PHAIO(2,2))/RADIAL(I)
  500 CONTINUE
      KKK1=KKK+1
      A=RADIUS(KKK1)
      WRITE(6,1200)A,KAI,KAIS
 1200 FORMAT(1H ,3H R=,F5.1,10(2H *),14H SEKIBUN KAISU,2I10)
      WRITE(6,1000)((PHAIO(K,J),K=1,2),J=1,2),((AMPO(K,J),K=1,2),J=1,2)
      IF(KKK.NE.4)GO TO 210
      DO 3000 M=1,2
      FMATRX(1,2,M,2)=0.
      FMATRX(2,M,1,2)=0.
      DO 3000 N=1,2
      FMATRX(1,1,M,N)=0.
 3000 CONTINUE
      RETURN
      END


      SUBROUTINE REI(LL,LK,NPN,NPP)
      DIMENSION C1(2),C2(2),C3(2)
      COMMON/SIG/SIGMA(4),SHERM(4,2)
      COMMON/BES/FJ(300,2),FNEU(300,2),RK(2),KR(2)
      COMMON/AASSLG/ASSLEG(2000,3)
      COMMON/FFSC/FSC(2,3,2)/AAAAMP/AAMP(2000,2,3,2),BBMP(300,2,3,2),
     1ABMP(300,2,3,2),BAMP(300,2,3,2)
C   F(I,K,K)  T,UP-UP ORUP-DOWN,,J,MAFNETIC QUANTUM NUMBWR,,KREAL OR IMAG
      DO 50 N=1,4
      SIGMA(N)=.0
      DO 50 M=1,2
      SHERM(N,M)=0.
   50 CONTINUE
      DO 60 K=1,3
      DO 60 M=1,2
      DO 60 L=1,2
      FSC(M,N,L)=0.
   60 CONTINUE
      DO 100 M=1,3
      M1=M-2
      DO 200 LL1=0,LL
      LLL1=LLL+1
      FLL=FLOAT(LLL1)
      IF(M1)300,400,500
  300 CONTINUE
      ALEG=ASSLEG(LLL1,2)
      ALEG1=ASSLEG(LLL1,3)
      C1(2)=(FLL/(2.*FLL+3.)/2.)**.5
      IF(LLL.EQ.0)GO TO 350
      C1(1)=((FLL+1.)/(2.*FLL-1)/2.)**5
      C2(2)=((FLL+1.)*(FLL+2.)/FLL/(2.*FLL-1.)/2.)**.5
      C2(1)=(FLL*(FLL-1.)/(FLL+1.)/(2.*FLL+3.)/2.)**.5
      GO TO 600
  350 CONTINUE
      C1(1)=0.
      C2(1)=0.
      C2(2)=0.
      GO TO 600
  400 CONTINUE
      ALEG=ASSLEG(LLL1,1)
```

```
00855          ALEG1=ASSLEG(LLL1,2)
00856          C1(2)=-((FLL+1.)/(2.*FLL+3.))**.5
00857          C2(1)=-(FLL*(FLL+2.)/(2.*FLL+3.)/(FLL+1.))**.5
00858          IF(LLL.LE.0)GO TO 450
00859          C1(1)=(FLL/(2.*FLL-1.))**.5
00860          C2(2)=((FLL+1.)*(FLL-1.)/FLL/(2.*FLL-1.))**.5
00861          GO TO 600
00862      450 CONTINUE
00863          C1(1)=0.
00864          C2(2)=0.
00865          GO TO 600
00866      550 CONTINUE
00867          C1(1)=0.
00868          C2(2)=0.
00869          GO TO 600
00870      500 CONTINUE
00871          ALEG=-ASSLEG(LLL1,2)
00872          ALEG1=ASSLEG(LLL1,1)
00873          C1(2)=(FLL/(2.*FLL+3.)/2.)**.5
00874          C2(1)=((FLL+2.)/(2.*FLL+3.))**.5
00875          C2(1)=C2(1)/2.**.5
00876          IF(LLL.LE.0)GO TO 550
00877          C1(1)=((FLL+1.)/(2.*FLL-1.))**.5
00878          C1(1)=C1(1)/2.**.5
00879          C2(2)=((FLL-1.)/(2.*FLL-1.)/2.)**.5
00880      600 CONTINUE
00881          C1(2)=C1(2)*((FLL+1.)/(2.*FLL+1.))**.5
00882          C2(1)=C2(1)*((FLL+1.)/(2.*FLL+1.))**.5
00883          C2(2)=C2(2)*(FLL/(2.*FLL+1.))**.5
00884          C1(1)=C1(1)*(FLL/(2.*FLL+1.))**.5
00885          IF(LLL.GT.LK+2)GO TO 610
00886          DO 700 I=1,2
00887          FSC(1,M,I)=FSC(1,M,I)+(AAMP(LLL1,2,M,I)*C1(1)-AAMP(LLL1,1,M,I)*
               1C1(2)+BBMP(LLL1,1,M,I)*C2(1)-BBMP(LLL1,2,M,I)*C2(2))*ALEG
00888          FSC(2,M,I)=FSC(2,M,I)+(BAMP(LLL1,2,M,I)*C1(1)-BAMP(LLL1,1,M,I)*
               1C1(2)*ABMP(LLL1,1,M,I)*C2(1)-ABMP(LLL1,2,M,I)*C2(2))*ALEG1
00889      700 CONTINUE
00890          GO TO 620
00891      610 CONTINUE
00892          DO 710 I=1,2
00893          FSC(1,M,I)=FSC(1,M,I)+(AAMP(LLL1,2,M,I)*C1(1)-AAMP(LLL1,1,M,I)*
               1C1(2))*ALEG
00894      710 CONTINUE
00895      620 CONTINUE
00896      200 CONTINUE
00897          DO 800 I=1,2
00898          FSC(1,M,I)=-FSC(1,M,I)*3.464101615
00899          FSC(2,M,I)=-FSC(2,M,I)*3.464101615
00900      800 CONTINUE
00901          DO 900 L=1,2
00902          DO 900 N=1,2
00903          SIGMA(M)=SIGMA(M)+FSC(L,M,N)*FSC(L,M,N)
00904      900 CONTINUE
00905          SIGMA(M)=SIGMA(M)*5.3294E-05
00906      100 CONTINUE
00907          FSC(2,2,1)=-FSC(2,2,1)
00908          FSC(2,2,2)=-FSC(2,2,2)
00909          DO 1000 M=1,3
00910          DO 1000 K=1,2
00911          SHERM(3,2)=SHERM(3,2)+2.*FLOAT((-1)**K)*FSC(1,M,K)*FSC(2,M,3-K)
00912          SHERM(3,1)=SHERM(3,1)+2.*FLOAT((-1)**(M+K))*FSC(1,M,K)*FSC(2,4-M,
               13-K)
00913      1000 CONTINUE
00914          DO 910 I=1,3
00915          SIGMA(4)=SIGMA(4)+SIGMA(I)
00916      910 CONTINUE
00917          SHERM(3,2)=SHERM(3,2)/SIGMA(4)*5.3294E-05
00918          SHERM(3,1)=SHERM(3,1)/SIGMA(4)*5.3294E-05
00919          RETURN
00920          END

00921          SUBROUTINE NA0(II,IK,NPN,NPP)
00922          DIMENSION SDL(3,2,2)
00923          COMMON/MATRIX/FMATRX(2000,2,2,2)
00924          COMMON/AAAAMP/AAMP(2000,2,3,2),BBMP(300,2,3,2),ABMP(300,2,3,2)
               1,BAMP(300,2,3,2)
00925          COMMON/TANDEI/TANDI(300,2,2)
00926          COMMON/SCDL/SINDL(300,2,2),COSDL(300,2,2),SCSQ(300,2,2)
C SDL (I,J,K)  I,J,L DR  -L-1 OF ELASTIC OR INELASTIC,,K,SIN OR COS
00927          LK=LK+2
00928          DO 1000 N=1,NPP
00929          DO 1000 NN=1,2
00930          DO 1000 NNN=1,3
00931          DO 1000 NNNN=1,2
00932          BBMP(N,NN,NNN,NNNN)=0.
00933          ABMP(N,NN,NNN,NNNN)=0.
00934          BAMP(N,NN,NNN,NNNN)=0.
00935      1000 CONTINUE
00936          DO 1100 N=1,NPN
00937          DO 1100 NN=1,2
00938          DO 1100 NNN=1,3
00939          DO 1100 NNNN=1,2
00940          AAMP(N,NN,NNN,NNNN)=0.
00941      1100 CONTINUE
00942          DO 100 I=1,2
00943          EXS=-1.
00944          JJ=2
00945          IF(I.EQ.2)GO TO 250
00946          JJ=1
00947          EXS=1.
00948      250 CONTINUE
00949          DO 200 J=JJ,LL
00950          J1=J+1
00951          AJ=FLOAT(J-1)
00952          IF(I.EQ.1)GO TO 350
00953          J1=J-1
00954      350 CONTINUE
00955          AJ1=FLOAT(J1-1)
00956          AL=FLOAT(2*J-1)*(FLOAT(2*J1-1))**.5
00957          IF(J.GT.LK+3)GO TO 310
00958          DO 300 K=1,2
00959          DO 300 M=1,2
00960          SDL(K,M,1)=SINDL(J1,M,1)*COSDL(J,K,2)+SINDL(J,K,2)*COSDL(J1,M,1)
00961          SDL(K,M,2)=COSDL(J1,M,1)*COSDL(J,K,2)-SINDL(J1,M,1)*SINDL(J,K,2)
00962      300 CONTINUE
00963          GO TO 320
00964      310 CONTINUE
00965          DO 330 K=1,2
00966          DO 330 M=1,2
00967          SDL(K,M,1)=.0
00968          SDL(K,M,2)=1.
00969      330 CONTINUE
00970      320 CONTINUE
00971          MM=1
00972          MMM=3
00973          IF(J.EQ.1)GO TO 600
00974          GO TO 700
00975      600 CONTINUE
00976          MM=2
00977          MMM=2
00978      700 CONTINUE
00979          DO 400 M=MM,MMM
00980          AM=FLOAT(M-2)
00981          DO 400 K=1,2
00982          EEXS=EXS*FLOAT((-1)**K)
00983          SF1=SDL(1,1,K)*FMATRX(J1,1,1,3-I)
00984          SF2=SDL(1,2,K)*FMATRX(J1,2,1,3-I)
00985          SF3=SDL(2,1,K)*FMATRX(J1,1,2,3-I)
00986          SF4=SDL(2,2,K)*FMATRX(J1,2,2,3-I)
00987          AAMP(J,I,M,K)=EEXS/AL*((AJ+AM)*(AJ1*SF1+(AJ1+1.)*SF2)+(AJ-AM+1.)
               1*(AJ1*SF3+(AJ1+1.)*SF4) )
00988          IF(J.GT.LK+3)GO TO 401
00989          BBMP(J,I,M,K)=EEXS/AL*((AJ+AM)*(AJ-AM+1.)*AJ1*(AJ1+1.))**.5*(SF1-S
               1F2-SF3+SF4)
00990          BBMP(J,I,M,K)=-BBMP(J,I,M,K)
00991          ABMP(J,I,M,K)=EEXS/AL*(AJ1*(AJ1+1.))**.5*(-(AJ-AM+1.)*(SF1-SF2)
               1-(AJ+AM)*(SF3-SF4))
00992          BAMP(J,I,M,K)=EEXS/AL*((AJ+AM)*(AJ-AM+1.))**.5*(-AJ1*(SF1-SF3)
               1-(AJ1+1.)*(SF2-SF4))
00993          BAMP(J,I,M,K)=-BAMP(J,I,M,K)
00994      401 CONTINUE
00995      400 CONTINUE
00996      200 CONTINUE
00997      100 CONTINUE
00998          WRITE(6,3500)
00999      3500 FORMAT(/////29H AAMP NO ZERO DE ARUBEKI ATAI)
01000          WRITE(6,3000)((AAMP(1,2,M,N),M=1,3)N=1,2)
```

```
      WRITE(6,3100)((BBMP(1,1,M,N),M=1,3),N=1,2)
      WRITE(6,3100)((BBMP(1,2,M,N),M=1,3),N=1,2)
      WRITE(6,3100)((BBMP(2,2,M,N),M=1,3),N=1,2)
      WRITE(6,3200)((BAMP(1,1,M,N),M=1,3),N=1,2)
      WRITE(6,3200)((BAMP(1,2,M,N),M=1,3),N=1,2)
      WRITE(6,3300)((ABMP(1,2,M,N),M=1,3),N=1,2)
      WRITE(6,3300)((ABMP(2,2,M,N),M=1,3),N=1,2)
 3000 FORMAT(1HO,6H AAMP=,6E15.5)
 3100 FORMAT(1H ,6H BBMP=,6E15.5)
 3200 FORMAT(1H ,6H BAMP=,6E15.5)
 3300 FORMAT(1H ,6H ABMP=,6E15.5)
      DO 2000 M=1,3
      DO 2000 N=1,2
      AAMP(1,2,M,N)=0.
      BAMP(1,1,M,N)=0.
      BBMP(1,2,M,N)=0.
      BAMP(1,2,M,N)=0.
      BBMP(1,2,M,N)=0.
      ABMP(1,2,M,N)=0.
      BBMP(2,2,M,N)=0.
      ABMP(2,2,M,N)=0.
 2000 CONTINUE
 3600 FORMAT(12E11.3)
      WRITE(6,3601)
 3601 FORMAT(6H AAMP=)
      WRITE(6,3600)((((AAMP(L,I,M,J),J=1,2),M=1,3),I=1,2),L=1,LK+2)
      WRITE(6,3605)
 3605 FORMAT(1HO      )
      WRITE(6,3600)((AAMP(L,I,1,2),I=1,2),L=LK+3,LL)
      WRITE(6,3602)
 3602 FORMAT(6H ABMP=)
      WRITE(6,3600)((((ABMP(L,I,M,J),J=1,2),M=1,3),I=1,2),L=I,LK+2)
      WRITE(6,3603)
 3603 FORMAT(6H BAMP=)
      WRITE(6,3600)((((BAMP(L,I,M,J),J=1,2),M=1,3),I=1,2),L=1,LK+2)
      WRITE(6,3604)
 3604 FORMAT(6H BBMP=)
      WRITE(6,3600)((((BBMP(L,I,M,J),J=1,2),M=1,3),I=1,2),L=1,LK+2)
      RETURN
      END
```

```
      SUBROUTINE TAE(LL,NPN,NPP)
      DIMENSION VPTEI(20000)
      DIMENSION FMTRX(300,2,2,2),FMTRX1(300,2,2,2)
      COMMON/HHABA/HABA(4)
      COMMON/WAVPOT/POTE(2,3),WAVEFU(3,2,2)
      COMMON/BES/FJ(300,2),FNEU(300,2),RK(2),KR(2)
      COMMON/SCDL/SINDL(300,2,2),COSDL(300,2,2),SCSQ(300,2,2)
      COMMON/MATRIX/FMATRX(2000,2,2,2)
      COMMON/RADAL/RADIUS(6)
      COMMON/FKF/FK(2)
      N99=20000
      LK=LL
      DO 60 I=1,NPP
      DO 60 J=1,2
      DO 60 K=1,2
      DO 60 M=1,2
      FMTRX1(I,J,K,M)=0.
   60 CONTINUE
      N=4
      HAB=1./FK(1)/41.958
      IF(HAB.LT.HABA(4))GO TO 70
      GO TO 80
   70 CONTINUE
      WRITE(6,90)
   90 FORMAT(//20(2H *),22H CAUTION TAE INCORRECT,20(2H *)
      HAB=HABA(4)+.01
   80 CONTINUE
      AA =(HAB/HABA(4)) **(1./FLOAT(N))
      RAD=(RADIUS(6)-RADIUS(5))/(AA**N-1.)*(AA-1.)
      NN=INT(RAD/HABA(4)/AA)
      HAB=RAD/FLOAT(NN)
      NN1=1
      NN2=NN
      WRITE(6,110)NN
  110 FORMAT(//18H TAE SEKIBUN KAISU,I10//)
      JI=1
      RADI=RADIUS(5)
      IF(NN.GE.N99)GO TO 4000
      GO TO 4100
 4000 CONTINUE
      WRITE(6,4200)
 4200 FORMAT(10X,32H CAUSION?? VPTEI DIMENSION OVER)
      GO TO 1200
 4100 CONTINUE
  400 CONTINUE
      DO 50 I=1,N99
      VPTEI(I)=0.
   50 CONTINUE
      DO 2000 I=1,NPP
      DO 2000 J=1,2
      DO 2000 K=1,2
      DO 2000 M=1,2
      FMTRX(I,J,L,M)=0.
 2000 CONTINUE
      DO 100 I=NN1,NN2
      FFI=FLOAT(I)
      R=RADI+HAB*FFI
      RK(1)=R *FK(1)
      RK(2)=R *FK(2)
      CALL BESEL1(LL,I,NPP)
      DO 300 J=1,2
      DO 300 K=1,2
      A1=WAVEFU(1,1,J)*WAVEFU(3,1,K)
      A2=WAVEFU(1,2,J)+WAVEFU(3,2,K)
      VPTEI(I)=VPTEI(I)+3.*A1/A2/A2 *(8./A2**3.*(1.-EXP(-A2*R))/R/R-(8.
     1/A2/A2/R+4./A2+R)*EXP(-A2*R))
  300 CONTINUE
      VPTEI(I)=VPTEI(I)*1.5437488
      DO 200 K=1,2
      JJ=1
      IF(K.EQ.2)JJ=2
      DO 200 J=JJ,LL
      J1=J+1
      IF(K.EQ.2) J1=J-1
      FMTRX(J,1,1,K)=FMTRX(J,1,1,K)+FJ(J,1)*VPTEI(I)*FJ(J1,2)*R*R
      FMTRX(J,1,2,K)=FMTRX(J,1,2,K)+FJ(J,1)*VPTEI(I)*FNEU(J1,2)*R*R
      FMTRX(J,2,1,K)=FMTRX(J,2,1,K)+FNEU(J,1)*VPTEI(I)*FJ(J1,2)*R*R
      FMTRX(J,2,2,K)=FMTRX(J,2,2,K)+FNEU(J,1)*VPTEI(I)*FNEU(J1,2)*R*R
  200 CONTINUE
  100 CONTINUE
      DO 3000 J=1,LL
      DO 3000 I=1,2

      DO 3000 K=1,2
      DO 3000 M=1,2
      FMTRX1(J,I,K,M)=FMTRX1(J,I,K,M)+FMTRX(J,I,K,M)*HAB
 3000 CONTINUE
      HAB=HAB*AA
      RADI=RADI+RAD*AA**(JI-1)
      WRITE(6,3100)R,RADI
 3100 FORMAT(1H ,3H R= ,E15.5, 9H DE OWARI,3H R=,E15.5,12H DE HAJIMARU)
      JI=JI+1
      IF(JI.NE.5)GO TO 400
      WRITE(6,3300)
 3300 FORMAT(1HO,8H FMTRX1=)
      WRITE(6,3200)((((FMTRX1(J,I,K,M),I=1,2),M=1,2,J=1,LL+2)
 3200 FORMAT(8E15.5)
      DO 1000 N=1,2
      JJ=1
      IF(N.EQ.2) JJ=2
      DO 1000 J=JJ,LL
      J1=J-1
      IF(N.EQ.2)J1=J-1
      DO 1000 I=1,2
      DO 1000 K=1,2
      FMATRX(J,I,K,N)=FMATRX(J,I,K,N)+COSDL(J,I,1)*COSDL(J1,K,2)*
     1FMTRX1(J,1,1,N)+SINDL(J,I,1)*SINDL(J1,K,2)*FMTRX1(J,2,2,N)-
     2COSDL(J,I,1)*SINDL(J1,K,2)*FMTRX1(J,1,2,N)-SINDL(J,I,1)*COSDL(J1,
     3K,2)*FMTRX1(J,2,1,N)
 1000 CONTINUE
      FMATRX(1,1,1,1)=.0
      FMATRX(1,1,2,1)=.0
      FMATRX(2,1,1,2)=.0
      FMATRX(2,2,1,2)=.0
      VP=.0
      DO 5400 J=1,2
      DO 5400 I=1,2
      A1=WAVEFU(1,1,I)*WAVEFU(3,1,J)
      A2=WAVEFU(1,2,I)+WAVEFU(3,2,J)
      VP=VP+6.*A1/A2**5
 5400 CONTINUE
      VP=VP*1.5437488
```

```
01158      5200 CONTINUE
01159           LL=LL+1
01160           AA=1.
01161           BB=1.
01162           DO 5100 J=1,LL-2
01163           FJ1=FLOAT(J)
01164           AA=AA*FJ1/(FJ1-.5)
01165           BB=BB*FJ1/(FJ1-1.5)
01166      5100 CONTINUE
01167           AA=AA/(FJ1+.5)/(FJ1+1.5)*(FJ1+1.)/(FJ1+2.5)
01168           BB=BB/(FJ1-.5)/(FJ1+.5)
01169           AA1=AA
01170           BB1=BB
01171           LAL=LL*10
01172           DO 5300 J=1,LAL+200
01173           FJ1=FLOAT(J)
01174           AA=AA*(FJ1-.5)/FJ1*(FJ1+FLOAT(LL-1))/(FJ1+FLOAT(LL-1)+1.5)
               1*(FK(2)/FK(1))**2
01175           BB=BB*(FJ1-1.5)/FJ1*(FJ1+FLOAT(LL-1)-1.)/(FJ1+FLOAT(LL-1)-.5
               1*(FK(2)/FK(1))**2
01176           AA1=AA1+AA
01177           BB1=BB1+BB
01178      5300 CONTINUE
01179           AA1=AA1*VP*(FK(2)/FK(1))**LL/FK(1)
01180           BB1=-BB1*VP*(FK(2)/FK(1))**(LL-2)/FK(1)
01181           DO 5500 I=1,2
01182           DO 5500 J=1,2
01183           FMATRX(LL,I,J,1)=AA1
01184           FMATRX(LL,I,J,2)=BB1
01185      5500 CONTINUE
01186           IF(LL.GE.NPN-5)GO TO 5600
01187           AB1=AMAX1(AA1,BB1)
01188           IF(AB1.GT.10E-4)GO TO 5200
01189      5600 CONTINUE
01190           FMATRX(LK+1,1,1,2)=-FMATRX(LK+1,1,1,2)
01191           FMATRX(LK+1,2,1,2)=-FMATRX(LK+1,2,1,2)
01192           FMATRX(LK+2,1,1,2)=-FMATRX(LK+2,1,1,2)
01193           FMATRX(LK+2,2,1,2)=-FMATRX(LK+2,2,1,2)
01194      1200 CONTINUE
01195           RETURN
01196           END
```

## REFERENCES I (REVIEW PAPERS AND BOOKS)


Tolhoek H.A., 1956, Rev. Mod. Phys., 28, 277.

McMaster W.H., 1961, Rev. Mod. Phys., 33, 8.

Farago P.S., 1965, Adv. Electron & Electronic Phys., 21, 1.

Mott N.F., and Massey H.S.W., 1965, "Theory of Atomic Collisions", (Oxford)

Kessler J., 1969, Rev. Mod. Phys.,41,3.

Eckstein W., 1970, IPP Report(7/1).

Farago P.S., 1971, Pep. Prog. Phys. 34, 1055.

Walker D.W., 1971, Advances in Phys., 20, 257.

Suzuki T., 1972, Butsuri, 27, 805. (in Japanese)

Kessler J., 1976, "Polarized Electrons" (Springer-Verlag).

## REFERENCES II


Alder H., Busch Q, Campagna M, Pierce D.T. and Siegmann H.C., 1973a, Vakuum Technik, 21, 139.

Alder H., Campagna M. and Siegmann H.C., 1973b, Phys. Rev. 8, 8, 2075.

Alvarado S.F., Eib W. and Siegmann H.C., 1975a, Phys. Rev. Letters,35, 860.

Alvarado S.F., Eib W., Meier F., Pierce D.T., Sattler K, Siegmann H.C. and Remeika J.P., 1975b, Phys. Rev. Letters, 34, 319.

Anderson, P.W., 1971, Proc. Roy. Soc., , 203.

Arnot F.L., 1929, Proc. Roy. Soc., A125, 660.

———— , 1931, Proc. Roy. Soc., A130, 655.

Arnot F. L. and Baines G.O., 1935, Proc. Roy. Soc., A151, 256.

Bänninger U., Busch G., Campagna M. and Siegmann H.C., 1970, Phys. Rev. Letters, 25, 585.

Bartlett J. H. and Welton T.A., 1941, Phys. Rev., 59, 281.

Bass J. N., Berg R.A. and Green A.E.S., 1974, J. Phys., B7, 1853.

Bates D.R. and Damgaard A., 1949, Phil. Trans. Roy. Soc., A242, 101.

Blum K. and Kleinpoppen H., 1974, Phys. Rev. A, 9, 1902.

Bonham R.A. and Strand T.G., 1963, J. Chem. Phys., 39, 2200.

Boyd R.G., Larson A.C. and Waber J. T., 1963, Phys. Rev., 129, 1629.

Bransden B.H., McDowell M.R.C., Noble C.J. and Scott T., 1976, J. Phys., B9, 1301.

Bransden B.H. and McDowell M.R.C., 1977, Physics Reports, 30, 207.

Breit G. and Bethe H.A., 1954, Phys. Rev., 93, 888.

Bromberg J.P., 1969, J. Chem. Phys., 51, 4117.

Browne H.N. and Bauer E., 1966, J. Chem. Phys., 16, 495.

Bühring W., 1965a, Nuclear Physics, 61, 110.

————, 1965b, Z. Physik, 187, 180.

————, 1968a, Z. Physik, 208, 286.

————, 1968b, Z. Physik, 212, 61.

Bullard E.C. and Massey H.S.W., 1931, Proc. Roy. Soc., A133, 637.

Bunyan P.J., 1963, Proc. Phys. Soc., 81, 816.

Bunyan P.J. and Schoufelder J.L., 1965, Proc. Phys. Soc., 85, 455.

Byatt W.J., 1956, Phys. Rev., 104, 1298.

Byrne J. and Farago P.S., 1965, Proc. Phys. Soc., 86, 801.

Campagna M., Pierce D.T., Sattler K. and Siegmann H.C., 1973, J. de Physique, supple, C6-87.

Campbell D.M., Brash H.M. and Farago P.S., 1971, Phys. Letters, 36A, 449.
Chrobok G., Hofmann M., Regenfus G. and Sizmann R., 1977, Phys. Rev. B , 15, 429.
Cohen S., 1960, Phys. Rev., 118, 489.
Coulthard M.A., 1967, Proc. Phys. Soc., 91, 44.
Cox H.L. and Bonham R.A., 1969, J. Chem. Phys., 47, 2599.

Darwin C.G., 1928, Proc. Roy. Soc., A118, 654.
Davis B. and Goucher F.S., 1917, Phys. Rev., 10, 101.
Dawson S.F., 1967, Phys. Rev., 163, 71.
Deichsel H., 1961, Z. Physik, 164, 156.
Deichsel H. and Reichert E., 1964, Phys. Letters, 13, 125.
———————————, 1965, Z. Physik, 185, 169.
Deichsel H., Reichert E. and Steidl H., 1966, Z. Physik, 189,212.
Dewames R.E. and Vredevoe L.A., 1967, Phys. Rev. Letters, 18, 853.
Dirac P.A.M., 1928, Proc. Roy. Soc., A117, 610.
Dirac P.A.M., 1930, Proc. Cambridge Phil. Soc., 26, 376.
Drachenfels W.V., et al., 1974, Z. Physik, 269, 387.
Düweke M., Kirchner N., Reichert E. and Schön S., 1976, J. Phys., B9, 1915.
Düweke M., Kirchner N., Reichert E. and Staudt E., 1973, J. Phys., B6, L208.

Eastmann D.E., 1973, Phys. Rev. B , 8, 6027.
Eckstein W., 1967, Z. Physik, 203, 59.
Eckstein W. and Müller N., 1975, Appl. Phys., 5, 71.
Eib W. and Alvarado S.F., 1976, Phys. Rev. Letters, 37, 444
Eitel W. and Kessler J., 1970, Phys. Rev. Letters, 24, 1472.
———————————, 1971, Z. Physik, 241, 355.
Eitel W, Jost K. and Kessler J., 1967, Phys. Rev.,159, 47.
———————————, 1968, Z. Physik, 209, 348.
Eldridge J.A., 1922, Phys. Rev., 20, 456.
Erskine G.A. and Massey H.S.W., 1952, Proc. Roy. Soc., A212, 521.

Fano U., 1969, Phys. Rev., 178, 131.
Farago P.S. and Siegmann H. Chr., 1966, Phys. Letters, 20, 279.
Feder R., 1973, Phys. Status sol., b58, K137.
————, 1974, Phys. Status sol., b62, 135.
————, 1975, Surface Science, 51, 297.
————, 1976, Phys. Rev. Letters, 36, 598.
————, 1977a, Phys. Rev., B51, 1751.

Feder R., 1977b, Solid State Commun., 21, 1091.
Feder R., Jennings P.J. and Jones R.O., 1976, Surface Science, 61, 307.
Fink M. and Yates A.C., 1970a, Tech. Rept. No.88 Electronic Research Center, The University of Texas.
———————— , 1970b, Atomic Data, 1, 385.
———————— , 1972, Atomic Data, 4, 129.
Foldy L.L. and Wouthuysen S.A., 1950, Phys. Rev., 78, 29.
Foard C.W., 1930, Phys. Rev., 35, 1187.
Franck J. and Hertz G., 1914, Verh. der Phys. Ges., 16, 457.
Franzen W. and Gupta R., 1965, Rhys. Rev. Letters, 15, 819.
Fujiwara K., 1961, J. Phys. Soc. Japan,16, 2226.

Gehenn W., Haug R., Wilmers M. and Deichsel H., 1969, Z. angew, Phys., 28, 142.
Gell-Mann H. and Goldberger M.L., 1953, Phys. Rev., 91, 398.
Gleich W., Regenfus G. and Sizmann R., 1971, Phys. Rev. Letters, 27, 1066.
Gluckstern R.L. and Lin S.R., 1964a, Phys. Rev., 136, B859.
———————— , 1964b, J. math. Phys., 5, 1594.
Granneman E.H.A., Klewer M. and Van der Wiel M.J., 1976, J. Phys., B9, 2819.
Grant I.P., 1961, Proc. Roy. Soc.,A262, 555.
Gregory D.C. and Fink M., 1974a, Atomic Data and Nuclear Data Tables, 14, 39.
———————— , 1974b, Tech. Rept. No160, Electric Research Center The University of Texas.
Gronemeier K.H., 1970, Z. Physik, 232, 483.

Hanne G.F., 1976, J. Phys., B9, 805.
Hanne G.F. and Kessler J., 1972, Phys. Rev. A, 5, 2457.
———————— , 1976, J. Phys., B9, 791.
Hanne G.F., Jost K. and Kessler J., 1972, Z. Physik,252, 141.
Hashimoto H. et al., 1962, J. Phys. Soc. Japan, 17 (suppl.BII) , 170.
Heindorff T., Höfft J. and Reichert E., 1973, J. Phys., B6, 477.
Heinrich et al., 1976, Use of Monte-Carlo Calculation in Electron Probe Microanalysis and Secondary Electron Microscopy (NBS Special Publication 460).
Heinzmann U., Kessler J. and Lorenz J., 1970, Z.Physik, 240, 42.
Heinzmann U., Kessler J. and Ohnemus B., 1971,Phys. Rev. Letters,27,1696.
Heinzmann U., Jost K., Kessler J. and Ohnemus B., 1972, Z. Physik,251, 354.
Heinzmann U. Heuer H. and Kessler J., 1975, Phys. Rev. Letters, 34, 441.
Hofman M., Regenfus G., Scharpf O. and Kennedy P.J., 1967, Phys. Letters, 25A,270.

Holtzwarth G. and Meister H.J., 1964a, Nuclear Physics, 59, 56.
———————————— , 1964b, Tables of Asymmetry, Cross-Section and related function for Mott scattering of electrons by Screened Au and Hg Nuclei (University of Munich)
Hughes V.W., Long R.L., Lubell M.S., Posner M. and Raith W., 1972, Phys. Rev. A, 5, 195.
Hughes A.L. and McMillen J.H., 1932, Phys. Rev. 39, 585.

Jennings P.J., 1970, Surface Science, 20, 18.
————————, 1971a, Surface Science, 26, 509.
————————, 1971b, Surface Science, 27, 221.
————————, 1975, J. Phys., C8, L285.
Jennings P.J. and Sim B.K., 1972, Surface Science, 33, 1.
Jost K. and Kessler J., 1966, Z. Physik,195, 1.

Kessler J. and Lindner H., 1965,Z. Physik,183, 1.
Kessler J. and Weichert N., 1968, Z. Physik,212, 48.
Kessler J., Lorenz H. and Rempp H., 1971, Z. Physik, 246,348.
Kessler J., Lucas C.B. and Vuskovic L., 1977, J. Phys., B10,, 847.
Kieffer L.J., 1970, Atomic Data, 3, 20.
King G.C. and Adams A., 1974, J. Phys., B7, 1712.
Kisker E. et al., 1976, Phys. Rev. Letters, 36, 982.
Kleinpoppen H., 1971, Phys. Rev. A, 3, 2015.
Koyama K., 1975, Z. Physik, B22, 337.
Kayama K. and Merz H., 1975, B20, 131.
Krause H.F., Johnson S.G., and Datz S., 1977, Phys. Rev. A, 15, 611.
Krefting E.R. and Reimer L.; Quantitative Analysis with Electron Microprobe and Secondary Ion Mass Spectrometry (Ed. E. Preuss, Zentral-bibliothek der KFA,Jurich GmbH)
Kuyatt C.E., Simpson J.A. and Mielczarek S.R., 1965, Phys. Rev. 138, A385.

Lafferty J.M., 1951, J. Appl. Phys., 22, 299.
Landolt M. and Campagna M., 1977, Phys. Rev. Letters, 38, 663.
Langstroth G.O., 1932, Proc. Roy. Soc.,A136, 558.
Latter R., 1955, Phys. Rev., 99, 510.
Laue M. von, 1948, Materiewellen und ihre Interferenzen (Akademische Verlag).
Liberman D., Wable J.T. and Cromer D.T., 1965, Phys. Rev., 137, A27.
Lin S.R., Shermann N. and Percus J.K., 1963, Nuclear Physics, 45, 492.
Lin S.R., 1964, Phys. Rev., 133, A965.

Lippmann B. and Schwinger J., 1950, Phys. Rev., 79, 469.
Loth R. and Eckstein W., 1966, Phys. Letters, 20, 390.
Loth R., 1967, Z. Physik, 203, 66.
Lurio A., 1965, Phys. Rev., 140, 1505.

Madison D.H. and Shelton W.N., 1973a, Phys. Rev. A, 7, 499.
———————————, 1973b, Phys. Rev. A, 7, 514.
Maslen V.W., 1956, Proc. Roy Soc., , 734.
Massey H.S.W. and Mohr C.B.O., 1940, Proc. Roy Soc., A177, 341.
Massey H.S.W., 1956, Rev. Mod. Phys., 28, 199.
Massey H.S.W. and Burhop E.H.S., 1969, Electronic and Ionic Impact Phenomena (Clarendon Press).
Mayers D.F., 1957, Proc. Roy. Soc.,A241, 93.
McConnell J.C. and Moiseiwitsch B.L., 1968, J. Phy S., B1, 406.
Mehr J., 1967, Z. Physik, 198, 345.
Meier F., Eib W. and Pierce D.T., 1975, Solid State Commun., 16, 1089.
Meister H.J. and Weiss H., 1968, Z. Physik,216, 165.
Mishra B., 1952, Cambridge Phil. Soc., 48, 511.
Mohr C.B.O. and Nicoll F.H., 1932, Proc. Roy. Soc.,A138, 229.
Mohr C.B.O. and Tassie L.J., 1954, Proc. Phys. Soc., 67, 711.
Mohr C.B.O., 1969, J. Phys., B2, 166.
Moiseiwitsch B.L., 1976, J. Phys., B9, L245.
Mott N.F., 1929, Proc. Roy. Soc.,A124, 425.
————, 1932, Proc. Roy. Soc.,A135, 429.
Müller N., Siegmann H. Chr. and Obermair G., 1967, Phys. Letters,24A, 733.
Müller N., Eckstein W., Heiland W. and Zinn W., 1972, Phys. Rev. Letters, 29, 1651.
Müller N., 1975, Phys. Letters, 54A, 415.
Murao T., 1972, Phys. Letters, 42A, 138.
———— , 1974, J. Phys. Soc. Japan, 37, 77.

Nigam B.P., Sundersen M.K. and Wu Ta-You, 1959, Phys. Rev.,115, 491.
Nishijima K., 1973, Sotaironteki-Ryoshirikigaku (in Japanese, Bai-Fu-Kan)

O'Neill M.R., Kalisvaart M., Dunning F.B. and Walters G.K., 1975, Phys. Rev. Letters, 34, 1167.

Peacher J.L. and Wills J.G., 1967, J. Chem. Phys., 46, 4809.

Pearson and Arnquist, 1931, Phys. Rev., 37, 970.
Penn D.R., 1975, Phys. Rev. B, 11, 3208.
Penney N.G., 1932, Phys. Rev., 39, 467.
Pierce D.T. and Siegmann H.C., 1974, Phys. Rev. B, 9, 4035.
Pierce D.T., Meier F. and Zurcher, 1975, Phys. Letters, 51A, 465.
Pierce J.R., 1954, Theory and Design of Electron Beams (Princeton).

Read F.H., 1970, J. Phys. E Sci. Instrum., 3, 127.
————, 1971, J. Phys. E Sci. Instrum., 4, 562.
Regenfus G. and Sütsch P., 1974, Z. Physik,266, 319.
Reichert E., 1963, Z. Physik,173, 392.
Rose M.E., 1957,Elementary theory of angular momentum (John Wiley & Sons).
Rotenberg M., 1966, Phys. Rev. Letters, 16, 969.

Satchler G.R., 1964, Nuclear Physics, 55, 1.
Sattler K. and Siegmann H.C., 1975, Z. Physik, B20, 289.
Sawada T., Purcell J.E. and Green A.E.S., 1971, Phys. Rev. A. 4, 193.
Schackert K., 1968, Z. Physik,213, 316.
Schiff L.I., 1968, Quantum Mechanics (McGraw-Hill).
Schonfelder J.L., 1966, J. Phys. Soc., 87, 163.
Shelton W.N. and Leherissey E.S., 1971, J. Chem. Phys., 54, 1130.
Sherman N., 1956, Phys. Rev., 103, 1601.
Sherman N. and Nelson D.F., 1959, Phys. Rev., 114, 1541.
Shimizu R., Kataoka Y., Ikuta T., Koshikawa T. and Hashimoto H., 1976, J. Phys. ,D9, 101.
Shull C.G., Chase C.T. and Myers F.E., 1943, Phys. Rev., 63, 29.
Siegmann H.C., 1975, Phys. Rept., 17, 37.
Skerbele A., Ross K.J. and Lassettre E.N., 1969, J. Chem. Phys., 50, 4486.
Skerbele A. and Lassettre E.N., 1970a, J. Chem. Phys., 52, 2708.
————————————, 1970b, J. Chem. Phys., 53, 3806.
————————————, 1972, J. Chem. Phys., 56, 845.
Slater J.C., 1951, Phys. Rev., 81, 385.
————, 1960, Quantum Theory of Atomic Structure (McGraw-Hill).
Smith N.V. and Traum H.M., 1971, Phys. Rev. Letters, 1388.
Spruch L., 1966, Phys. Rev. Letters, 16, 1137.
Steidl H., Reichert E. and Deichsel H., 1965, Phys. Letters, 17, 31.
Strand T.G. and Bonham R.A., 1964, J. Chem. Phys., 40, 1686.
Suzuki T. and Tanaka H., 1973, J. Phys. Soc. Japan, 34, 566.
Suzuki T., Tanaka H.,Saito M. and Igawa H., 1975, J. Phys. Soc. Japan, 39, 200.

Tanaka T., Bannai E., Kawai S. and Yamane T., 1975, J. Crystal Growth,30, 193.
Thomas L.H., 1927, Phil. Mag., 3, 1.
Tietz T., 1962, Ann. der Physik, 9, 295.
Tolhoek M.A., 1956, Rev. Mod. Phys., 28, 277.

Unertl W.N.,Celotta R.J. and Pierce D.T., 1977, 50th Anniversary of the discovery of electron diffraction 19-21 September.

Walker D.W., 1969, J. Phys., B2, 356.
————, 1970, J. Phys., B3, 788.
Watson G.N., 1966, Theory of Bessel Functions (Cambridge University Press).
Weast, 1972, Handbook of Chemistry and Physics, 53rd edition.
Weiss H.F., 1969, Z. Physik, 229, 299.
Whitney J.D., 1929, Phys. Rev., 34, 923.
Wilmers M., Haug R. and Deichsel H., 1969, Z. angen. Physik, 27, 204.
Wohlfarth E.P., 1971, Phys. Letters, 36A, 131.
————, 19722, Phys. Rev. Letters, 38, 524.
Wu T.Y. and Ohmura T., 1962, Quantum Theory of scattering (Prentice Hall)

Yamazaki Y., Shimizu R. and Hashimoto H., 1976, J. Phys. Soc. Japan, 41, 721.
———————————————, 1977a, Techno. Rept. Osaka Univ., 27, 317.
———————————————, 1977b, Optik, to be published.
Yamazaki et al., 1977c, J. Phys. Soc. Japan, submitted.
————, 1977d, J. Phys. B10, L1.
————, 1977e, J. Phys. Soc. Japan, to be published.
Yates A.C. and Strand T.G., 1968, Phys. Rev., 170, 184.
Yates A.C. and Fink M., 1969, Phys. Rev. Letters, 22, 1.
Yavorskii B.M., 1947, Zh. Eksp. Fiz., 17, 315.
Yennie D.R., Ravenhall D.G. and Wilson R.N., 1954, Phys. Rev., 95, 500.

PUBLICATION LIST

Y. Yamazaki, R.Shimizu and H.Hashimoto : "Calculation of Electron Spin Polarization for Polarization Detector" J.Phys.Soc.Japan 41 (1976) 721.

Y. Yamazaki, R.Shimizu and H.Hashimoto: "Electron Spin Polarization Detector for Hundreds eV Electrons" Technol. Rept. Osaka Univ. 27 (1977) 317

Yamazaki, R.Shimizu and H.Hashimoto: "Basic Experimental Study of ESP detector Using Electron-Mercury Scattering" Optik (to be published)

Y.Yamazaki, R.Shimizu, K.Ueda and H.Hashimoto: "Electron Impact Spectra of Mercury in Intermediate Energies" J. Phys. Soc. Japan (submitted)

Y.Yamazaki, R.Shimizu, K.Ueda and H.Hashimoto: "Influence of Atomic Wave Function on Spin Polarization and Differential Cross Section for Electron Impact Excitation of Mercury" J. Phys. B10 (1977) L1

Yamazaki, R.Shimizu, K.Ueda and H.Hashimoto: "Spin-Polarization and Differential Cross Section of Electron-Mercury Inelastic Scattering J.Phys.Soc. Japan (to be published)

R.Shimizu, M.Aratama, S.Ichimura, Y.Yamazaki and T.Ikuta : "Application of Monte-Carlo Calculation to Fundamentals of Scanning Auger Electron Microscopy" appl. Phys. lett. 31 (1977) 692.